UNIVERSITY OF SOUTHAMPTON

FACULTY OF PHYSICAL SCIENCES AND ENGINEERING

School of Electronics and Computer Science

Influence of Contamination on the Electrical Performance of Power Transformer Oil

by

Shekhar Mahmud

1st Supervisor: Prof. George Chen
2nd Supervisor: Dr. Igor Golosnoy

PhD thesis

April 2015

ABSTRACT

Transformer failure statistics from all over the world showed that almost 30% of them were due to insulation. Large amount of those failures were due to particles in transformer oil. Main focus of this research is to effects of contamination on electrical performance of transformer oil. A literature review of major causes of transformer failure, breakdown mechanisms of transformer oil has been conducted. The experimental setup and results from the pressboard-dust-contaminated transformer mineral oil test are also discussed. Several experiments have been carried out with cellulose particle contaminated transformer mineral oil. The experiments of bridge formation are conducted under the influence of DC, AC, and DC biased AC voltages. Samples with several levels of contaminant are tested under different voltage levels. The influence of different electrode systems is also tested i.e. bare electrode, covered electrode, bare electrodes with paper barrier, spherical and needle – plane electrodes. These experiments revealed that the bridges are always formed under the influence of DC voltages. The particles are attracted towards high electric field due to Dielectrophoretic (DEP) force and become charged once in contact with the electrode surface. Long fiber particles were attached to the electrodes and aligned parallel to electric field towards the other electrode. More particles attached to the initial fibers and the process continued until a full bridge formed between the electrodes. The conduction current increased with contamination levels as the bridge thickened with increment of contaminations.

There is no complete bridge formed under AC electric field. The particles were attracted to the high electric field and attached to the electrodes but the particles are not been able to charge before the polarity of AC electric field alters with spherical electrodes. The current for AC remained unchanged with the increment of particle contamination levels as there is no bridge formed. However, when the DC biased AC signal is applied, the bridge is formed for all the three voltage levels tested. DC and AC breakdown tests were also conducted for several contamination levels.

Experiments with kraft paper covered spherical electrodes confirmed that a tightly bonded cover does not stop the bridge; only a loose bonded cover stopped the bridging. Another test with a paper barrier between bare electrodes also did not stop the bridging. Partial discharge (PD) and breakdown test of the contaminated transformer oil is also measured but the results were not conclusive.

An initial mathematical model of pressboard dust accumulation using Finite Element Analysis (FEA) software, COMSOL multiphysics has been conducted. The result of the simulation model for charging-discharging and bridging showed similar trend as experimental results. There are a number of changes that can result in improved simulations. There are several variables affecting the simulation i.e. the pressboard dust particle shape, size, conductivity of impregnated pressboard fiber etc.

ACKNOWLEDGEMENTS

In the name of Allah, the Beneficent, the Merciful.

Firstly, I would like to express my deepest thanks to Allah for giving me the efforts to finish this thesis successfully. Without His permission, I would never be able to reach at this stage.

Secondly, I would like to acknowledge the support of Power Network Research Academy and National Grid for the sponsorship.

Next, I would like to express my deepest gratitude to my first supervisor, Prof. George Chen and second supervisor Dr. Igor Golosnoy for their valuable suggestions, guidance and encouragement that have substantially helped in my work through the last three years. I would also like to thank Prof. Paul Lewin for his continuous advices through my PhD; especially on image and signal processing techniques. I would also like to thank all the colleagues of Tony Davies High Voltage Lab for their co-operation.

Lastly, I would like to extend my deepest gratitude to my parents, Abdul Mannan and Sufia Hasna Jahan, my wife, Suraiya Islam and the rest of my family as well as all my friends for their support and encouragement.

LIST OF PUBLICATIONS

1. S. Mahmud, G. Chen, I. O. Golosnoy, G. Wilson, and P. Jarman, "Bridging phenomenon in contaminated transformer oil". Proceedings of 2012 International Conference on Condition Monitoring and Diagnosis, Piscataway, US, Institute of Electrical and Electronics Engineers, 4pp, 180-183.

2. S. Mahmud, I. O. Golosnoy, G. Chen, G. Wilson, and P. Jarman, "Numerical simulations of bridging phenomena in contaminated transformer oil". Proceedings of 2012 IEEE Conference on Electrical Insulation and Dielectric Phenomena, Montreal, Canada, 14 - 17 Oct 2012.4pp, 383-386.

3. S. Mahmud, G. Chen, I. O. Golosnoy, G. Wilson, & P. Jarman, "Bridging in contaminated transformer oil under DC and AC electric field". Journal of Physics: Conference Series, 472(1), 12007, 2013.

4. S. Mahmud, G. Chen, I. O. Golosnoy, G. Wilson, and P. Jarman, "Bridging in Contaminated Transformer Oil under AC, DC and DC Biased AC Electric Field". Proceedings of IEEE Conference on Electrical Insulation and Dielectric Phenomena, Shenzhen, China, 20 – 23 Oct, 2013.

5. S. Mahmud, G. Chen, I. O. Golosnoy, G. Wilson, and P. Jarman, "Effect of Kraft Paper Barriers on Bridging in Contaminated Transformer Oil". Proceedings of IEEE Conference on Electrical Insulation and Dielectric Phenomena, Des Moines, Iowa, USA, 19 – 22 Oct, 2014.

6. S. Mahmud, G. Chen, I. O. Golosnoy, G. Wilson, and P. Jarman, "Effect of Different Shapes of Electrodes on Bridging in Contaminated Transformer Oil". Proceedings of IEEE Conference on Electrical Insulation and Dielectric Phenomena, Des Moines, Iowa, USA, 19 – 22 Oct, 2014.

7. S. Mahmud, G. Chen, I. O. Golosnoy, G. Wilson, & P. Jarman, "Experimental Studies of influence of DC and AC Electric Fields on Bridging in Contaminated Transformer Oil". IEEE Transactions on Dielectrics and Electrical Insulation, Vol. 22, Issue 1, pp. 152-160, February 2015.

8. S. Mahmud, G. Chen, I. O. Golosnoy, G. Wilson, & P. Jarman, "Experimental Studies of Influence of Different Electrodes on Bridging in Contaminated Transformer Oil". IEEE Transactions on Dielectrics and Electrical Insulation, 2015. (in press)

CONTENTS

ABBREVIATIONS

AC	Alternating current
CFD	Computational Fluid Dynamic
CIGRE	International Council on Large Electric Systems
DC	Direct Current
DEP	Dielectrophoresis
EPRI	Electric Power Research Institute (US)
FEA	Finite Element Analysis
FEM	Finite Element Method
GSU	Generator step-up (transformer)
GPIB	General Purpose Interface Bus
HV	High voltage
IEEE	Institute of Electrical and Electronics Engineers
OLTC	On-Load Tap Changer
PD	Partial discharge
PPM	Parts per million

LIST OF SYMBOLS

σ_p Conductivity of pressboard particle

σ_{oil} Conductivity of oil

σ_{mix} Conductivity of oil and particle mixture

$a, a_1, a_3 \; and \; a_3$ are constants for oil and particle mixture

m is constant for velocity equation to stop the particles

c is the concentration of the particles

$c_{critical}$ is the critical concentration when particle will stop

ε_0 Dielectric permittivity of air

ε_p Dielectric permittivity of pressboard particle

ε_{oil} Dielectric permittivity of oil

μ_{oil} Viscosity of Oil

v_p Velocity of particle

F_{drag} Drag force

F_{DEP} Dielectrophoretic force

F_C Coulomb force

r Pressboard Particle radius

d Pressboard Particle diameter

l Pressboard Particle length

γ aspect ratio of particle length and diameter

q Charge acquired by Particle

E Electric field

V Applied Voltage

D_p diffusion coefficient

∇ Electric field gradient

CHAPTER ONE: INTRODUCTION

1.1 OVERVIEW

Power transformers are key components in high voltage transmission and distribution systems and their reliable operation is of paramount importance to energy utilities and users. However, as more transformers are approaching or exceeding their designed lifetime, transformer failures in power systems have gathered pace. Analysis has revealed that insulation/oil contamination is a major factor, accounting for nearly 30% of the total failures [1]. Therefore, it is essential to understand the failure mechanisms/processes so the proper measures can be taken to prevent failure and remove the huge cost caused by the failure in terms of asset loss and business interruption [2].

Oil is an important part in power transformers. It serves as both the electrical insulation and coolant and is in direct contact with metals, iron core and the paper insulation. So that the transformer oil is very easy to be contaminated [3, 4]. Contaminants such as metal filings or cellulosic residual can be formed in the oil, especially for transformers with aged paper insulation. Non-uniform fields are present within the transformer during normal operation. These contaminants tend to move towards high field regions due to dielectrophoresis (DEP) forces and could form a bridge over a period of time. The bridge may potentially act as a conducting path between two different potentials within the transformer structure, leading to partial discharges or insulation failure. Initial work on cellulosic particles has demonstrated that pre-breakdown phenomena are closely related to the level of contamination [5].

Demand for HVDC transformer has increased as renewable energy sources like solar gaining popularity and more long distance DC transmission lines are to be built to meet energy requirements for 21st century [6, 7]. Analysis on operational HVDC transformer revealed that some parts of these HVDC converter transformers experience combined effect of AC and DC electric field [8].

HVDC systems in operation today are mostly based on line-commutated converters (LCC). This configuration uses a three-phase bridge rectifier or six-pulse bridge that contains six electronic switches. Each of these switches connecting one of the three phases to one of the two DC rails. A phase change only every 60° and considerable harmonic distortion is produced at both the DC and AC terminals when this arrangement is used [9].

When two units of six pulse converters are connected in seris, star or delta configuration are udes on the DC side for harmonic cancellation. LCC HVDC transformers are placed between converter and AC busbar and before the AC harmonic filters. These tharnsformers have to withstand DC stress

and low order harmonics. An LCC HVDC converter transformer is also subjected to a DC offset voltage depending upos the position with respect to ground [10].

Previously conduction current, partial discharges, resistivity [5, 11, 12] of bridging in transformer oil with DC and AC electric fields have been studied.

1.2 DESCRIPTION OF THE RESEARCH

This project extends the initial work of Chen and Zuber [5] to consider insulating particles under both DC and AC voltages. This is extremely important to power converter transformers which are one of the key components in high voltage DC transmission systems. Power converter transformers experience the combination of DC and AC voltages during operation.

To fully understand the characteristics of contaminants under the combined dc and ac voltage, bridging characteristics under dc and ac voltage will be studied separately. In addition to live optical observation and capturing of bridging phenomena between two spherical electrodes in oil under different voltages, contamination levels and oil and paper insulation conditions, electrical conduction currents and partial discharges will also be measured simultaneously during bridging. Finally, the electric breakdown tests of these various contaminated oil will be carried out.

To simulate extreme cases of non-uniform electric field and its influence on pre-breakdown characteristics of contaminated transformer oil, a needle-plane electrode system will be further investigated. Similar tests to the two spherical electrodes outlined in the above section can be performed.

As the project develops forward, practical application will be considered such as the effects of electrode shape. The influence of coated/wrapped electrode on bridging dynamics can be explored. As transformer coils are typically covered, therefore, it is vital to extend the above research to reveal effects of covered electrodes. Particle bridging characteristics with a barrier between electrodes is also vital to understand as all the cores in a transformers are separated by pressboard barrier. The comprehensive experimental results will allow us to establish a good understanding of contamination and its relation to pre-breakdown phenomena.

To aid the understanding of bridging dynamics in the contaminated oil, a numerical model of particle movements and their accumulation in high field regions will be developed. It will be based on the hydrodynamic drift-diffusion approximation for the particles' motion under dielectrophoresis (DEP) forces. Additionally, the effect of particles shape and surface roughness on dust migration will be studied and an average (and easy measurable) parameters to characterise a wide variety of

dust particles will be found from the simulation. This will create a link between the simulation and the practice, plus provide a verification tool for the model. The model assumptions will be tested by experiments with variety of dust particle (bunches of different sizes and shapes).

By assigning appropriate conductivity values to the oil and contaminant, it is possible to obtain the current that flows during the bridging. It will be compared with the electrical conduction current measured under various conditions. Furthermore particles' percolation as a function of particles geometry and volume fraction will be modeled and the effects of dust accumulation around the electrodes on breakdown initiation will be understood.

This step by step approach will provide essential knowledge of pre-breakdown phenomenon of contaminated transformer oil so that a set of criteria about oil contamination levels can be established to reduce potential transformer failures in power systems.

1.3 Research Objective and Scope

By the end of the research, it is expected to achieve the following objectives:

1. To investigate and analyse the effect of pressboard particles on AC, DC and DC biased AC electric field based on experiments using spherical-spherical and needle-plane electrode system.
2. To measure partial discharge and conduction current during the experiments.
3. To investigate pressboard dust accumulation with covered electrode and paper barrier between electrodes.
4. To develop a mathematical model of pressboard dust accumulation in transformer oil and conduction current measurement with different size and shape of pressboard particles.
5. To verify the simulation results against experimental data to the highest possible degree that can describe the phenomena of interest.

The research scopes are planned limited to the following aspects:

1. The experiments and simulation model will be based on optical observation experimental setup to study the effect of pressboard dust in transformer oil.
2. The experiments and simulation model will consider room conditions of moisture, temperature and voltage source.

1.4 THESIS SUMMARY

Chapter 1

This chapter discusses the impurities due to pressboard and metallic particles in transformer oil and its consequences. It also identifies the experimental works that need to be conducted to explore the mechanism behind the breakdown phenomenon. To justify the experimental result, a mathematical model also has been identified and described. Finally, research objectives and scopes are described.

Chapter 2

Related literature is described in this chapter. These are described under the following topics; transformer failures statistics, failure due to particle, theories of dielectric liquid breakdown, different streamers modes, and previous experiment on contaminated transformer oil.

Chapter 3

The description of experimental setup for all the tests has been given in this chapter. Two different electrode system it used under the influence of DC, AC and DC biased AC voltages. Sample preparation, experimental procedure are explained. Sample tank and electrote system for the breakdown test are also discussed in this chapter.

Chapter 4

In this chapter, all the experimental results of bridging with two bare spherical electrodes with different electric potential have been described. Four different particle sizes were investigated. Conduction current measurement between the electrodes is also included. There were three different levels of pressboard particle contamination and three voltages levels of DC, AC and DC biased AC are considered for these tests.

Influences of DC, AC and DC biased AC electric field on contaminated oil were investigated using spherical electrodes covered with loose and tight bonded kraft paper as well as a paper barrier between two bare spherical electrodes. There were six different levels of contamination tested with three different levels of voltages for each sample. There were complete bridges formed for all the experiments with tight bonded electrode test and paper barrier test under the influence of DC and DC biased AC.

The experimental results of DC, AC and combined AC & DC test with a needle – plane electrode system. There were three different levels of DC electric field applied with six different

contamination levels. A complete bridge formed for most of the concentration level under DC. Three different levels of AC and three level of DC biased AC electric field were also investigated. But no bridges were observed.

Chapter 5

This chapter discusses the breakdown test carried on several contamination levels under DC and AC electric field. Statistical analysis on the breakdown results are computed. The breakdown strength was reduced by adding the contaminated particles for DC and AC voltages.

Chapter 6

The partial discharge experiments and results were explained in this chapter. Several contamination levels of pressboard fibres were tested with spherical and needle – plane electrode system. There was no PD for spherical electrode system. PD was observed for needle – plane electrode system.

Chapter 7

A simulation model based on the dielectrophoresis, electrostatic theory is developed and described in this chapter. Two different models are developed to explain particle charging-discharging and bridging mechanism. The results from these simulations have been analysed, interpreted and compared with the experimental results. Both of the overall characteristics of simulated results were consistent with the experimental results.

Chapter 8

This chapter summarizes the overall conclusion drawn in this PhD thesis and suggests further work to continue the study of particle contamination effect in transformer oil.

CHAPTER TWO: LITERATURE REVIEW

This chapter describes a brief overview of transformer oil and pressboard. It also includes the statistics of transformer failures and their causes from all over the world. Theories of liquid breakdown mechanisms and streamers also discussed. Finally, previous research on particle contaminated transformer oil are also presented.

2.1 TRANSFORMER APPLICATION

Power transformers are the most important components of any electrical transmission network. The typical generator voltage levels are on the order of tens of kilovolts. The power transformer increases the voltage to transmission voltage levels, ranging anywhere from 110 kV to 1000 kV. Power transformers are also used at the end of a transmission line for stepping down the voltage from transmission to distribution levels. Power transformers facilitate the economic transmission of electricity by providing the step-up and step-down functionality [13].

2.2 TRANSFORMER OIL

The greater electrical breakdown strength and thermal conductivity of dielectric liquids than the gaseous insulators make them a useful component for high voltage insulation and power apparatus cooling. Additionally, these can be conformed to complex geometries which are practically more valuable than solid insulators. On the other hand, if the liquid dielectric fails to fulfil the purpose, it can lead to severe damage to power equipment as well as the surrounding environment.

Transformer oil is mainly a mixture of hydrocarbon compounds: alkanes and naphthenes, and is made by refining crude oil. The chemical and electrical properties of the oil may be greatly influenced by a minor part of the ingredients which are polar and ionic species. In general, the molecules of transformer oil have little or no polarity. “Polar compounds found in transformer oil usually contain oxygen, nitrogen, or sulphur. Ionic compounds would typically be organic salts found only in trace quantities” [14]. A more detailed review on the characteristic of transformer oil is given in [4]. This section just concentrates on the elements that are important for this research.

Based on field measurements particle counting in contaminated transformer oil reported by various countries, CIGRE Working Group 12.17 recommended that the contamination level encountered in service should classified as indicated in Table 2-1.

Table 2-1 Typical contamination levels encountered on power transformer insulating oil [15]

ISO class	Maximum count per 100 ml		Contamination designation	Typical occurrence
	5 µm	15 µm		
Up to 8/5	250	32	Nil	IEC cleanliness requirement for sample bottle filled with a clean solvent
9/6 to 10/7	1000	130	Low	Excellent oil cleanliness encountered during factory acceptance test and transformer commissioning
11/8 to 15/12	32000	4000	Normal	Contamination level typical for transformers in service
16/13 to 17/14	130000	16000	Marginal	Contamination level found on a significant number of transformers in service
18/15 and above			High	Contamination level rare and usually indicative of abnormal operating conditions

2.2.1 CHARACTERISTICS OF OIL [16]

Unaged, clean and dry oil usually exhibits the following characteristics:

- From 60℃ to 70℃ the water content is 10-15 ppm or less
- At 90℃ the dissipation factor is 0.5% or less.
- Oil is practically non-polar and typical permittivity is $\varepsilon_m = 2.2$.
- Neither the conducting nor the non-conducting visible particles are present.

Transformer oil used for all the experiments reported in this thesis is manufactured by Nynas Inc. The product is called Nytro Gemini X. According to the manufacturer's datasheet, the dielectric strength of this mineral oil along with some other useful parameters are shown in Table 2-2.

Table 2-2 Properties of the mineral transformer oil

PROPERTY	TEST METHOD	TYPICAL DATA	UNIT
Viscosity, 40°C	ISO 3104	9.2	mm^2/s
Water content	IEC 60814	<20	mg/kg
Density, 20°C	ISO 12185	0.870	kg/dm^3
Breakdown Before Treatment	IEC 60156	40-60	kV
Breakdown After Treatment	IEC 60296	>70	kV

2.3 PRESSBOARD

The textile and paper processing industries used pressboard in the electric machines for more than hundred years. The efforts of Hans Tschudi-Faude in H. Widemann Limited in the late 1920's resulted in a better type of pressboard meeting the requirements of large power transformers. The pressboard is made with high-grade sulphate cellulose, and consists solely of pure cellulose fibres without any binder [14]. Wood is the main source of cellulose fibre. Wood contains 40 to 50% cellulose, 20 to 30% lignin and 10 to 30% hemicellulose and polysaccharides in a dry condition. Structure of glucose and cellulose are shown in Figure 2:1. Cellulose is a linear polymer composed of individual anhydrous glucose units linked at the first and fourth carbon atoms through a glucosidal bond [17]. Insulation paper can be completely dried, degassed, oil impregnated and manufactured to different density, shape, and other properties for different applications [14].

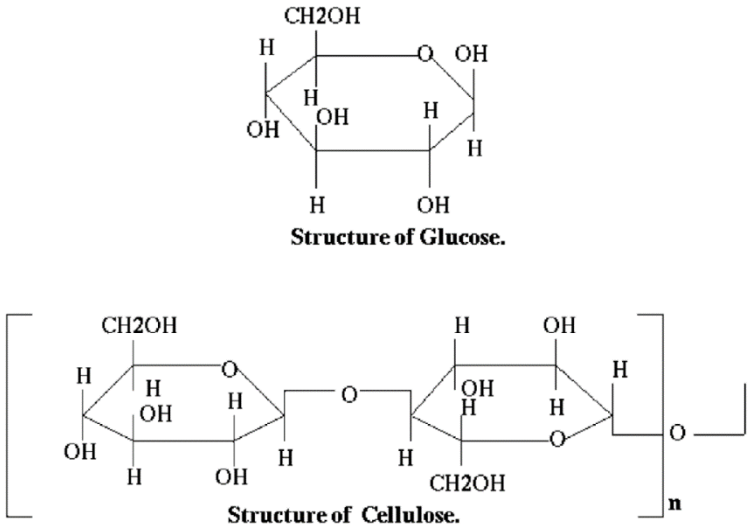

Figure 2:1 Structure of glucose and cellulose.[17]

2.3.1 CHARACTERISTICS OF PRESSBOARD

Undamaged, dry and clean oil-impregnated insulation usually exhibits the following characteristics [16]:

- Water content in the barrier is 0.5 – 1.0% or less.
- A dry and clean surface.
- No irreversible damage due to partial discharge activity.
- A dissipation factor for solid insulation from 20℃ to 70℃ is less than 0.5%.
- Insulation dc conductivity at 20℃ is $\sigma = 2.5 \times 10^{-13}\Omega^{-1}m^{-1}$.
- A practically constant dielectric permittivity of the pressboard, typically: $\varepsilon_p = 4.5$.

2.4 FAILURE ANALYSIS OF POWER TRANSFORMERS

Sokolov [18] has summarised different surveys in a paper regarding transformer failure. Table 2-3 shows the statistics of different failure modes and their occurrence in percentages from the various surveys worldwide. CIGRE working group 12.05 [19] has summarised over 1,000 of power transformers failures rated 72 kV and above for the period 1968-1978. The annual failure rate was 2%, and 5% for extra high-voltage transformers. The most frequently damaged components were winding insulation and terminals arising out of design defect and manufacturing material. The IEEE survey [20] also found 164 failure events in which 51% was dielectric faults arising also because of design and manufacturing problems. On the other hand, winding insulation was the main cause of failure as has been reported by Indian Power Grid accounting for 73.3% of failures; Australia and New Zealand amounting to 30% rate of failure; and China shows a 21% rate of failure. Similar reports of failure were also conveyed by utility companies in Mexico, Romania and Japan. Furthermore, in 1999, an EPRI failure survey on 45 Generator Step-Up (GSU) transformers installed in the US found that major failures were associated with bushings and winding insulation. Hence, it can be concluded based on various survey reports worldwide (as shown in Table 2-3) that most of the failures in transformers accounted from defects in windings/insulation, bushing, on load tap changers, tank and dielectric liquid.

Table 2-3 Failed components and failure modes [18]

Faulty component	CIGRE Survey 1983 (%)	IEEE 1986 (%)	EPRI GSU US (%)	Australia-New Zealand 1985-95 (%)	India Power Grid (%)	China 220kV (Numbers)
Windings/insulation	29	41		30	73.3	21
Dielectric issues			21			
Mechanical			11			
Magnetic circuit	11	10				4
Terminals	29	9	5			
OLTC	13			25		15
Bushing	5	13	30	19	13.3	45
Tank and dielectric liquid	13	3				16
Cooling and others		17	12		13.3	22
Total failure observed	>1000	164	45	498	15	176

Research, however shows that the cause of failure of such transformers was due to corrosive oil and winding insulation arising out of conductive deposit of copper sulphide on paper insulation [18]. Since, most of the data accumulated by Sokolov [18] was in countries like Colombia, Brasilia, India, Rwanda, Thailand, Italy, and South of USA , it may also account for that of transformer failures due to hot and humid environments.

2.4.1 TRANSFORMER FAILURE ATTRIBUTED TO PARTICLES

The CIGRE Working Group 12.17 [15] conducted a series of research projects to determine the reasons of failures in transformers in different parts of the world. From their study, it was reflected that in Venezuela, two 800-kV GSU transformers failed within 15 minutes of operation arising out of causes of particles in the oil used in the transformer. The inspection of those transformers revealed that the filter had been destroyed in the unit where the oil processing is accomplished. To solve the problem, the filters were replaced and later the problem was not encountered again. Similar instances were also observed in Brazil. Here, there were four cases of 800-kV GSU transformer failures and all such cases were attributed to the presence of large paint flakes. Most of such failures occurred within two to six weeks after the units were returned from servicing. Such flashover took place between the high voltage lead shielding and the tank [15].

Other cases of transformer failures were also due to malfunction of the main insulation because of presence of aluminium particles. Such reports were gathered from Canada on 765-kV units over the 30 years by the CIGRE working group. It was also found that the aluminium particles originated from the cooling system. Moreover, in France, the reports of the CIGRE working group between the years of 1980 and 1990 found that 10 of the transformer failures have been attributed to similar particles in the oil. All of the flashovers took place in these 400-kV transformers between the bushing shield and the turret. Similar failures were reported in four cases in 220 to 750 kV transformers in the Ukraine. In this case, the suspected particles seem to have appeared from the cooling system or from excessive heating of the bushing connection. On the other hand, a 400-kV transformer failure occurred in Norway during a lightning storm. Since no other cause of failure could be found, the effect of the particles is considered to be the only possible explanation.

In conclusion, CIGRE working group's survey revealed that most of the failures in the high-voltage power transformers, attributed to particles arising from flashover between the bushing shield and the tank wall. These cellulose particles came from the time of manufacturing the transformer and they caused many cellulose barriers in transformer. A test was conducted for checking the voltage, and it showed that flashover took place in EHV transformers with voltage ratings as low as 120 kV within a long oil gap when there was several visible particles. Although in practice, such flashovers should

have not taken place in a clean oil environment in the transformer. Hence, manufacturers have predicted that the probability of flashover can be significantly reduced if oil is filtered before proceeding with the dielectric tests.

It can be stated from the field and factory experience, that particles are known to be a source of concern mainly for transformers rated 400 kV and above. The transformer component at risk appears to be the bulk oil surrounding the high-voltage lead and the high-voltage bushing shield. However, it is observed that there is very little experimental data which explores the relative severity of factors such as the nature, size and quantity of particles, along with the aggravating effect of moisture and hence, warrants further research.

2.4.2 DIELECTRIC STRENGTH OF PARTICLES CONTAMINATED OIL

To understand the consequence and depict the effects of the particles on the dielectric strength of the insulating oil of transformers has been an interest of researchers. A CIGRE working group reported varying dielectric strengths of the liquid due to the presence of particles. There remains further scope to investigate what mechanisms cause such change in dielectric strength due to the presence of particles.

2.4.3 BARE ELECTRODES

Most of the reported experiments [15] were made using bare electrodes, using test cell as specified by IEC 156 or ASTM D-1816. Experimental findings showed that the conducting materials or cellulose fibre particles reduce the average breakdown voltage. However, the reduction factor fluctuated extensively. Findings further showed that such fluctuation cannot be attributed to the oil volume under stress, voltage application method or type of contaminant.

In the study of Miner [21], it was observed that using contamination particles of iron, copper, and cellulose of 45 µm. The reduction on breakdown voltage was 50, 40, and 25 per cent respectively. In this research, such efforts need also to see what variation in the nature of the particles will attribute to the respective breakdown voltage. In the studies of Sinz [15], where they used cellulose dust and fibres, it appeared that when the researcher used less than 100 µm of the particles, no reduction in breakdown voltage was experienced, but when the size was increased from 100 to 1000 µm, several variations in breakdown voltage was experienced ranging from 40-65 percent. Jorendal [15] reported that 52 percent reduction of breakdown voltage was experienced. The tests were conducted on contaminated transformer oil with 1 ppm cellulose and 14 ppm water.

2.4.4 *Covered Electrodes*

The CIGRE working group reports that there is limited experimental data available to explore the effect of particles with electrodes coated with insulating material. Only research by Nakagawi [15] has reported that plane electrodes covering 0.5 mm pressboard (PB) with contamination amounted to a reduction of 29% on the average breakdown voltage. Future research needs to explore the effect of breakdown voltage using covered electrodes.

2.4.5 *Contamination Deposited on Insulating Surface*

To quantify the impact of conducting particles deposited on insulating structures Hydro-Quebec, in collaboration with EHV Weidmann [15], has investigated the effect of aluminium deposited on spacers in the transformer's main insulation. The findings showed a reduction in average breakdown value by 24% for the single duct and 14% for the double oil duct.

2.5 Breakdown Induced by Many Particles

The influence of particles on the dielectric strength of transformer oil have been carried out by means of measuring the breakdown voltage induced by a given concentration of particles, in relation to the particles composition and size. The following conclusions have been drawn [21-26]. The dielectric strength of the liquid is affected much more by conducting particles than insulating particles. Breakdown voltage increases with decreasing concentration of particles; and particles of larger size have more damaging effects. These experimental results may lead to contradiction because of the possible formation of agglomerates [25].

Alignment of particles have been observed in millimetre gaps [25, 27, 28] but it is not clear whether they induced breakdown or not. Normally the breakdown occurred when the bridges have broken off or perhaps due to a large particle. The attraction of particles towards the high field region and for the formation of these bridging chains [29] are due to Dielectrophoretic force. When the electric field reaches more than a certain point which depends on the gap distance, the particles are ejected out of the gap due to the electrohydrodynamic motion of the oil [27, 28, 30-32].

2.6 Breakdown Induced by a Single Particle

Early work by Dakin and Hughes investigated the influence of a single calibrated particle [33] in order to carry out a quantitative and comprehensive study of the particles effects on dielectric strength of transformer oil. They reported that spherical metal particles of 1 to 3 mm diameter lifted off at very low fields (around 3 kV/cm for 1 mm aluminum spheres). The breakdown under AC voltage was initiated at a lower voltage when the particle was moving freely than when it was fixed

to an electrode and the breakdown occurred when the particle was in contact with the positive electrode. The breakdown voltage also reported to be induced by a 1 mm diameter sphere in a 5 mm gap [34]. The study of [35] revealed that AC breakdown occurs when the free moving particle touches the positive electrode and the breakdown happens at low voltage. Under impulse breakdown conditions with AC voltage, the free moving particle initiates breakdown at much lower voltage than the same particle were to kept fixed. Other reported research with a single particle are mainly related to the particle motion under dc or ac fields [36-41] and its contribution to the liquid conductivity [42-44], or to the micro-discharges induced by a particle approaching the electrodes [31, 37].

2.7 THEORIES OF LIQUID BREAKDOWN

The phenomenon of liquid breakdown cannot be explained by a single theory; rather several issues such as complex nature of liquids, difficulty for production of pure liquid etc. should be considered in defining liquid breakdown. There are three theories presented to explain liquid breakdown phenomenon- bubble theory, suspended particle theory and electronic breakdown theory [45].

2.7.1 BUBBLE THEORY

The most predominant theory of liquid breakdown is the bubble theory which considers both liquid and gaseous component for breakdown. According to this theory, an electronic amplification process is initiated by the formation of bubble near the electrode tip. The formation of bubble may be by local heating, cavitation or electrical stress. When the energy injection is occurred locally in liquids, it generates hot electrons having more energy in excess of the thermal energy [46]. It is thought that field enhancement caused by a region of lower permittivity induces more charges into the vapour phase which actuates the amplification process.

A mechanical model for bubble formation was put forth by T.J. Lewis [47]. This model for the formation of a bubble or low density region is derived from the mechanical properties of very large electric fields near breakdown, 10^8 to 10^9 V/m. The electric field boosts the thermal generation of ruptures throughout the liquid not just at the electrode/liquid interface. The results will be of having the holes in the liquid which will lead to develop weak spots in the molecular structure of the liquid and hence create a “crack” in the liquid to form at the cathode surface. Findings show that such crack is a low density or even a vacuum region, occasionally referred to as a vacuole where electrons can be injected. The vacuole’s formation arises from mechanical stress of the cathode surface and not of energy injection. The demonstrations of the activities that take place are depicted in Figure 2:2.

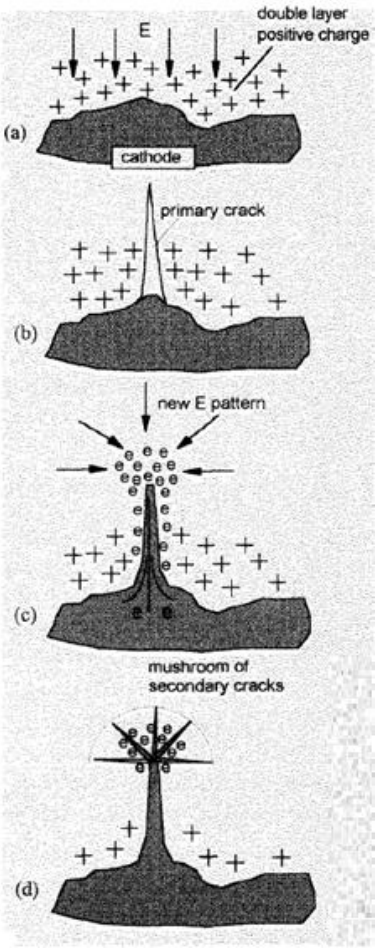

Figure 2:2 Illustration of crack development at the cathode surface. (a) pre-breakdown conditions. (b) "crack" develops at the surface of the cathode. (c) jet of electrons from the cathode surface act as an extension of the cathode and severely distort the local field. (d) an array of secondary cracks develop in the radial field. [47]

2.7.2 SUSPENDED PARTICLE THEORY

The concept of suspended particle theory has its basis on existence of impurities in a liquid. A suspended particle is anything within the liquid that does not carry a charge. The theory states that the particle will be polarisable or charged when subject to an electric field. The velocity of the particle arising from the polarisation is controlled by the viscosity of the liquid. It acts like an extension of the electrode after reaching an electrode and can alter the local field leading to breakdown [48].

2.7.3 ELECTRONIC BREAKDOWN THEORY

Theoretically it is unlikely that electrons when injected into a liquid will produce significant ionization to develop an amplification process. However, cathode initiation attempts for such electron injection. During such a state, the electrons will collide with molecules locally heating the

liquid through collisional impacts. The heating of the liquid reduces the density allowing future electrons to obtain more energy from the field before colliding with another molecule [45].

Such impacts ionizing a molecule will leave two slow electrons to drift in the field. The build-up of low energy electrons at the front of the streamer "marks the onset of spherical expansion under the Coulombic forces of the consequent cloud of negative charge" [49]. The streamer will expand and appear thick and bushy as it proliferates across the gap. The lower the density of the region the faster electron amplification will take place. The obvious extreme of this process is the formation of an avalanche within a bubble [45].

2.8 Mechanisms Behind Positive Streamers

Scientists and engineers have devoted themselves for many years studying properties of dielectric liquid due to insulation failure in power transformers, specially focusing on the mechanism for electrical breakdown to reduce its likelihood [50-52].

A great deal of the work has been done on formation of electrical streamers. These are low density conductive structures that form in regions of oil that are over-stressed by electric fields on the order of $1 \times 10^8 V/m$ or greater [51]. It tends to elongate, growing from the point of initiation towards a grounding point. Sustained over excitation can result in a streamer short circuiting the oil gap between electrodes. When this happens an electric breakdown arc will form in transformer oil [53].

Experimental observation has revealed that streamers have propagation characteristics that are strongly dependent on the voltage excitation to the liquid [50-52, 54-57].

The positive streamers are classed into 4 different modes, called the 1st, 2nd, 3rd, and 4th modes, for lightning impulse voltage excitations in transformer oil. The magnitude of the excitation voltage for the 1st mode is the lowest and the 4th mode at the highest. The 1st mode streamers have a bush-like structure and propagate at velocities on the order of 100 m/s [58]. The 2nd mode initiates slightly below the breakdown voltage *Vb*, which denotes 50% probability of breakdown, and dominates up until the acceleration voltage *Va* [56]. These streamers are filamentary in shape with several main branches [54],[56]. Near the acceleration voltage, the streamer propagation transitions to the fast 3rd mode where the propagation velocity rises dramatically and the streamer shape is more branched [56]. With a slight increase in applied voltage above the acceleration voltage, the streamer propagation quickly changes to the fast event 4th mode, which is extremely filamentary with one or two main branches [54],[56]. The velocity and shape of streamer changes dramatically with increased applied voltage. The 1st, 2nd, 3rd, and 4th streamer modes propagate with velocities on the order of 0.1 km/s, 1 km/s, 10 km/s, and 100 km/s, respectively [54, 56]. The transition from

the 2nd to 3rd mode, which occurs near the acceleration voltage *Va*, is of great importance because 3rd mode streamers propagate at extremely fast velocities such that they quickly traverse the oil gap to the cathode before the applied voltage impulse can be extinguished causing electrical breakdown.

There is some reported research about postulated charge generation mechanisms that result in streamer propagation. Several commonly hypothesized charge generation mechanisms are electric field dependent ionic dissociation [59, 60], Fowler-Nordheim electron injection from the cathode [51], vaporization [59], and collisional ionization [61].

2.9 PARTIAL DISCHARGE IN CONTAMINATED OIL UNDER AC

Partial discharge measurements of transformer oil and oil impregnated pressboard for HVDC application have been studied by researchers for many years [62]. Partial discharge patterns recognition and interpretation have been proven very useful for the diagnostics of insulating condition of the high voltage apparatus. PD takes place when the local electric field exceeds the threshold value and produces a partial breakdown of the surrounding insulating material [63, 64]. The manufacturers diagnose the quality of the insulation of the converter transformer by carrying out certain routine tests before installation, which includes AC voltage withstand test, DC voltage test with simultaneous partial discharge measurement, polarity reversal test with partial discharge (PD) measurement etc [65, 66]. A lot of research has been carried out on measuring partial discharge activity using UHF sensors in transformer oil insulation, e.g., [67-69].

Researchers had reported that conducting particles affect the breakdown strength of the transformer oil more than insulating particles [70]. The movement of particles in transformer oil has been studied by Birlasekaran under the influence of DC and AC electric fields both by theoretically and experimentally [39, 71]. His observation from the experiment revealed that the conductive particles transport charge by contact with electrodes under DC voltages. He also observed the discharge current in the form of a fast rising current pulse and slowly increasing displacement current [71]. The observation of Tobazeon revealed when the charged conductive particle comes close to opposite electrode, charge transfer occurs and produces a current peak as well [41].

Transformer oil with different level of cellulose particles were tested in [11]. They had observed bridging under 6 kV AC electric field with moisture and cellulose particles. The partial discharge also measured during the AC test with spherical and needle plane electrode system. The PD pulses decreased with increment of cellulose particle contamination as shown in Figure 2:3. The peak values of the PD were recorded up to 80 pC. The PD activities were decreased when the bridge was forming. There was no more PD observed after a stable bridge was formed.

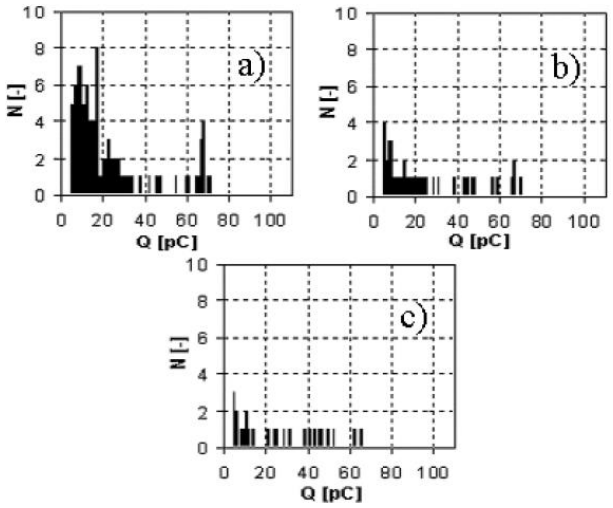

Figure 2:3 Frequency amplitude distributions of PD charge with different levels of cellulose particles: a) 0.008, b) 0.016 and c) 0.024% [11].

2.10 PRESSBOARD DUST IN OIL

Although the suspended particle theory cannot explain all the phenomena observed before a liquid breakdown, extensive experimental studies have shown that conducting particles accumulate in high electric field will move towards the region of highest electric field intensity due to dielectrophoresis [5, 11, 12].

Even if oil undergoes important cleaning procedures during its production, impurities can still contaminate oil during storage and shipping. This is particularly the case during operation where cellulose paper fragments, due to electrical and thermal stresses, will become present in the transformer oil [1]. Fibrous dust particles from pressboard insulation were investigated in [1] for three predetermined levels of contamination. The experiment was conducted as follows:

2.10.1 PREVIOUS EXPERIMENTAL SETUP

Basically, two spherical electrodes of 10 mm diameter, spaced to 10 mm, were in the middle section of a sample tank, filled with 300 ml of transformer oil that completely submerged the electrodes. The goal of the test was to observe the bridge formation across the electrodes and to measure the current flowing through the electrode gap when three different DC voltages of 2 kV, 7.5 kV and 15 kV were applied to the sample tank. The typical experimental setup is summarized in Figure 2:4 below:

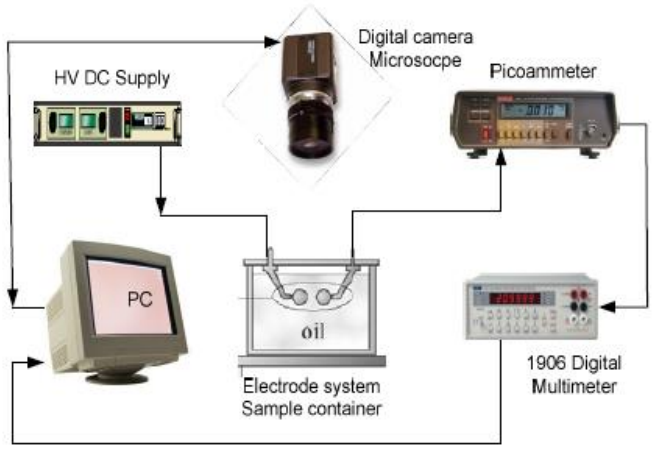

Figure 2:4 Experimental Setup Used for the Observation of Dust Particles Accumulation in Transformer Oil [5]

2.10.2 PREVIOUS OBSERVATIONS

For each level of contamination, the same measurements were made. After switching on the power supply, contaminant particles were moving back and forth in the electrode gap. After a while, the particles started to attach to the two electrodes and, then, connected themselves to form a partial bridge at the surface of the electrodes. The bridge kept growing until a complete bridge was formed.The first important result is that the bridge formation was accelerated when greater DC voltages were applied.

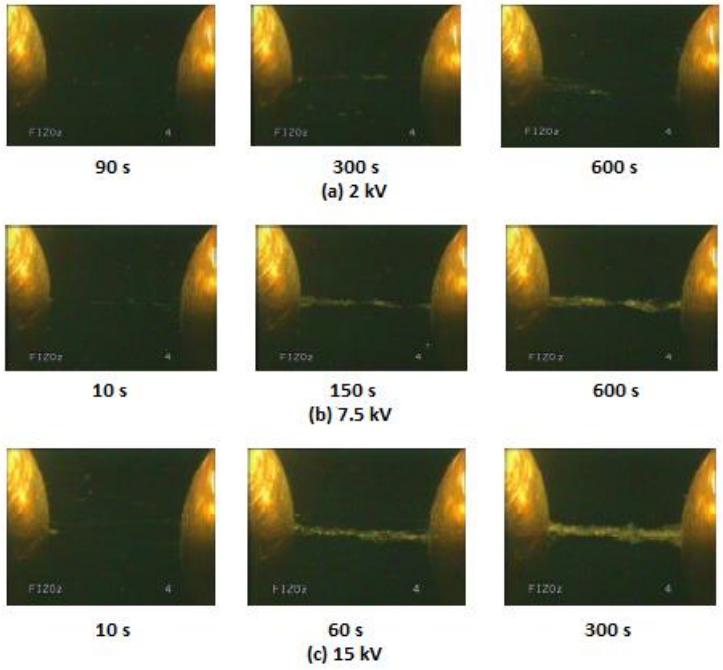

Figure 2:5 Bridge Formation at Low Level of Contamination (0.0025% by weight) and at Different Applied DC Voltages [5]

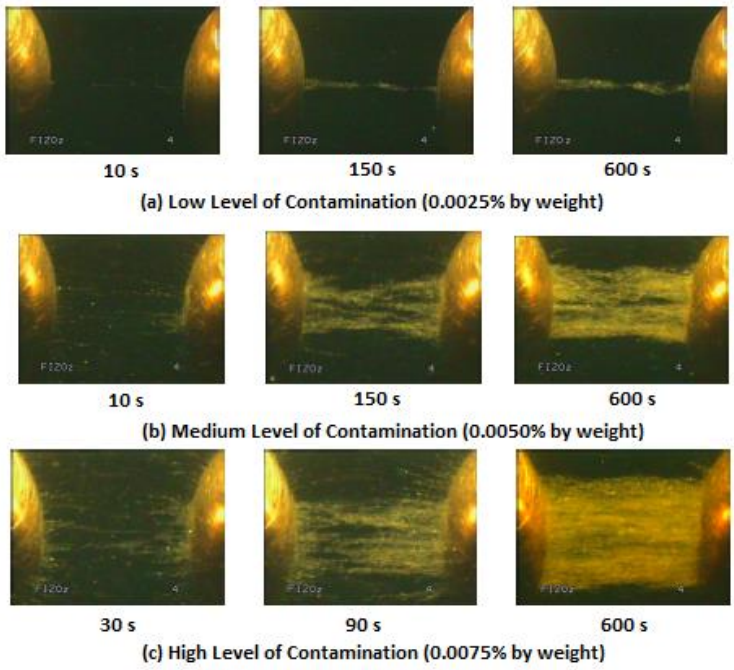

Figure 2:6 Bridge Formations at 7.5 kV and at Different Level of Contamination[5]

The second important result was that the complete bridge was thicker when dust particle concentration was increased. The two observations are illustrated in Figure 2:5 and Figure 2:6.

2.10.3 CURRENT THROUGH THE BRIDGE

The current flowing through the bridge was measured with a Keithley picoammeter. It was observed that the current rose during a very short period of time, due to polarization, then gradually rose until reaching saturation. It was also observed that the saturation currents were higher with increasing DC voltages. An example is shown in Figure 2:7 below.

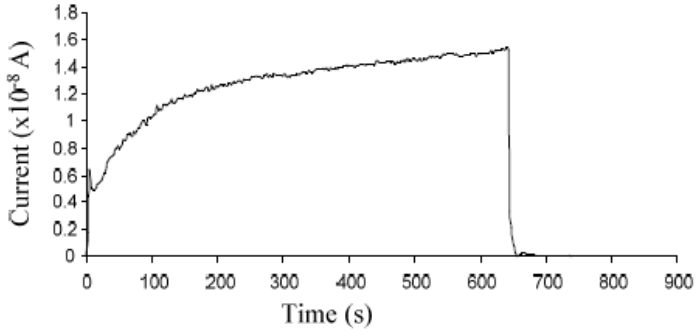

Figure 2:7 Current through the Bridge in Function of Time at 7.5 kV and Medium-level of Contamination [5]

The saturation currents were also plotted as a function of the contamination levels at 2 kV, 7.5 kV and 15 kV. The plots are shown in Figure 2:8 below.

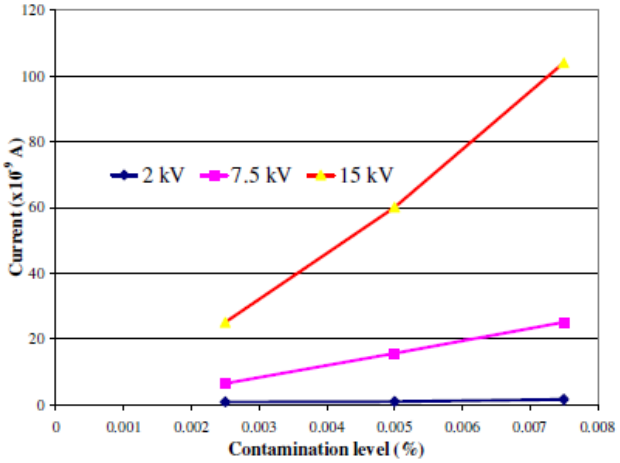

Figure 2:8 Saturation Currents as a Function of Contamination Levels at 2 kV, 7.5 kV and 15 kV [5]

An important result can be deduced from Figure 2:8. In fact, it seems that saturation currents are proportional to contamination levels at given applied dc voltages.

2.11 SUMMARY

Ideally, the transformer oil should be particle free. But in reality there are particles present in oil. The consequence of these particles contaminations are many. The particles create bridge between two different electric field which leads to leakage current, PD as well as it lowers the breakdown strength of transformer oil. In some condition these contaminants lead to total failure of power transformers. Therefore it is very important to investigate the behavior of the particles under the influence of different electric field which will enable researchers to prevent the further failure due to particles.

CHAPTER THREE: EXPERIMENTAL SETUP

Inside a power transformer, any exposed conductors in a winding or leads are usually insulated. But to understand the behavior of a particle under worst case scenario and provide an ideal condition to observe the effect easily, we have started our investigations with a bare electrode system.

3.1 SAMPLE TANK AND ELECTRODES ARRANGEMENTS

3.1.1 SAMPLE TANK WITH BARE ELECTRODE

The sample tank used for all the experiments was glass built and the total volume of this tank was 550 ml.

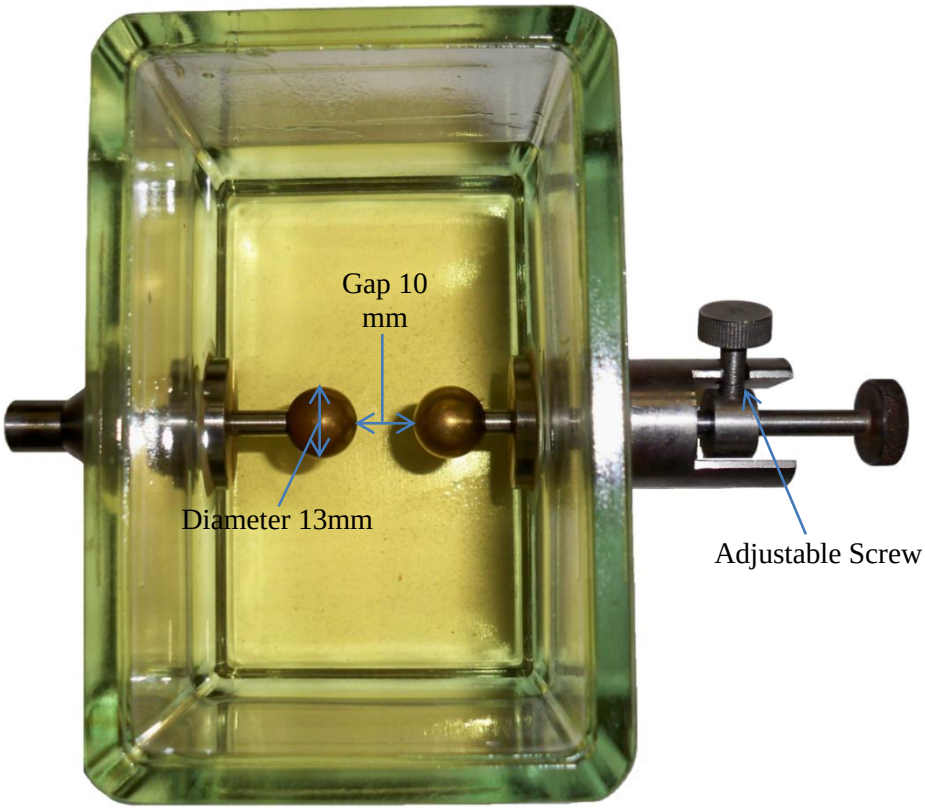

Figure 3:1 Test Cell with spherical bare electrodes

A pair of spherical brass electrodes with 13 mm diameter have been used for the experiments. The electrodes were attached to either side of the test cell wall from which they extended towards the middle of the cell. The position of one electrode was fixed and another electrode could be moved using a screw drive. The distance between the electrodes was kept constant at 10 mm for all the experiments. For these experiments, only 300ml of transformer mineral oil was used and the sphere

electrodes were completely submerged in the transformer oil. The sample tank is shown in the Figure 3:1.

3.1.2 COVERED ELECTRODE SYSTEM

A new piece of 100 µm thick kraft paper was used to cover the surface of both spherical electrodes. A single layer of kraft paper was wrapped around the electrodes and was kept without tied to the rod attached to electrodes which was the case of loose bonded test. These tests was conducted with a new single layer of kraft paper wrapped around the electrodes as well as it was held tightly to the rod of the electrodes using a cable tie as shown in Figure 3:2. The kraft paper covers were submerged in oil for a day to ensure that the papers are fully impregnated by oil and no air trapped between the electrode surface and paper cover.

Figure 3:2 Covered electrode system with tight bonded paper kraft

3.1.3 ELECTRODES WITH PAPER BARRIER

There was a craft paper of 100 µm thickness placed between the electrodes to replicate real transformer operating condition. These experiments carried out to investigate the effect of a paper barrier on the bridge formation under the influence of DC electric field. These experiments were performed with the paper barrier placing in the mid-point of the electrodes as shown in Figure 3:3. A zoom in picture of the electrodes arrangement with paper barrier is shown in Figure 3:4. The paper barrier was inserted in two plastic foams from either side of the electrodes. These foams were used to keep the paper barrier in the mid-point between the electrodes and kept it vertical. The paper barrier was couple of millimeters wider than the diameter of the electrodes to stop the particles from going over or under the barrier.

Figure 3:3 Sample holding tank for paper barrier test

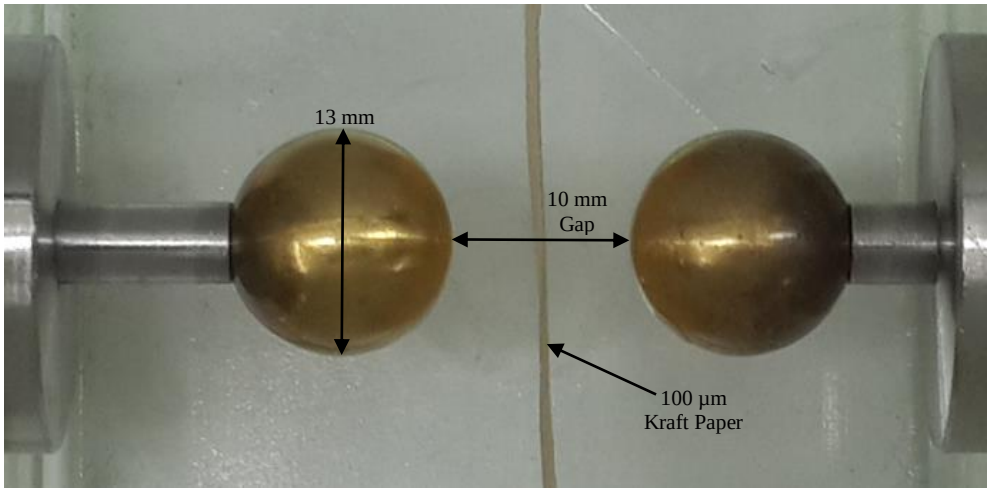

Figure 3:4 Inset view of electrodes with a paper barrier in the middle

3.1.4 NEEDLE – PLANE ELECTRODES SYSTEM

The test cell used for needle – plane electrodes was the same as the one used for previous tests. The needle electrode is made of tungsten and it was produced in the laboratory from a tungsten wire. Chemical etching technique was used to make the needle shape. The body of the needle is 1 mm of diameter and the slope of the tip started from about 5 mm above. The tip curvature of the needle is approximately 100 µm of diameter. The material of plane electrode is brass and it has a diameter of 50 mm with a thickness of 5 mm. The edge of the plane electrode was rounded to avoid electric field enhancement. The gap between the electrodes was kept constant at 10 mm for the entire

experiments. The needle electrode was connected to the power supply and the plane electrode was attached to earth via a Picoammeter (DC) and Multimeter (AC) to monitor the conduction current. The plane electrode was connected to earth for DC biased AC test as the current was not monitored. Rest of the setup for the DC, AC and combined DC & AC test were the same as for spherical electrodes which have been precisely explained in the earlier section.

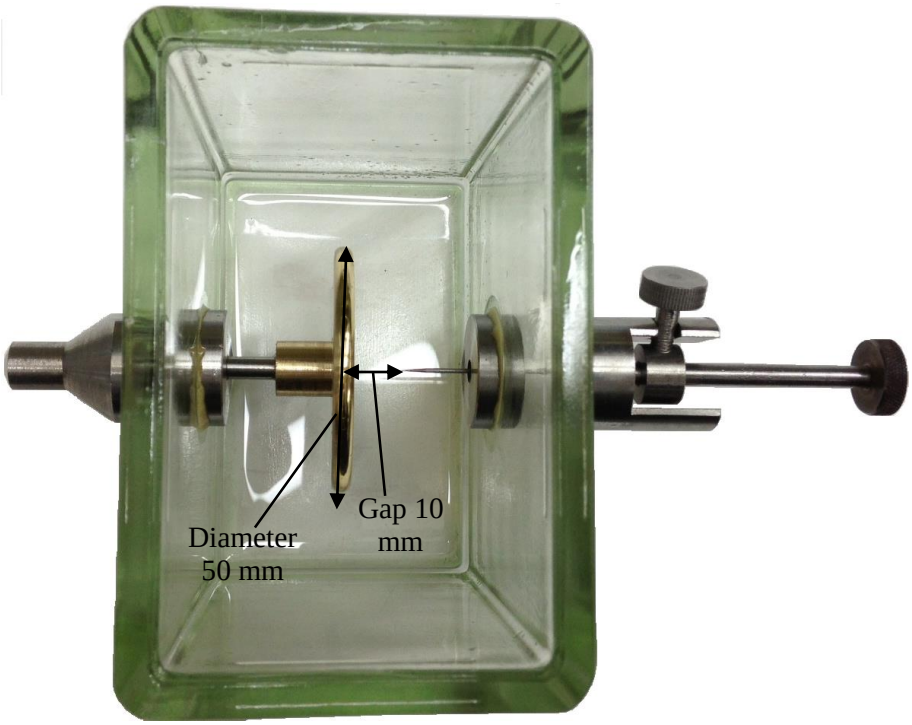

Figure 3:5 Test cell with Needle – Plane electrode system

3.2 SAMPLE PREPARATION

A predetermined amount of pressboard dust was prepared to simulate the presence of contaminants in a power transformer. Cellulose fiber dust was produced by rubbing a piece of new pressboard used as a solid insulation in high voltage transformer by metal files with different cut sizes. It was not possible to control the size of the particle by filling with hand. Different sizes of sieves were used afterwards to separate the fibers. As a result, the particles were separated by the fiber diameter rather than length. The particles were categorized into four different size groups i.e. 250-500 µm, 150-250 µm, 63-150 µm and less than 63 µm. All the four sizes of particles were tested under DC electric field. Only the results from 150-250 µm and 250-500 µm tests are discussed in this thesis. Only 63-150 µm size particles were investigated for AC and DC biased AC experiments to enhance the bridging. The contamination levels for each size of particles were 0.001%, 0.002%, 0.003%, 0.004%, 0.006%, 0.008%, 0.016% and 0.024% by weight. A digital measurement scale capable of measuring microgram was used to achieve the highest accuracy. For DC experiments only 0.001 to

0.004% contaminant were investigated whereas for AC all the above contamination levels used. In the case of DC biased AC, only 0.024% which was the highest contamination level was tested along with 1 kV, 3 kV, 5 kV and 6 kV DC biased with 5 kV, 10 kV, 15 kV and 20 kV AC voltages.

The contamination particles content was taken significantly higher in comparison with real operational conditions of HV transformers. It speeds up the process and allows to visualize the bridge formation without affecting the underlying physics.

The sample tank was cleaned with a soap solution in hot water then it was dried in hot air flow before starting a new test with a new size of particle. The sample tank was first rinsed with clean oil then the test cell was rinsed thoroughly with cyclohexane before repeating a test with same particle size to ensure that there no particles left from previous test.

A new experiment was always started with adding 300 ml of transformer mineral oil into the test cell which was enough to submerge the electrodes completely under oil. The lowest contamination level of pressboard fibers was then added to the oil. The test cell was covered with cling film to protect from dust and moisture. The sample tank was covered during whole experimental period apart from adding the next level of contaminants. The sample tank was stirred prior to every test on a magnetic stirrer for 2 minutes to disperse the particles evenly.

Moisture in the oil can affect the dielectric constants and conductivities of both oil and the pressboard particles. To make sure that all experiments done at the same conditions, the water content of the oil was monitored by Karl Fischer titration method [72]. For all experiments presented in this thesis the moisture content was measured between 20 ppm and 24 ppm.

3.3 EXPERIMENTAL SETUP

The experimental setup has been modified from the experiment [5] explained in literature review. The experimental set up consists of a high voltage dc power supply, sample tank, microscope, digital camera, picoammeter, GPIB card and a computer. A stereo microscope from GX Optical, model XTL3, equipped with GXCAM-1.3 digital camera was used to record images and videos. The sample tank was positioned under a stereo microscope that had a digital camera mounted on the top to record the optical images of the particles accumulation. For experiments with DC electric field, the microscope along with the test cell was placed inside an aluminium box which acts as a Faraday cage to reduce the effect of possible noise on measurements of the conduction current. One of the spherical electrodes was attached to the high voltage source. The other electrode was connected to the ground via a Keithley picoammeter 6485 (DC). A desktop computer was used to

control the digital camera, to collect data from the camera, and also for the conduction current measurement. Figure 3:6 shows a block diagram of the DC experimental setup.

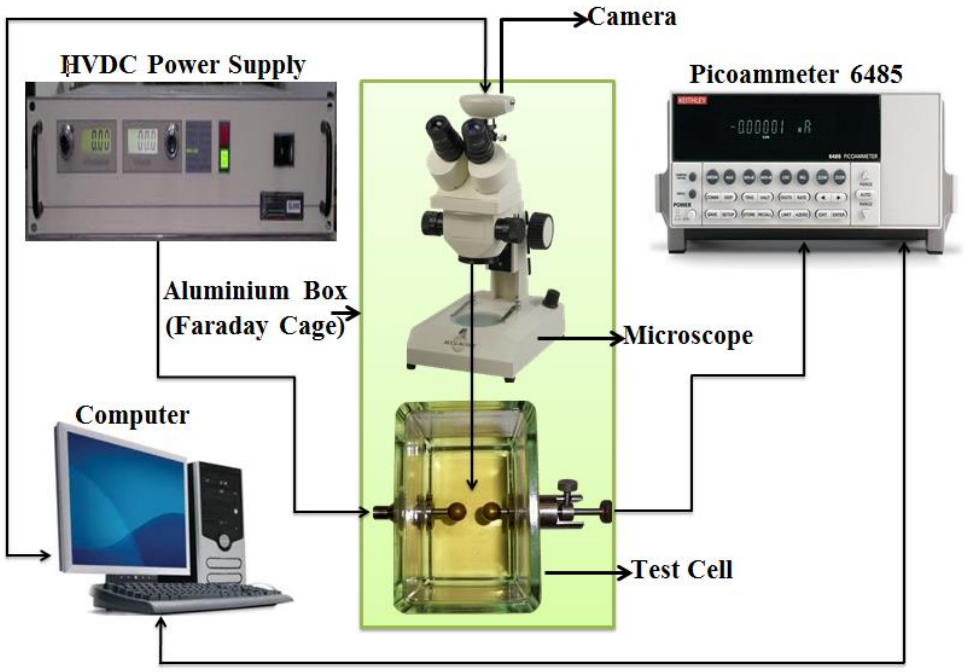

Figure 3:6 Block diagram of experimental setup for DC test [73]

LABView software was used to develop a program to interface with the Picoammeter and Multimeter. The block diagram and interface of LABView program is included in appendix A. A GPIB card is used to communicate with the Picoammeter. The monitoring program was set to take the current measurement every second. The data were then saved on the computer.

The sample tank for AC test (Figure 3:7) was the same as for the DC test. The experimental set up consists of a high voltage ac transformer, variac, sample tank, microscope, digital camera, multimeter, GPIB card and a computer. A new Keithley 2001 multimeter has been used to measure the conduction current through the gap.

The AC voltage was calibrated using a calibrator. A set of predetermined voltages were measured using the calibrator and the corresponding voltages were recorded using digital multimeter as a reference. The same multimeter were then used to monitor the output voltage of the transformer to achieve the consistent voltage supply.

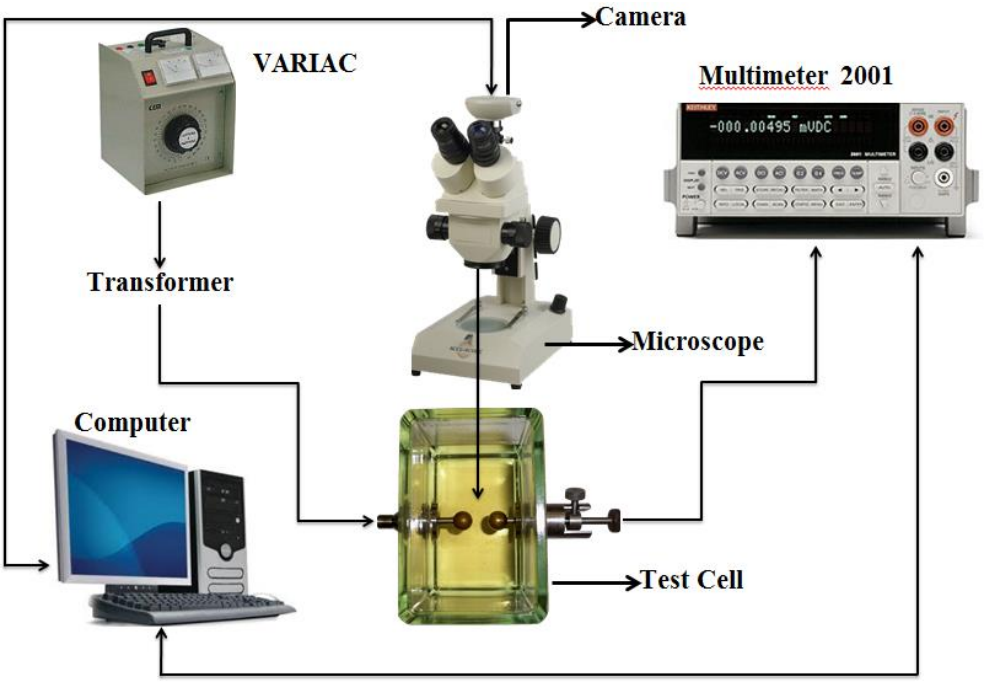

Figure 3:7 Block diagram of experimental setup for AC test [74]

A block diagram of complete experimental setup for DC biased AC tests is shown in Figure 3:8.

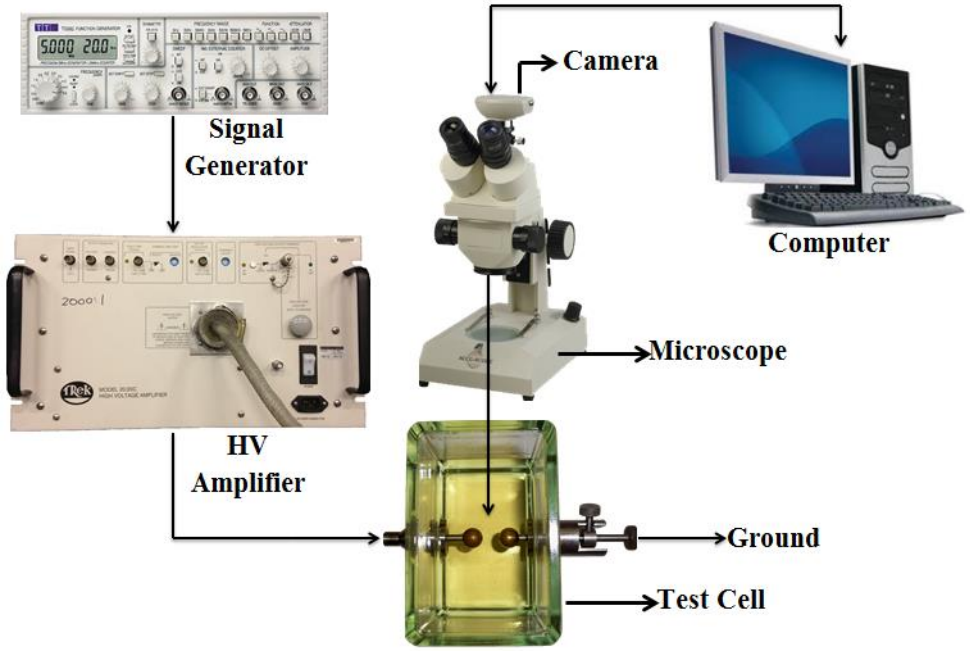

Figure 3:8 Block diagram of experimental setup for DC biased AC test [75]

This experimental setup for DC biased AC test consisted of a signal generator, high voltage amplifier, sample tank, microscope, digital camera and computer. As for AC and DC biased AC test the aluminium box was not used. A signal generator was used to produce the sinusoidal voltage of

50 Hz with a DC offset. This signal was amplified with the high voltage amplifier from TREK, Inc. The ratio of the amplification was 2000:1. The amplified signal was send to one electrode. The high voltage amplifier was also connected to an oscilloscope and the output voltage was monitored. The current were not measured for DC biased AC test so the electrode was directly attached to the ground.

3.4 Experiments Under Different Fields

Three different voltage levels were investigated for each category, such as positive DC (2 kV, 7.5 kV and 15 kV), AC (10 kV, 15 kV and 20 kV peak-peak with constant supply frequency of 50 Hz) and DC biased AC (1 kV, 3 kV and 5 kV positive DC offset with 5 kV, 10 kV and 15 kV AC peak-peak with constant supply frequency of 50 Hz). Each experiment was carried out until a complete bridge was created between the electrodes or maximum of 25 minutes where there was no bridge. A stereo microscope equipped with digital camera was used to record images and videos. Images were taken in a regular time interval during the entire test to record the bridging process along with some videos. All tests were conducted at ambient room temperature. The temperature of the aluminium box was monitored during DC test. The temperature was within on average 3 degrees difference for all the DC experiments. Most of the tests were conducted three times for each voltage level to observe the repeatability of the obtained results.

3.5 Summary

The pressboard fiber weight needed to be measured very carefully to ensure the ration of oil and fiber remain same for every test. It is very important to clean the test cell after every test and the test cell should be dried properly to ensure that there is no moisture left. The conduction current measurement also had to be carried out with extremely carefully as any slight variations could result in a wrong data.

CHAPTER FOUR: BARE ELECTRODE TEST

The influence of DC Electric field started with bare spherical electrode system. Then electrodes were covered with kraft paper to stop the bridge creation between the electrodes. The effect of divergent electric field system was also investigated with needle-plane electrode system.

4.1 BARE ELECTRODE TEST UNDER DC ELECTRIC FIELD

Although the conductors in a real transformers are always covered but to understand the phenomenon of DC electric field with the worst case scenario and to accelerate the bridging process, bare electrode systems are chosen. Several contamination levels with different levels of voltages were investigated. Influence of particle sizes on bridging were also tested with four different sizes of particles.

4.1.1 BRIDGE FORMATION AND CONDUCTION CURRENT WITH A CONTAMINATION LEVEL OF 0.001%

The contaminant particles moved back and forth in the gap between two electrodes immediately after 2 kV was applied. The particles were charging and discharging under the dc electric field. Those particles start to attach themselves to the two electrodes first and then connect themselves to form a partial bridge at the surface of the electrodes after some time. Initially the long fibers were attached to the electrodes and then the other small particles started attaching themselves to the long fibers. The bridge continues to grow in this fashion. A very thin bridge formed at 2 kV after 600 s for 150-250 µm particles as shown in Figure 4:1. There was no complete bridge formed for the 250-500 µm particles as Figure 4:2 even after 900 s. The reason behind non-formation of complete bridge is because the dielectrophoretic force was not strong enough to move the bigger size particles. This phenomenon simulated and results are presented in chapter 7.

The particles movements were intensified in the oil when the applied voltage was increased to 7.5 kV. A thin bridge formed after 240 s for 150-250 µm particles which was faster than that at 2 kV. The thickness of the bridge increased with time until at 600 s as shown in Figure 4:1. No change was observed after that. The thickness of the bridge was larger at the surfaces of the electrodes than the bridge in the midpoint of the gap. A thin bridge formed at 270 s and started to grow until 900 s as for 250-500 µm particles (Figure 4:2). The completed bridge for the bigger particles was not as thick as for the smaller particles.

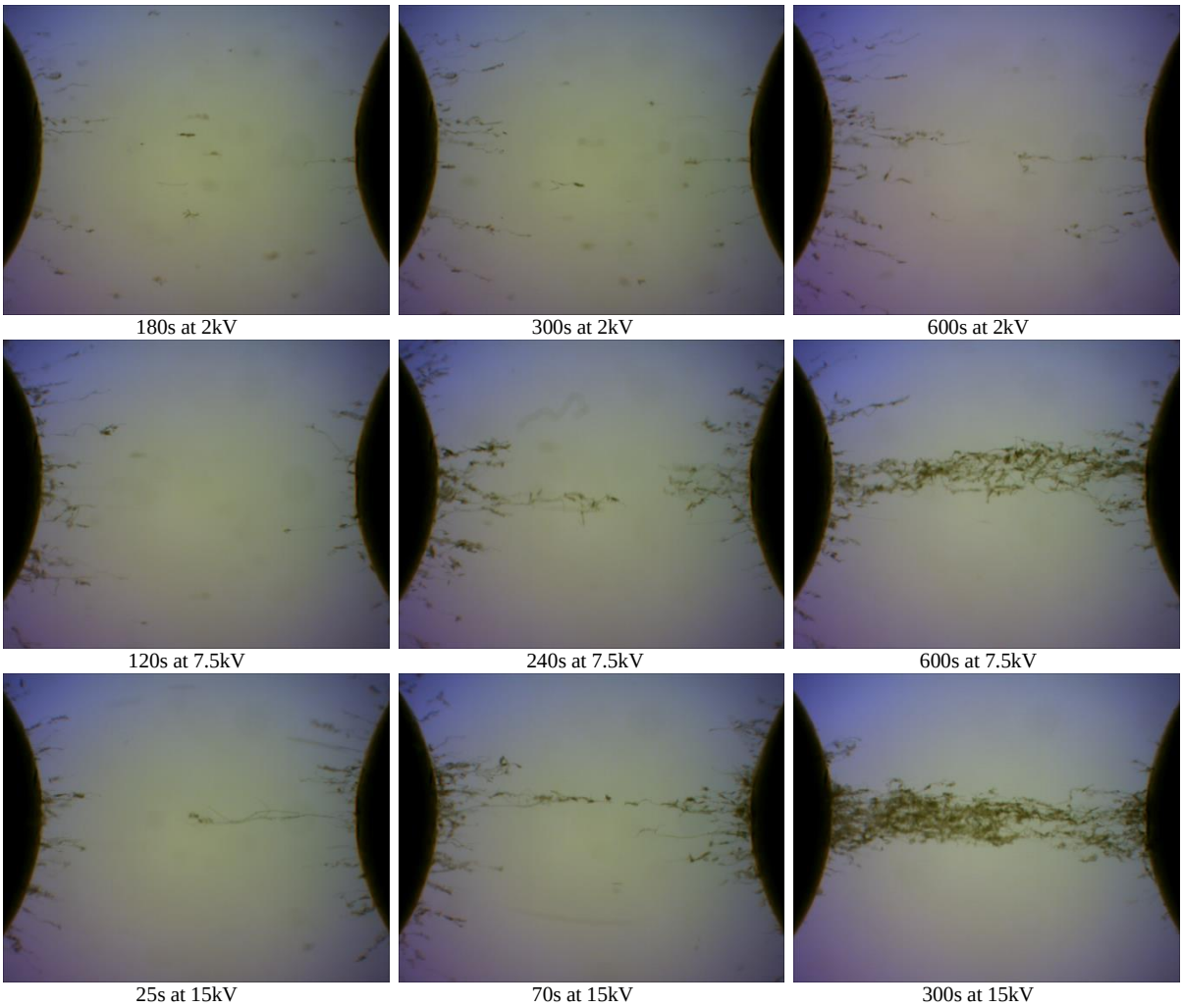

Figure 4:1 Optical microscopic images of bridging in contaminated transformer oil with 150-250 µm pressboard fiber, concentration level 0.001%

After applying 15 kV to the oil gap, the contaminants started to move rapidly. A threadlike stretched bridge was created within 70 s after the voltage applied (Figure 4:1). More particles were attracted in the gap between the electrodes because of the higher electric field and they formed a thicker bridge than previous electric field. The bridge was thickened up to 300 s for 150-250 µm samples. As for the bigger size particle, it took 90 s to form a complete thin bridge. The bridge continued to grow thicker until 600 s. The bridges were thicker near the electrodes and thinner towards the middle for both particles sizes.

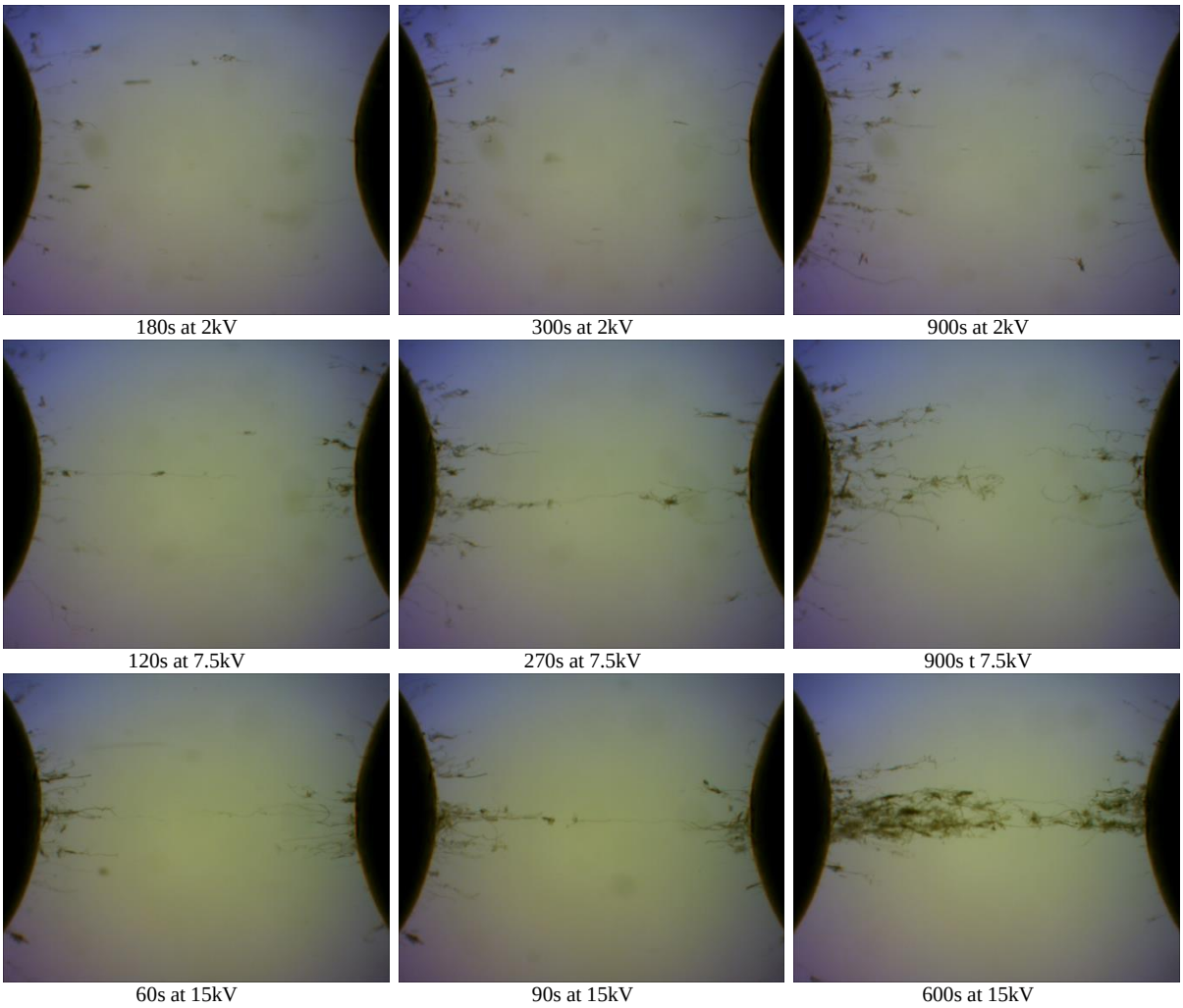

Figure 4:2 Optical microscopic images of bridging in contaminated transformer oil with 250-500 µm pressboard fiber, concentration level 0.001%.

The conduction current for the two particle sizes under three different voltage levels are shown in Figure 4:3. The currents measurement were made at 1 second intervals and are the average of 20 separate measurements. As soon as the voltage was applied, there was a high polarization current observed in most of the experiments. After that the slow growing current was stabilized. It has been noticed that the current flowing through the gap increases gradually throughout the testing period from $0.3x10^{-9}$A to $0.4x10^{-9}$A for smaller size particle and from $0.2x10^{-9}$A to $0.3x10^{-9}$A for bigger size particle. The reason for this very small rise of current is the thickness of the bridge for 2 kV test is not very significant. The existence of the current can be explained by charging of the particles at the electrodes and transfer the charge across even if the bridge is not formed yet. The gradual increment process of current slowly stopped after 600 second. The currents reached to the saturation level after the bridge was formed. The thickness of the bridge and the bond between the particles were the main determining factor for the conduction currents. It is crucial to emphasize that the saturation of current reached after a complete bridge is formed.

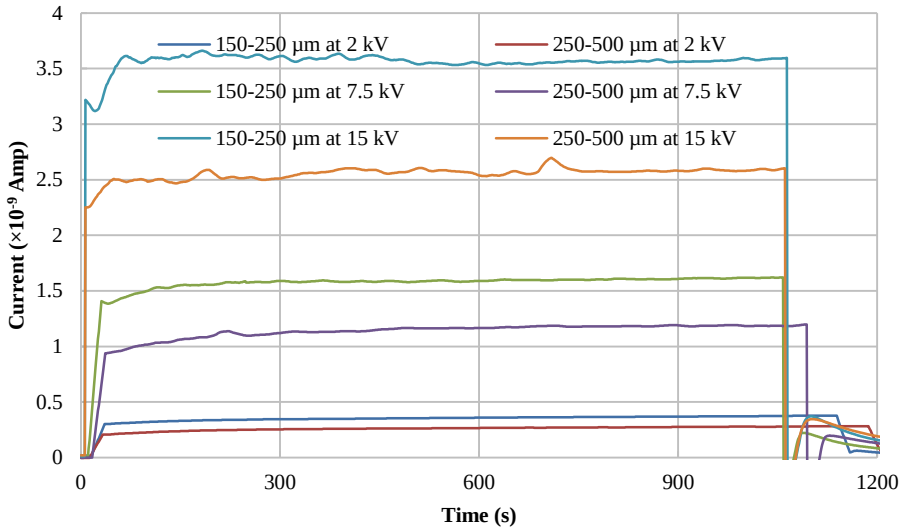

Figure 4:3 Current at different DC voltages with 0.001% concentration for 150 – 250 µm and 250 – 500 µm particles

For 7.5 and 15 kV test, the conduction current increased. The higher the applied voltage, the higher the current flows through the gap. The increment of the voltage has two features. Firstly, the time elapsed for reaching to the saturation current is reduced. Secondly, as the voltage varies, the saturated current magnitude rises nonlinearly. Once a bridge is created the current increase rate reduced which is shown in Figure 4:3. This may be due to the difference in electrical properties of each individual particle. Having difficulty in reaching a test for distinction, it is considered that some particles may have a slightly higher conductivity than the others. Those having higher conductivity will form an initial bridge due to a strong dielectrophoresis, leading to a major contribution to the current. And therefore, further addition of less conducting particles to the bridge contributes less to conducting current. The conduction current for the smaller size particles was almost 1.5 times higher than bigger particles in the case of 7.5 kV and 15 kV. From these experiments it was clear that the particle size plays a vital role on conduction currents.

Two more particle sizes were also investigated 63 – 150 µm and less than 63 µm. But the size of the particles were small and did not have many long fibers to start the bridging hence there was no consistent bridging occurred. The images of the bridging and conduction currents are available in Appendix B.

4.1.2 Bridge Formation and Conduction Current with a Contamination Level of 0.002%

These tests were conducted with concentration level of 0.002% by weight. As shown in Figure 4:4, within the first 60 s upon switching the 2 kV voltage supply, the contaminant particles were

attracted to the gap between the electrodes and attached to surfaces of the electrodes for 150-250 µm particles (Figure 4:4). At 330 s elongated partial bridges were created; the thicknesses of the bridges develops up until they joint together to form complete bridges at 625 s. On the other hand, a thin bridge was observed only after 900 s for the 250-500 µm particles (Figure 4:5). It was also observed that the bridges were denser at the surface of the electrodes and thinning away as it gets to the midpoint of the gap.

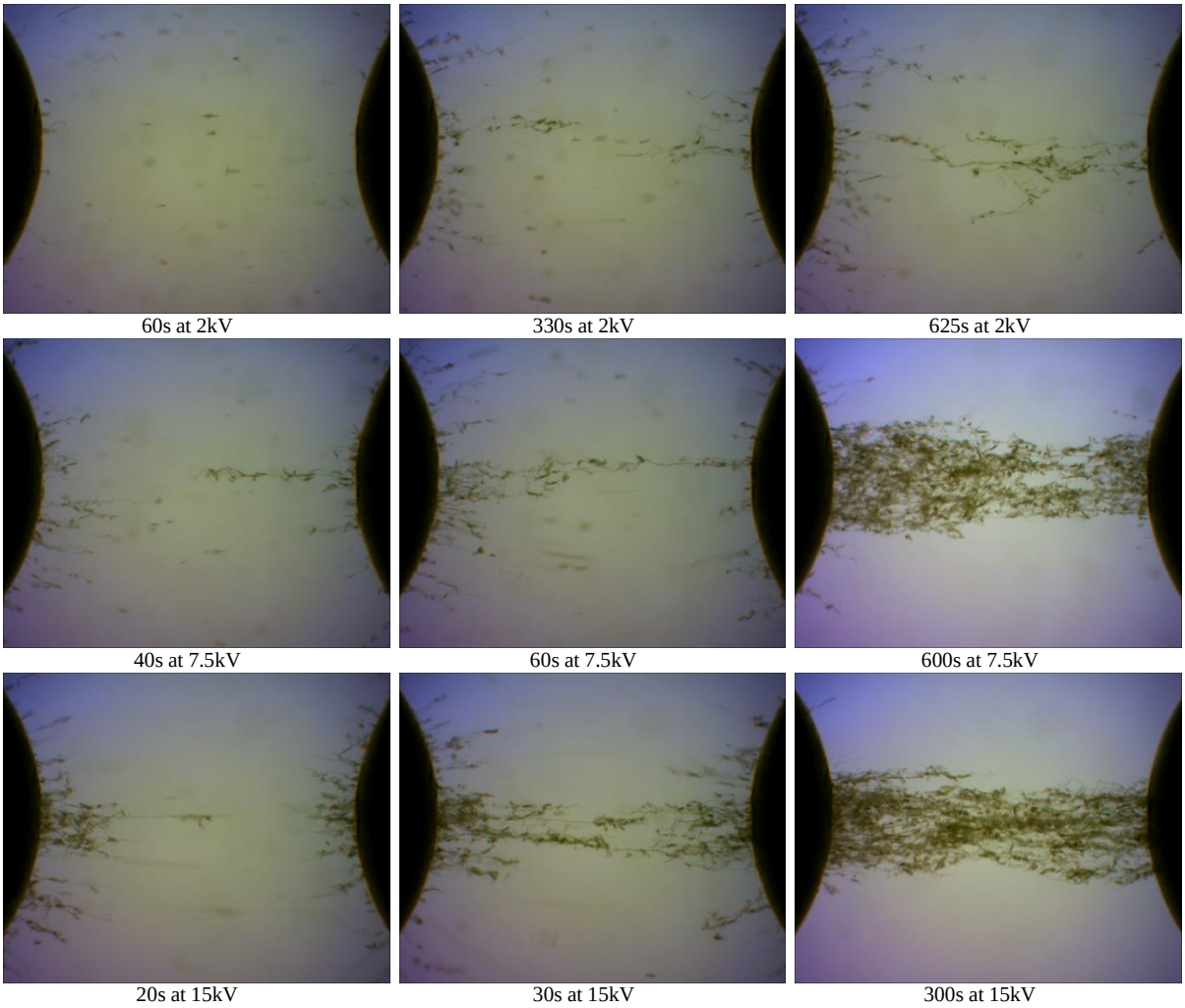

Figure 4:4 Optical microscopic images of bridging in contaminated transformer oil with 150-500 µm pressboard fiber, concentration level 0.002%.

Similarly, when the applied voltage was increased to 7.5 kV for 150-250 µm particles, within 60 s of switching on the voltage, a thin bridge was built on the surfaces of the electrodes. It took 240 s to create the first thin bridge for the bigger particles of 250-500 µm. The bridges were thickened as time progressed and several branches were created between the two electrodes for both particle sizes. Finally, within 600 s, a thick bridge in the gap was formed for the smaller particles (Figure 4:4) and thinner bridge was observed for bigger size particles.

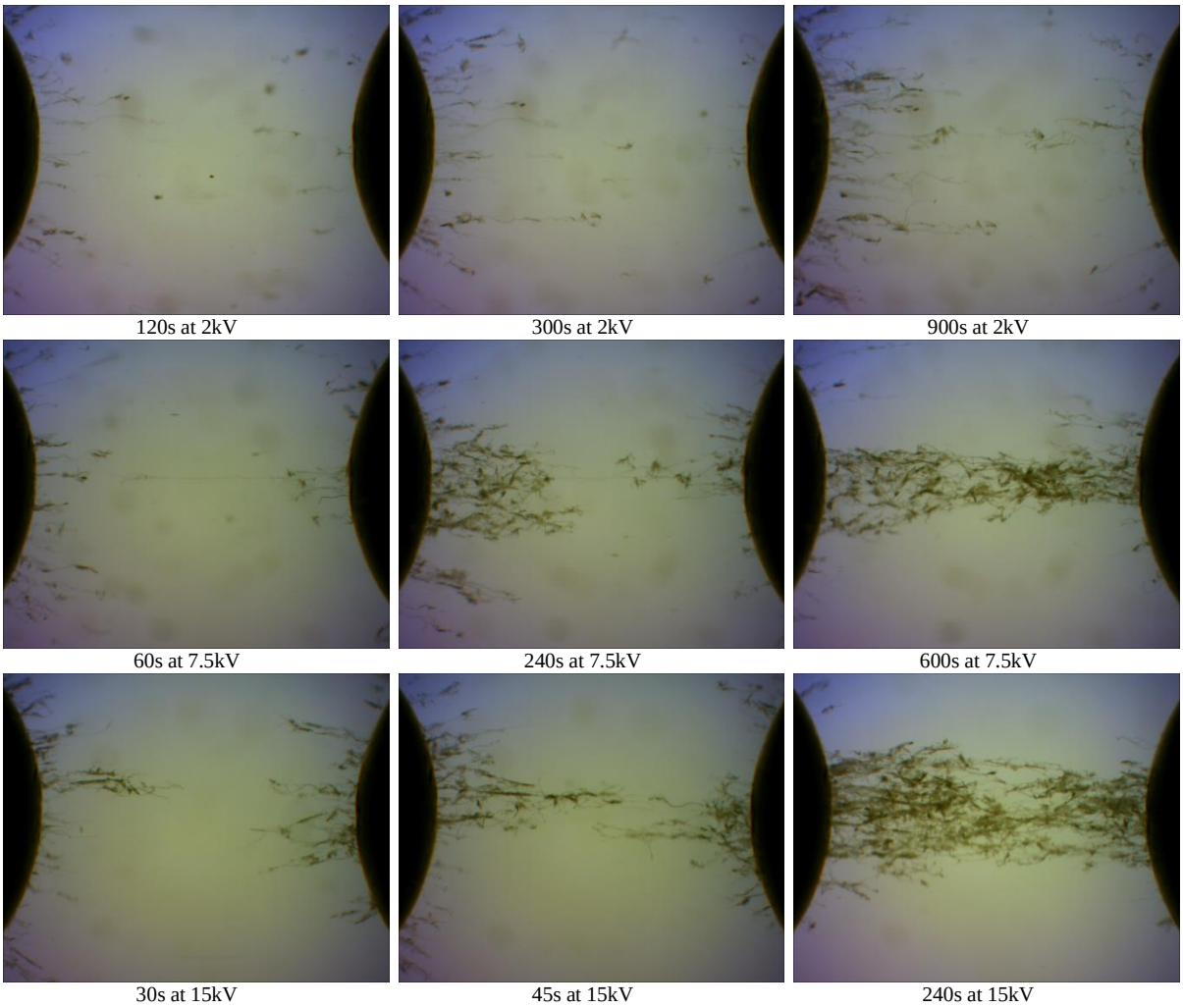

Figure 4:5 Optical microscopic images of bridging in contaminated transformer oil with 250-500 µm pressboard fiber, concentration level 0.002%.

Under the same experimental conditions, within 20 s of switching on 15 kV, multiple partial bridges branch out from surfaces of the electrodes and a thin bridge was formed for smaller particles. After 60 s a thin bridge was observed for bigger particles. Subsequently, the partial bridges were joining together from the either side of the electrodes, leading to form complete bridges connecting the two electrodes resulting in thicker branches close to the surface of the electrodes and eventually leading to a thinner density to the midpoint of the gap. Gradually, the bridges then coalesce together to form a solid bridge within the gap. The bridge was strongly bonded for smaller size (150-250 µm) particles than the bigger ones (250-500 µm).

It was also observed that the magnitude of the currents flowing through the gap increased with the level of contamination. The conduction currents of different applied voltages for both particles sizes shown in Figure 4:6. In this case, polarisation current is smaller than the steady conducting current.

The 150-250 µm size particle always had higher conduction currents than the 250-500 µm particles due to the thick and strongly bonded bridge.

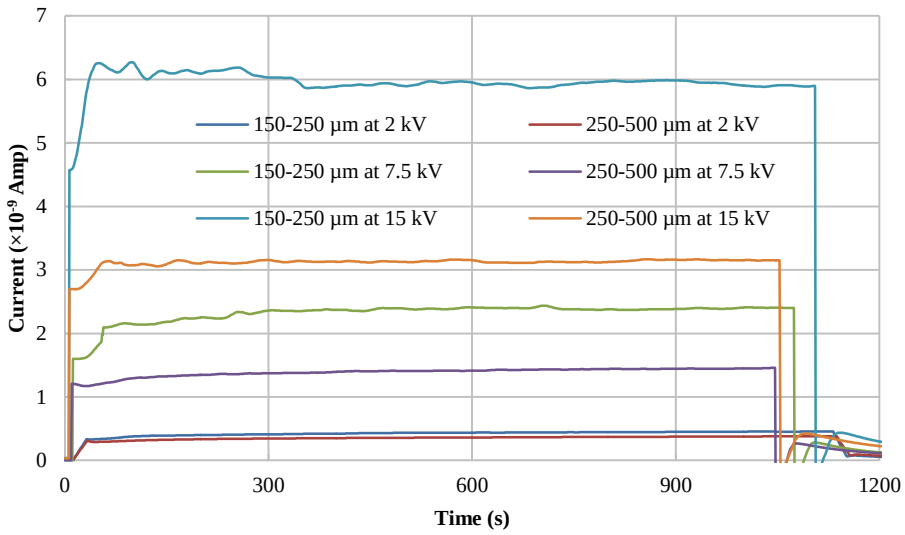

Figure 4:6 Current at different DC voltages with 0.002% concentration for 150-250 µm and 250-500 µm particles

The increment ratio of currents between smaller size and bigger size particles had intensified than lower contamination level.

4.2 Mechanism of DC Bridging

It has been found that pressboard particles started moving between the electrodes after applying the DC electric field. The reason behind the movement of particles could be explained in the following way. As soon as the power is pplied to the system, under DC electric field the particles start to become polarized. The fiber then align themselves parallel to the field. Due to non-uniform electric field, the particles experience DEP force [76]. It can be seen at the initial stages of the experiment that fibers move towards the electrodes. Once the particles touch the electrode surface they acquire charges from the electrode. When the charge transferred to the fiber reaches a certain level and its repelling Coulomb force is greater than the attractive DEP force, the particle gets off the electrode surface and travel towards other electrode under a combined action of the Coulomb force, DEP force and the drag force from viscous oil. At this stage the motion is mainly controlled by a balance between Coulomb and drag forces since DEP is relatively weak. The particle finally reaches the opposite electrode, where it discharges and acquires charge of different polarity. The dielectric particles travel back and forth from one electrode to the other in this fashion.

The described behavior is clearly seen on the current profiles, Figure 4:9. Initially the current is small, but since more and more fibers get an electric charge the current increases until it reaches a saturation which is different for different voltages and particles size. Previously this phenomenon has been investigated by several researchers [5, 38, 39, 71, 73, 77-80] with conductive and dielectric particles. They have calculated the amount of charge acquired by both conductive and dielectric particles.

To understand the dynamics of the fibers we need to note that for long fibers of length l and sectional radius r:

Drag force [81] $F_{drag} \sim l(\mu_{oil} v_p)$ **4:1**

Coulomb force [39] $F_C \sim qE \sim r^2 V^2, q \sim r^2 E$ **4:2**

DEP force [82] $F_{DEP} \sim r^2 l \nabla(E^2) \sim a^2 l V^2$ **4:3**

with E, V, μ_{oil}, v_p being electric field, applied potential, oil viscosity and fiber velocity respectively. Many parameters in the above equations depend on moisture content. Since the moisture content remains the same during all experiments, the qualitative analysis can be done without taking into account these moisture effects.

The particles which did not acquire enough charge were stick with the electrodes surface due to strong DEP force. So the fibers move from one electrode to another electrode until they reach the point at the electrode surface where DEP force is high, which is close to the central line between the electrodes. The charged particles that are in contact with the electrode attracted other particles with oppositely charges due to Coulomb force. The other attractive forces between particles within short distances are van der Waals force, dipole and quadrupole interactions. As the particles are under a DC field, quadrupole forces can be ignored. The main component of the attractive force is the dipole interaction, when the voltage is switched off and the polarisation is removed, the particle fall down to the bottom of the tank under the gravity. Due to these inter-particle interaction forces, the pressboard particles started to form chain between two electrodes. These chains also align themselves parallel to electric field lines as can be seen in Figure 4:7, the particles at upper or lower side of electrodes elongated following electric field lines. Initially the electric field strength is maximum at the electrodes surfaces so is the DEP force. But since more and more particles stick to the electrodes surface, the maximum field and DEP force move to the ends of these particles chains closer and closer to the mid-point between the two electrodes. So the higher the voltage, the stronger DEP force pushes the fibers toward the electrodes at the start of the process and towards

the central line at the bridge development stage. Consequently, for higher voltages the thinner, denser bridges are formed, see Figure 4:7 and Figure 4:8. Initially, longer fiber particles first stick on both electrodes where the DEP force is maximum. They start the bridging process by attracting other particles with smaller l on their surface forming a skeleton of the bridge which progresses towards the opposite electrode. Eventually the fibers chains from both electrodes joining up in the middle [83].

4.2.1 Bridge Formation and Conduction Current with a Contamination Level of 0.003%

After applying 2 kV there was a thick bridge created after 600 s for 150-250 µm particles as shown in Figure 4:7.

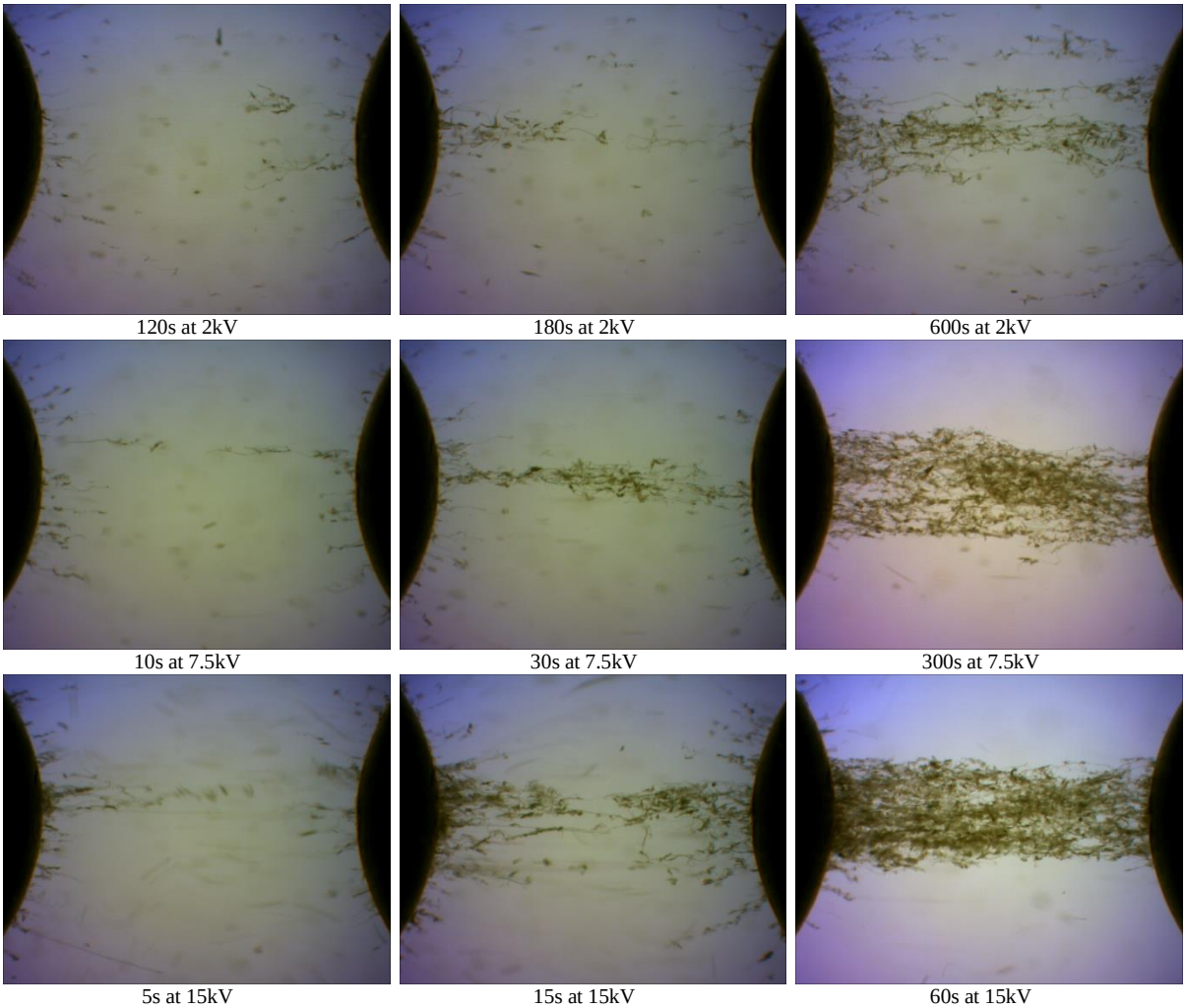

Figure 4:7 Optical microscopic images of bridging in contaminated transformer oil with 150-250 µm pressboard fiber, concentration level 0.003%.

It took 180 s to make a complete thin bridge. There was a complete very tiny bridge formed after 180 s for the 250-500 µm particles as shown in Figure 4:8. A very shallow bridge was observed

after 600 s. A couple of different branches were attached from one electrode to the other. The observed behaviour agrees with the proposed force balance in section 4.2. With increase of l (for the same r) the drag force increases whereas Coulomb force stays the same and it slows the particle motion towards the central region between the electrode. Note that the fibers have to be dragged towards the centre first and only after that the DEP force moves them to create the bridge.

For 7.5 kV, a thin bridge formed after 10 s for 150-250 µm particles. The bridge was thickened until 300 s (Figure 4:7). There was no change of bridge formation observed after that. For 250-500 µm particles, a thin bridge formed at 30 s and started to grow until 300 s as shown in Figure 4:8. The completed bridge for the bigger particles was shallow as compared with the smaller particles.

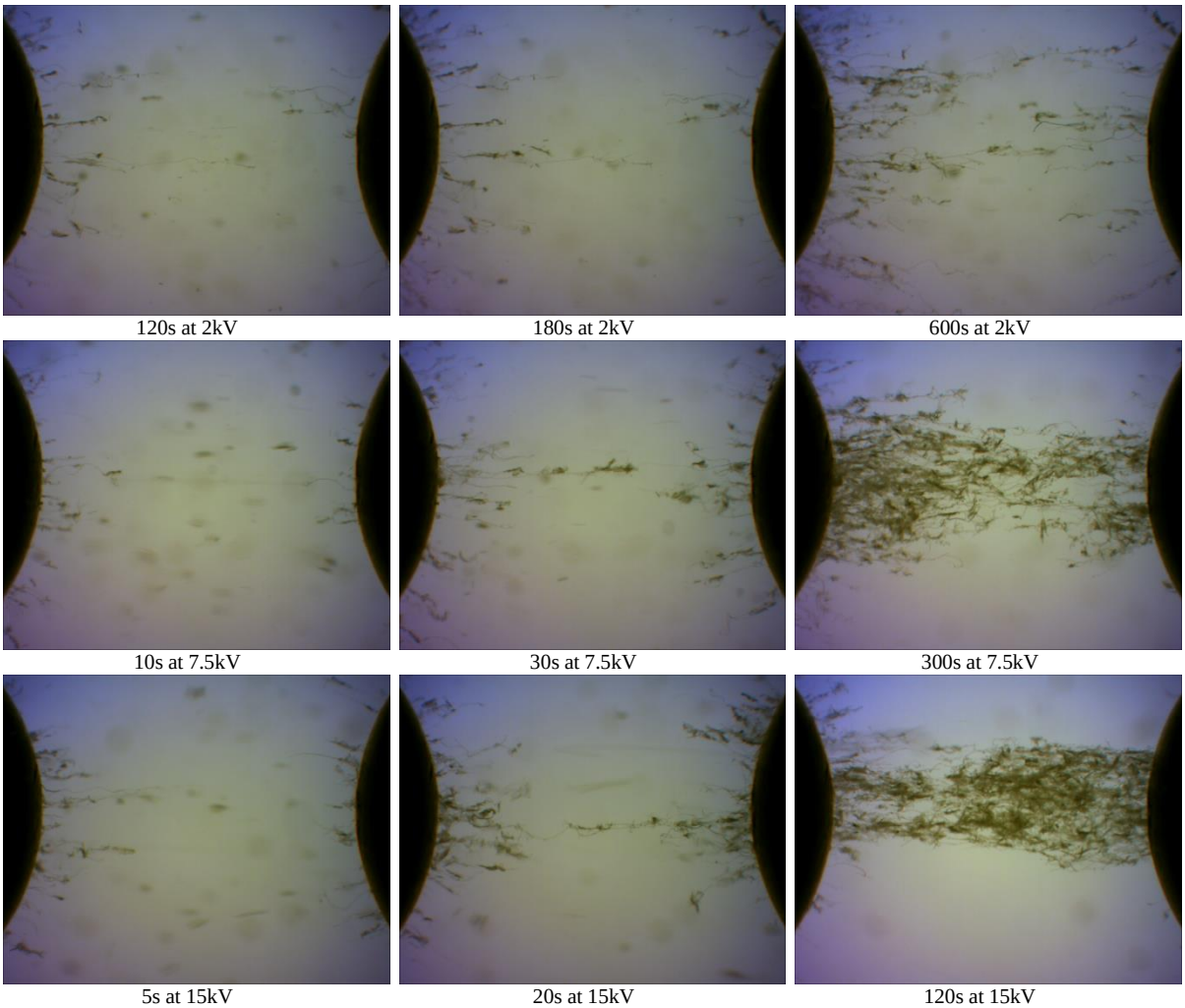

Figure 4:8 Optical microscopic images of bridging in contaminated transformer oil with 250-500 µm pressboard fiber, concentration level 0.003%.

Similar observations were made after applying 15 kV. A thin complete bridge was made within 5 s, and thickened up to 60 s for 150-250 µm samples. On other hand, it took 20 s to form a complete bridge for bigger size particle. Within 120 s a thick bridge was created. The main point to be noted

is that the thickness of the bridge and the bond between the particles of for smaller particles were far better than that for bigger size particle. It contradicts to the simplified force balance suggested in the thesis. For larger fibers, further bridge compression is expected after 300 s with forming denser bridge. It does not happen partially probably due to higher friction forces between longer fibers as well a different quadruple interactions. But it is mainly due to the modification of electric field between the electrodes when the bridge is formed. The field gradient will be along the bridge in this case which stops the further bridge growth, see Figure 4:8.

The conduction current for the two particle sizes under the influence of three different voltage levels are shown in Figure 4:9. As soon as the voltage was applied, there was a high polarization current observed in most of the experiments. After that the slow growing current was established. The existing of the current can be explained by charging of the particles at the electrodes and transfer the charge across even if the bridge is not formed yet. Then the currents were gradually increased until a complete thick bridge formed. It is clear based on current results that charge transportation is taking place through the pressboard particles under a DC electric field.

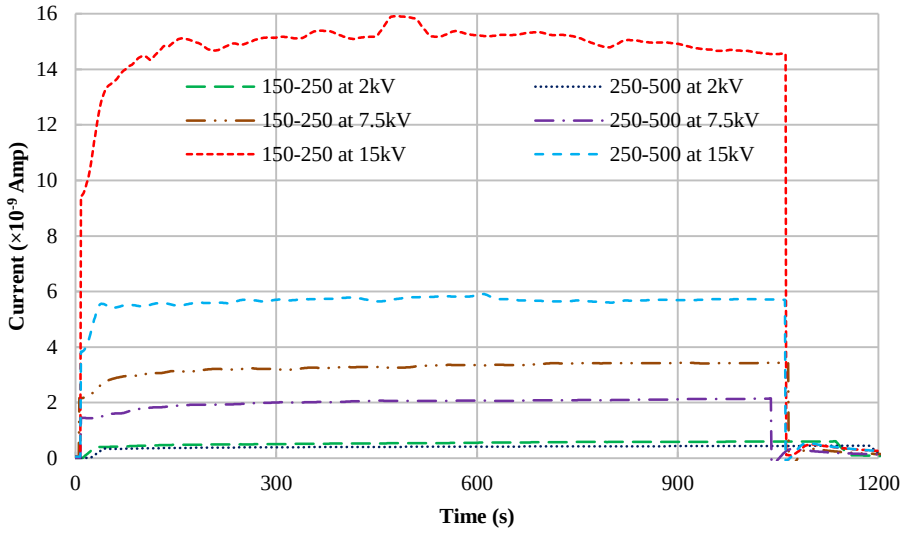

Figure 4:9 Current at different DC voltages with 0.003% concentration for 150-250 µm and 250-500 µm particles

The currents were almost steady after the bridge formation. The thickness of the bridge and the bond between the particles were the main determining factor for the conduction currents after this time. Although the bulk conductivity of the pressboard is several hundred times less than the transformer mineral oil. However the fiber surface conductivity is not very clear from the literature and it might be higher than the bulk conductivity. So it is assumed that the pressboard fibers transferring a charge over the outer surface. The currents for all the contamination levels increase

with the contamination rise. The increment ratio of currents for smaller size and bigger size particles is different.

4.2.2 Conduction Current Comparison in Different Concentration Level

The maximum conduction current (at the bridge stage) with respect to contamination levels for all the experiments are summarized in Figure 4:10. The highest point of steady conduction currents was taken for this graph. The two region of the process can be clearly identified for these plots. For low voltage of 2 kV, the current weakly depends on the particle size and contamination level. It is probably because the dielectrophoretic force (DEP) is small to overcome friction force. Even the large number of particles are available to form the bridge, they cannot be compressed enough to form a long bridge. The current is approximately constant at 7.5 kV up to 0.003% contamination. After that it starts to rise. At 15 kV the non-linear dependence becomes obvious. These results are in line with previous studies [5]. The most important observation out of this investigation is that the conduction current for 150-250 µm is always higher than 250-500 µm particles. To be more specific, the larger the size of the particles, the lower is the conduction current. The magnitudes of the conduction currents for smaller particles are 1.5, 2 and 3 times larger at 0.001%, 0.002% and 0.003% concentration level respectively for applied voltage of 15 kV as shown in Figure 4:10. Since it measured at steady state bridge, the contacts formed by smaller particles are always better. Note that after the bridge is formed the mobility of the particles is irrelevant and the current is an indication of the bridge quality and its size.

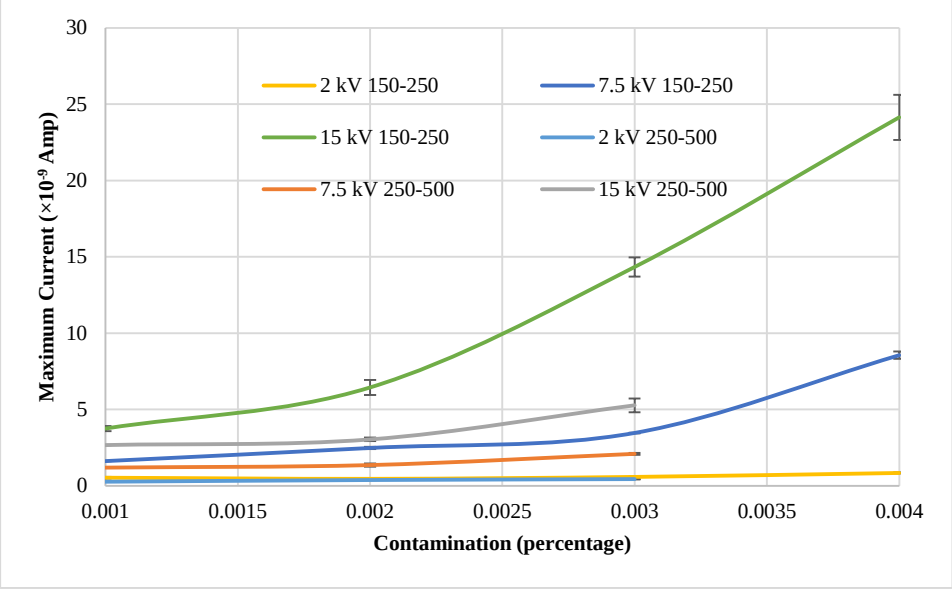

Figure 4:10 Maximum Conduction current in different concentration levels for 150 – 250 µm and 250 – 500 µm particles

4.2.3 *Pixel Counting Analysis of the Images*

The images for particle accumulation were analysed using pixel counting technique. The first image of a particular experiment was taken as background and it was subtracted from all the later images. The result was obtained as a grey image with a specified tolerance level which was fixed for all the analysis to obtain consistent result. Then the resultant images were converted into black and white. After that all the black pixels were counted. The quantity of pixel count does not correspond to the particles number but the increment of the pixels shows the particles accumulation between the electrodes.

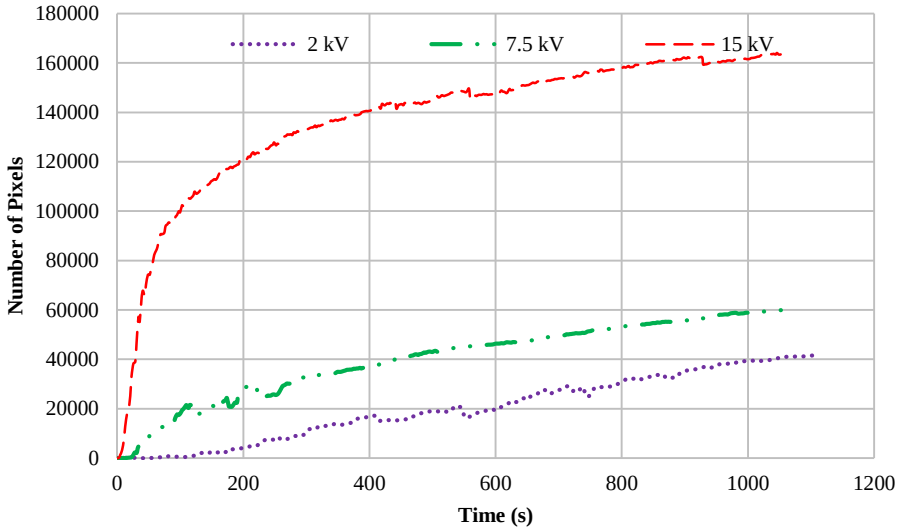

Figure 4:11 Increment of pixels in microscopic images under influence of DC electric field with 0.003% concentration, particle size 150-250 µm

The plots in Figure 4:11 shows the pixel counts for optical microscopic image taken during the test. The graph clearly indicates the increments of bridge density with time. But the current in Figure 4:9 reaches the saturation level much quicker. In other words, the additional particles which are brought in after the central bridge formation do not go towards the central region. It may be understood by considering the electric field changes as the bridge has been formed. The bridge itself is a reasonably conductive and the field gradient will be along the bridge. So DEP force moves fibers towards the electrode in this situation, not making the bridge thicker in the middle. Despite of changing the bridge density (Figure 4:11) with time, the current (Figure 4:9) remain same because higher resistance of the outer side of the bridge had a very little effect on total conduction current.

4.3 BARE ELECTRODE TEST UNDER AC ELECTRIC FIELD

Several contamination levels were tested under the influence of three different levels of AC electric field

4.3.1 BRIDGE FORMATION AND CURRENT UNDER 10 KV AC

The particles were slowly moving after the 10 kV AC supply turned on as shown in Figure 4:12.

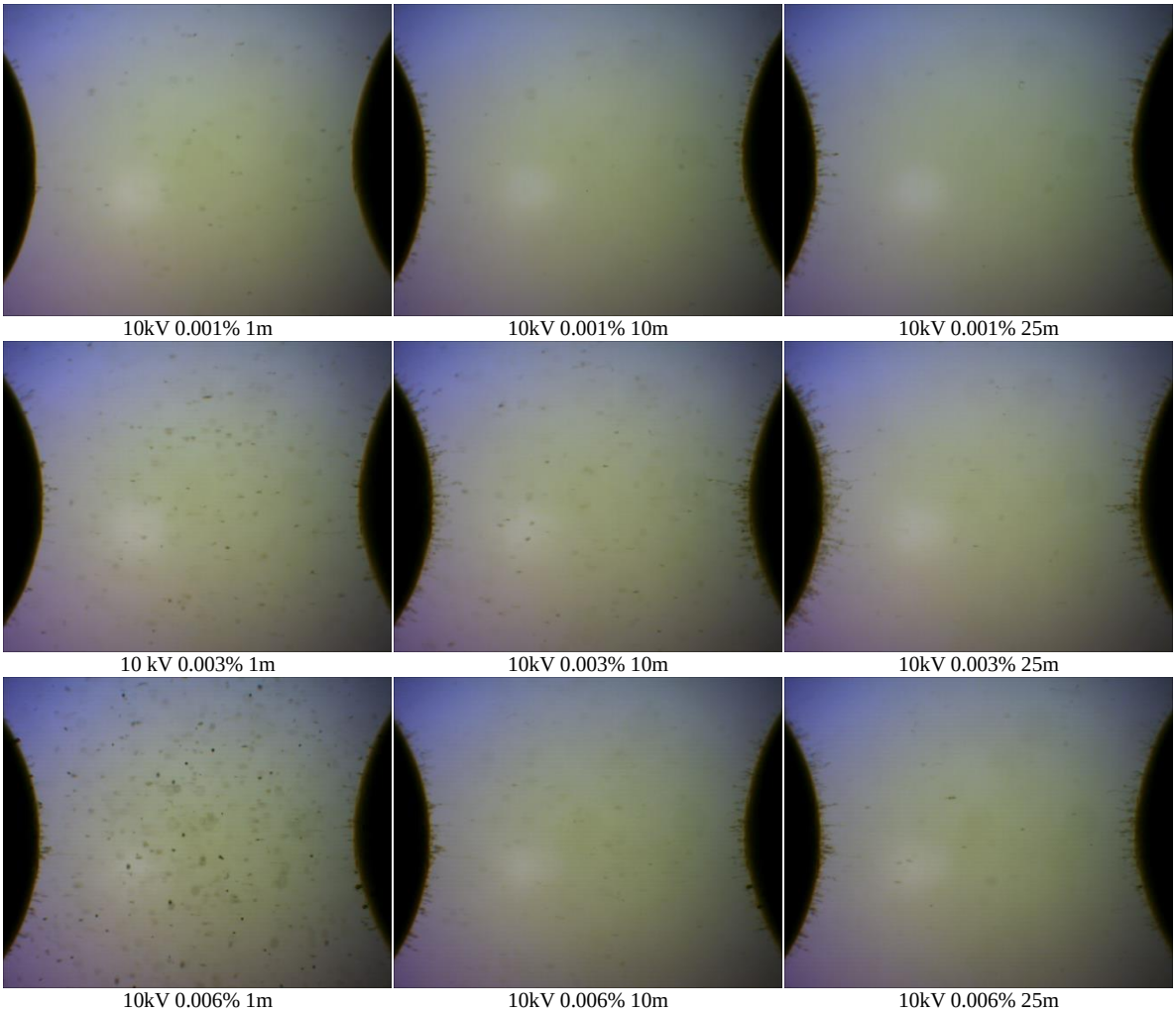

Figure 4:12 Optical microscopic images of bridging in contaminated transformer oil with 150-250 µm pressboard fiber, applied voltage 10kV. (Part 1)

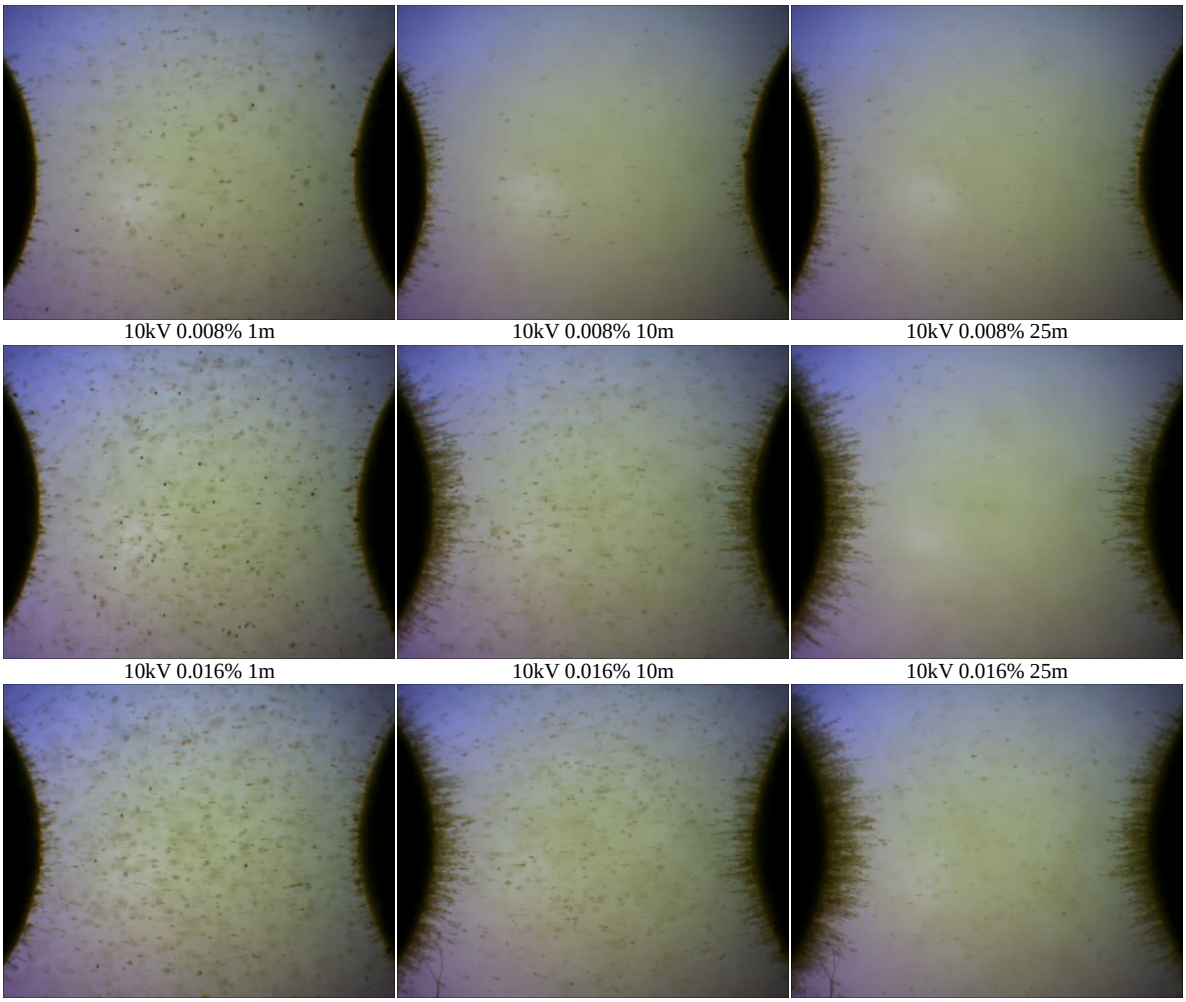

Figure 4:12 Optical microscopic images of bridging in contaminated transformer oil with 150-250 µm pressboard fiber, applied voltage 10kV. (Part 2)

They started to move towards the high electric field region and started attaching themselves to the electrodes slowly because of dielectrophoretic force. More particles were attached to the electrodes as time elapsed.These experiments were carried out on several contamination levels i.e. 0.001%, 0.002, 0.003, 0.006%, 0.008%, 0.016% and 0.024%.As the concentration increased the particle accumulations to the electrodes increased. But they never formed a complete bridge between the two electrodes. It was reported by [12] that bridging were observed with spherical and wrapped electrode system in moistened and pressboard fiber concentrated samples under AC electric field of 6kV and 8 kV for spherical and formed wire electrodes respectively.

The conduction currents were also recorded during the entire test for all contamination levels. The conduction current didn't fluctuate with time during any of the tests as shown in Figure 4:13. The currents for all the test of different concentration levels were also almost constant for the 10kV supply. The current were measured by Keithley 2001 multimeter and it can only measure the RMS value of the AC current. As for AC voltage, the dielectric liquid act as a capacitor. So the capacitive

current is the dominant part and the resistive current is much smaller. Further investigation is needed to measure the conductivity under range of frequencies which will indicate if there is any change which relates to particle concentration level.

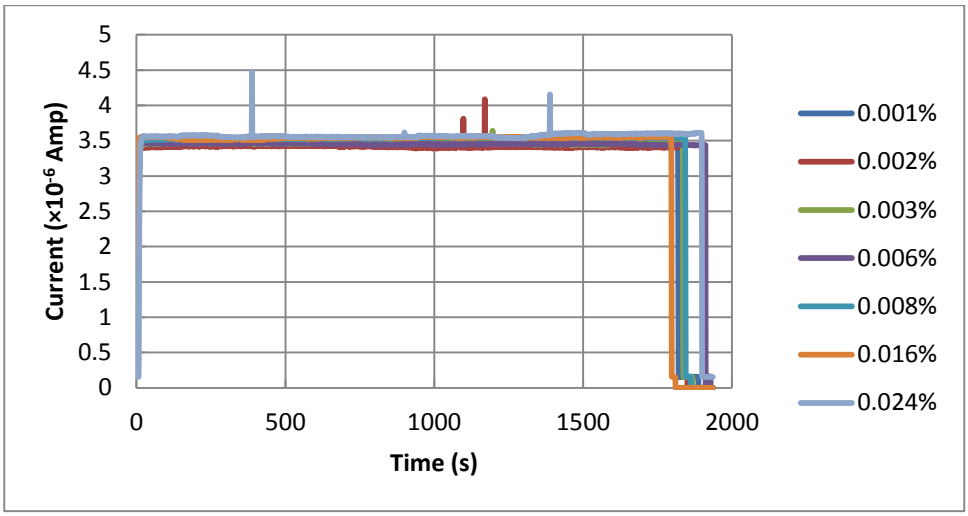

Figure 4:13 Current in different concentration level under influence of 10 kV AC electric field

4.3.2 Bridge Formation and Current under 15 kV AC

Figure 4:14 shows the images from 15 kV AC experiments. The particles were moving faster than before due to the increased of intensity of electric field after the power supply turned on. They started to move towards the high electric field region and started attaching themselves to the electrodes. More particles were attached to the electrodes as time elapsed. The particle accumulations to the electrodes increased with concentration level and the increased voltage level. For the applied voltage of 15 kV, there was no complete bridge formed between the two electrodes as before.

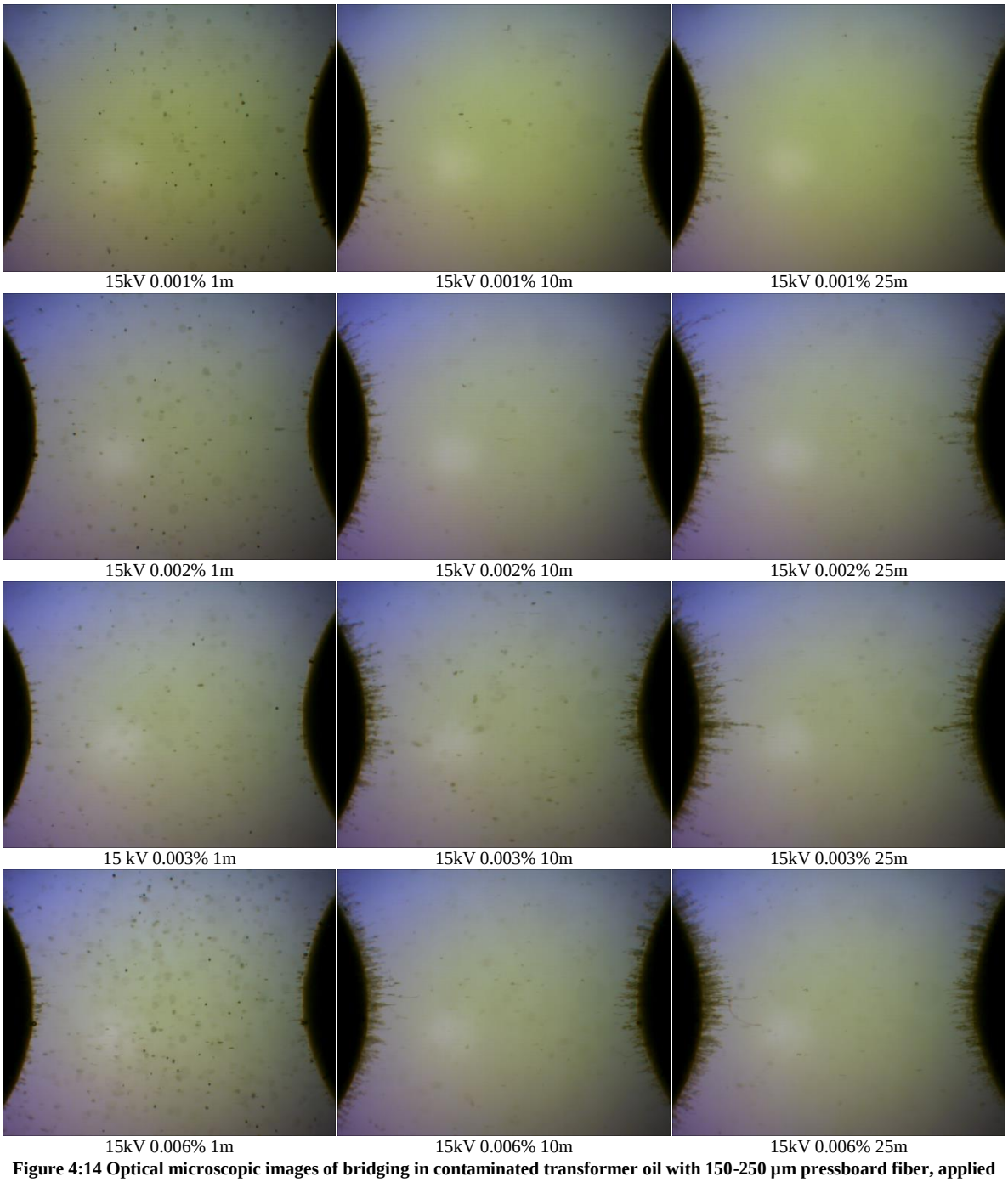

15kV 0.001% 1m | 15kV 0.001% 10m | 15kV 0.001% 25m

15kV 0.002% 1m | 15kV 0.002% 10m | 15kV 0.002% 25m

15 kV 0.003% 1m | 15kV 0.003% 10m | 15kV 0.003% 25m

15kV 0.006% 1m | 15kV 0.006% 10m | 15kV 0.006% 25m

Figure 4:14 Optical microscopic images of bridging in contaminated transformer oil with 150-250 µm pressboard fiber, applied voltage 15kV. (Part 1)

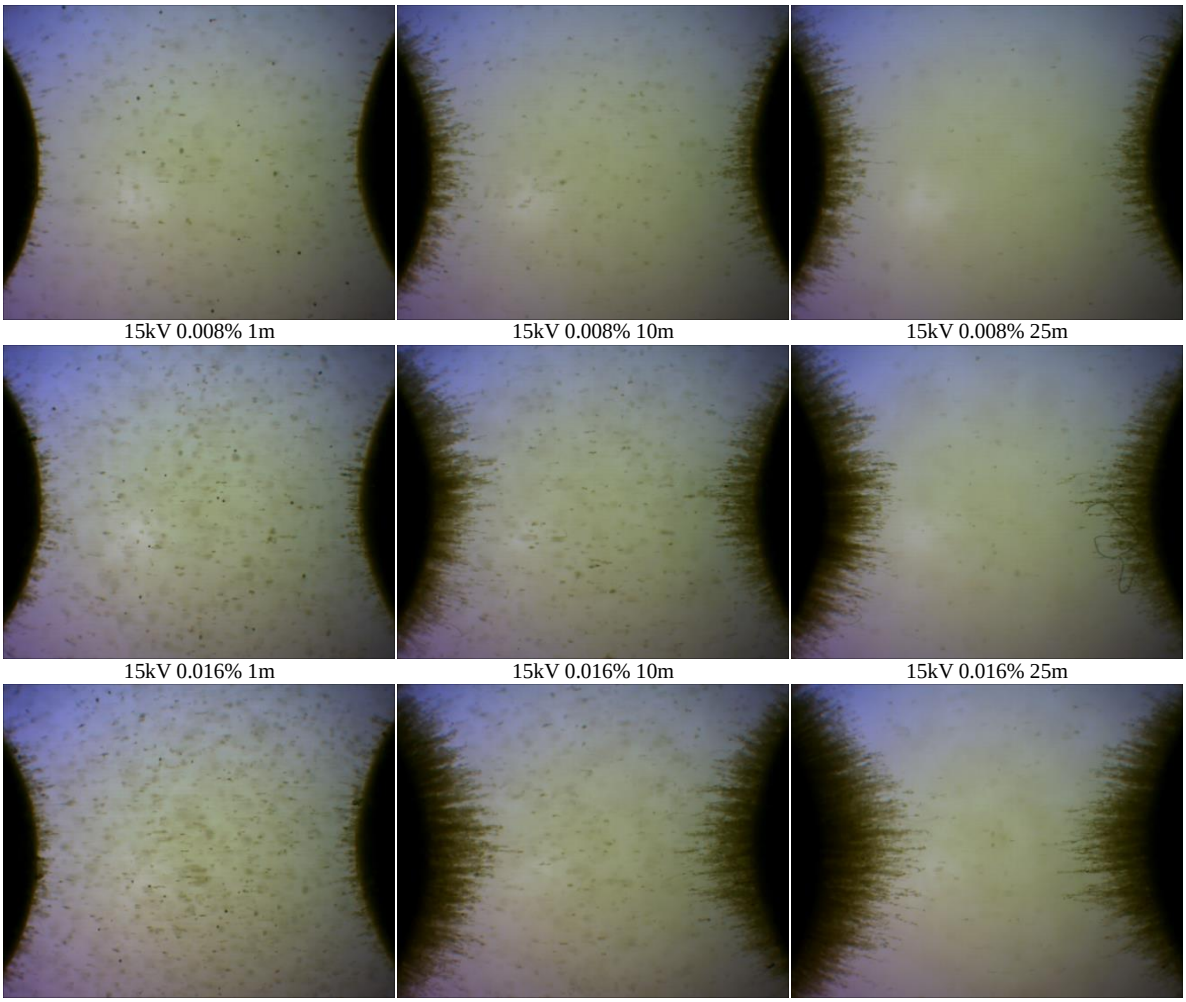

Figure 4:14 Optical microscopic images of bridging in contaminated transformer oil with 150-250 µm pressboard fiber, applied voltage 15kV. (Part 2)

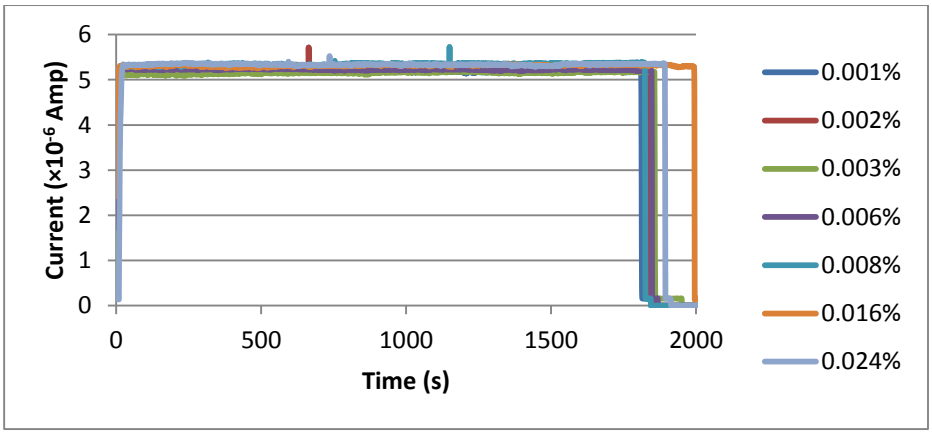

Figure 4:15 Current in different concentration level under influence of 15 kV AC electric field

The conduction currents were increased with the applied voltage of 15 kV shown in Figure 4:15. The currents were almost constant during the entire test. The currents for all the test of different concentration levels were also remained constant for the 15 kV supply.

4.3.3 *Bridge Formation and Current under 20kV AC*

The particle movement were intensified for 20 kV AC test as shown in Figure 4:16. The particle accumulations were also increased with the applied voltage.

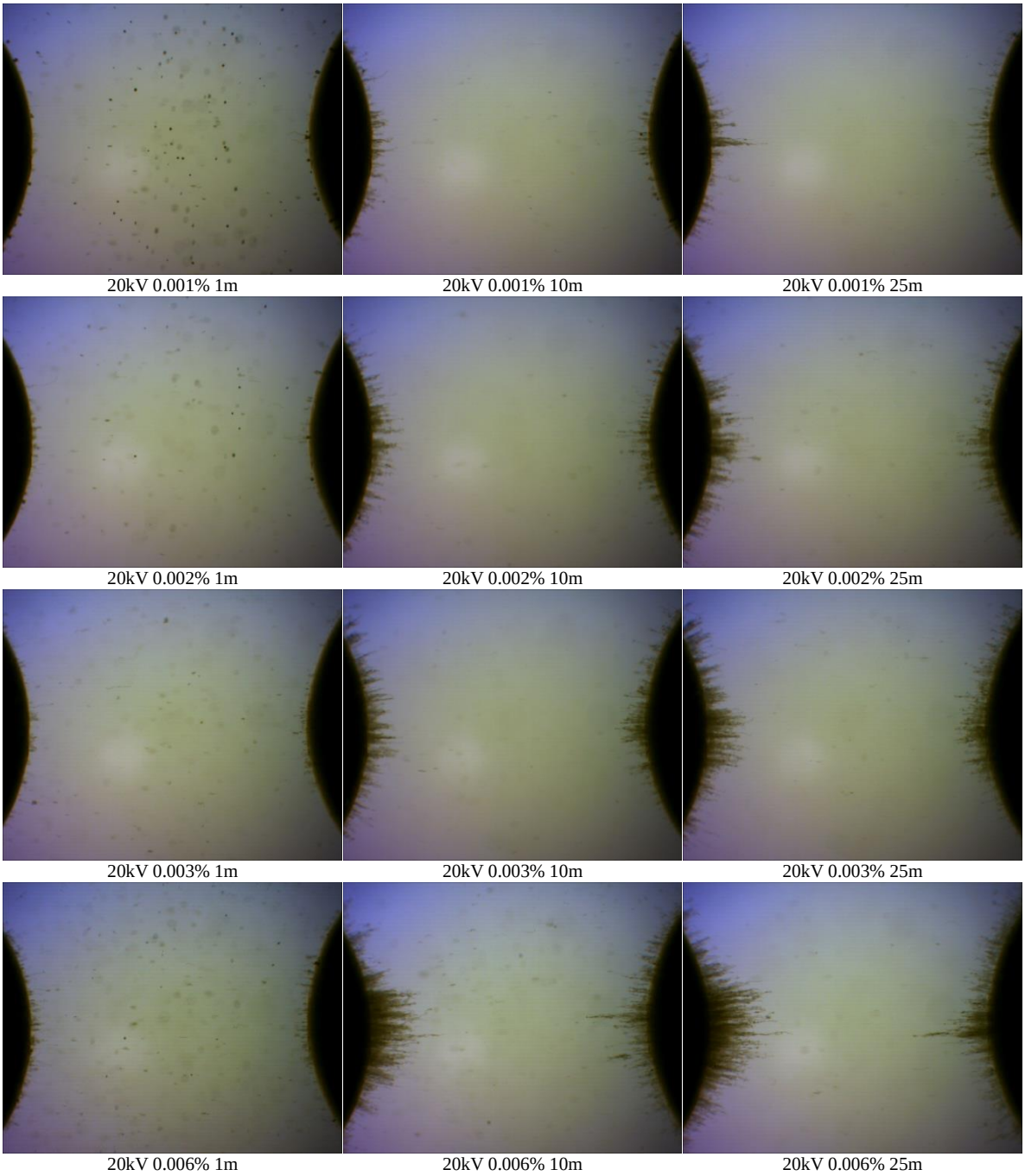

Figure 4:16 Optical microscopic images of bridging in contaminated transformer oil with 150-250 µm pressboard fiber, applied voltage 20kV. (Part 1)

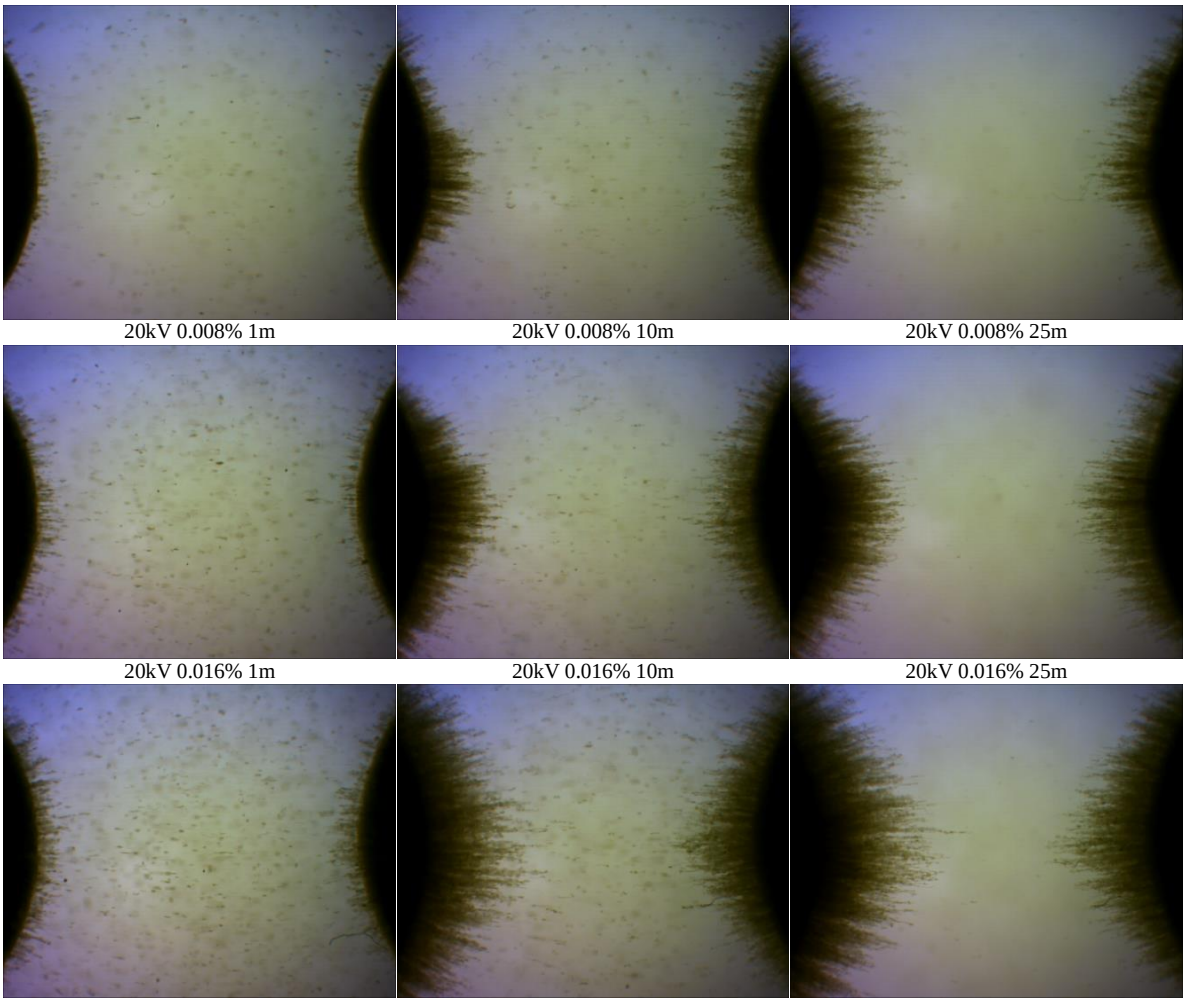

Figure 4:16 Optical microscopic images of bridging in contaminated transformer oil with 150-250 µm pressboard fiber, applied voltage 20kV. (Part 2)

This test had the highest particle attachment to the electrodes. But there was no complete bridges formed between the electrodes for any of the experimental conditions.

The conduction currents again increased with the voltage as shown in Figure 4:17 but they remained almost constant for the all the contamination levels.

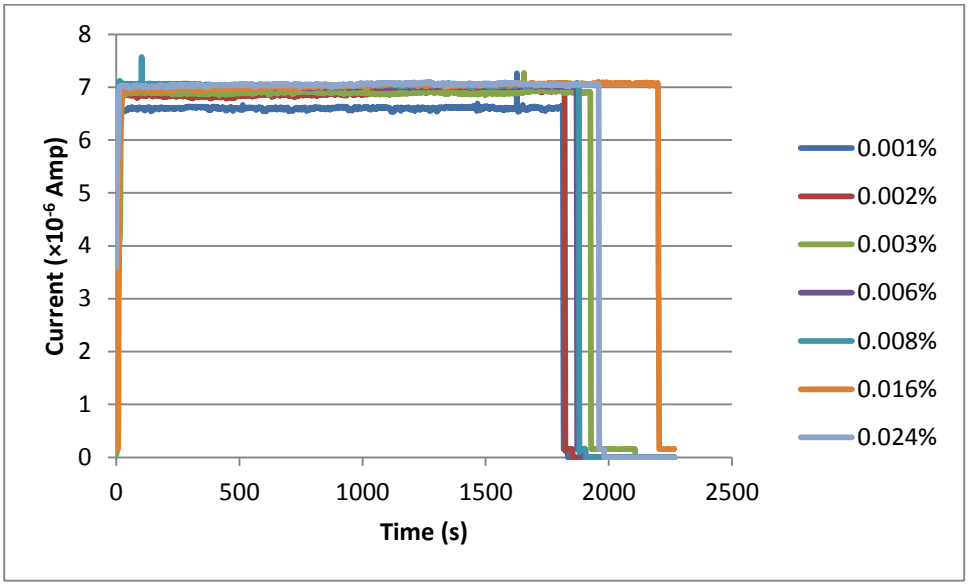

Figure 4:17 Current in different concentration level

4.4 MECHANISM OF AC "BRIDGING"

Particle cloud formation at lower stress and dispersion at higher stress were previously observed and quantified by researchers [84, 85]. Figure 4:18 shows the images obtained at three different AC voltages for the highest concentration (0.024%) of fiber particles. It is clear that instead of forming a bridge, the particles are attached to the surface of the electrodes more or less evenly. This behaviour is related to the alternation of the electric field. It is worth to note that The DEP force is 280 times higher than gravitational force estimated by [85] for a 50 micrometer diameter particle at 1 MV/m and gravity has a minor effect on the experiment. Once again, when the particles made a contact with the electrodes, they become charged. The particles which could not acquire enough charge to detach themselves from electrode surface (a balance between Coulomb and DEP force) stay on the electrode surface. Other particles may attach to these particles. These particle chains also elongate towards the other electrode parallel to electric field lines and form a beard as seen in Figure 4:18. If the charge is large enough, Coulomb force detaches the particles from the surface and they continue to move in the gap. But under AC, the particles travel towards opposite electrode only during a half cycle, after that the particles dragged back to the initial electrode. So, the particles make a short journey along the electric field line but the return journey is different mainly due to DEP force (which does not change the direction) and flow disturbance force caused by other particles.

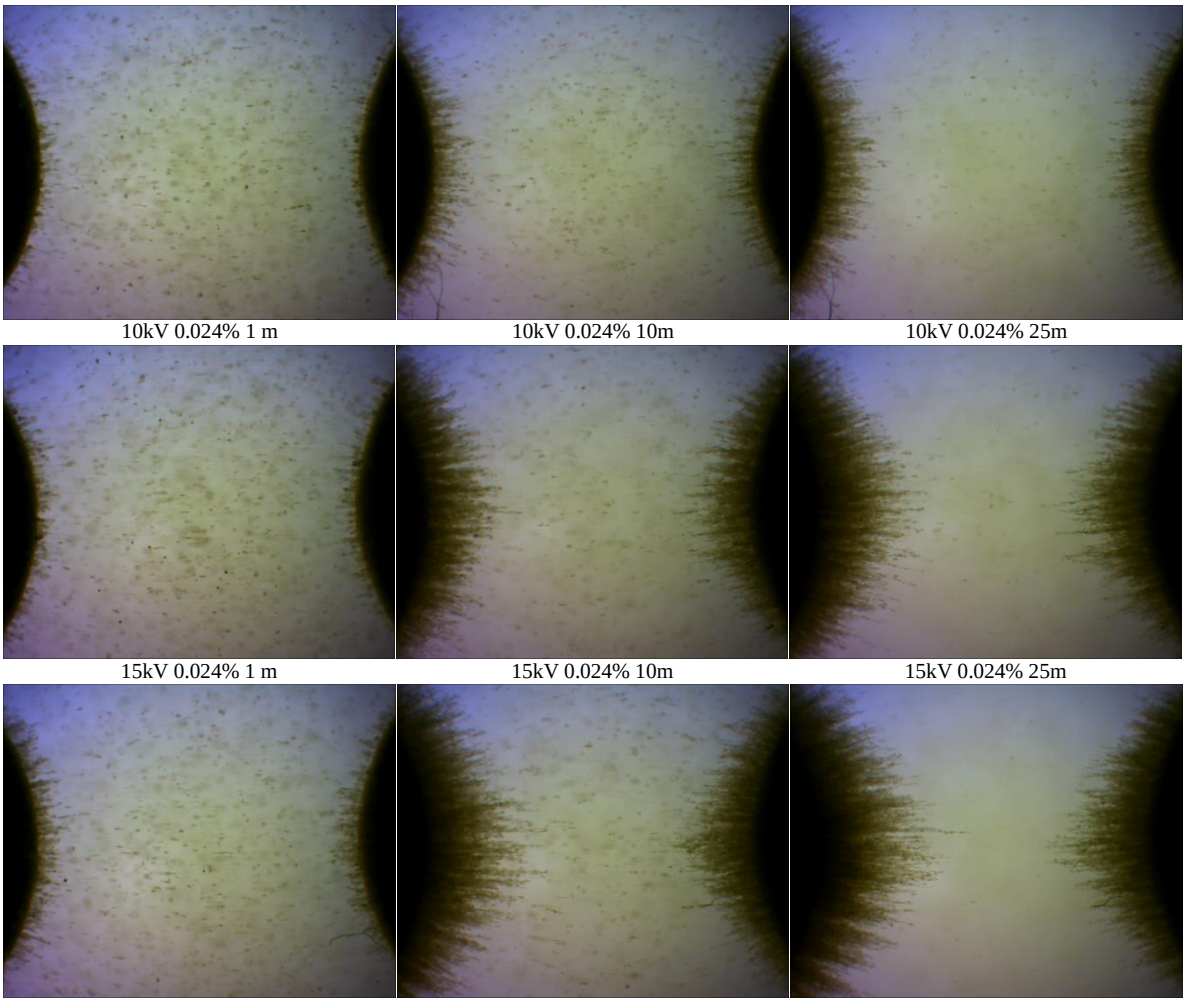

Figure 4:18 Optical microscopic image for bridging under influence of AC electric field with 0.024% concentration of 63-150 µm cellulose particles.

Inter-particle interaction and DEP forces are the main reasons for particle segregation. The inter-particle force is not large, but it is sufficient to hold the particles attached to each other even when they form a conductive bridge. For example analysis of 50 µm diameter particle at 1.33 MV/m field showed [85, 86] that short range inter-particle interactions exceed the gravitational weight of the particle to the distances up to 6 particle radiuses. So while alternating field shaking the particles near the electrodes the DEP force, which does not dependent on the polarity of charge of the particle, drags the particles toward the central region of electrode surface where the distance is shortest between the electrodes and the electric field is the highest. Fluid movement due to the particles motion also helps in dragging neighbouring particles towards the electrodes. A single particle would drag all the particles at the distance of 10 times its radius along the direction of its movement [85]. A combination of the factors mentioned above and the electric field changes due to the formation of a conductive electrodes cover of cellulose particles, results in evenly coverage of the electrodes without bridge formation. In the AC case the Coulomb force does not bring the

particle to the central line between electrodes region between electrode and it prevents a bridge formation [83].

Several contamination levels i.e. 0.001, 0.002, 0.003, 0.006, 0.008, 0.016 and 0.024% were tested under influence of 10, 15 and 20 kV AC electric field. The pressboard particles started moving slowly when the 10 kV AC supply was applied. As time elapsed, particles were attached to both electrodes evenly, Figure 4:18. The particles accumulations increased to the electrodes surface with increment of both voltage and contamination levels. A complete bridge between the two electrodes was never created as for DC experiments because of the alternating polarity of the voltage. These results are in conflict with some previous reports [11] where the bridging was observed between spherical electrodes. Although the experiments used lower voltage, i.e. at 6 kV, they were done in moistened transformer oil which may affect DEP force.

4.4.1 Pixel Counting Analysis for AC

Figure 4:19 shows the pixel counts graph under influence of different AC voltages.

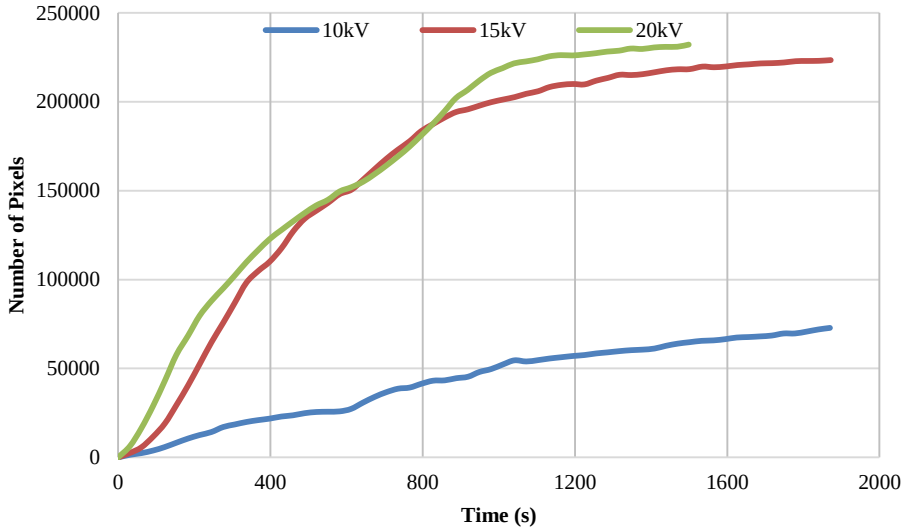

Figure 4:19 Increment of pixels in microscopic images under influence of AC electric field with 0.024% concentration

The particle accumulation for 10 kV was slow because of weaker DEP force. Particles were attached to the electrodes almost at a steady pace during the whole experiment. The amount of particles accumulated for 15 kV was only little less than for the 20 kV test in spite of large increase in DEP force. Almost all the particles were collected by the electrodes at higher voltage. For both 15 and 20 kV the particles accumulation was fast until 1000 s then it flattened. At this point, almost all fibers were consumed and the accumulation was stopped due to the lack of the fibers.

4.4.2 *Maximum Current Comparison for Different AC Voltages*

The current measured for the different voltage levels is given in Table 4-1. It is clearly observed from the table that currents were linearly increased with voltages which also suggest that the particles were not conducting for AC.

Table 4-1 Maximum current at different applied AC voltage levels.

Applied Voltage (kV)	Current ($\times 10^{-6}$ Amp)
10	3.566
15	5.343
20	7.074

4.4.3 *Bridging Under Different Frequencies*

These experiments were carried out with 150 – 250 μm particles to verify the particle accumulation process with bare spherical electrodes under different frequencies, such as 1, 2, 5, 10, 70, 100, 180 Hz. As shown in Figure 4:20, a complete thin bridge between electrodes were only formed for 1 Hz and 2 Hz frequency. The bridge for 1 Hz is thicker than 2 Hz. The particles acquired enough charge during half cycle of the sinusoidal voltage to travel towards the other electrode only for the first two tests. As frequency increased, they did not have enough time to be charged before the voltage alternated. But the DEP force is still present despite of alternating frequency. This is why the particles are attracted towards both of the electrodes and attached to the surface.

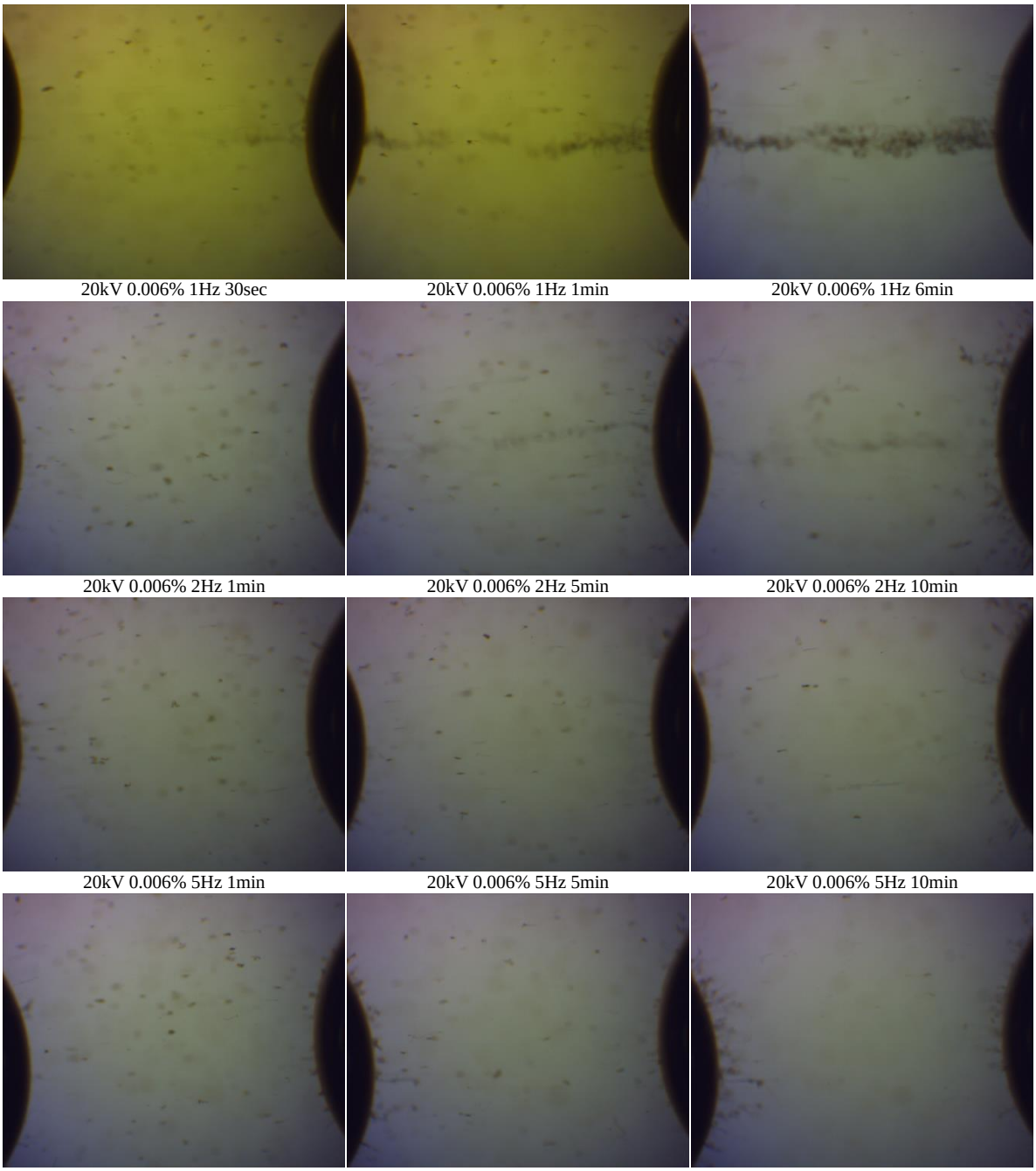

20kV 0.006% 1Hz 30sec | 20kV 0.006% 1Hz 1min | 20kV 0.006% 1Hz 6min

20kV 0.006% 2Hz 1min | 20kV 0.006% 2Hz 5min | 20kV 0.006% 2Hz 10min

20kV 0.006% 5Hz 1min | 20kV 0.006% 5Hz 5min | 20kV 0.006% 5Hz 10min

20kV 0.006% 10Hz 1min | 20kV 0.006% 10Hz 5min | 20kV 0.006% 10Hz 15min

Figure 4:20 Optical microscopic images of particle accumulation in contaminated transformer oil under influence of different frequencies, applied voltage 20 kV. (Part 1)

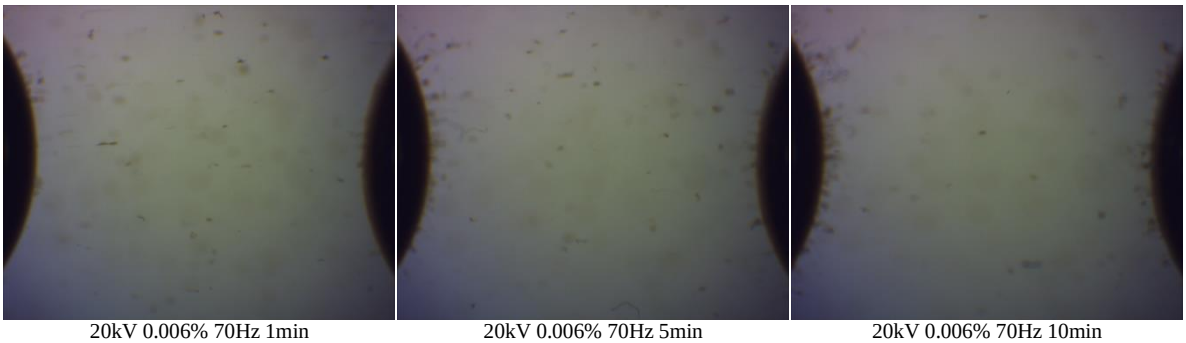

20kV 0.006% 70Hz 1min | 20kV 0.006% 70Hz 5min | 20kV 0.006% 70Hz 10min

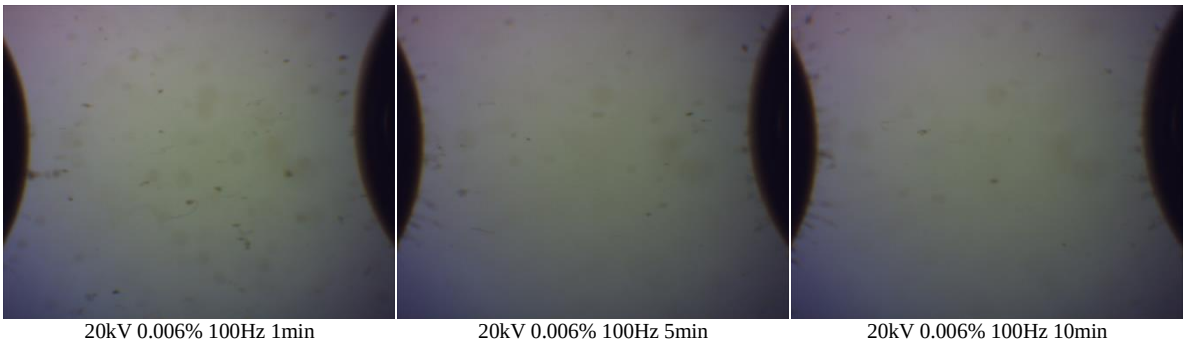

20kV 0.006% 100Hz 1min | 20kV 0.006% 100Hz 5min | 20kV 0.006% 100Hz 10min

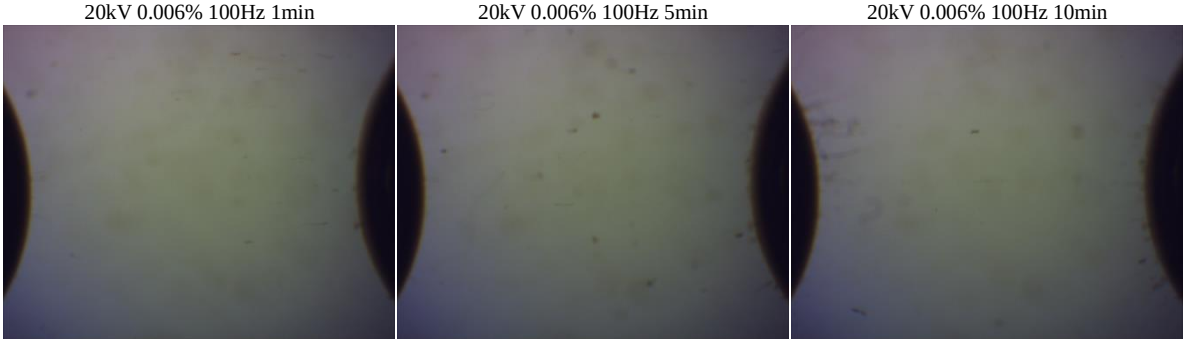

20kV 0.006% 180Hz 1min | 20kV 0.006% 180Hz 5min | 20kV 0.006% 180Hz 10min

Figure 4:20 Optical microscopic images of particle accumulation in contaminated transformer oil under influence of different frequencies, applied voltage 20 kV. (Part 2)

4.5 BARE ELECTRODE TEST UNDER POSITIVE DC BIASED AC ELECTRIC FIELD

Three different DC offset levels investigated i.e. at 1 kV, 3 kV and 6 kV with 150 – 250 µm particles. The AC voltage of 10 kV, 15 kV and 20 kV were imposed over the DC bias. All of these three levels of DC voltage showed that as the AC voltage increased, the thickness of the bridge also increases.

4.5.1 INFLUENCE OF 1KV DC BIASED AC

The first row of the Figure 4:21 shows the bridging under influence of 1 kV pure DC electric field to compare the difference. For these tests 1 kV DC was applied with three different levels of AC which were 10 kV, 15 kV and 20 kV. The particles were started to draw closer to the high electric field region. They started to move from one electrode to the other. For one of the voltage combination it was observed that the particles were vibrating all together one side to the other because of the change of polarity.

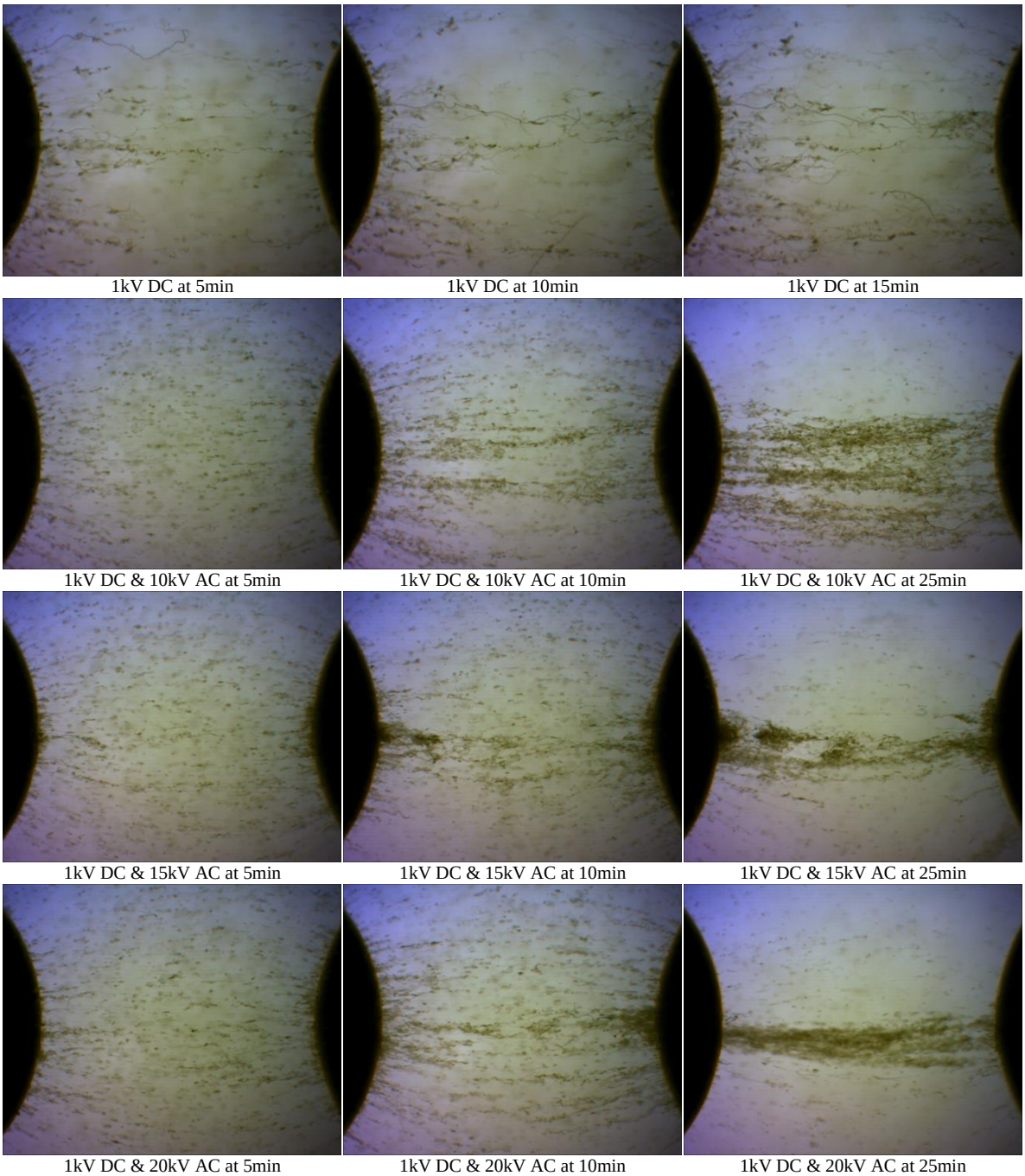

Figure 4:21 Optical microscopic images of particle accumulation in contaminated transformer oil under the influence of combined 1 kV DC and different levels of AC, concentration level 0.024%.

4.5.2 INFLUENCE OF 3KV DC BIASED AC

Figure 4:22 shows the typical observation. The first row of Figure 4:22 shows the result of 3 kV DC electric field. Then the followings rows are the result from 3 kV DC biased with AC voltages which enable us to visualize the difference bridging dynamics as a function of the level of AC voltage. There are many branches of the bridge which were formed within 30s after the 3 kV DC supply was switched on. The thick bridge was formed over a period of 15 min but it was a shallow bridge with

lots of different branches. When the 3 kV DC was combined with 10 kV AC, a very thin bridge was created after 20 minutes and many branches of pressboard particle chain elongated from either side of the electrodes aligned themselves parallel to electric field lines. For 15 and 20 kV AC, complete bridge formed between the electrodes after 10 minutes and 5 minutes respectively. So the particle accumulation and bridging process is much slower in comparison to pure DC electric field.

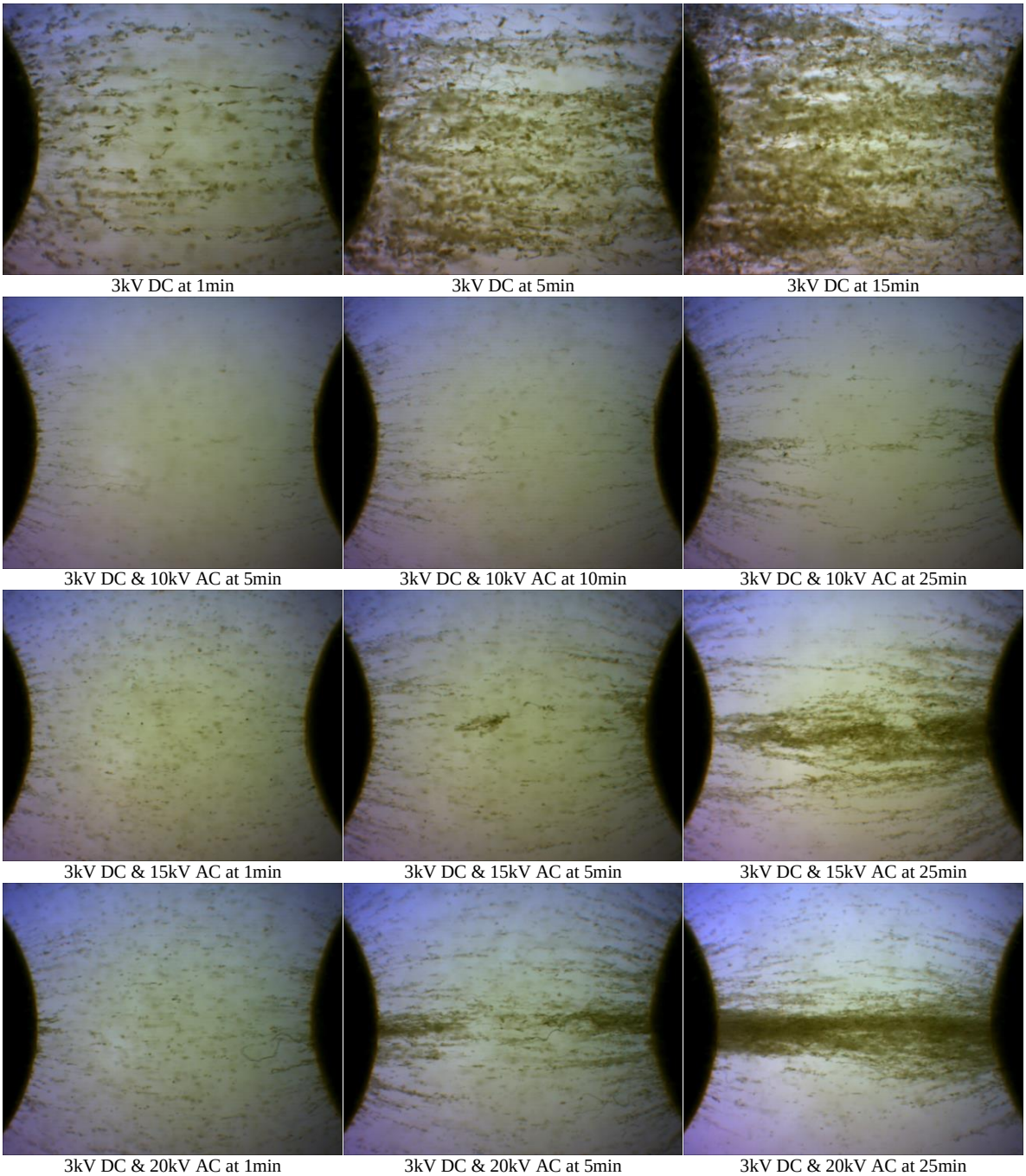

Figure 4:22 Optical microscopic images of particle accumulation in contaminated transformer oil under the influence of combined 3 kV DC and different levels of AC, concentration level 0.024%.

4.5.3 *Pixel Counting Analysis of DC Biased AC Test*

The optical images from above experiments were analyzed using pixel counting technique to determine the particle accumulation with time. Figure 4:23 shows the pixels counts under the influence of 3 kV DC biased with three different levels of AC electric field. The count for 10 kV AC did not increase much which is in line with the images of Figure 4:22. The growth is noticeable for 15 and 20 kV cases. It is worth to notice that the particles accumulation was very slow until around 200 s for 15 and 20 kV. It is probably the time for sufficient number of "active" fibers to arrive to the electrodes surface. After that the growth takes place at constant rate up to the end of the experiments for both cases. The ratio of the slopes is approximately proportional to the applied voltage. It is an indication that the process is quite complex. It is controlled by a combination of the particles migration towards the electrodes, charging of the fibers together with DEP force both of which are proportional to V^2. The particle accumulation (pixel counting) curve had a very fast rise for DC at the beginning on the test then it slows down. But for DC bias AC, the curve has a very slow increment at the beginning and after a while it had a steady increase through the whole test.

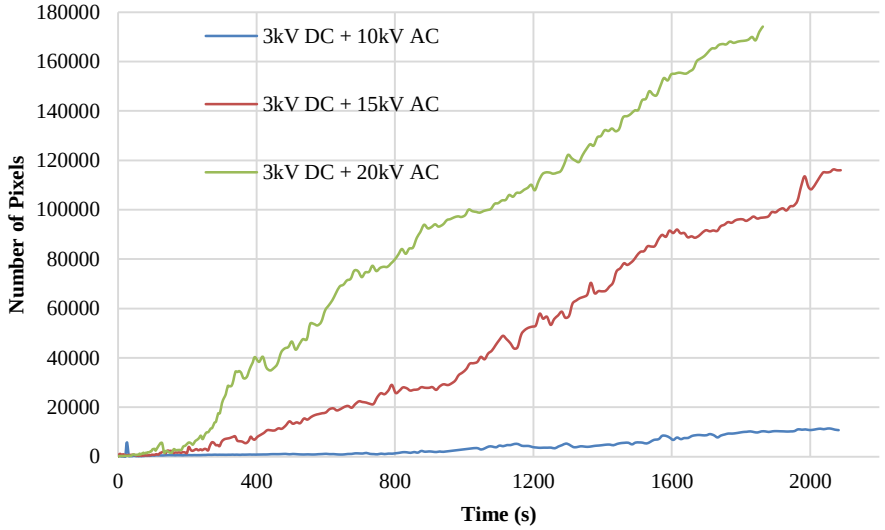

Figure 4:23 Increment of pixels in microscopic images under influence of DC biased AC electric field with 0.024% concentration

4.5.4 *Influence of 6kV DC Biased AC*

There were many branches of bridge were formed within 30 s of turning the 6 kV DC supply. The bridge was forming over a period of 15 min but it was a shallow bridge with lots of different branches which is on the first row of Figure 4:24. When the 6 kV DC was combined with 10 kV AC, the bridge was very strongly bonded. For 15 kV AC, the bond became stronger and more particles joined the bridge than 10 kV. The particles which were on the side of the electrodes were

going to discharge on the other side and eventually attracted to the middle of the bridge. That is how the bond of the bridge became stronger for the higher electric field. These three levels of DC voltage shows that as the voltage increased, the thickness of the bridge also increases. The bridge thickness increased with increment of DC voltage level under fixed AC voltage.

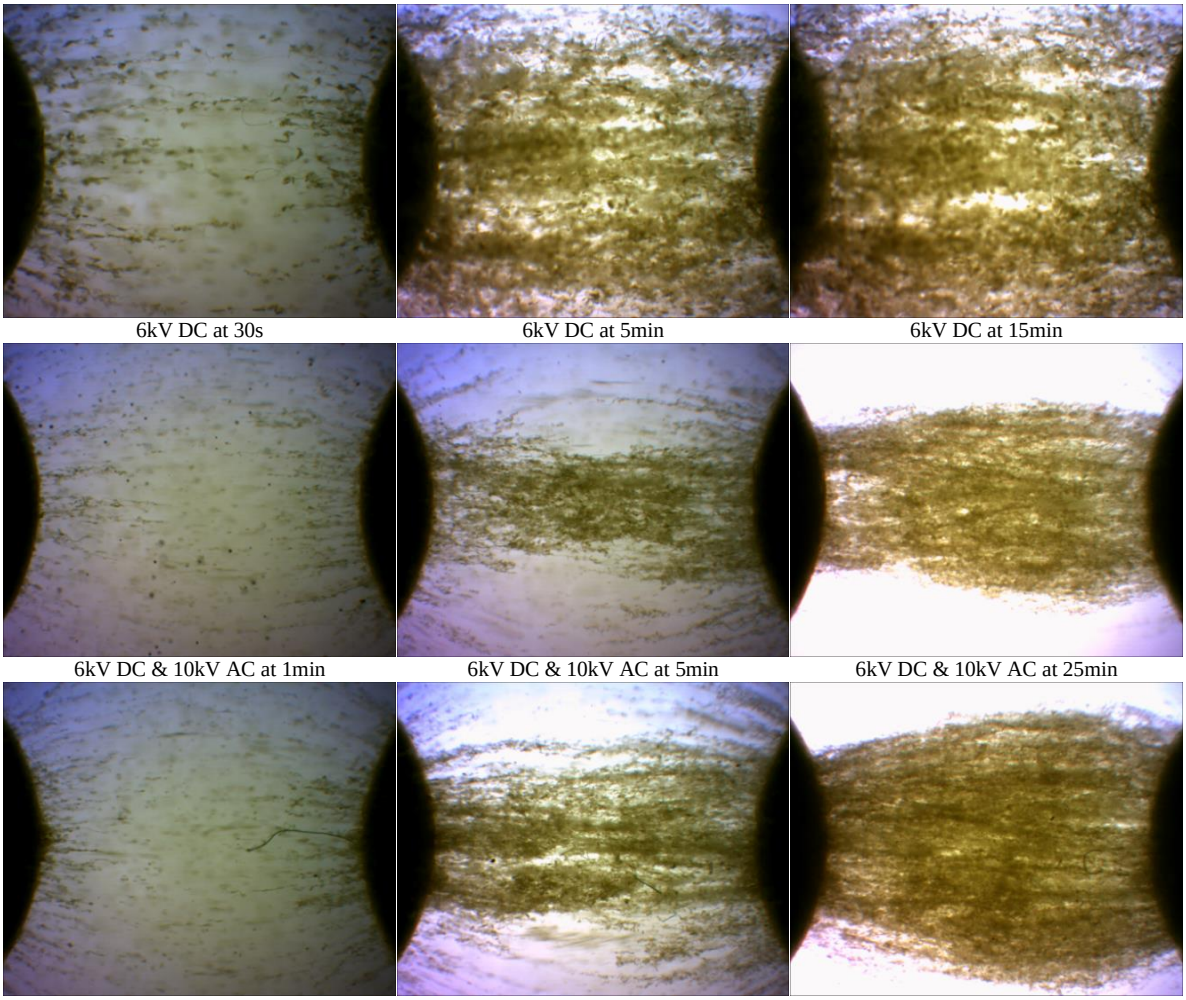

Figure 4:24 Optical microscopic images of particle accumulation in contaminated transformer oil under the influence of combined 6 kV DC and different levels of AC, concentration level 0.024%.

4.5.5 MECHANISM OF DC BIASED AC BRIDGING

To form the bridge the particles have to travel first to the electrodes, get a charge, be detached from the surface, move towards the opposite electrode by Coulomb force and be pushed towards the central line by DEP. It is the DC voltage which dictates the average value of Coulomb force, whereas RMS of DC+AC affect DEP force. It means the addition of AC forces the fibers to stick to the electrodes and only a fraction of fibers can travel between electrodes. So it takes longer for the same number of "active", highly charged fibers to arrive to the electrodes. As the result the bridging dynamics is much slower. But the DEP force is much stronger with AC addition, it pushes fibers to

the central line and makes the bridge much denser. The particles chains which are on either side of the electrodes operate as conductive extensions of the electrodes with new fibers attaching to these chains [83].

4.6 SUMMARY

Bare spherical electrode testes under DC and DC biased AC electric field showed that there was always a complete bridge former between the electrodes. It indicates that charge transfer took place during all the experiments under DC and DC biased AC electric field. However, there were no complete bridge formed with any of the contamination levels tested under AC electric field. Only DEP force was dominating for AC experiments and it enabled the particles to stick on the surface of the both electrodes.

CHAPTER FIVE: COVERED ELECTRODE TEST

All the conductors within each windings and leads are covered by paper insulation in a power transformer [87]. Moreover, between the winding, there are also cellulose based pressboard barrier used to separate them. Hence, it will be very crucial to investigate the similar situation. I have conducted three separate set of electrode arrangements to understand the consequence on pressboard particles. As all the conductors are covered in a real transformer, to replicate the similar scenario, experiments were conducted with kraft paper cover the electrodes to experience similar behaviour. Two types of covered electrodes were tested; loose bonded to the electrode surface and tight bonded electrodes. Further investigations also carried out with a kraft paper barrier placed between the electrodes to replicate the pressboard barrier between the windings. Three different electric fields were tested with three different levels of voltages for each experimental setup.

5.1 TIGHTLY BONDED COVERED ELECTRODE TEST UNDER DC ELECTRIC FIELD

Covered electrode test was conducted under influence of DC electric field with several concentration levels such as 0.001%, 0.002%, 0.003%, 0.006% and 0.008%. Few of the images from 0.001%, 0.003% and 0.006% tests are shown in Figure 5:1 Covered electrode test with 0.001% concentration

, Figure 5:2 and Figure 5:3 respectively. All of these contaminated samples were tested under three voltage levels i.e. 2 kV, 7.5 kV and 15 kV which are on the same levels as bare electrode test with DC electric field.

The pressboard particles started moving back and forth between the electrodes as soon as 2kV was applied to 0.001% contaminated sample. They were charging and discharging from one electrode to the other. They were initially drawing near the electrodes due to DEP force, once they touch the kraft paper covered electrode surface, they acquired charge from the surfaces. The kraft paper is acquiring charge from the electrode surface as it is in direct contact. These charges are accumulating on the paper surface which are ready to be transferred to the fibre particles. As the particles gathered charge, Coulomb force started to repel the particles from the electrodes due to the same polarity. When repelling Coulomb force became greater than attracting DEP force, the particles finally started moving towards the other electrode. A detailed explanation of this process is given in [83]. The fibres started to attach on the paper cover of electrodes after a while. Initially the long fibres were attached to either of the electrodes and then the other small particles started attaching themselves to the elongated fibres. The bridging process started in this fashion and continued to

grow. A very thin bridge formed for 2 kV supply after 230 s. There were few shallow bridges which were created until 900 s.

The movement of the particles along with bridging process intensified when the supplied voltage was increased to 7.5 kV. A complete bridge was formed within 34 s. The bridge between the electrodes were denser than previous test at 2 kV. The bridging process continued for 900 s whereas no significant change observed.

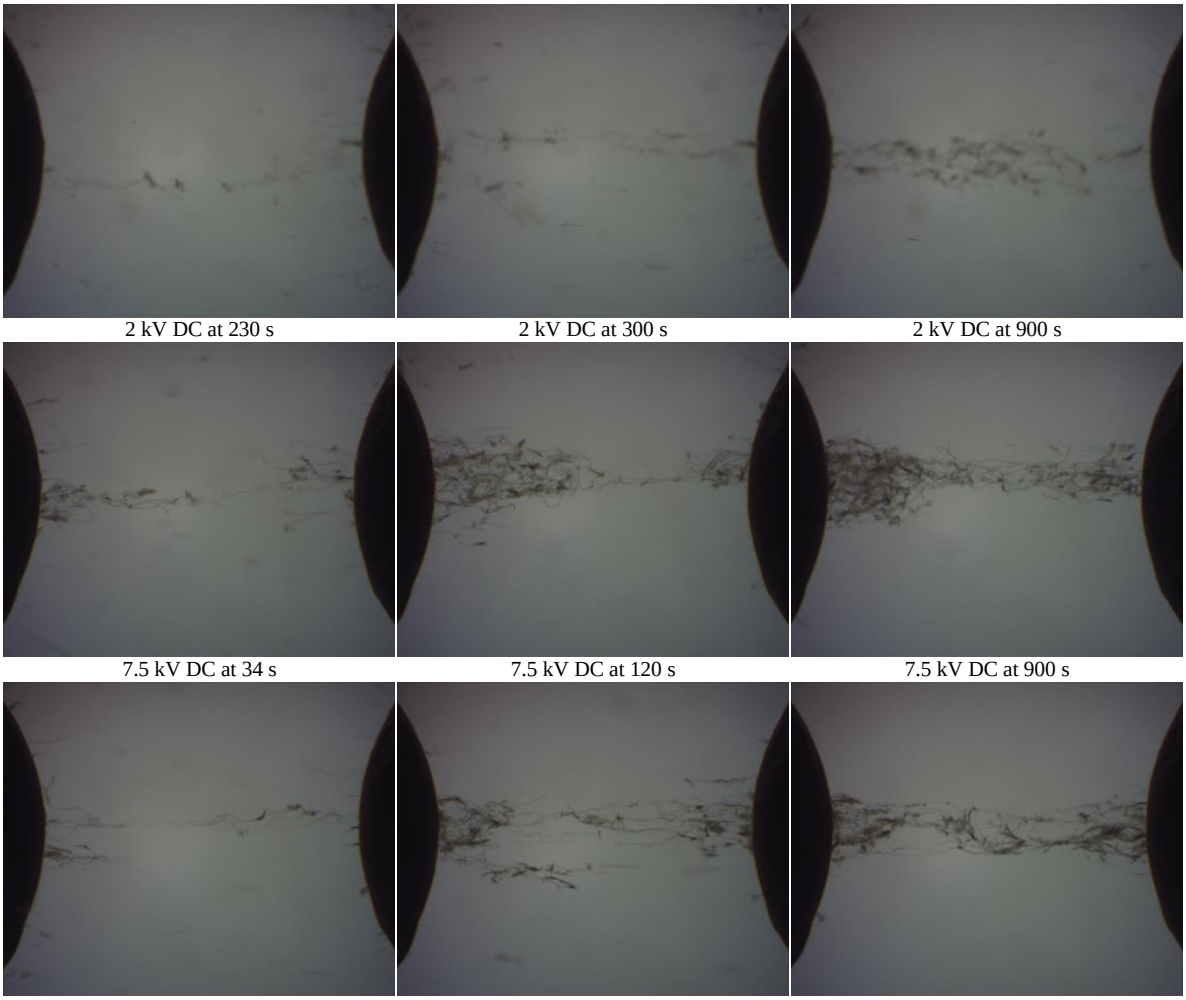

Figure 5:1 Covered electrode test with 0.001% concentration

The particles were moving between the electrodes more violently after the 15 kV supply turned on. It took only 6s to form the first thin bridge. The bridge became more strongly bonded and the thickness on the bridge was narrower in the middle and broadened towards the surface of the electrodes. Almost all the particles near the vicinity of the electrodes were drawn in to the bridge within 300s.

After applying 2 kV voltage to the sample with 0.003% concentration, there were very slow movement observed in the tank (Figure 5:2). Fibre particles were drawing near to the electrodes due to DEP force. Then the fibres started to attach on the paper cover of electrodes. Bridging process always starts with long fibres. They attach to either of the electrodes first and then the other small particles started attaching themselves to the elongated fibres. For 2 kV supply, after 50 s a very thin bridge formed. There was a shallow bridge created until 600 s whereby no obvious change to the bridge found. The movement of the fibers was intensified when the supplied voltage was increased to 7.5 kV. It took only 20 s to form a complete bridge. The bridging process continued for 300 s. This time the bridge was thicker.

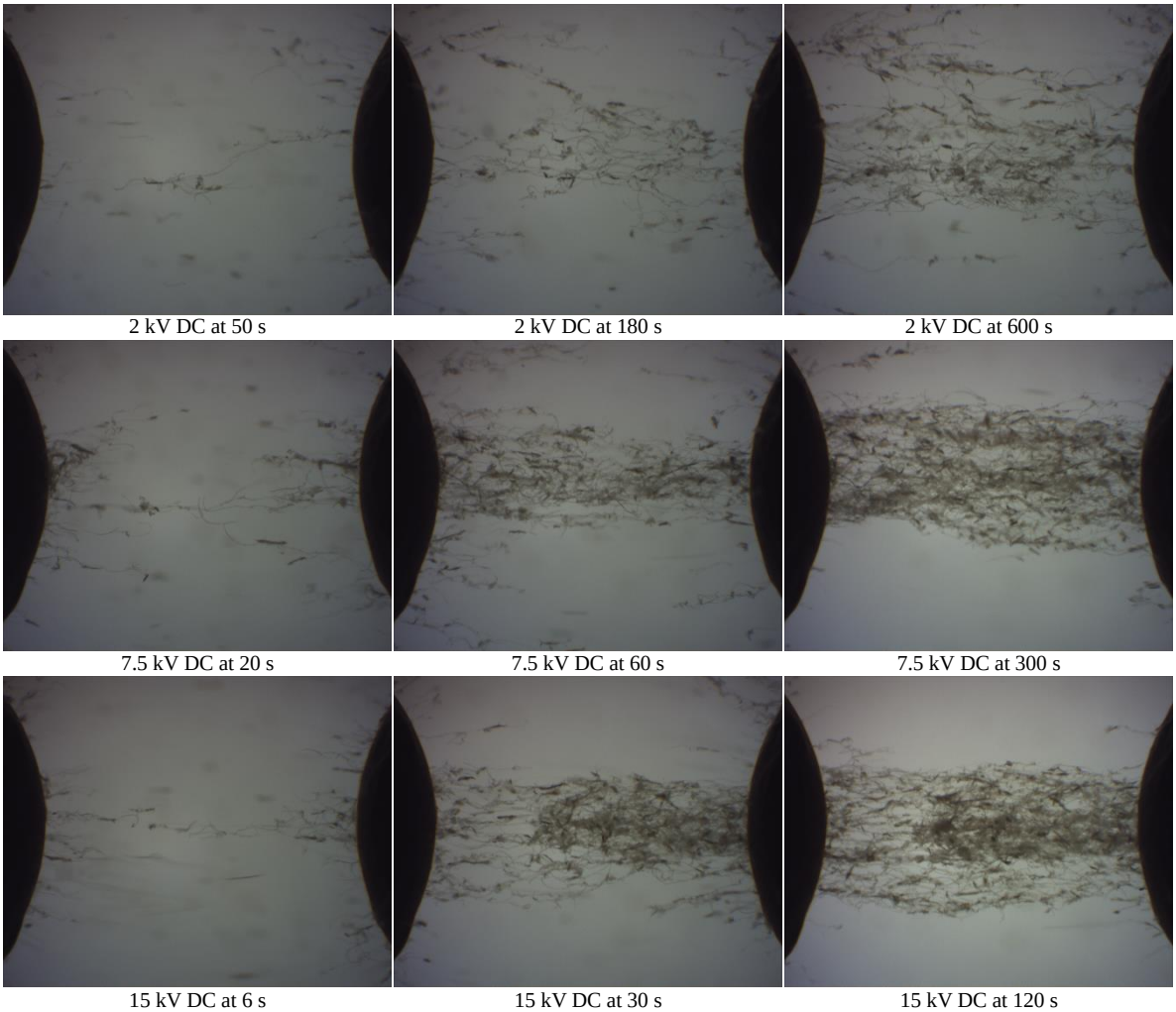

2 kV DC at 50 s | 2 kV DC at 180 s | 2 kV DC at 600 s

7.5 kV DC at 20 s | 7.5 kV DC at 60 s | 7.5 kV DC at 300 s

15 kV DC at 6 s | 15 kV DC at 30 s | 15 kV DC at 120 s

Figure 5:2 Covered electrode test with 0.003% concentration

The particles were aggressively moving towards the electrodes after the applied voltage of 15 kV. The first thin bridge was formed only within 6s. Almost all the particles near the vicinity of the electrodes were drawn towards the bridge within 120s. The bridge did not have any noticeable change after that time.Images from the 0.006% contaminated transformer oil test under influence of

DC electric field are shown in Figure 5:3. The process of bridging were similar to the previously described tests. Only difference was the amount fibres taken part to form the bridge were a lot more than the previous which we would be normally expecting as the contamination level became doubled.

The overall bridging dynamics are similar to bare electrodes experiments for all the experiments conducted on tightly bonded covered electrode system. The density of the bridge for covered electrodes are less than bare electrodes. The time to form the bridge is slower than bare electrode system. As the voltage level increased, the bridge thickness also increased for the same concentration level. The particles accumulation and the bridge thickness increased with contamination level which was also the case for bare electrode experiments.

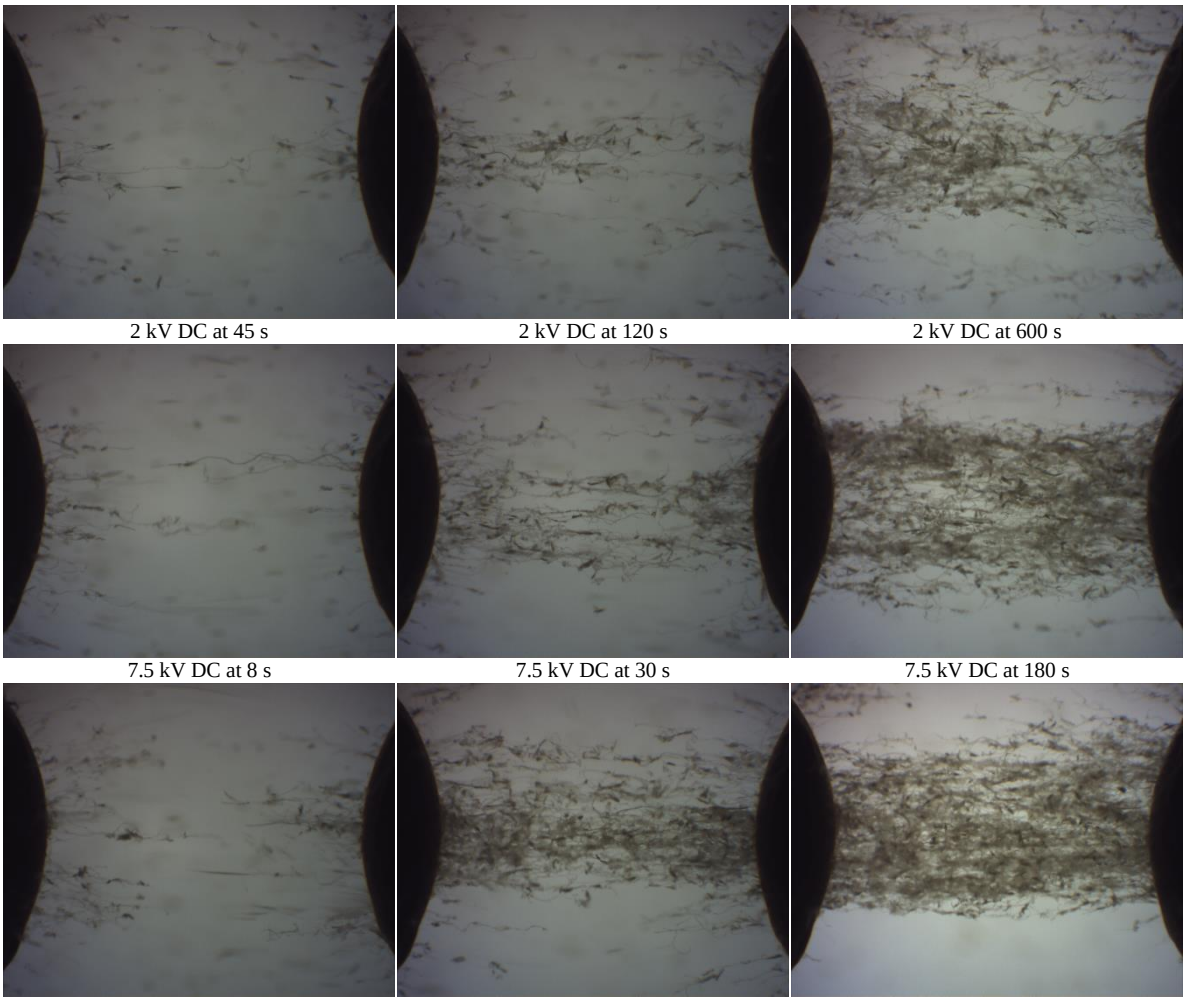

Figure 5:3 Covered electrode test with 0.006% concentration

5.1.1 *Conduction Current Comparison for different contamination level*

Conduction currents were also recorded during all the DC tests for covered electrodes. The conduction currents for two contamination levels under the influence of three different voltage levels are shown in Figure 5:4. As soon as the voltage was applied, there was a high polarization current observed in most of the experiments which was also observed for bare electrode system (see Figure 4:9). After that the slow growing current was established after a while for lower voltage level i.e. 2 kV and 7.5 kV. However, for 15 kV, the current initially increased and slowly decreased to a steady state with time. The existence of the current even before the bridge formed can be explained by charging of the particles at the electrodes and transfer the charge across. The currents were then gradually increased until a complete thick bridge formed. It is clear based on conduction current results that charge transportation is taking place through the pressboard particles under DC electric field.

The currents were almost steady after the bridge formed which was also observed for bare electrodes. The thickness of the bridge and the bond between the particles were the main determining factor for the conduction currents after this time. Although the bulk conductivity of the pressboard is several hundred times less than the transformer mineral oil, the high fiber surface conductivity allows the pressboard fibers to transfer a charge over the outer surface. The magnitude of the currents increased a great deal with the increment of contamination level from 0.001% to 0.003%. The conduction currents for all the voltage levels increase with the contamination levels. The increment ratio of currents for two levels of contaminated particles were almost similar by visual inspection.

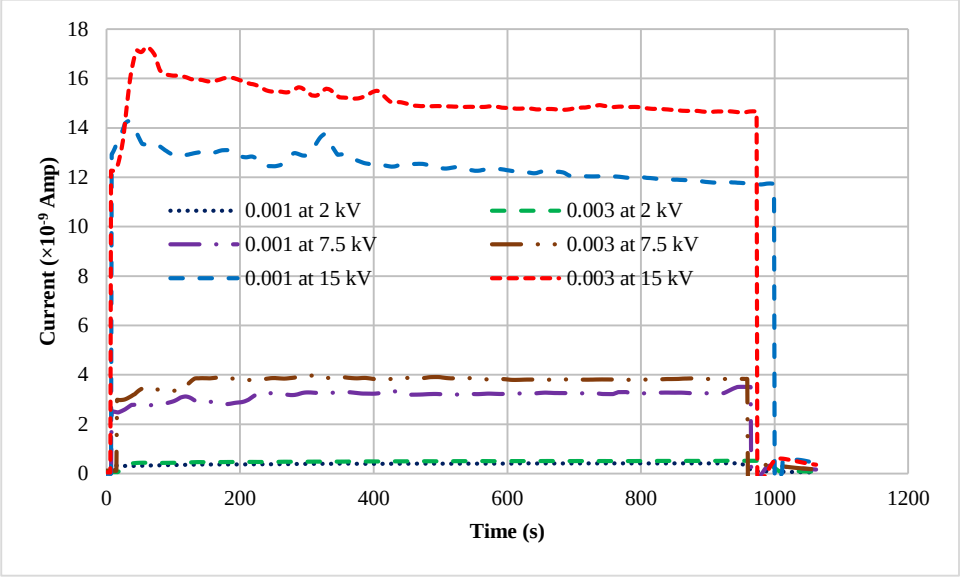

Figure 5:4 Conduction current comparison under influence of different levels of DC voltages with 0.001% and 0.003% contaminated transformer oil

5.2 COVERED ELECTRODES TEST UNDER AC ELECTRIC FIELD

There was three different levels of AC voltages investigated i.e. 10 kV, 15 kV and 20 kV. The kraft paper cover was tightly bonded to the electrode surface for all these test carried with AC electric field. Several level of contaminated samples were tested i.e. 0.001%, 0.002%, 0.003%, 0.006%, and 0.008%.

5.2.1 COVERED ELECTRODE TEST WITH 10 KV AC

The particles did not have much movement after the 10 kV applied to the samples. As time elapsed very slowly some particles started to move towards both electrodes. The overall motion of the particles was much slower than the bare electrode system. There was not many particles attached to the electrodes for lower contamination level and it was increased with higher contaminated sample as shown in Figure 5:5. Overall particles accumulations on the electrode surfaces was decreased compared to bare electrode system. The DEP force was reduced by the kraft paper and hence particles movement.

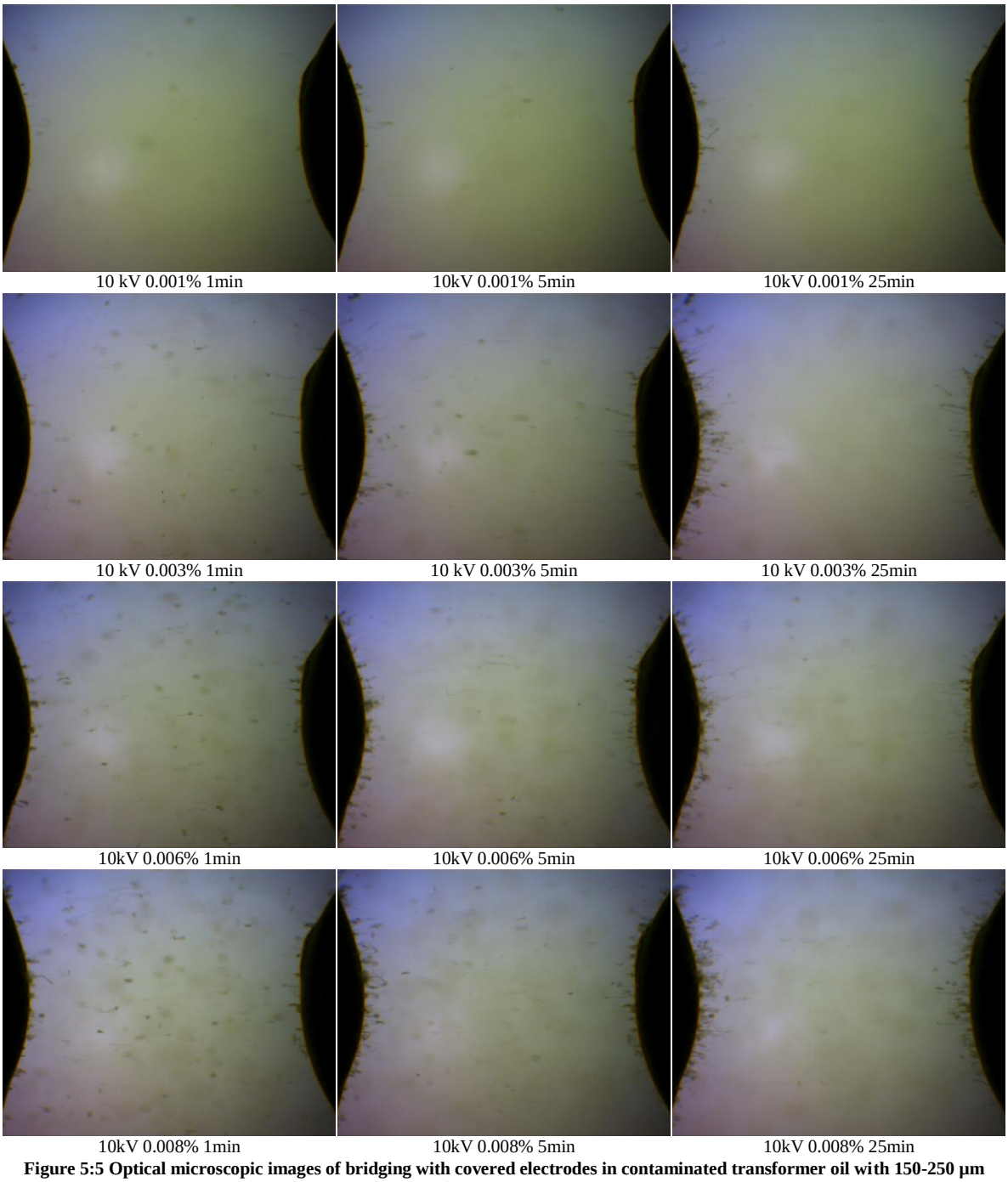

Figure 5:5 Optical microscopic images of bridging with covered electrodes in contaminated transformer oil with 150-250 µm pressboard fiber, applied voltage 10kV.

5.2.2 COVERED ELECTRODE TEST WITH 15KV AC

When the applied voltage increased to 15 kV, the particle movement started to increase a bit. The particle accumulation towards the surface of the covered electrodes increased with higher electric field as the DEP force is stronger. There was not a great deal of difference in particles accumulation observed for 0.003%, 0.006% and 0.008% as shown in Figure 5:6. It might be due to the long-time

taken to bring the particles to the electrode-surfaces under the influence of DEP force. The gravitational force on the particles bringing the other particles in the vicinity of the electrodes down.

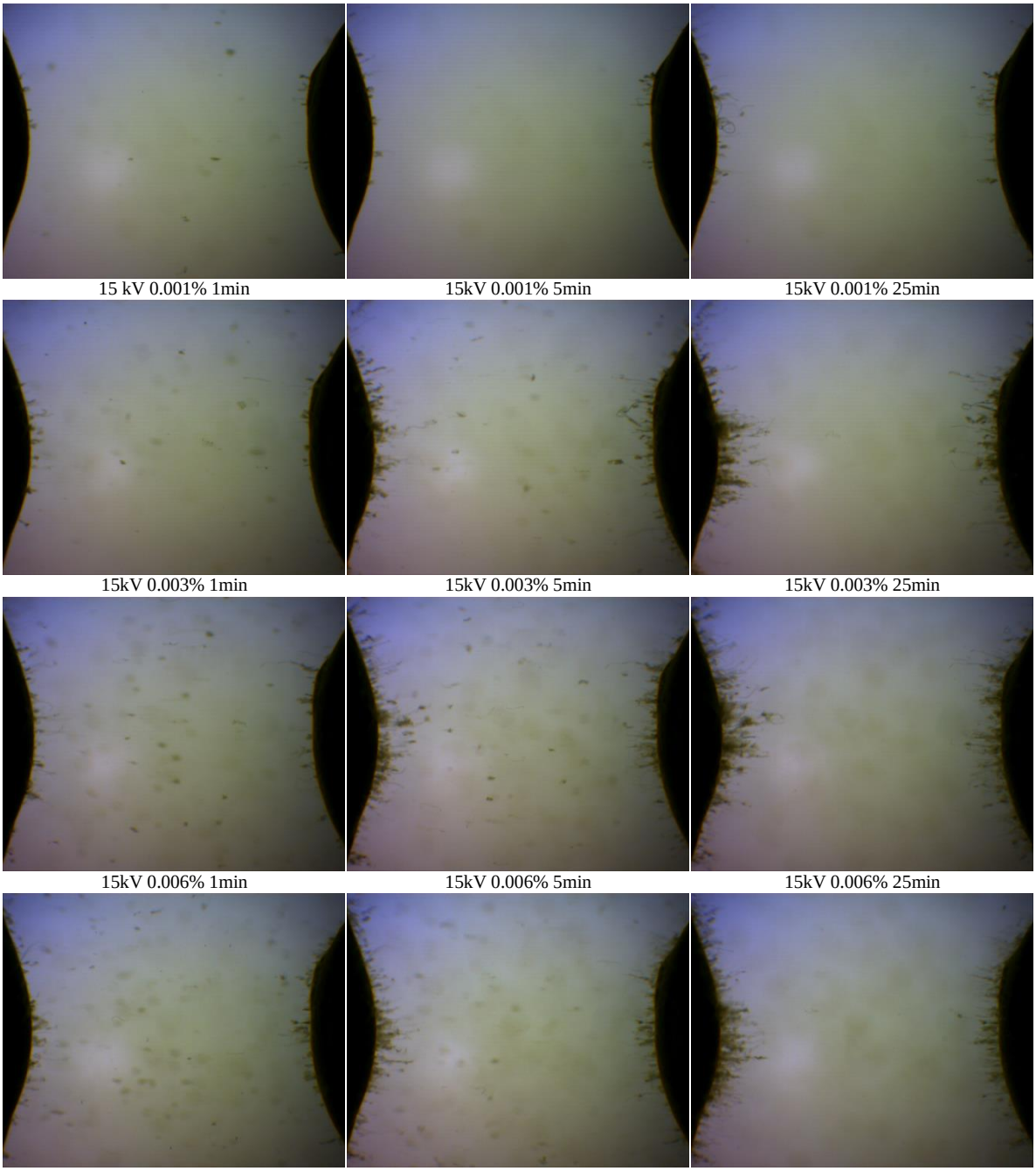

Figure 5:6 Optical microscopic images of bridging with covered electrodes in contaminated transformer oil with 150-250 µm pressboard fiber, applied voltage 15 kV.

5.2.3 COVERED ELECTRODE TEST WITH 20KV AC

The fibre particles were moving faster with 20 kV applied voltage. The overall particle accumulation was higher than previous test as expected with higher DEP which is shown in

Figure 5:7. The current was not recorded for any of the AC test with covered electrode as the current from bare electrode test with AC did not have significant changes.

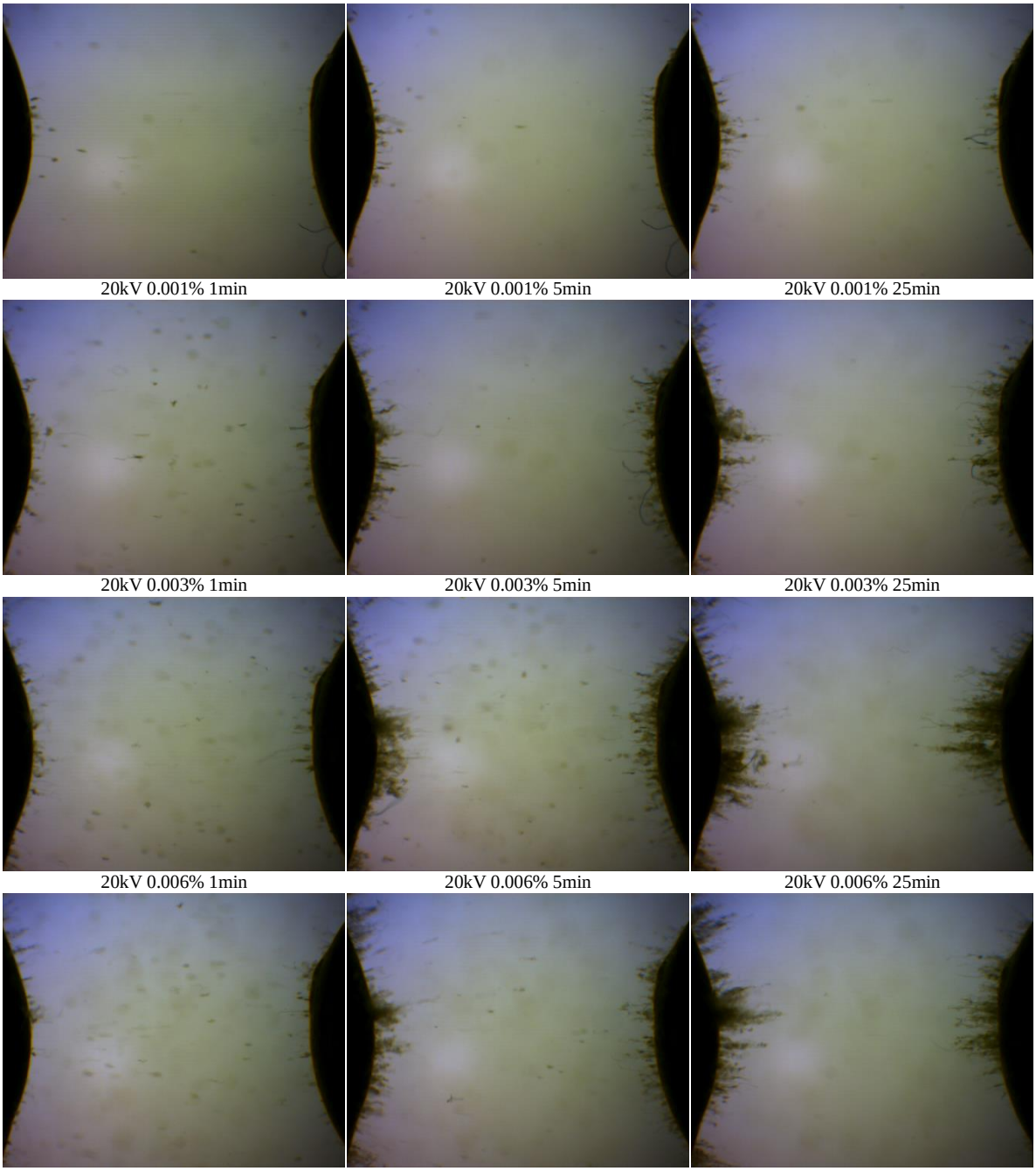

Figure 5:7 Optical microscopic images of bridging with covered electrodes in contaminated transformer oil with 150-250 µm pressboard fiber, applied voltage 20 kV.

5.3 COVERED ELECTRODE TEST UNDER DC BIASED AC ELECTRIC FIELD

Three different DC offset levels investigated at 1 kV, 3 kV and 6 kV with particle size of 150 – 250 µm. The AC voltage of 10 and 15 were imposed over the DC bias. All of these three levels of DC voltage showed that as the AC voltage increased, the thickness of the bridge also increases.

5.3.1 INFLUENCE OF 1 KV DC BIASED AC

Images from 1kV DC biased with 10 kV and 15 kV AC are shown in Figure 5:8. The first row shows the result of purely 1 kV DC electric field. Then the followings rows are the result from 1 kV DC biased with AC voltages which enable us to visualize the difference bridging dynamics as a function of the AC voltages.

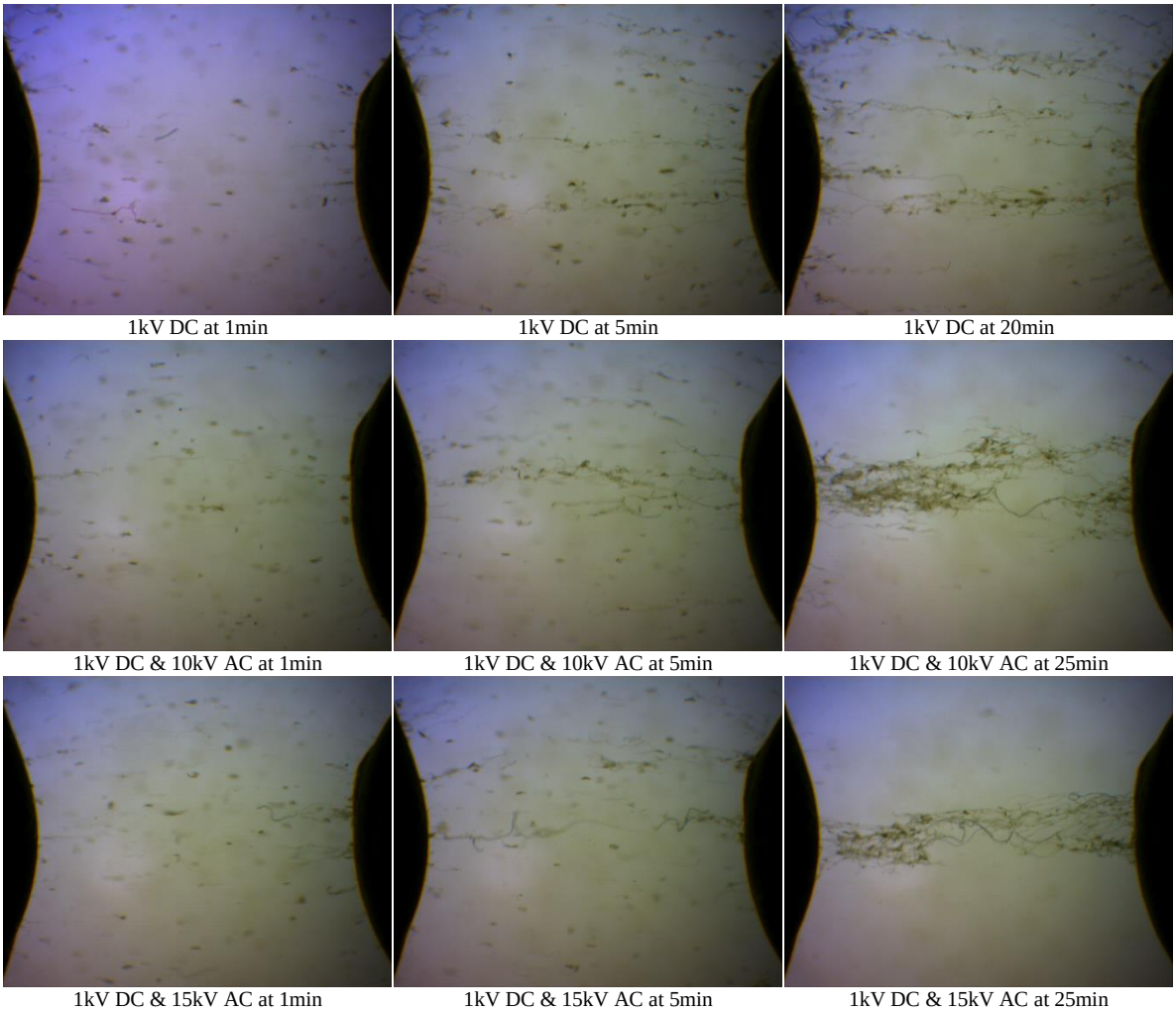

Figure 5:8 Optical microscopic images of particle accumulation with covered electrodes in contaminated transformer oil under the influence of combined 1 kV DC and different levels of AC, concentration level 0.024%.

There are two branches of very thin bridge were formed within 5 min after the 1 kV DC supply applied. A very shallow bridge with barely three branches formed over a period of 15 min. When

the 1 kV DC was combined with 10 kV AC, a thin bridge was created after 5 min. As time progressed, a complete thicker bridge was observed after 25 min. For 15 kV AC, complete bridge formed between the electrodes after 5 min. The particle accumulation and bridging process is much slower in comparison to bare electrodes with same conditions. This indicates the extra time required for charge transfer through the paper.

5.3.2 INFLUENCE OF 3 KV DC BIASED AC

Figure 5:9 shows the images from 3 kV DC biased AC tests.

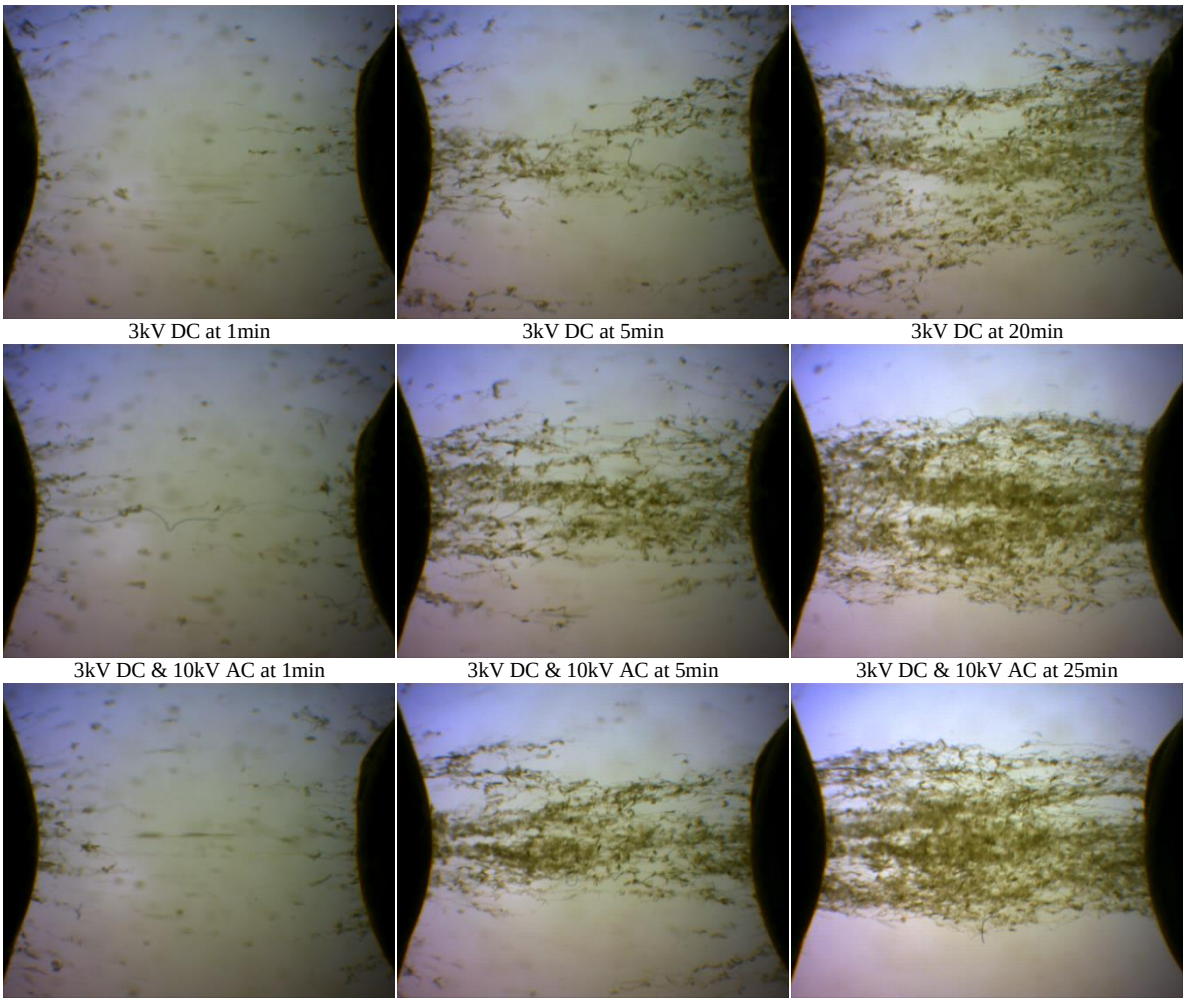

Figure 5:9 Optical microscopic images of particle accumulation with covered electrodes in contaminated transformer oil under the influence of combined 3 kV DC and different levels of AC, concentration level 0.024%.

The first row shows the result of pure 3 kV DC electric field. Then the followings rows are the results from 3 kV DC biased with AC experiments. There are many branches of the bridge which were formed within few minutes after the 3 kV DC supply was switched on. A wide-spread bridge was formed over a period of 20 min but the particles were not densely populated. When the 10 kV AC was combined, a very thin bridge was created after few minutes. Many branches of pressboard

particle chain elongated from either side of the electrodes aligned themselves parallel to electric field lines after 5min. A very thick complete bridge formed between the electrodes after 25 minutes.

5.3.3 INFLUENCE OF 6 KV DC BIASED AC

Figure 5:10 shows the result of 6 kV DC electric field on its first row. Then the subsequent rows are the result from 6 kV DC combined with AC voltages. There are many branches of the bridge which were formed within 1 min after the supply was switched on. The thick bridge was formed over a period of 20 min. It was a shallow bridge with lots of different branches. When the 6 kV DC was combined with 10 kV AC, a very thin bridge was created after 20 minutes and many branches of pressboard particle chain elongated from either side of the electrodes aligned themselves parallel to electric field lines.

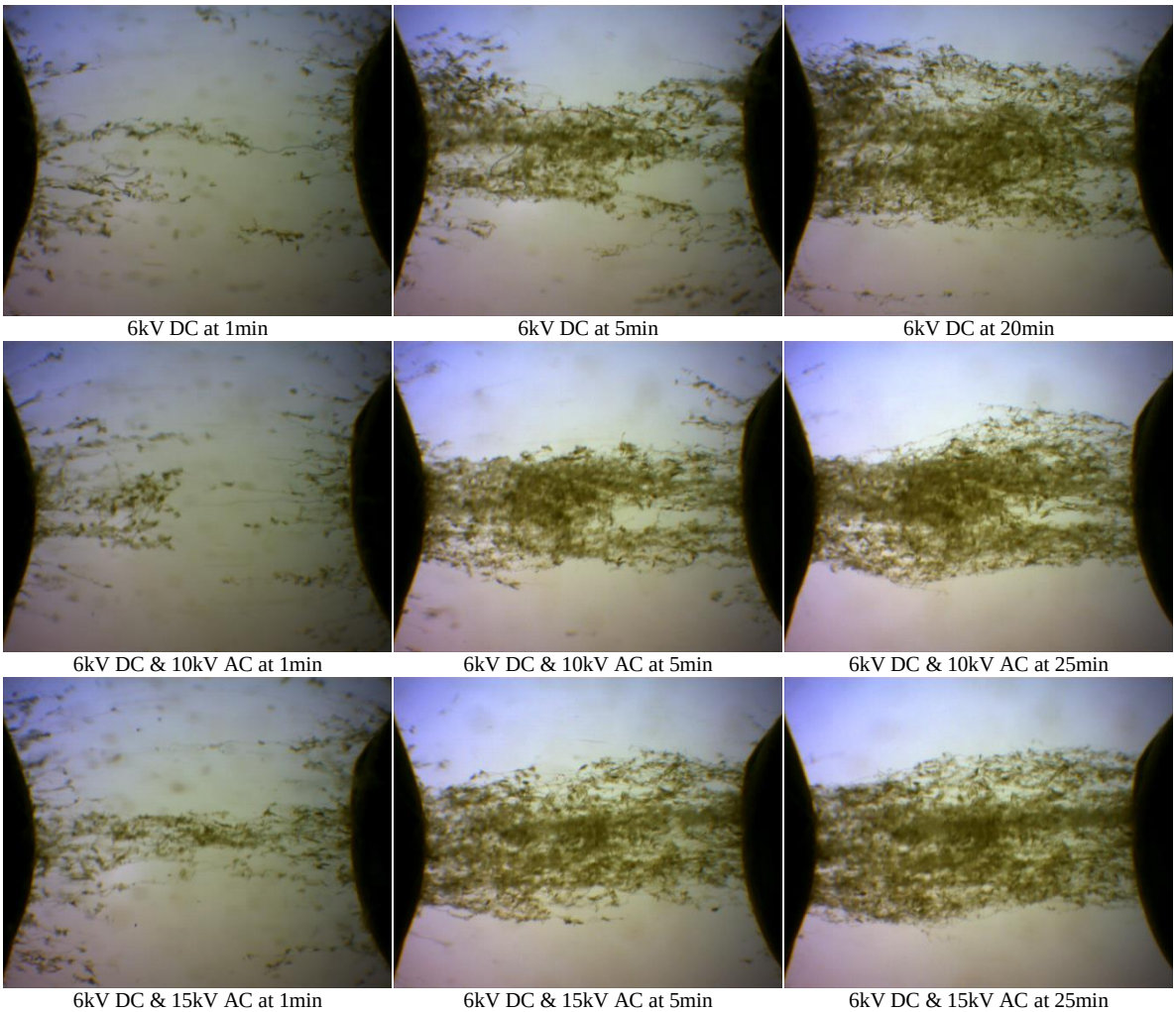

Figure 5:10 Optical microscopic images of particle accumulation with covered electrodes in contaminated transformer oil under the influence of combined 6 kV DC and different levels of AC, concentration level 0.024%.

For 15 kV AC, a complete bridge formed between the electrodes within less than 1 minute and it continued to grow until 25 min whereby a very thick and densely populated bridge was observed.

The bridging mechanism could be explained similar to bare electrode system with exception to the charge transfer via kraft paper cover. To form the bridge the particles have to get a charge by travelling first to the covered electrodes surfaces driver by DEP force. Then it has to be detached from the electrodes surface by acquiring enough charge which penetrated throw the kraft paper surface which give rise to electrostatic force for overcoming the attractive DEP force. At this point the particle will move towards the opposite electrode by Coulomb force and be pushed towards the central line by DEP force. The average value of Coulomb force is dictated by the DC voltage, whereas RMS of DC+AC affects DEP force. It means the addition of AC forces the fibers to stick to the electrodes and only a fraction of fibers can travel between electrodes. Thus it takes longer time for the same number of "active", highly charged particles to arrive to the electrodes. The added problem comes from the kraft paper cover on the electrode surface which made even difficult to get charged. This explains why bridging dynamics is much slower. The DEP force is much stronger with AC addition, it pushes fibers to the central line and makes the bridge much thicker than pure DC voltage.

5.4 KRAFT PAPER BARRIER BETWEEN ELECTRODES

These experiments were carried out to investigate the effect of a paper barrier on the bridge formation under the influence of DC electric field. Pressboard barriers are normally used in between the windings in a transformer to strengthen the insulation and to make the structure mechanically strong. The kraft paper used as a barrier for this test was same as covered electrode experiments. Ideally, a pressboard should have been used for this experiment, but it would need higher voltage to creat a bridge. The effect of a same thickness barrier would also give a comparable result in terms of charge transfer with covered electrode test under same levels of DC electric field.

5.4.1 PAPER BARRIER TEST UNDER THE INFLUENCE OF DC ELECTRIC FIELD WITH 0.001% CONCENTRATION

Images from DC experiments of 0.001% contaminated transformer oil has shown in Figure 5:11. The cellulose fibres started moving closer the electrode surfaces as soon as 2 kV supply was applied to the sample due to DEP force. The particles were then getting charged by touching the bare electrodes. When the particles had enough charge to generate electrostatic repulsive force greater than attractive DEP force, they took off from the surface and started going toward the other electrode. Once the particles reaches to the mid-point, they hit the paper barrier. The kraft paper then get the charge from particles. As the charges coming from both side to the paper barrier which are with different polarity, this gives rise to high electric field and the charge passes through the paper barrier. After a while some particles start to attach on the electrodes surfaces and on both

sides to the paper barrier. The initial bridging process starts with a longer fibre attached to the electrodes and barrier surfaces. Afterwards, they progress towards each other until they touch each other to make complete bridge between the electrodes and paper barrier. Other small particles attracted towards the long fibres. The bridge grows in this way from both electrodes to the paper wall. A thin complete bridge formed to both side of the barrier after 180 s and it continued to grow thicker until 900 s as shown in Figure 5:11.

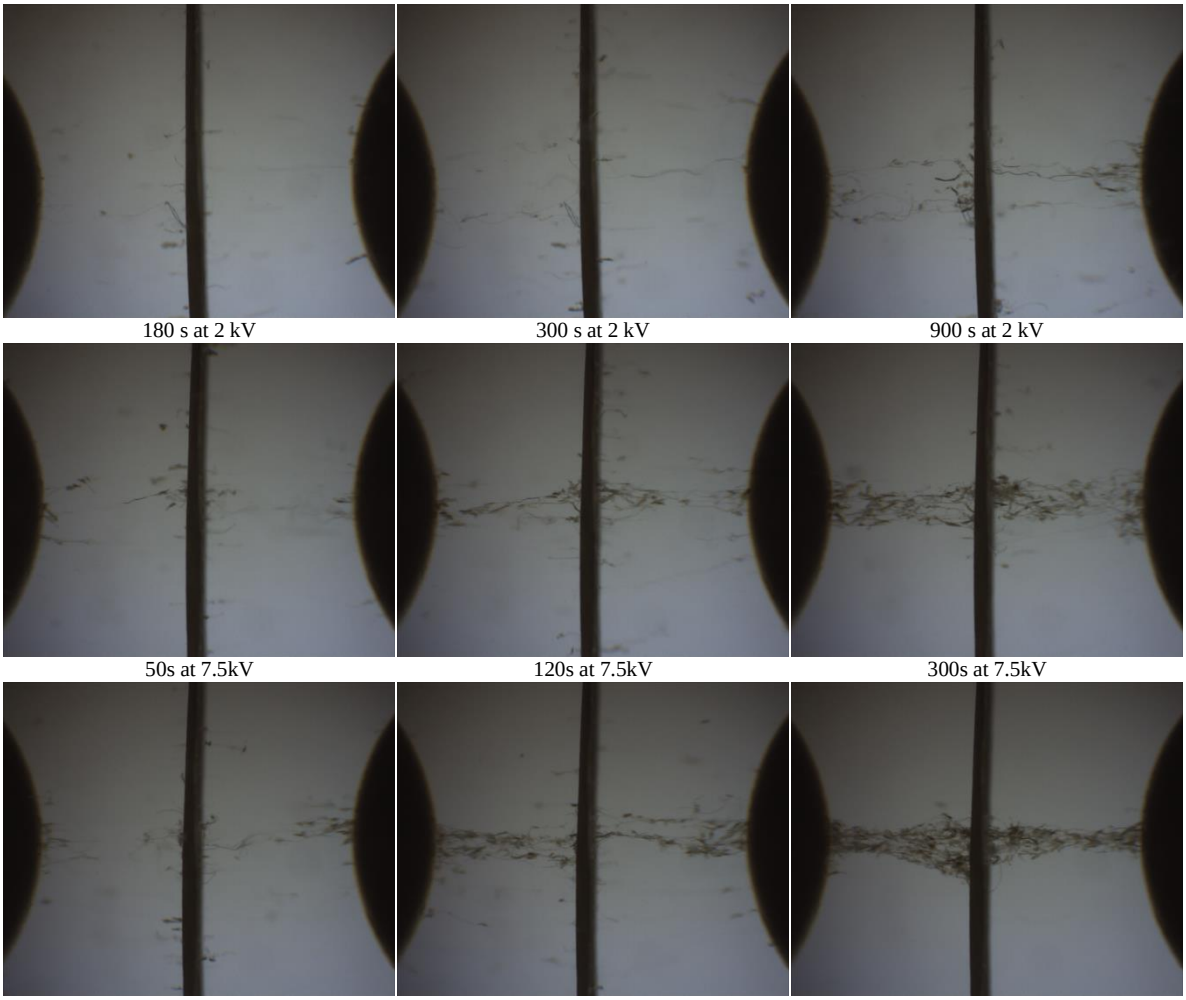

Figure 5:11 Optical microscopic images of particle accumulation with paper barrier in contaminated transformer oil under the influence of different levels of DC electric field, concentration level 0.001%.

After applying 7.5 kV DC, the pressboard fibres movement became quicker. The charging and discharging process were intensified. The first complete bridge was observed after 50s. The particle accumulation to the bridge continued until 300 s.

The particle movement was increased rapidly for 15 kV test. A very thin bridge was formed within 30s from either side of the barrier. The bridge continued to grow thicker until 300 s. There was no apparent change observed after this point.

Conduction currents for the 0.001% contaminated transformer oil are shown in Figure 5:12. A high polarization current was observed for all the voltage levels tested. Then current slowly increased to their saturation levels. The conduction currents for 2 kV and 7.5 kV were flat and smooth when they became stabilized. The current for 15 kV were always fluctuating. The reason for this might be related to some particles still moving back and forth which might have increased and decreased the current.

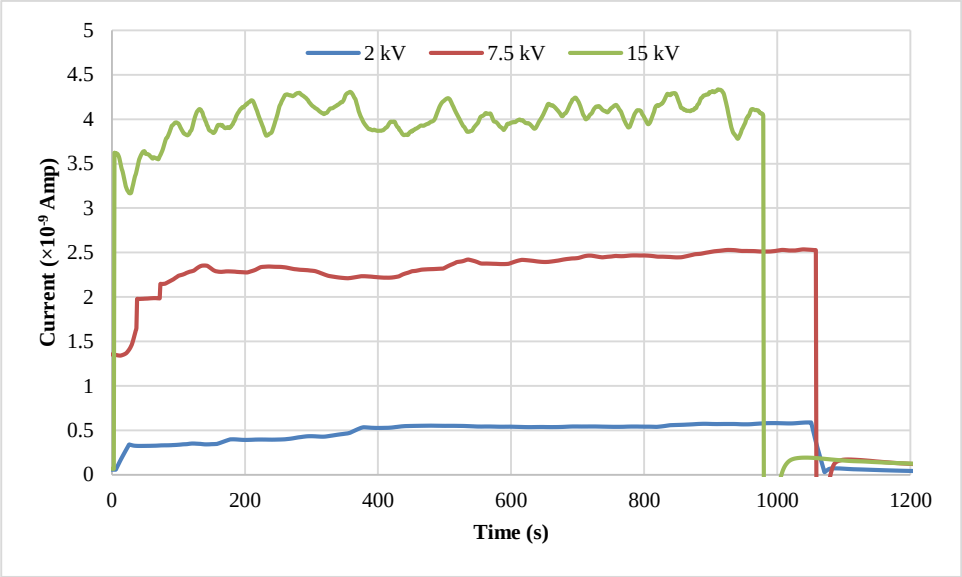

Figure 5:12 Conduction current for paper barrier test under different levels of DC electric field with 0.001% contaminated transformer oil

5.4.2 Paper Barrier Test under the Influence of DC Electric Field with 0.002% Concentration.

Images from 0.002% contaminated test are shown in Figure 5:13. The particles started moving back and forward as soon as 2 kV was applied. After 130 s, a thin complete bridge formed on both side of the barrier and it continued to grow thicker until 900 s.

When the applied voltage was increased to 7.5 kV, the fibres started moving quicker. A thin complete bridge was created within 18 s. The bridge continued to grow thicker until 600 s. There was no significant change observed after that.

The particle accumulation process was intensified for 15 kV. A thin complete bridge was formed within 6 s from either side of the barrier. The bridge continued to grow thicker until 600 s. There was no apparent change observed after this time.

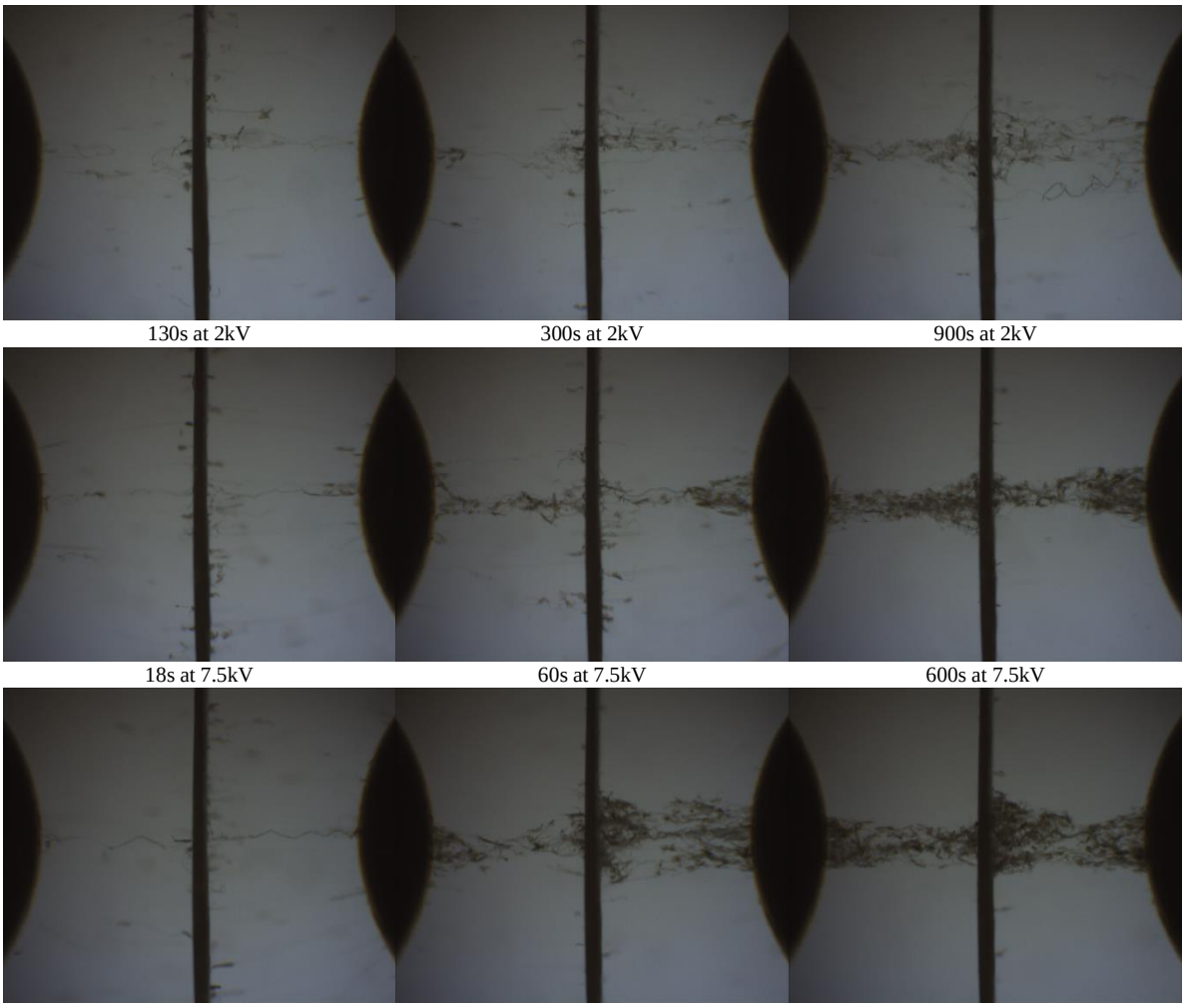

Figure 5:13 Optical microscopic images of particle accumulation with paper barrier in contaminated transformer oil under the influence of different levels of DC electric field, concentration level 0.002%.

Conduction currents for paper barrier experiment under DC electric field are shown in Figure 5:14. The magnitude of the currents for all voltage levels are higher than the previous test which might can be explained as the final thickness of the bridge for all voltage levels were greater than 0.001% test. The thickness and density of particles in a bridge also had determinant factor for higher current for bare and tightly bonded covered electrode test under DC electric field. There is a decline of current observed after 200 s for 15 kV. This is believed to be due to the increment of temperature.

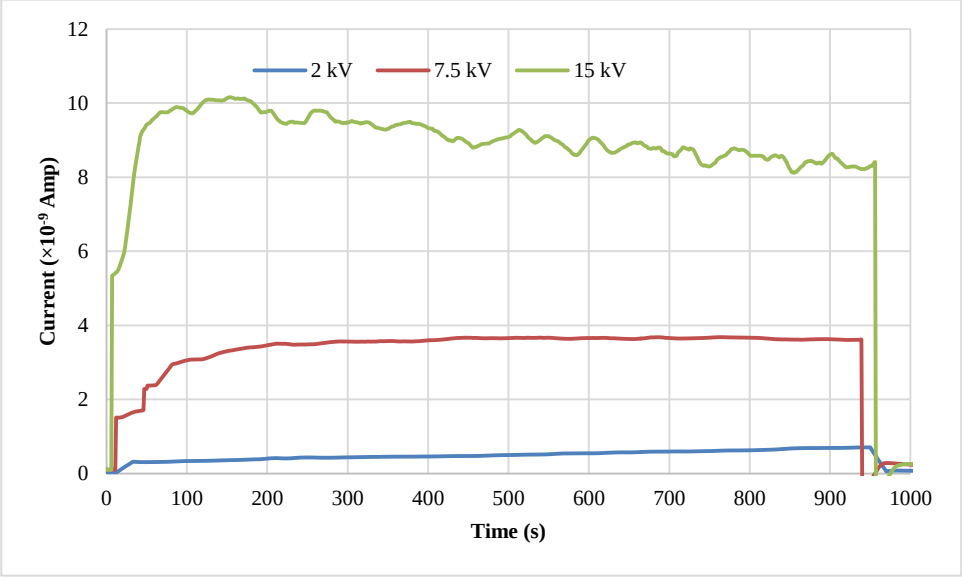

Figure 5:14 Conduction current for paper barrier test under different levels of DC electric field with 0.002% contaminated transformer oil

5.4.3 Paper Barrier Test under the Influence of DC Electric Field with 0.003% Concentration.

The cellulose fibers started moving back and forward as soon as 2 kV was applied. After 60 s, a thin complete bridge formed on both sides of the barrier and it continued to grow thicker until 600 s as shown in Figure 5:15.

The pressboard fibers started moving more quickly after applying 7.5 kV DC. For the 2nd observation within 20 s without any significant change the bridge continued to grow thicker until 300s.

The particle movement was intensified for 15kV. This time the same bridge was formed within 10s from either side of the barrier with no changes until 180s.

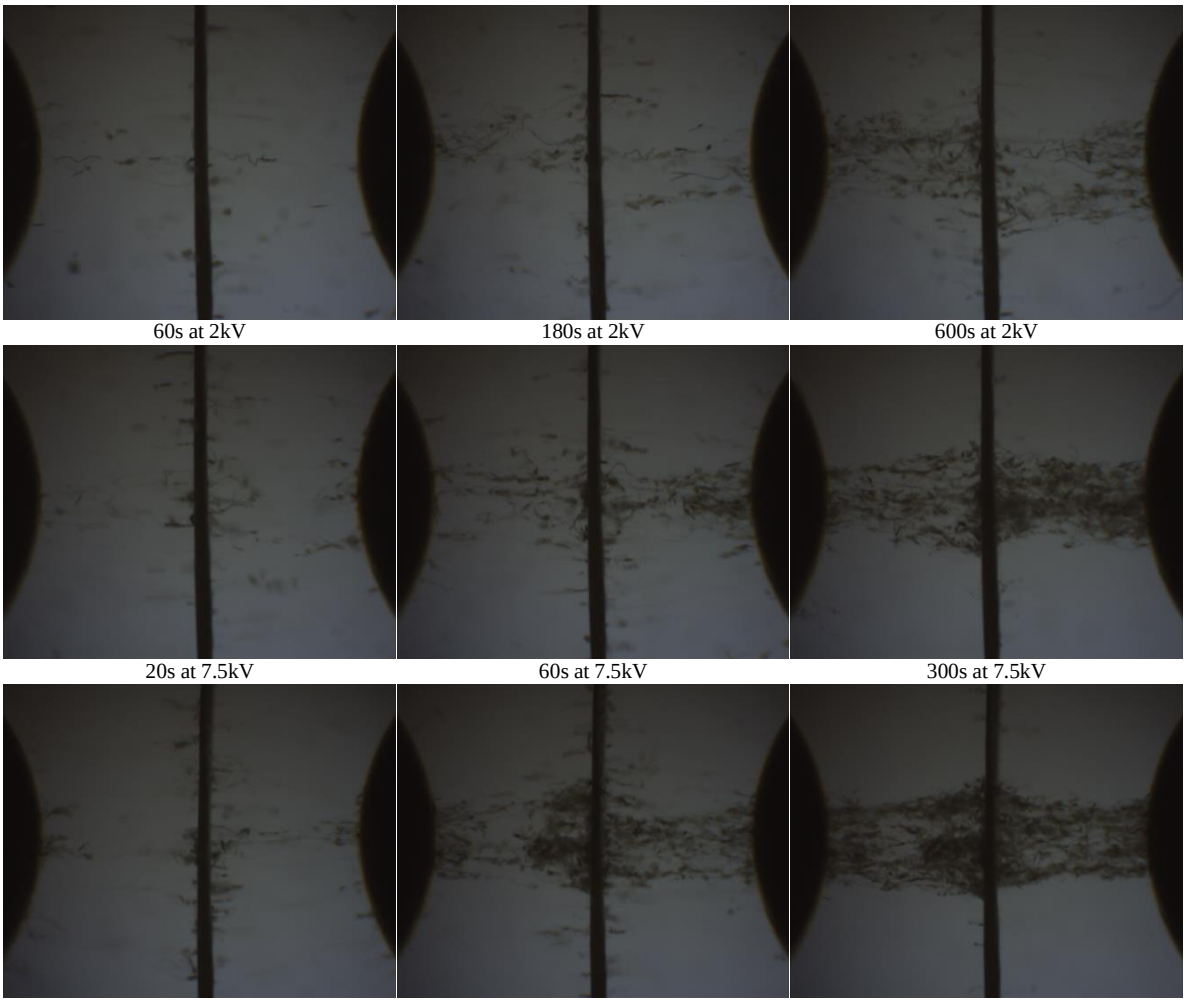

Figure 5:15 Optical microscopic images of particle accumulation with paper barrier in contaminated transformer oil under the influence of different levels of DC electric field, concentration level 0.003%.

Conduction currents for paper barrier experiment under DC electric field with 0.003% contamination are shown in Figure 5:16. All the conduction current for this test were increased significantly than the previous two tests.

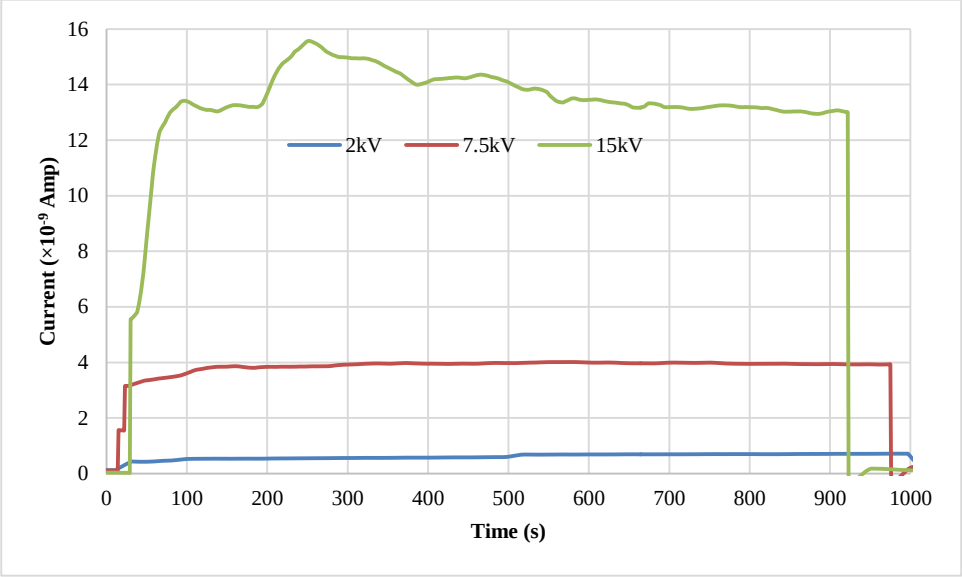

Figure 5:16 Conduction current for paper barrier test under different levels of DC electric field with 0.003% contaminated transformer oil

5.4.4 Current Comparison of All Concentration Levels

The conduction currents under the influence of 15kV DC electric field are shown in Figure 5:17. The lowest current in the graph is for clean oil with the paper barrier inserted and rest of them are with different contaminant levels. All the contamination levels had a similar trend of conduction current. The currents increased almost linearly with the increment of particle contamination. The effects of the ion conduction in oil are not clear, but it probably plays a major role in clean oil [88-90]. The particles also charge by contacting the electrode and discharge to the other electrode. So in contaminated oil the conduction is driven by the particles.

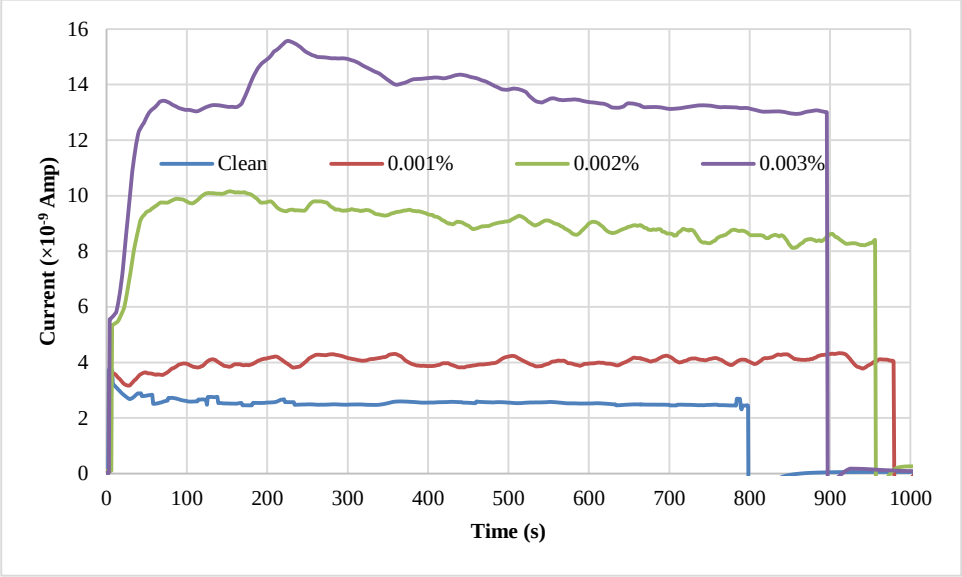

Figure 5:17 Conduction current comparison under the influence of 15 kV DC electric field with clean oil and different levels of contaminated transformer oil [91]

Figure 5:18 summarized all the maximum currents with respect to contamination levels for all the experiments conducted with DC electric field. The highest point of conduction currents were plotted for this graph. The two regions of the process can be clearly identified for these plots. For low voltage of 2 kV, the current weakly depends on the contamination level as shown in Figure 5:18. It is probably because the DEP is small to overcome friction force. Even the large number of particles is available to form the bridge, they cannot be compressed enough to form a thick bridge. The current is approximately constant at 2 kV. There is a slow increase in current for 7.5 kV. The most important observation out of this investigation is that the conduction current always increases with particle contamination level. The maximum magnitudes of the conduction currents for 0.001%, 0.002% and 0.003% concentration level are 4, 10 and 15 nA respectively for the applied voltage of 15 kV. Note that after the bridge is formed the mobility of the particles is irrelevant and the current may be serves as an indication of the bridge quality and its size.

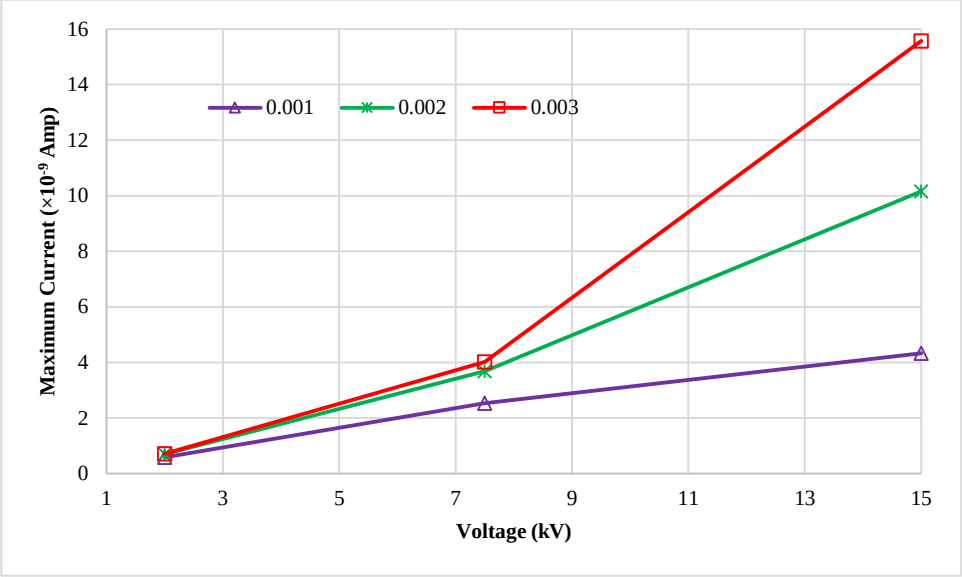

Figure 5:18 Maximum conduction current from all concentration levels plotted with respect to current vs applied voltage

5.5 Paper Barrier Test under DC Biased AC Electric Field

These experiments carried out to investigate the influence of DC offset in AC electric field. This investigation is very important for HVDC converter transformer. Three levels of positive DC voltages (1 kV, 3kV and 5kV) biased with three different levels AC voltages (5 kV, 10 kV and 15 kV) were applied to the samples.

5.5.1 Influence of 1 kV DC and AC Electric Field with 0.003% Concentration

Three different levels of AC electric field with 1 kV DC was applied to the one of the electrode and the other one was connected to the ground. The particle size of all the experiments carried out with paper barrier is 150 – 250 µm. The very first row of Figure 5:19 shows images from bridge formation under 1 kV DC electric field. There were couple of branches of shallow bridge formed within 5 min. The thickness of the bridge increased up to 15 min.

When 1 kV DC biased voltage applied with 5 kV AC, within 1 min a complete thin bridge was created on both side of the barrier. The thickness of the bridge with AC was not significantly different but the bridging formation rate was quicker that purely DC voltage. Particle accumulation for 10 kV and 15 kV AC was higher as previously seen in the bare electrode system. The bridge became more compressed with AC electric field than DC only.

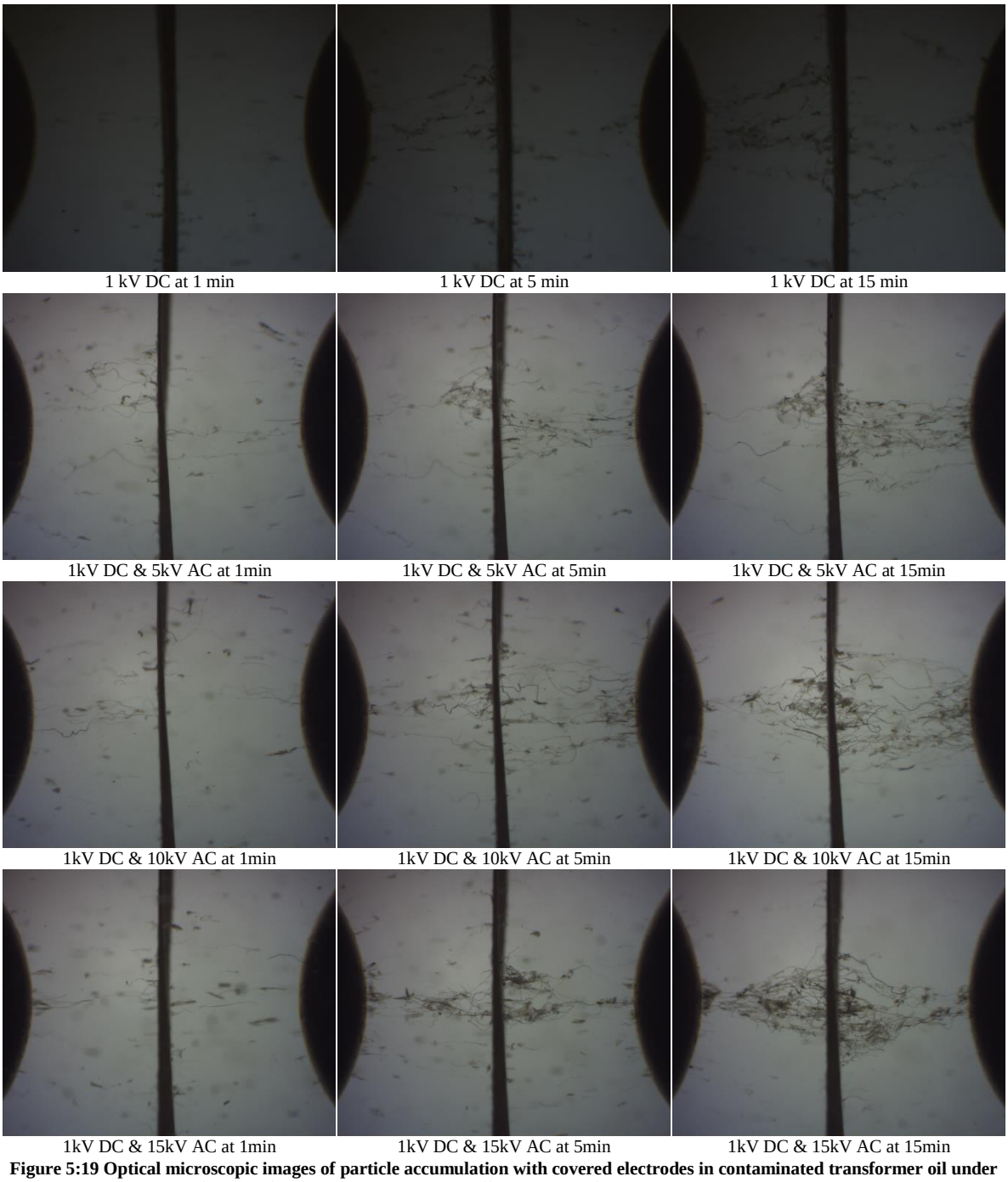

Figure 5:19 Optical microscopic images of particle accumulation with covered electrodes in contaminated transformer oil under the influence of combined 1 kV DC and different levels of AC, concentration level 0.003%.

5.5.2 Paper Barrier Test under the Influence of 3 kV DC and AC Electric Field

The bridge with purely 3 kV DC has shown in Figure 5:20. Bridge formation rate increased than 1 kV DC. A thick and denser bridge was formed with increased voltage level. The combination of AC voltage increased the bridge formation rate and more particle gathered to create the bridge.

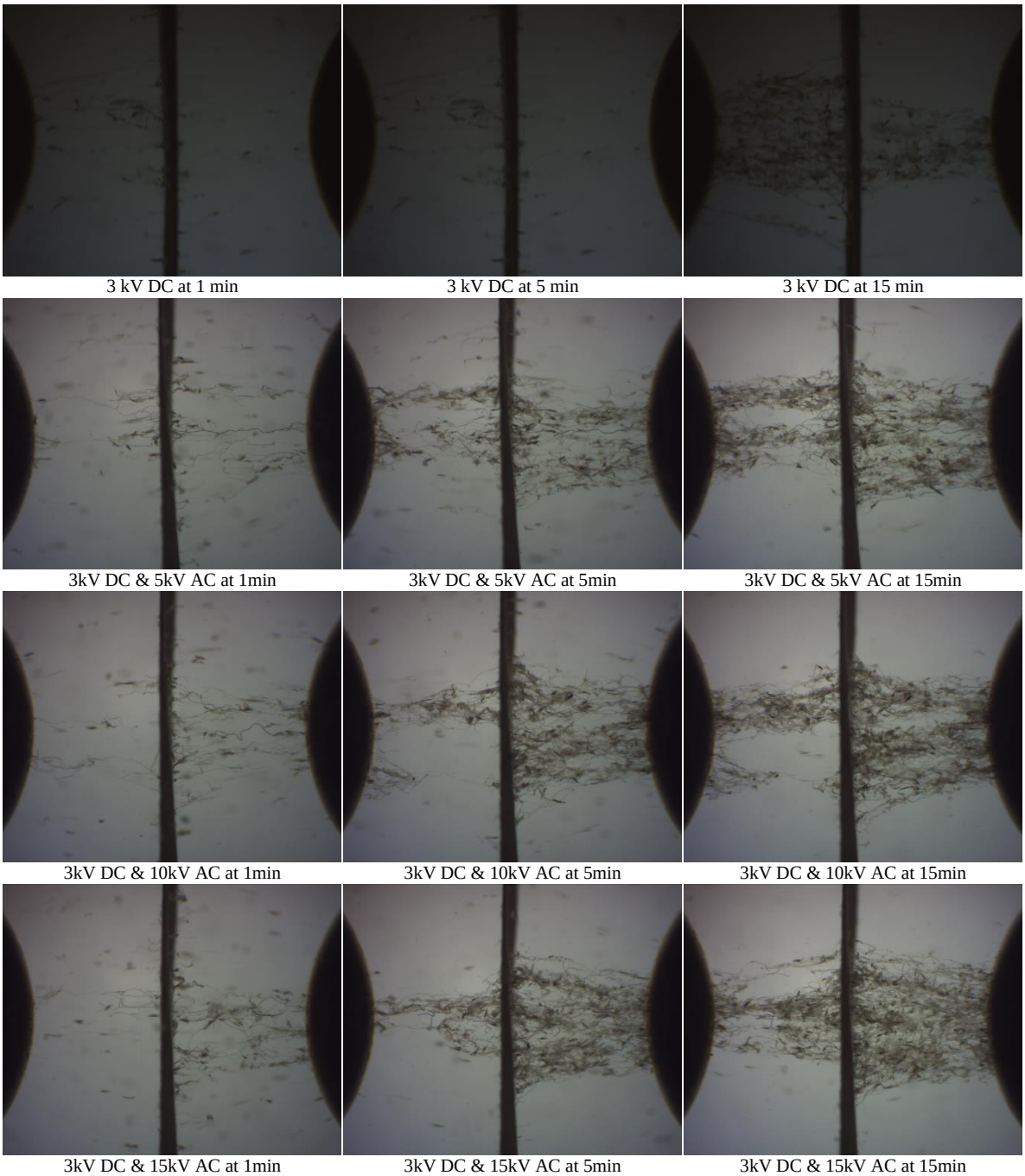

Figure 5:20 Optical microscopic images of particle accumulation with covered electrodes in contaminated transformer oil under the influence of combined 3 kV DC and different levels of AC, concentration level 0.003%

5.5.3 Paper Barrier Test under the Influence of 5 kV DC and AC Electric Field

The highest level of DC electric field was 5 kV tested for DC biased AC test in this case. Bridging process for purely DC electric field is on the first row followed by combination of AC electric field on the next rows of images shown in Figure 5:21. Similar observation is found as the previous two tests.

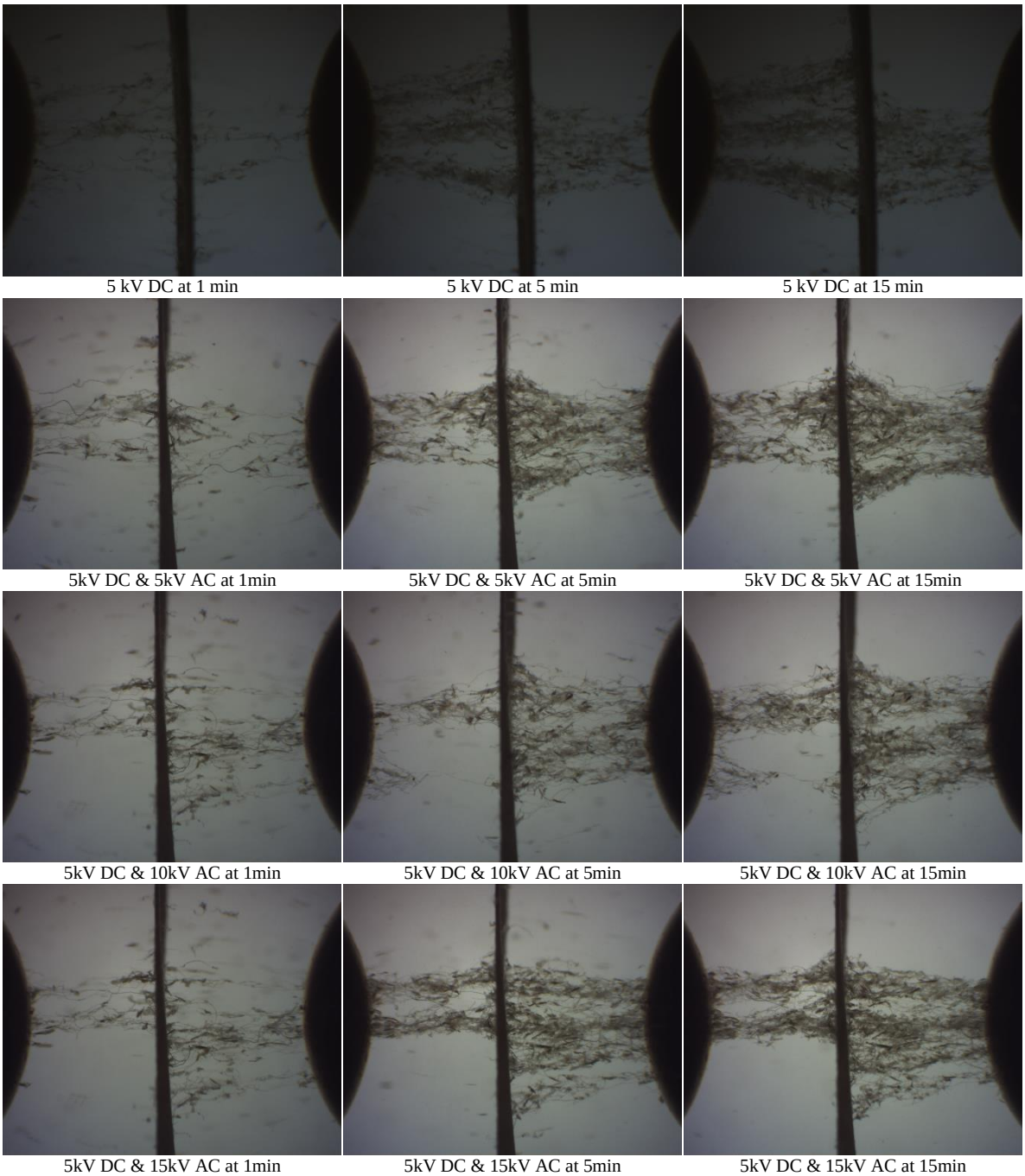

Figure 5:21 Optical microscopic images of particle accumulation with covered electrodes in contaminated transformer oil under the influence of combined 5 kV DC and different levels of AC, concentration level 0.003%

5.6 SUMMARY

Tightly bonded covered electrode experiments revealed that there is always a bridge formed for all the concentration levels tested under DC and a DC biased AC electric field. The conduction current also increases with the level of contamination. A kraft paper barrier between the electrodes also could not prevent bridge formation. The current also increased with the level of concentration, which is an indication of charge transfer through the paper barrier. There were no complete bridge

formed with any of the concentration levels, when there was a loose bond between the electrode surface and the kraft paper. The results for loosely bonded tests are shown in the appendix section.

CHAPTER SIX: NEEDLE - PLANE ELECTRODE TEST

Inside a transformer there are many places where the electric field is non-uniform. One of the places where very non-uniform electric field exist is near the vicinity of high voltage leads between winding terminators and lower bushing connections [92]. Therefore, it is very important to understand the behavior of the contaminant particles under these circumstances. Previous tests with sphere – sphere electrode systems was quasi-uniform but not asymmetric. Several experiments were conducted to replicate situation where non-uniform and divergent electric field condition might be present inside an operating transformer. Needle – plane electrode system was used for this purpose which might be extreme case and might not be found in a real transformer but it will reveal the worst case scenario. The investigation of different electric fields with several levels of voltages also accomplished.

6.1.1 INFLUENCE OF DC ELECTRIC FIELD

These tests were carried out with 0.001, 0.002, 0.003, 0.006, 0.016 and 0.024% fibre particle concentrated transformer oil. A complete bridge between the electrodes was only formed for 0.016 and 0.024% contaminated transformer oil. The particle size for 0.001 to 0.016% experiments was 150 – 250 µm. Only the test with 0.024% concentration was conducted with 63 – 150 µm sized particles. Polarity reversal test was also carried out with 0.016% contamination level with particles size of 150 – 250 µm where the plane electrode were positive and needle were grounded.

There were some pressboard particles attached to the needle electrode after 60 s of the 1 kV applied. There was a thin bridge formed within 300 s. There was no noticeable change to the bridge observed after 900 s for the needle-plane electrode system as shown in Figure 6:1.

The intensity of particles movement was increased with the applied voltage of 3 kV. Particles were accumulated towards the electrodes and started to attach themselves within 35 seconds of the power supply started. There were a few branches of the bridge formed within 60 s. The bridge continued to grow until 600 s. The bridge for 3 kV supply was shallow. The bridge structure seems to follow the electric field.

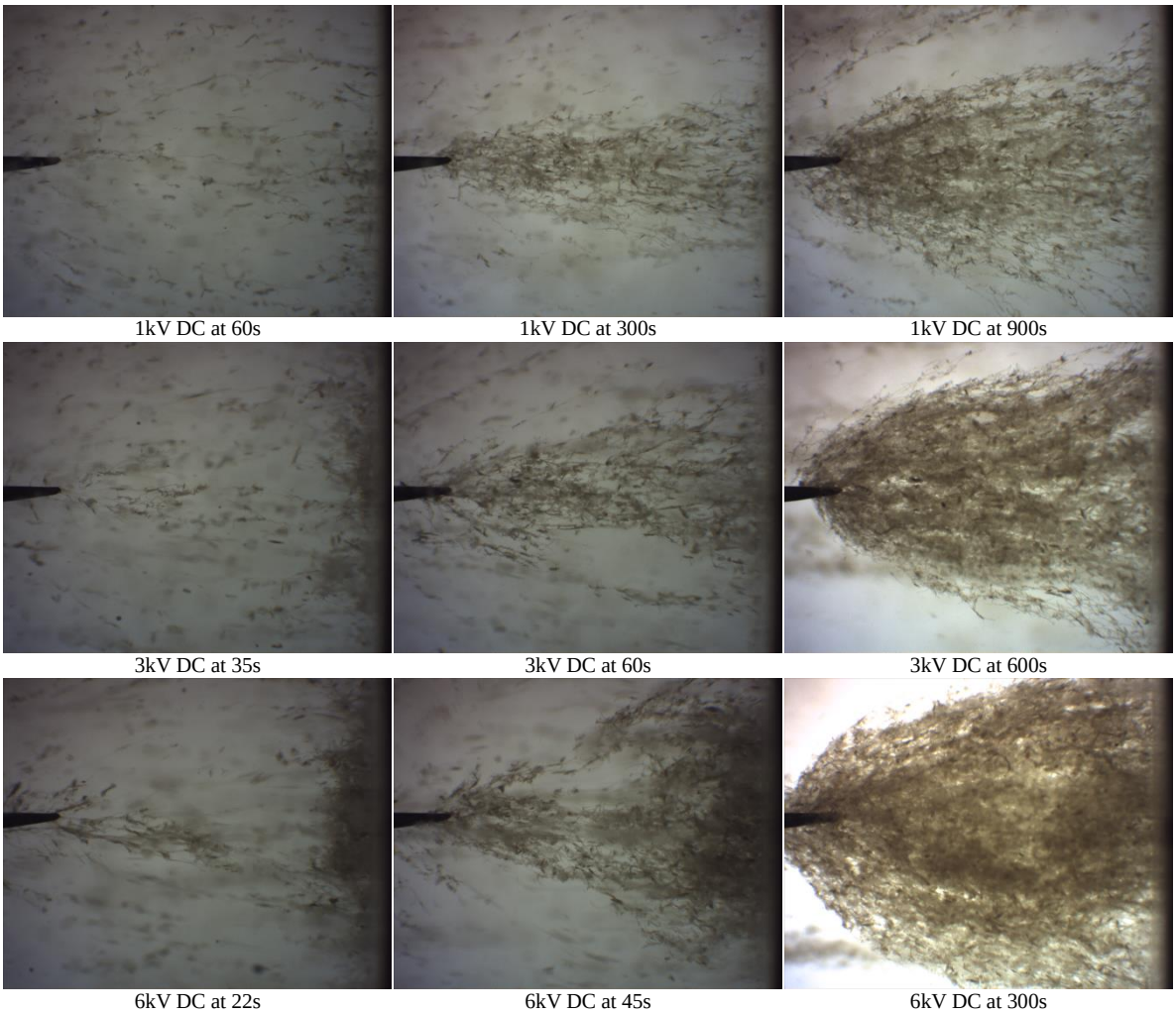

Figure 6:1 Optical microscopic images of bridging in contaminated transformer oil with 150 - 250 µm pressboard fiber under DC voltage, concentration level 0.016%.

The bridging process increased dramatically with an applied voltage of 6 kV. Within few seconds of starting the test, the particles were attaching themselves to form the bridge. One or two branches of the bridge formed as soon as 22 s. The bridge was forming until 300 s thereafter there was no change occurred. The bridge was more compact than 3 kV. The bonding between the branches was stronger than the previous one because of the stronger electric field.

There was a high polarization current observed as soon as the power supply was turned on for needle-plane electrodes (Figure 6:2) for most of the experiments. Then the current dropped slightly and a slow increase of current was observed for 1 kV and 3 kV clean oil. There was a sudden high current observed for clean oil under 6 kV possibly due to partial discharge or strong charge injection. Conduction currents for all voltage levels had slow increment and they settled when they reached saturation point after a while. It is worth to note that for the case of spherical electrodes the "steady" current is approximately proportional to voltage squared at high voltage, but for needle-plane case the dependence is more complex. In latter case the strong field exist in the vicinity of the

needle even for low voltages. But the large volume of oil is still under the low field. The presence of the near needle region gives some non-linear rise in the current as can be seen for 6 kV case in Figure 6:2. The conduction current for contaminated oil was always higher than the clean oil for needle plane electrodes as well. The value of the current was three times and five times higher than clean oil under 3 kV and 6 kV respectively.

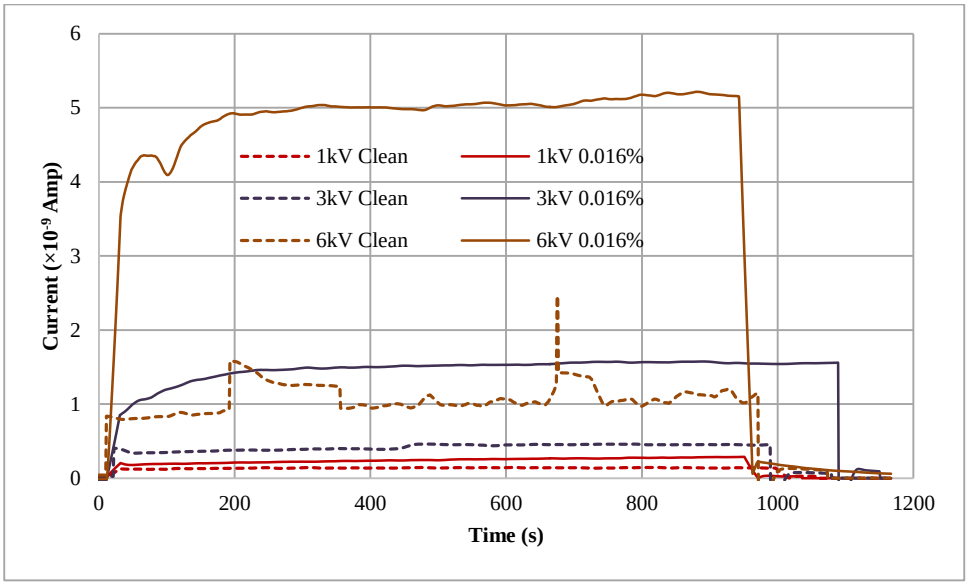

Figure 6:2 Conduction current under different DC voltages with clean oil and 0.016% contaminated transformer oil

The contamination level was 0.024% and particle size was 63 – 150 µm for the experiment shown in Figure 6:3. The contaminant particles were started to move back and forth between the electrodes as soon as 1 kV was turned on. The particles were first polarized due to the DC electric field. Because of the gradient of the electric filed the particles were experienced dielectrophoretic force and they started to draw close towards high electric field region. Then the particles were charged from the cathode and discharging on the other side. The spherical and fiber particles were attaching themselves to both electrodes. The initial bridging process always started from the fiber particles. The fibers attached to the needle and align themselves parallel to the electric field. Then the spherical/small particles attached to the fibers and some more fiber attached to the end of the fibers. This process continues until they form a full bridge between the electrodes. The particles were slowly attaching themselves after 120s of 1 kV applied. The process continues until 900s and after that there was no more change observed. There was no complete bridge created for 1 kV supply.

The particles movement was increased with the applied voltage of 3 kV. Particles were accumulated towards the electrodes and started to attach themselves within 30 seconds of the power supply

started. There were few braches of the bridge formed within 120 s. The bridge was continued to grow until 600 s. The bridge for 3 kV supply was shallow.

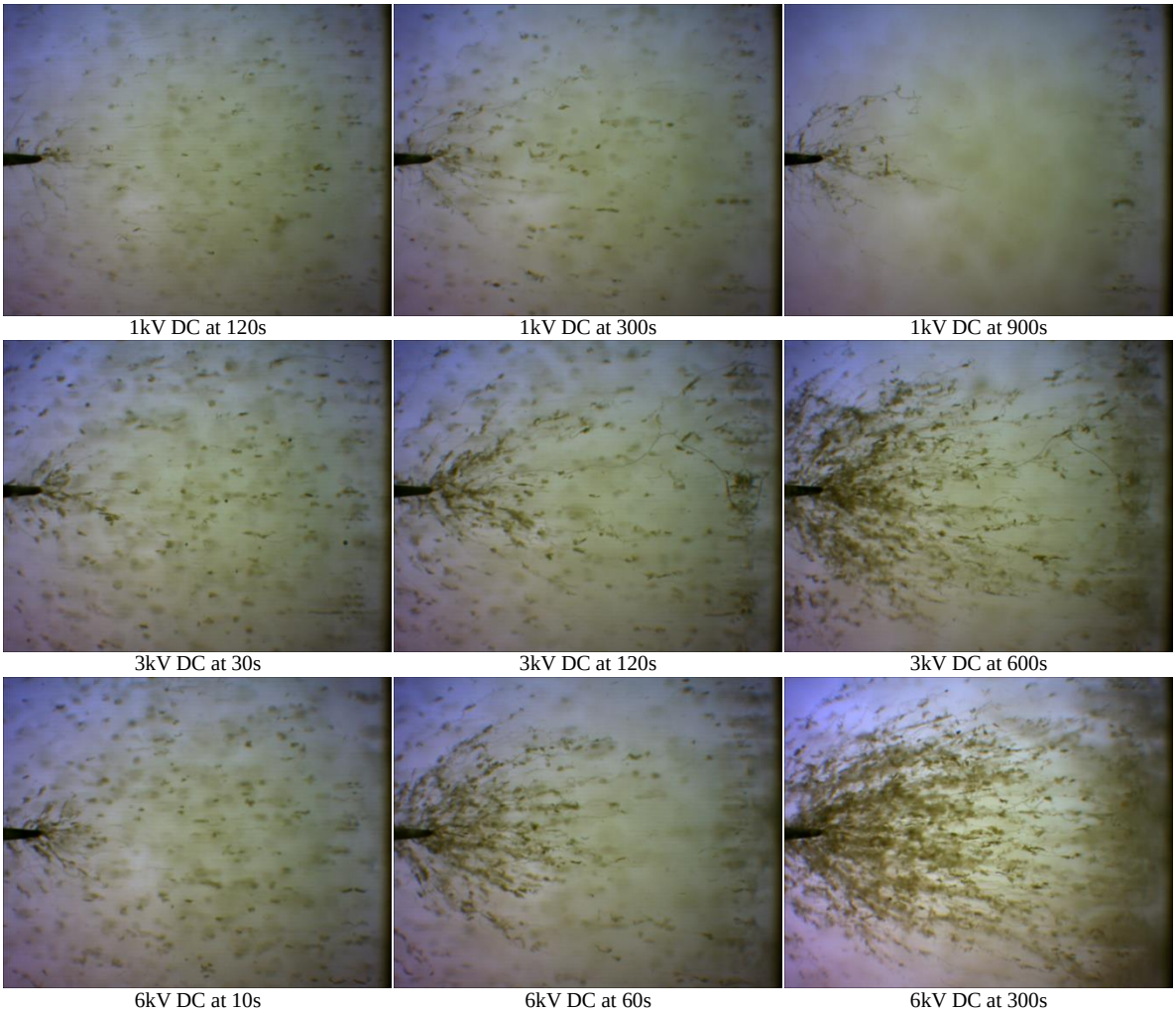

Figure 6:3 Optical microscopic images of bridging in contaminated transformer oil with 63 - 150 µm pressboard fiber under DC voltage, concentration level 0.024%.

The bridging process increased dramatically with applied voltage of 6 kV. Within 10 s of starting the test, the particles were attaching themselves to form the bridge. One or two branches of the bridge formed as soon as 60 s. The bridge was forming until 300 s whereby there was no change occurred. The bridge was more compact than 3 kV. The bonding between the branches was stronger than the previous one because of the stronger electric field.

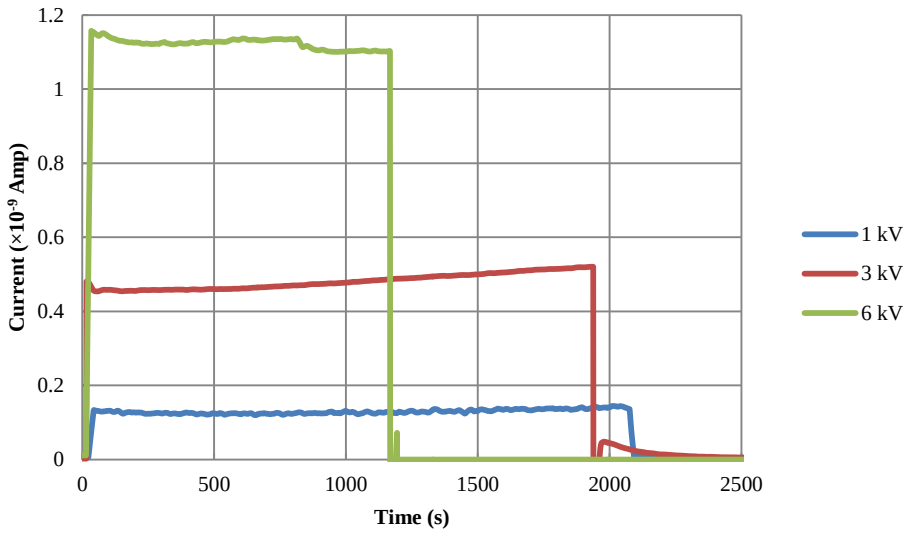

Figure 6:4 Conduction current under different DC voltages with concentration level of 0.024%

The conduction currents were also recorded during the entire experiments. There was a high polarization current observed as soon as the power supply was turned on. Then the current (Figure 6:4) decayed and a slow increase of current was observed for 1 kV and 3 kV. The conduction current increased non-linearly with the applied voltage which was also observed for spherical electrodes.

6.1.2 Test with Negative DC Electric Field

These tests had been carried out to observe the effect of changing the polarity of the divergent electric field. The plane electrode was connected to positive and needle electrode was grounded. The images from the experiments are shown in Figure 6:5. The particles started to move towards needle electrode as soon as the 3 kV DC power supply was turned on. Once the particles touch the needle, they acquired charge and they were shot towards the plane electrode following a straight line path from needle. Most of the particles were coming from either side of needle electrode and after touching the needle, they were going to plane electrode. The particles were first gathered on the plane little bit wide spread as shown in the first row of Figure 6:5 after 300 s. Then the particles gathered like cone shaped and slowly going closer the needle tip after 600 s. Eventually, the particles touched the needle tip and former a complete bridge as can be seen after 900 s. The bridge was thicker and covered almost 1/2 mm of needle electrode when the same voltage were applied with needle positive as can be seen on Figure 6:1 above.

The particles movement was intensified with voltage increased to 6 kV. The particle accumulation time was almost half than 3 kV. It took half the amount of time to make a denser bridge than the

previous. The shape of the overall bridge were similar to previous test (Figure 6:1) where the needle electrode was positive but there was almost double the amount of particles gathered to make a very thick bridge for needle positive test than polarity reversal test (Figure 6:5).

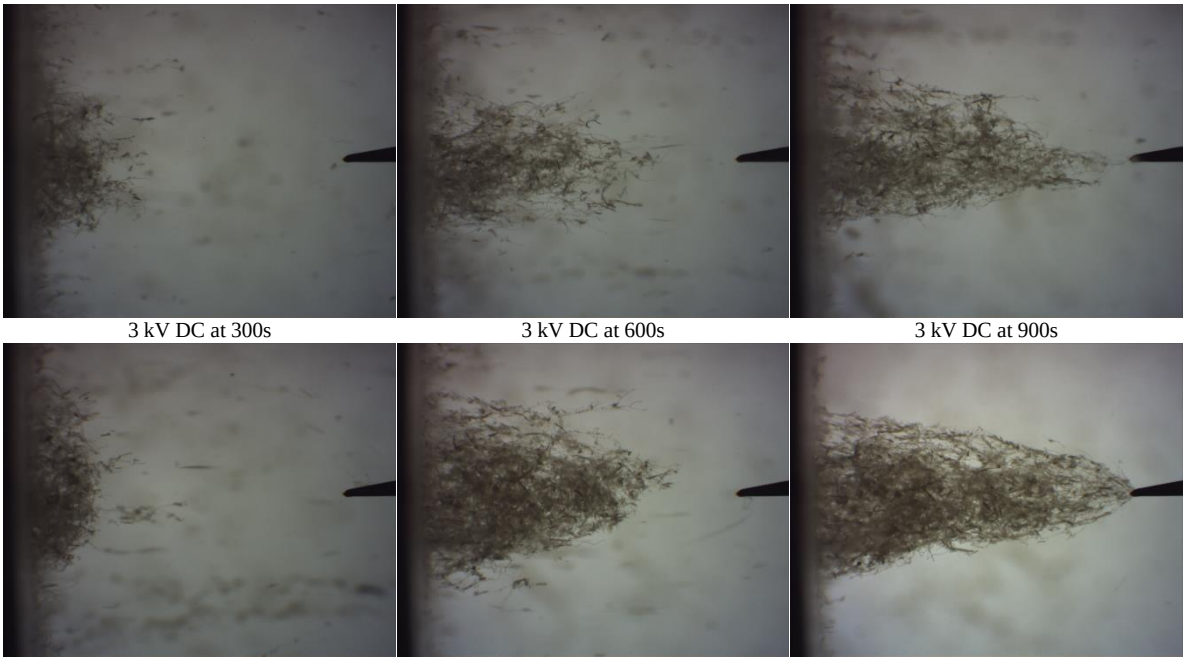

Figure 6:5 Optical microscopic images of bridging with polarity of the electrode reversed in contaminated transformer oil with 150 - 250 µm pressboard fiber under DC voltage, concentration level 0.016%.

Conduction currents of the polarity reversed test are shown in Figure 6:6. The conduction current for 3 kV DC were stabilized to 0.75 nA. There was a high current observed for 6 kV DC due to a lot of particles shooting to and from the needle electrode and it reaches to 2 nA when it became stable. The conduction current for 3 kV and 6 kV were 1.5 nA and 5 nA respectively which are almost double when the needle was positive. It reflects the bridge size observed for the both experiments. The particle accumulation and so is the thickness of the bridge for polarity reversal test were almost half than the test with positive needle as can be visually observed, the conduction current also reflected similar behavior.

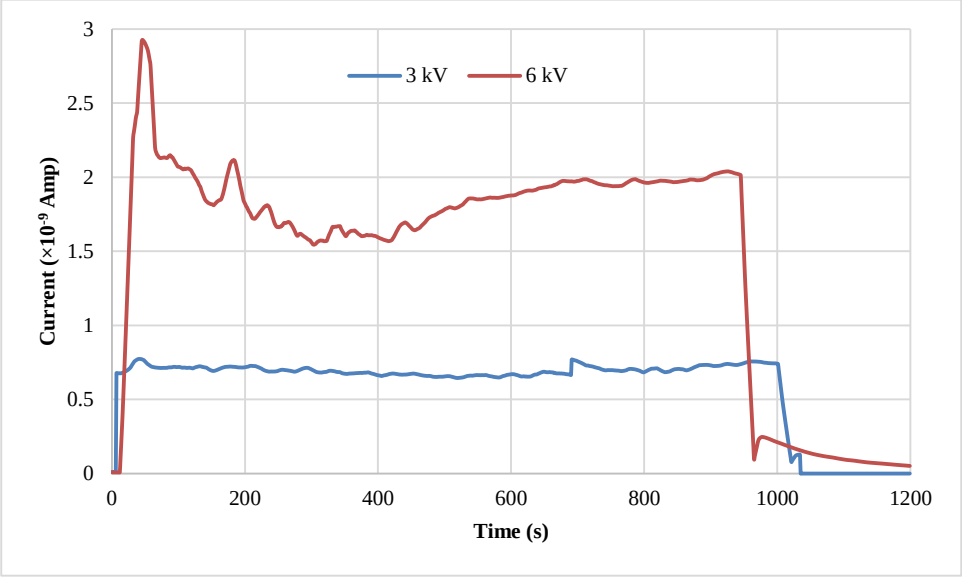

Figure 6:6 Conduction current for polarity reversal test with needle plane electrode

6.1.3 INFLUENCE OF AC ELECTRIC FIELD

The AC voltage was slowly increased to desired level of 5 kV. Images from the needle-plane electrode system under AC electric field are shown in Figure 6:7. The particles were started to move slowly towards the high electric field gradient region because of the DEP force. They started to gather mainly on the needle tip but some of them were going towards the plane electrode. After 1 minute there were some particles observed on the tip of the needle and not many particles attached to the plane electrode. As time progressed more particles accumulated on the needle tip until 25 min thereafter there was no apparent change taken place. There were a small number of particles attached to the plane for the 5 kV testing voltage.

5 kV AC at 1 min | 5 kV AC at 5 min | 5 kV AC at 25 min

10 kV at 1 min | 10 kV at 5 min | 10 kV at 25 min

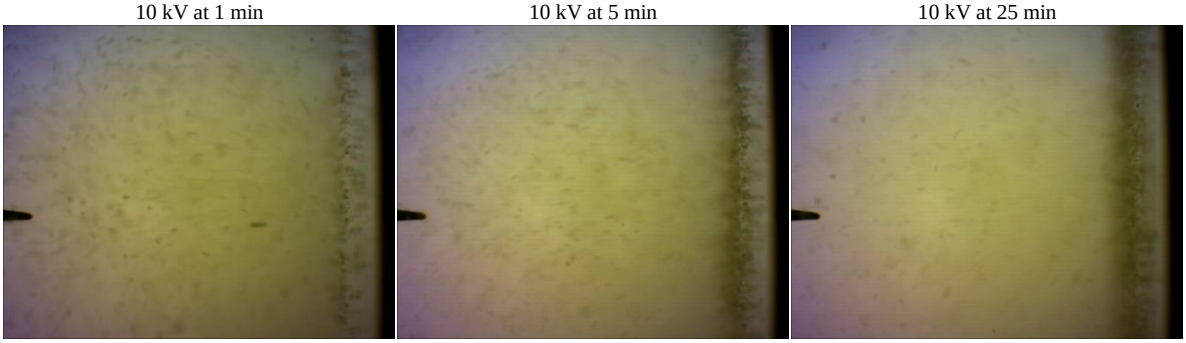

15 kV at 1 min | 15 kV at 5 min | 15 kV at 25 min

Figure 6:7 Optical microscopic images of particle accumulation in contaminated transformer oil with 63 - 150 µm pressboard fiber under different levels of AC, concentration level 0.024%.

The particle accumulation dynamics were changed for higher electric field of 10 kV AC. The particles were started to move from the needle towards the plane electrode. They were shooting to the plane electrode then after hitting the plane electrode, some of them attached to the plane and others were moving away from the plane electrode. The motion of the particles was consistent with electro-convective flow due to charge injection into a dielectric liquid [93]. In this case the high electric field creates two turbulence waves propagating from the needle to the plane and returning back at the sides [94]. In dielectric liquids, space charges (ions) are mainly created by two mechanisms: one is the dissociation and recombination phenomenon [95], the other one is the charge injection [96]. It has been demonstrated that in blade plane geometry the dissociation/recombination phenomenon induces a flow from plane to blade [97-99] while liquid flows in the opposite direction when an injection occurs [100, 101]. In this experiment there were very few particles accumulated at the very beginning of the test but later on all the particles were attached to the plane which is completely opposite of what was observed for 5 kV. It suggests that

there were charge injected to the oil at the needle and the oil moves towards the plane dragging the fibre particle. To explain completely different regions for the observed fibre accumulation at 5kV and 10kV we have to assume that the charge injection is only noticeable at voltages above 10kV. The particles accumulated on the surface of plane electrode experience a combination of DEP force and the drag force due the oil flow. These forces are low at the surface of the plane electrode and the particles were stuck on the surface. Similar phenomenon was observed for 15 kV.

Taking into account observation described in the previous section, AC produces unexpected results for needle-plane system. DEP force is proportional to voltage squared whereas electro convective force (velocity) linearly depends on voltage for blade electrodes [100]. So accumulation of fibers is expected at the needle tip as the voltage increases. The opposite behaviour is observed. It may be explained by exponential increase in charge injected into the oil with increase of the voltage for our experiment.

6.1.4 Influence of 3kV DC Biased AC

There were three different levels of AC voltages i.e. 5 kV, 7 kV and 10 kV were used with a DC offset of 3 kV for needle-plate system and the images from these tests are shown in Figure 6:8. The particles started to detach and move from the needle to the plane electrode after the 3 kV DC biased 5 kV AC was applied. They accumulated on the both electrodes initially. As time progressed there were more particles attached to the plane than the needle tip. At the end of 25 min all the particles left the needle tip as it was observed on AC test. Taking into account observation described in previous sections, AC+DC combination produces results similar to the AC case for needle-plane system. Strong electro convective force does not allow particles to stay at the needle tip, they are pushed towards the plane electrode. But this time more particles were attached to the plane electrode than pure AC test. So the effect of DC was to accumulate more particles at the plane electrode.

As the AC voltage was increased to 7 kV and 10 kV, the velocity of the particles was increased but the particle accumulations were not increased significantly.

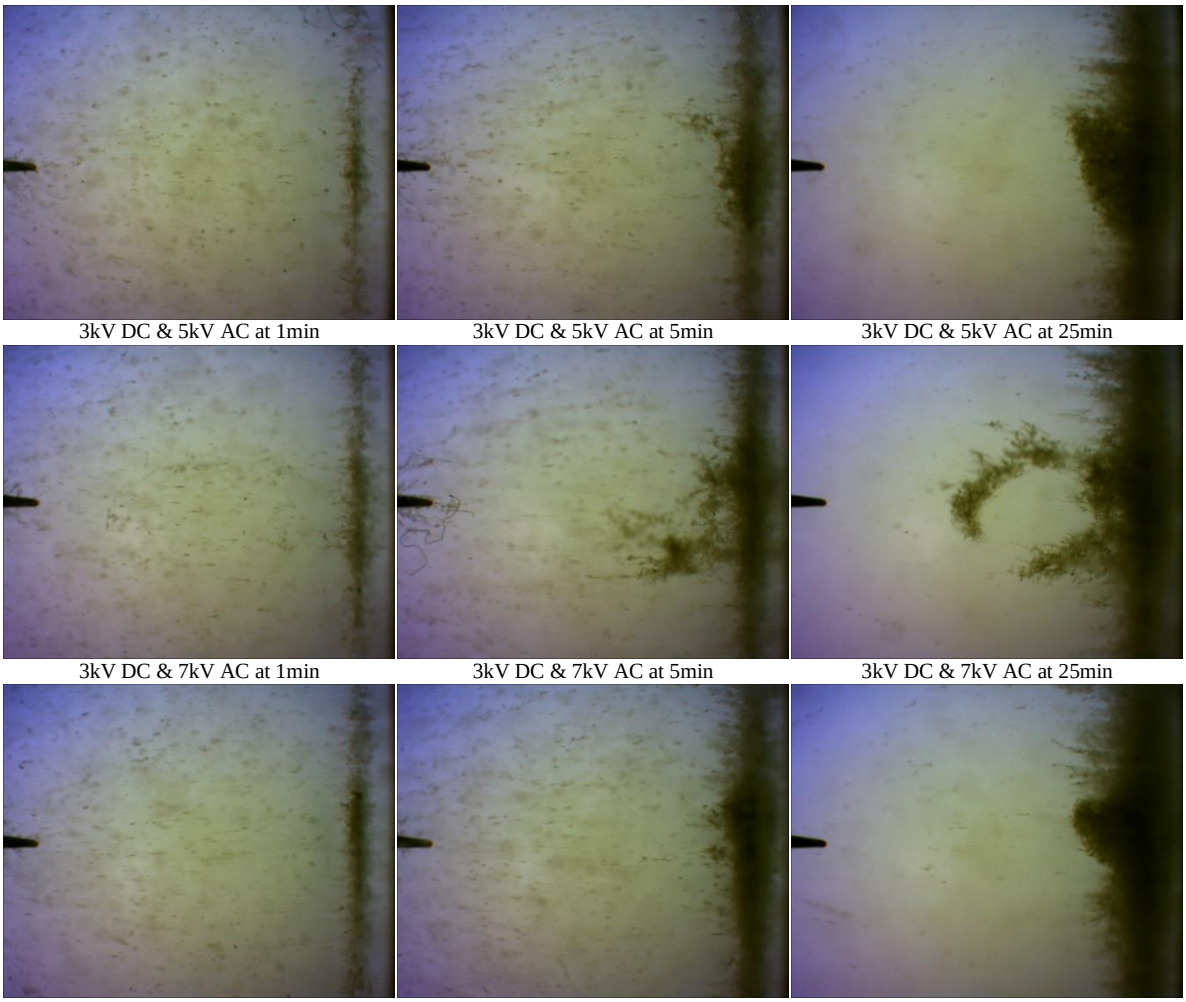

3kV DC & 5kV AC at 1min | 3kV DC & 5kV AC at 5min | 3kV DC & 5kV AC at 25min

3kV DC & 7kV AC at 1min | 3kV DC & 7kV AC at 5min | 3kV DC & 7kV AC at 25min

3kV DC & 10kV AC at 1min | 3kV DC & 10kV AC at 5min | 3kV DC & 10kV AC at 25min

Figure 6:8 Optical microscopic images of particle accumulation in contaminated transformer oil under the influence of combined 3 kV DC and different levels of AC, concentration level 0.024%.

6.1.5 INFLUENCE OF 6KV DC BIASED AC

For these experiments, 6 kV DC was combined with 5 kV, 7 kV and 10 kV AC as shown in Figure 6:9. As soon as the voltage applied, the particles were started to move from the needle to the plane electrode. The behavior of the particle accumulations were the same as observed in the previous test. The only difference was the particle accumulations on the plane electrode were much higher than the 3 kV test.

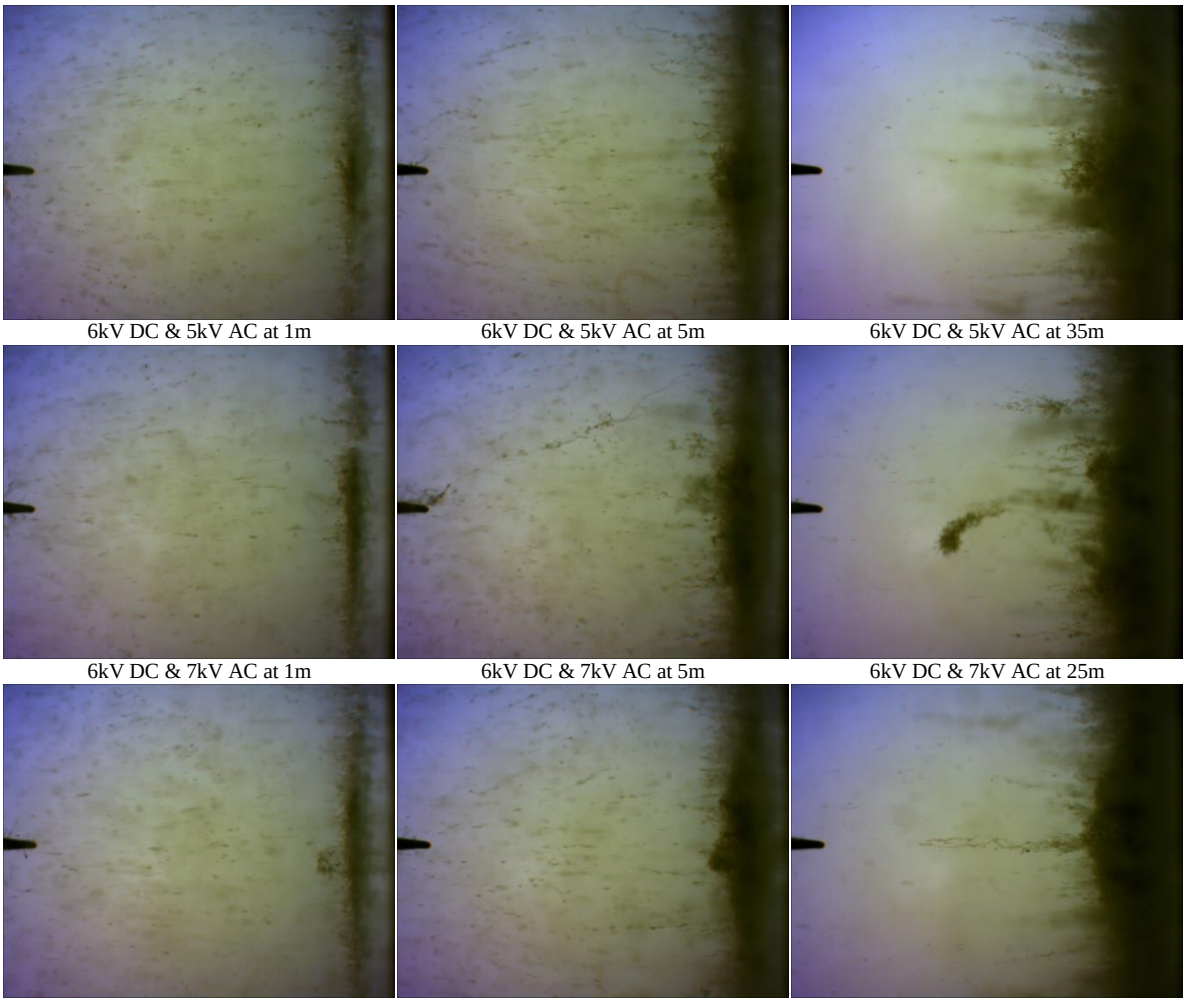

6kV DC & 5kV AC at 1m | 6kV DC & 5kV AC at 5m | 6kV DC & 5kV AC at 35m

6kV DC & 7kV AC at 1m | 6kV DC & 7kV AC at 5m | 6kV DC & 7kV AC at 25m

6kV DC & 10kV AC at 1m | 6kV DC & 10kV AC at 5m | 6kV DC & 10kV AC at 25m

Figure 6:9 Optical microscopic images of particle accumulation in contaminated transformer oil under the influence of combined 3 kV DC and different levels of AC, concentration level 0.024%.

6.1.6 NEEDLE – SPHERE ELECTRODE SYSTEM

A quick test was carried out with needle-sphere electrode system to observe the effect of different geometry of electrodes. This test also showed similar characteristics, all the particles were accumulated on the spherical electrodes. The bridge was progressing from the spherical electrode towards the needle.

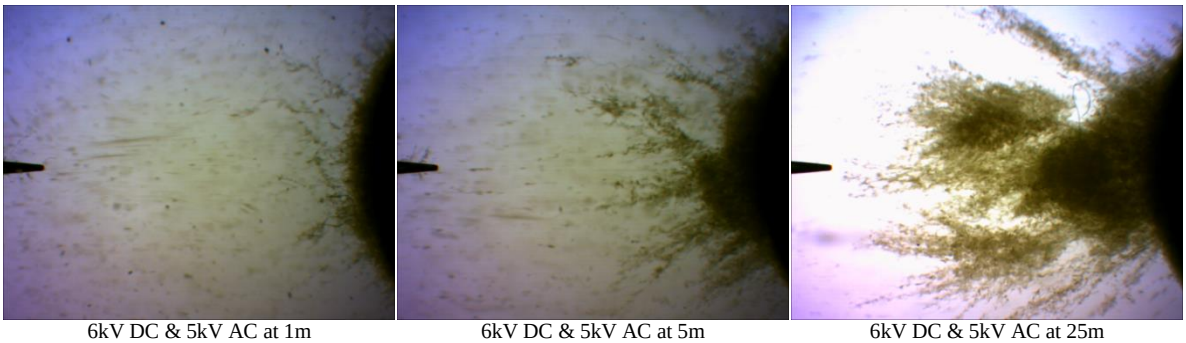

6kV DC & 5kV AC at 1m | 6kV DC & 5kV AC at 5m | 6kV DC & 5kV AC at 25m

Figure 6:10 Optical microscopic images of particle accumulation in contaminated transformer oil under the influence of combined 6 kV DC and 5kV AC, concentration level 0.024% with needle-sphere electrodes.

6.2 SUMMARY

Bare spherical electrodes, covered spherical electrode and barrier between spherical electrode experiments under DC biased AC electric field showed that there were always a complete bridge between electrodes created. Whereas with needle-plane electrode system had different results for DC biased AC test. All the experiments with needle and plane electrodes were subjected to positive DC electric field had a complete bridge between electrodes. There were no bridge with positive DC biased AC electric field for any of the contamination level. The bridge started from needle electrode when the needle were positive DC and the bridge started from plane electrode when the plane were subjected to positive DC voltage. This could cause by changing the electro-convective flow direction in oil for different polarity and the charge transfer mechanism for positive and negative electrode might be different.

CHAPTER SEVEN: SIMULATION STUDIES

7.1 MATHEMATICAL MODELING

In 2010, N. N. A. Jaafar attempted to model the experimental results [5] as a part of BEng final year project using COMSOL [102]. Some of the experimental observations were successfully simulated. For example, it showed that the dust particles were attracted and attached to the surface of the two electrodes where the electric field was the highest. However, it failed to simulate bridge formation for any of the three voltages applied (2 kV, 7.5 kV and 15 kV).

In 2011, Naciri, N. improved the model further using COMSOL as a part of MSc thesis [103]. In this case, only the spherical particles were considered for modelling as it was observed in the experiments that the fibre particles are mainly responsible to form the bridge. So this model is based on fibre particles. The findings of [103] is further developed and reported in this chapter.

7.2 PARTICLE DYNAMICS

Observation from experiments revealed that, dust particles in transformer oil moved towards the region of highest electric field and eventually form a bridge between the two electrodes. The forces applied to a dust particle are necessary to find an expression for the particles velocity.

The dust particles fall down in the transformer oil within 600s, therefore the gravitational force is greater than the buoyancy. The buoyancy force is neglected in this case as the particles are in the range of hundreds of micrometers in size. Moreover, the non-uniform electric field has an effect on dielectric mixture and so does the transformer oil on the moving particles [103]. So the dielectric particles are affected by many forces.

Dascalescu had modelled conductive particle movement under the influence of DC electric field [104]. The equation he used for the motion of a particle in transformer oil under an applied electric field is,

$$ma = \boldsymbol{F}_e + \boldsymbol{F}_d \pm \boldsymbol{F}_g \qquad \textbf{7:1}$$

Where m is the mass of the particle, a is the particle acceleration, $\boldsymbol{F}_e$ is the electrostatic force, $\boldsymbol{F}_d$ is the viscous drag force and $\boldsymbol{F}_g$ is gravitational force. The drag force is a function of particle shape, size and the viscosity of the liquid.

Other researchers also proposed a more comprehensive force model called Electro-Dielectrophoretic force [77]. In this mechanism, the particles will be drawn closer to the electrodes due to dielectrophoretic force due to polarization. Once the particles touches the electrodes, they will acquire charge and will be affected by the electrostatic force as well. Charging of the particle is discussed in the following section. As the particles will be polarized (DEP) and later acquired charge (electrostatic), they will also be influenced by the inter-particle interaction forces. Other hydrodynamic forces such as drag and gravity will also be present. Therefore the total force exerted to the particles are,

$$ma = \boldsymbol{F}_{dep} + \boldsymbol{F}_e + \boldsymbol{F}_d + \boldsymbol{F}_{pr} \pm \boldsymbol{F}_g \qquad 7{:}2$$

Where $\boldsymbol{F}_{dep}$ and $\boldsymbol{F}_{pr}$ are dielectrophoretic force and particle-particle interaction force.

7.2.1 DIELECTROPHORESIS (DEP)

A neutral body placed in an electric field becomes polarized and is equivalent to an electric dipole with an excess of positive charge on one end and negative charge on the other. The forces acting on the two ends do not balance for non-uniform electric field resulting in the movement of the particles. This phenomenon is called dielectrophoresis first introduced by Pohl [76]. Dielectro- means the dielectric polarization, and -phoresis means swim in Greek. In short, Dielectrophoresis is a force exerted by an inhomogeneous electric field on a small, polarized but non-charged particle [105]. An early analysis of dielectrophoresis was published by Placzek [106]. Extensive reviews of dielectrophoresis have been published by Pohl [82, 107]. DEP depends on the dielectric properties of a matter, its structure, composition and the properties of the electric field.

7.2.1.1 Mechanism of DEP

The effect of DEP is a motion of suspended particle superimposed by inhomogeneous electric field due to dielectric polarization. Any particle suspended in an electric field will become polarized with free charges on the interface resulted in the formation of double layers of free charges, as shown in Figure 7:1 (a). The polarization of a dielectric particle under an electric field is moving charges bound within the dielectrics at short distances to form induced dipoles Figure 7:1 (b).

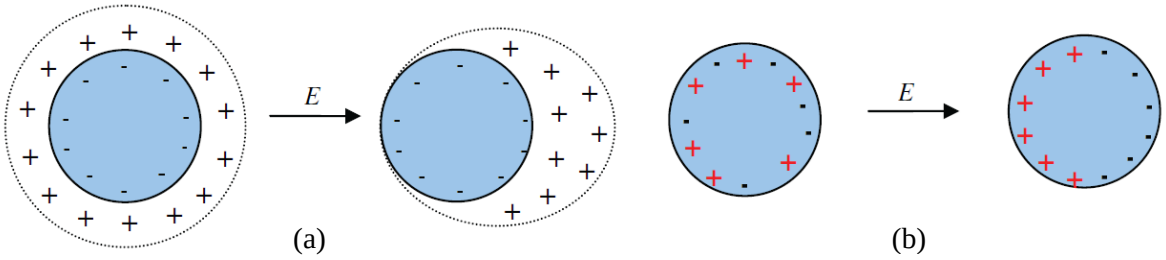

Figure 7:1 Polarization mechanisms of particle with free charges on interface (a) and dielectric particle (b) in a uniform electric field [108].

The local electric field and resulting forces on both sides of the particle are different for non-uniform electric field, causing a net force to arise. This force is termed as the dielectrophoretic force (*FDEP)*. The general expression for the dielectrophoretic force is [105, 109]:

$$\overrightarrow{F_{dep}} = (\overrightarrow{p_{eff}} \cdot \nabla)\overrightarrow{E_0} \qquad \textbf{7:3}$$

where $\overrightarrow{p_{eff}}$ is the effective dipole moment and $\overrightarrow{E_0}$ the non-uniform electric field. If the electric field is uniform, then $\overrightarrow{F_{dep}} = 0$.

For many years, researchers focused on calculating dielectrophoretic forces for different particle geometries. Dielectrophoretic force depends on the dielectric field, the volume of the particles, the complex permittivity of the particles and the medium [105, 110, 111]:

$$\overrightarrow{F_{dep}} = f(volume, medium\ and\ particles\ permittivities)\vec{E}\nabla\vec{E} \qquad \textbf{7:4}$$

Expressions for the dielectrophoretic force exerted on spherical particles for AC or DC voltages are outlined in [105, 110, 111]:

For AC voltages and for conducting spherical particles of radius r, the most general expression is given by [18]:

$$\overrightarrow{F_{dep}} = 4\pi r^3 \varepsilon_{oil} K \vec{E}\nabla\vec{E} \qquad \textbf{7:5}$$

where K is the Clausius-Mossotti factor given by:

$$K = \frac{\varepsilon_p^*(\omega) - \varepsilon_{oil}^*(\omega)}{\varepsilon_p^*(\omega) + 2\varepsilon_{oil}^*(\omega)} \qquad \textbf{7:6}$$

where $\varepsilon_p^*(\omega)$ and $\varepsilon_{oil}^*(\omega)$ are the particles and medium complex permittivities respectively, such as $\varepsilon^*(\omega) = \varepsilon - j\frac{\sigma}{\omega}$ with σ and ω represent the conductivity and the angular frequency respectively.

For DC voltages and conducting spherical particles in transformer oil, the complete expression is given by [110]:

$$F_{dep} = 2\pi r^3 \varepsilon_{oil} \left[\frac{\sigma_p - \sigma_{oil}}{\sigma_p + 2\sigma_{oil}} \left(1 - e^{-t/\tau}\right) + \frac{\varepsilon_p - \varepsilon_{oil}}{\varepsilon_p + 2\varepsilon_{oil}} e^{-t/\tau} \right] \nabla E^2 \quad \textbf{7:7}$$

Where ε_{oil} and σ_{oil} are the dielectric permittivity and conductivity of the transformer oil respectively.

This Clausius-Mossotti factor was derived by Pohl [76] first, and recently by Lorrain et al [108], using extrapolation by solving potential inside and outside of a dielectric sphere with boundary conditions based on Gauss's law and the divergence of electric flux density equal to the free volume charge density. It represents a relaxation in the effective permittivity (real part) or polarizability of the particle with a relaxation time of (imaginary part),

$$\tau = \frac{\varepsilon_p + 2\varepsilon_{oil}}{\sigma_p + \sigma_{oil}} \quad \textbf{7:8}$$

where τ is the inverse of the angular frequency ω.

When t > τ, the dielectrophoretic force is given by:

$$F_{Dep} = 2\pi r^3 \varepsilon_{oil} \left(\frac{\sigma_P - \sigma_{oil}}{\sigma_P + 2\sigma_{oil}} \right) \nabla E^2 \quad \textbf{7:9}$$

The particle dielectric motion velocity v_{DEP} can be given by balancing DEP force with the drag force F_{Drag} [76],

$$F_{DEP} = -F_{Drag} = 6\pi \eta_{oil} r v_{DEP} \quad \textbf{7:10}$$

where, η_{oil} is dynamic viscosity of the medium. Therefore, the dielectric velocity of a spherical particle can be expressed as,

$$v_{DEP} = \frac{r^2}{3\eta_{oil}} \varepsilon_{oil} \left(\frac{\sigma_P - \sigma_{oil}}{\sigma_P + 2\sigma_{oil}} \right) \nabla E^2 \quad \textbf{7:11}$$

Here the Reynolds number is assumed to be low enough to ensure the motion of the particle is in the Stokes-regime.

7.2.2 GRAVITATIONAL FORCE

If a particle of mass density ρ_p is suspended in a medium of density of ρ_m, then the effective mass of the particle is equal to the volume of the particle times the difference in mass densities between the particle and the suspending medium [112]. Therefore the magnitude of the gravitational force, $\boldsymbol{F}_g$ is given by [113]:

$$\boldsymbol{F}_g = m_p \boldsymbol{g} \frac{(\rho_p - \rho_m)}{\rho_p} \quad \textbf{7:12}$$

where $\boldsymbol{g}$ is the acceleration due to gravity, m_p is mass of the particle.

7.2.3 ELECTROSTATIC FORCE DUE TO PARTICLE CHARGE TRANSFER

This theory is described by [39]. "If a conducting particle is suspended in an insulating liquid and it is in direct contact with an electrode surface, the particle will become charged to the same polarity as the electrode. The attraction force of a particle to an electrode of opposite polarity and repulsion force from the same polarity electrode will cause the particle to move to the distant electrode. The transit of the particle between the electrodes will register as a current in an external circuit. When the particle collides with the opposite-polarity electrode, it will deliver up its charge and then charge up to the same polarity as the electrode it now contacts. This discharge will produce a sharp current pulse. The particle will then proceed back to the first electrode. This oscillatory motion continues indefinitely if there are no other disturbances in the gap".

The electric field *E* between two large plane parallel electrodes is uniform. The amount of charge q will be acquired by a small metal ball of radius r touching the electrodes given by [114-116],

$$q = \frac{2}{3}\pi^3 \varepsilon_m \varepsilon_0 r^2 E \quad \textbf{7:13}$$

here $\varepsilon_m, \varepsilon_0 \; and \; E$, are the relative permittivity of the liquid , the permittivity of free space and electric field (V/m) respectively.

The above equation is for a conducting particle touching on a plane electrode. For a dielectric particle, the amount of charge will be reduced by several factors e.g. electrode material, particles shape are few of them. So there is no universal equation suggesting that it will be different for each application. One of the way to determine the factor of this reduction is to measure the velocity of the particle and plot the results. A suitable value can then be obtained from a curve fitting technique which has been validated by [77-80]. In this simulation the reduction factor was not obtained from the above method, instead it was chosen by trying different values so as to match the experimental results. Point of contact is also a very important factor as explained by [117] where he carried out the calculation of charge transfer for a cylindrical conducting particle lying on a plane electrode.

The pressboard samples used in the experiments had many different shapes and sizes. Some of them are fibre like, some are not very rounded spherical shape with rough edges. All the particles are observed to be charging and discharging. Fibre liked shaped large particles took longer time to charge and discharge. Smaller particle were quicker to charge and discharge. For simplicity,

spherical particles shape is chosen for this simulation since the Particle Trajectory Module of COMSOL can only model spherical particles. The diameter of the particles tested for the experiments are 250 – 500 µm, 150 – 250 µm, 63 – 150 µm, and less than 63 µm. For simulation purposes, three different particle diameters are used i.e. 100,200and 300 µm. The reduction factor of charge transfer to the dielectric particles was chosen by trial and error method and it was selected to be 0.7.

The experimental results of the fibre particles bridging had a very complex phenomenon. Charging-discharging of the particles and bridge formation are only two main phenomenon among many others. Attempt was made to simulate these mechanisms in this project with two different approaches which are discussed in the following sections.

7.3 CHARGING AND DISCHARGING OF PARTICLES

After establishing the forces involved with the particle movement, a model needs to be chosen and implemented in order to test its validity. At first, suitable software has to be found that will allow the implementation of the force equations. Comsol multiphysics software [118] chosen for the task. This software provides a readily available module called 'Particle Tracing' which is a suitable platform to implement the particle movement.

7.3.1 INTRODUCTION TO PARTICLE TRACING MODELLING

Particle tracing solves ordinary differential equations using Newton's law of motion that requires particle mass, and all forces acting on the particle. Force either due to external fields or due to interactions between particles are calculated. Forces due to external fields are typically computed from a finite element model. For each particle, either one, two or three differential equations are solved for each component of the position vector depending on whether the model is 1D, 2D or 3D respectively. The forces acting on each particle are derived from the external fields at the current particle position at every time step. The particle position is then updated, and the process continues until simulation converges. The equation used in COMSOL to solve particle motion is,

$$\frac{d}{dt}(m_p \boldsymbol{v}) = \boldsymbol{F}_d + \boldsymbol{F}_g + \boldsymbol{F}_{ext} \qquad \textbf{7:14}$$

Where, $\boldsymbol{F}_d, \boldsymbol{F}_g \; and \; \boldsymbol{F}_{ext}$ are drag, gravity and external force respectively.

7.3.2 Model Geometry and Meshing

The experimental setup consisted of two 10 mm diameter spherical electrodes and the gap between them is 10mm, placed in the middle of a 550 ml glass tank. The exact geometry of electrode used in the experimental setup has been chosen for the mathematical model. Therefore, two spherical electrodes drawn and placed in a rectangular oil-filled tank as shown in Fig. 7:2.

Needle-plane electrode system was also tested in the sample tank as above. Diameter of the needle was 1 mm which started to curve from 5 mm above the needle tip as illustrated in Fig. 7:3. The diameter of the needle tip was approximately 100 µm. The diameter of the plane electrode was 50 mm and its thickness was 5 mm.

Ideally the model should be 3D, however it will require a lot of computation time. Therefore, 2D model was chosen for both spherical and needle-plane electrode system models. This can be another source of error to the result as it assumes a plane geometry.

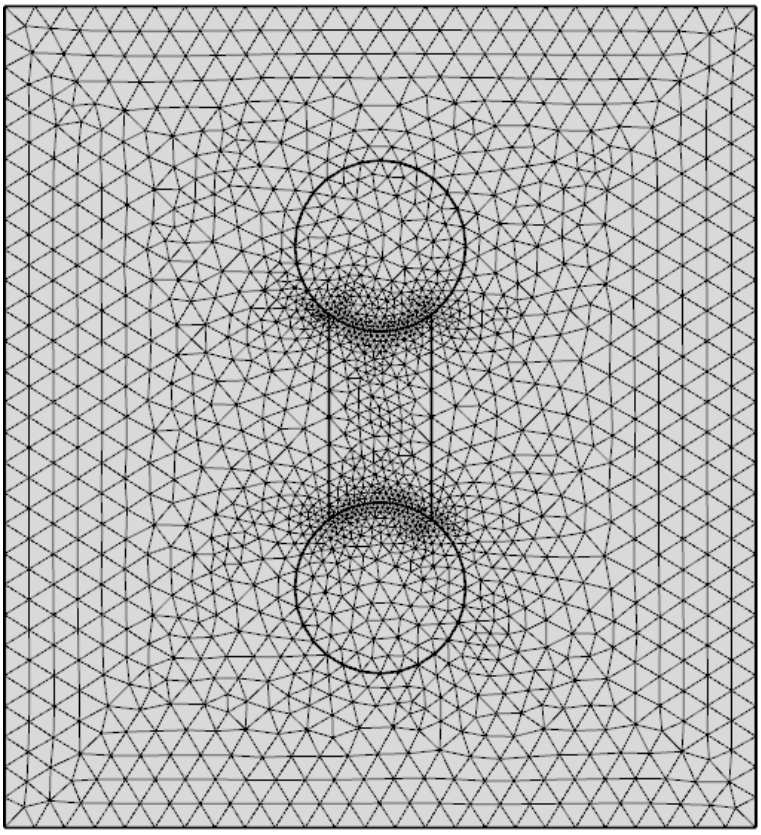

Figure 7:2 2D Model geometry of spherical electrode system with mesh

It is important to find an appropriate meshing for the problem as COMSOL uses Finite Element Analysis. Normal mesh is taken for the tank. A section of the tank between the electrodes identified from the experimental results where the particles are more likely to travel and contact with the edge

of the electrodes. Finer mesh is applied around this area. The optimum selection of the mesh type and density is chosen from trials and errors. For a very densely populated mesh, the simulation takes a very long time to converge.

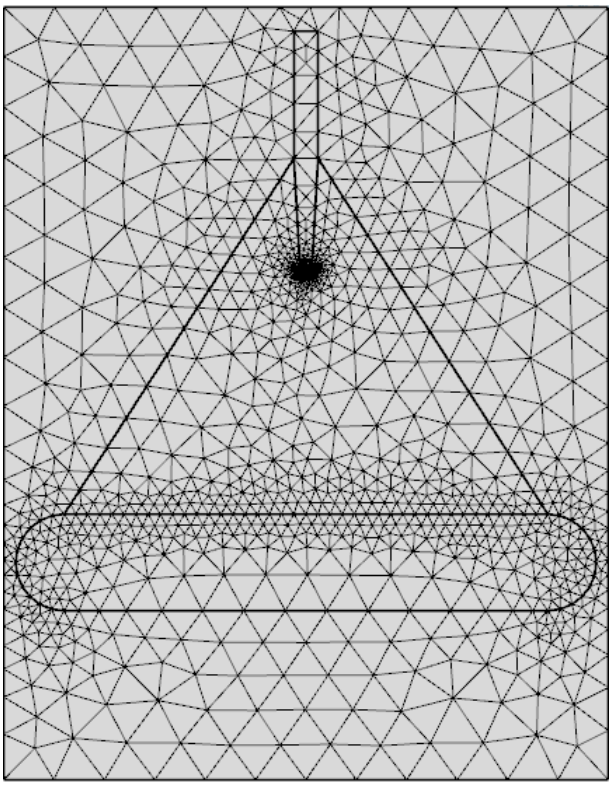

Figure 7:32D Model geometry of needle-plane electrode system with mesh

Choosing a suitable mesh was very difficult for needle-plane electrode system as the electric field intensity is very high only at the needle tip. Table 7-1 summarizes the parameters values used in the simulations.

Table 7-1 Constants and parameters used for charging and discharging model

Constants		Parameters	
ε_0	$8.85 \cdot 10^{-12}\ F/m$	V_0 (applied DC voltage)	2 kV, 7.5 kV and 15 kV
ε_P	$4.5\varepsilon_0$	r	100,200 and 300 μm
ε_{oil}	$2.2\varepsilon_0$	Charge Reduction Factor	0.7
η_{oil}	$0.02\ \mathrm{kg/m \cdot s}$		
ρ_p	$1500\ kg/m^3$		
ρ_m	$870\ kg/m^3$		

7.4 Simulation Results of Charging and Discharging Particle

Figure 7:4 shows the simulation result for a spherical electrode system. The DEP force appears to be significant near the large surface area of the electrodes and the fibers would be attracted to these points on the surface. The arrow indicates the direction of the force acting on the particles. Under DEP force the particles should accumulate from either side of the electrodes, but their motion is not directed straight towards the electrodes. Many particles move first towards the central line between the spherical electrodes and near this line they turn toward the electrodes. Such behavior explains the bridging dynamics found in the experimental results.

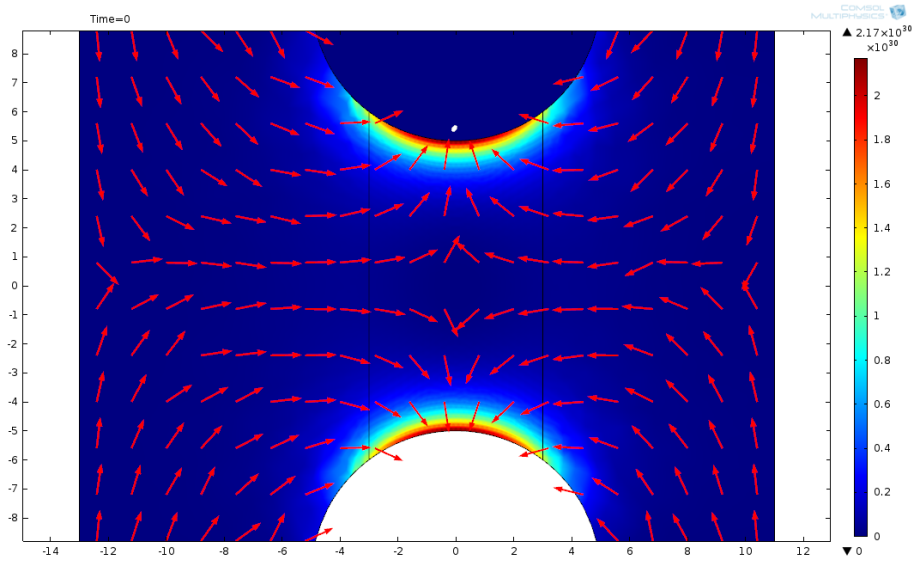

Figure 7:4 Simulation of electric field for spherical electrode system. The color surface represents the intensity of the gradient the electric field squared. The red arrows point towards the direction of the force.

The electric field distribution for needle plane electrode system is shown in Figure 7:5. Again, the particle will tend to move towards the electrode, but they are still attracted to the central line between the needle and the plane. So the bridge grows slowly from the needle. At low voltage there is no particles' accumulation at the plane electrode, but as voltage increases the particles can be seen at the plane surface as well. It can be attributed to electro convective flow. There is a charge injection to the particles from the needle which force them to move under combined action of Coulomb, DEP and the drag force. The drag force is large in the vicinity of the needle but weak near the plane electrode.

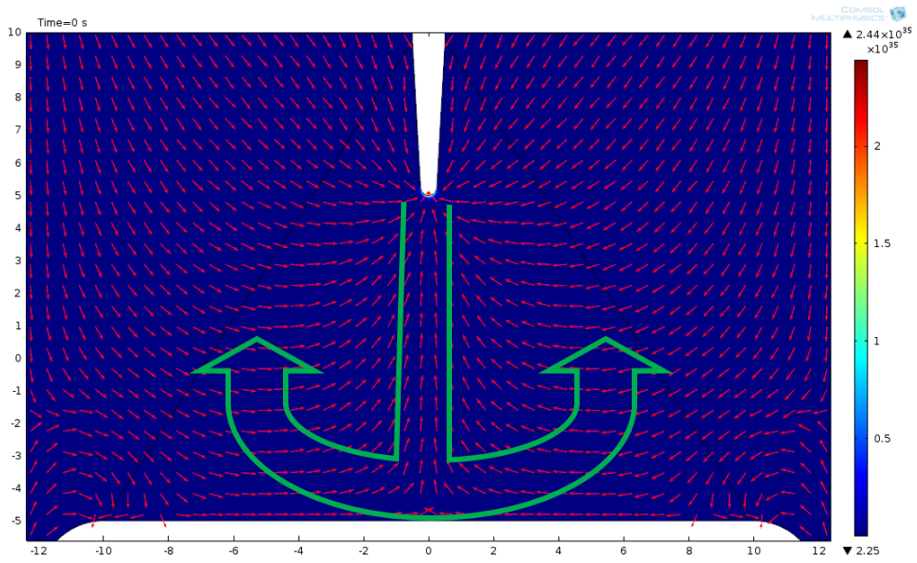

Figure 7:5 Simulation of electric field gradient for needle-plane system. The color surface represents the intensity of the gradient of electric field squared. The red arrows point towards the direction of the force. The green arrows indicate qualitatively the convective oil flow introduced by charge injection in strong electric field according to [100].

The close view of the needle electrode in Figure 7:6 indicates that the DEP force is really small in the oil volume except the region next to the needle tip. It means that even if the particles are attracted to the needle they can be easily swept away by electro-convective flow at high voltages. On the other hand the convective flow is not strong in the vicinity of the plane electrode and it explains an accumulation of the particles at the plane electrodes for high voltages observed in experimental results.

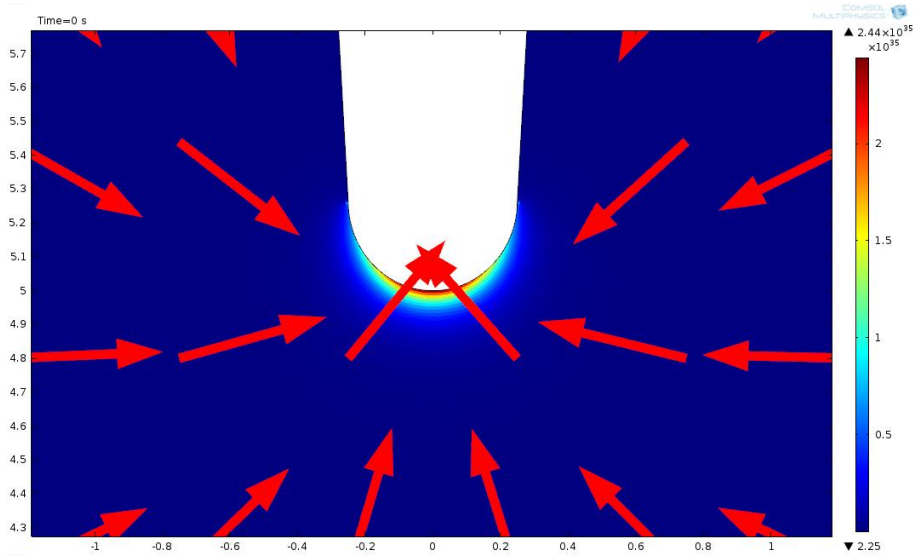

Figure 7:6 The zoom in view of the needle electrode. The notations are similar to Figure 7:5

7.4.1 IMPLEMENTATION OF FORCES

The forces used for all these simulation results are dielectrophoreic, drag, electrostatic and gravitational forces. The simulation begins with the assumption that the particles are not charged. So, the particles will experience only DEP, drag and gravitational forces. The distance between the center of the spherical particles and the center of the electrodes are calculated in each time step. Once the particles reached at a distance which is equal or less than the radius of the electrodes and radius of the particle plus a very small thresh hold, then the particles will be charged. At this point, the particles will experience electrostatic repulsive force from the same polarity of electrode and will be repelled if its value is greater than the DEP force. Once the particle reaches mid-point of the electrode, it will be attracted by electrostatic force towards the opposite polarity electrode and DEP force. Once the particle reaches the other electrode, it will be discharged first and then charged with the same polarity and the process will continue. Note that the gravitational force is acting towards – y axis (left side of the page) so the particles will be leaning toward that axis. Once the particles reaches to a point where the DEP and electrostatic force is less than the gravity, the particle will fall to the bottom of the tank. Although a number of experimental observations have been explained adequately using the simulated results but the particle-particle interaction force could not been simulated successfully. A solution was worked for two particles but for multiple particles this did not work.

The particle charging and discharging simulation model tested with the influence of applied different DC voltage, times, and the particle sizes. The results are discussed in the following sections.

7.4.2 THE EFFECT OF DIFFERENT LEVELS OF DC VOLTAGES

For this study, only the applied DC voltage (2 kV, 7.5 kV and 5 kV) are varied while the other parameters are kept constant. The particle size for these simulations is assumed to be 100 μm.

The trajectories of the particles over the first 10 s of DC electric fields are shown in Figure 7:7, Figure 7:8 and Figure 7:9 for 2 kV, 7.5 kV and 15 kV respectively:

Bottom

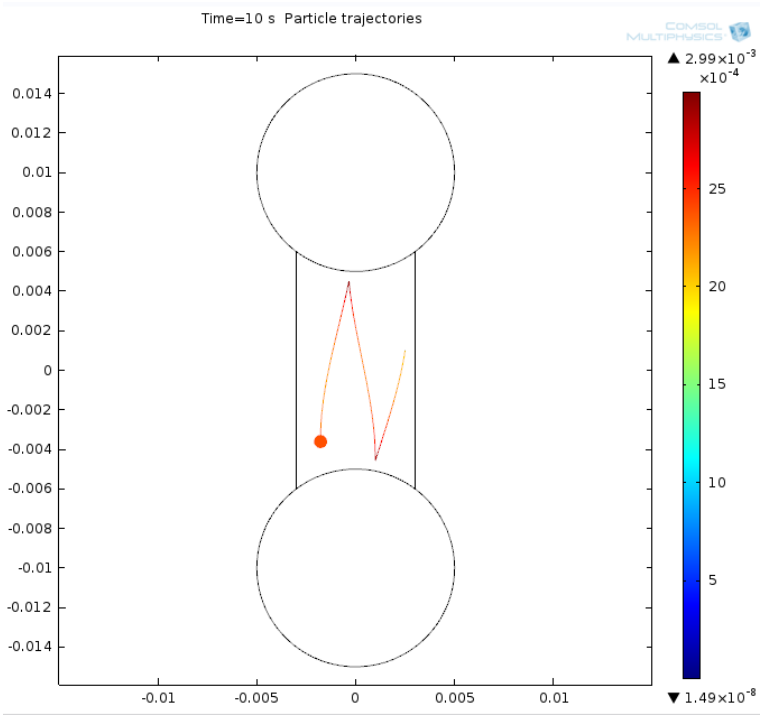

Top

Figure 7:7 Particle trajectory of 100 µm particle under 2 kV DC electric field after 10 s with spherical electrode

Bottom

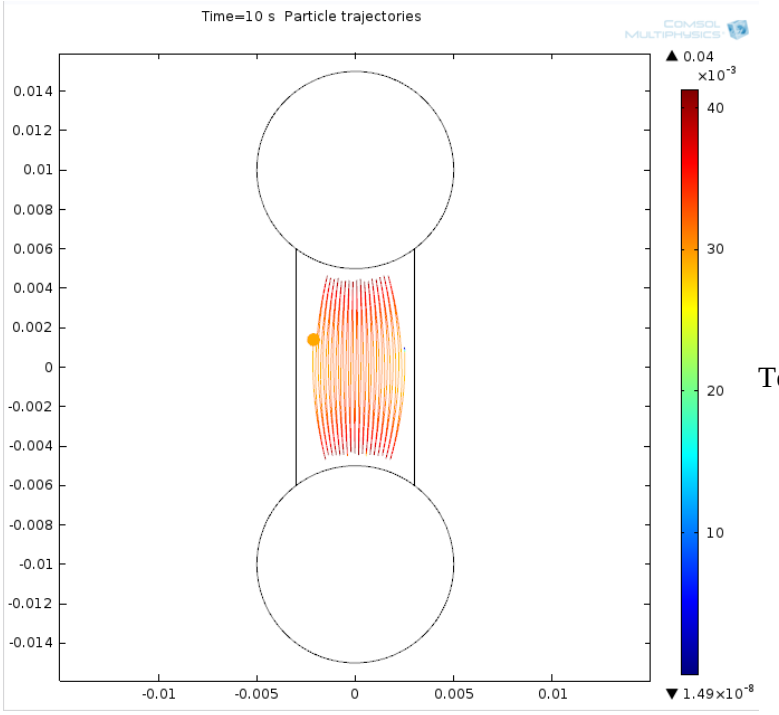

Top

Figure 7:8 Particle trajectory of 100 µm particle under 7.5 kV DC electric field after 10 s with spherical electrode

Bottom

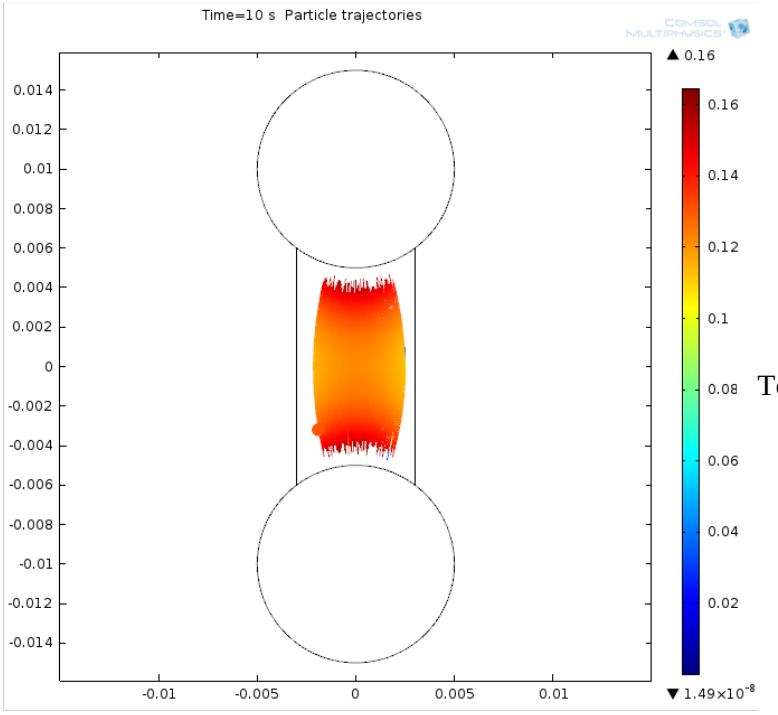

Top

Figure 7:9 Particle trajectory of 100 µm particle under 15 kV DC electric field after 10 s with spherical electrode

From the above particles trajectories it is clear that at lower voltage the particles did not have enough force to charge and discharge from one electrode to the other electrode. The particles movement increased rapidly at higher voltages similar to that observed experimentally. The velocity from the simulation could not be validated against experimental results as the particle velocity could not be measured during the experiments. But the visual observation of the particles movement during experiments agree with the simulation results.

7.4.3 The Effect of Elapsed Time

The evolution of the particle trajectory under the influence of DC electric field as a function of time is also investigated. The particle size for these simulations is assumed to be 200 µm while the applied voltage is 7.5 kV. The times chosen for these simulations are at 0s, 2.5 s, 5 s and 10 s which are presented in Figure 7:10, Figure 7:11, Figure 7:12 and Figure 7:13 respectively.

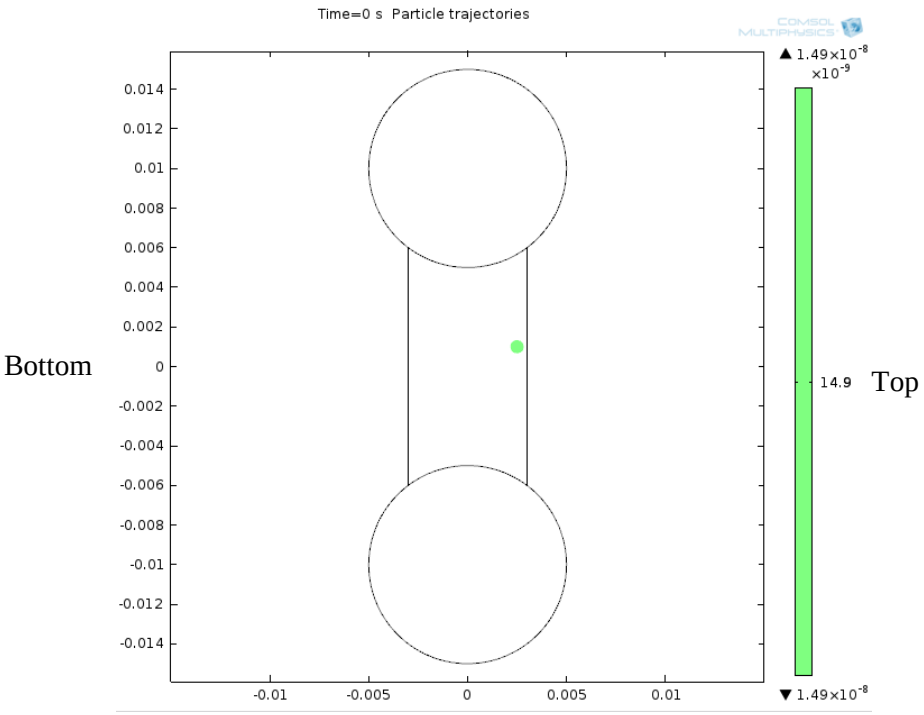

Figure 7:10 Particle trajectory of 200 µm particle under 7.5 kV DC electric field at 0 s with spherical electrode

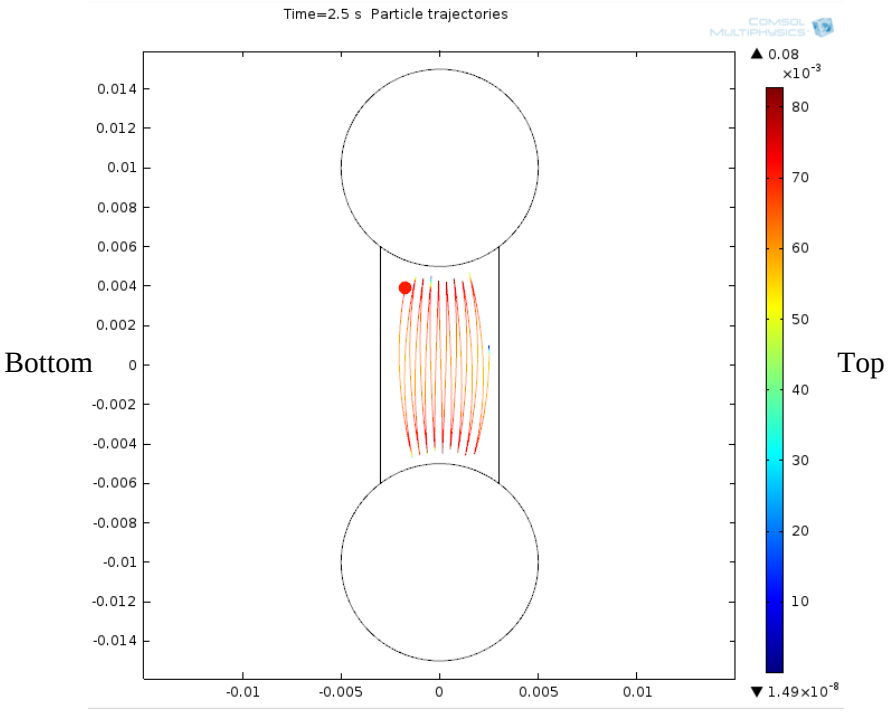

Figure 7:11 Particle trajectory of 200 µm particle under 7.5 kV DC electric field at 2.5 s with spherical electrode

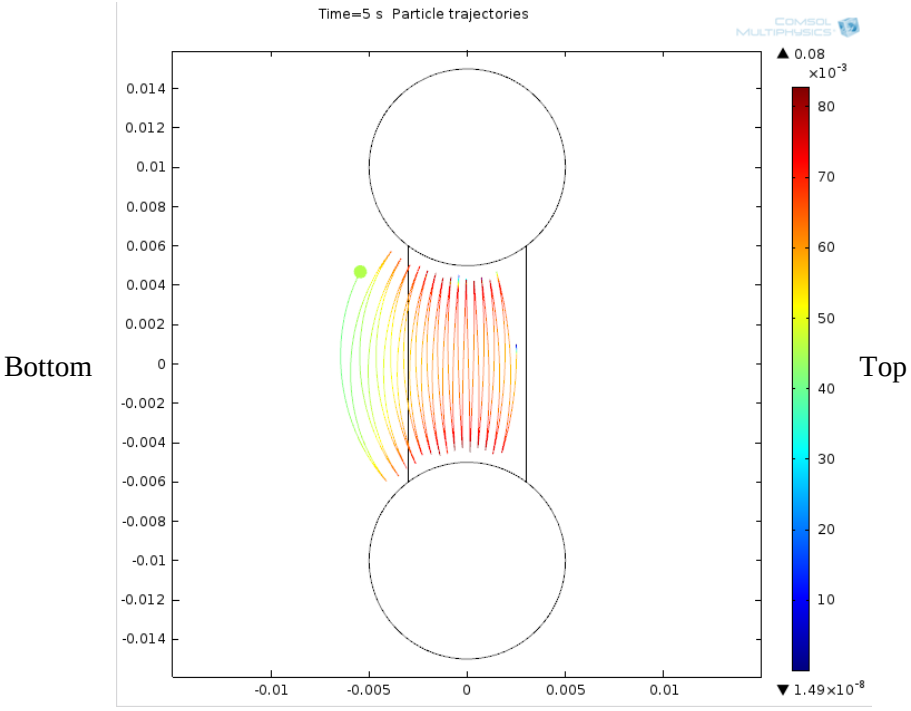

Figure 7:12 Particle trajectory of 200 µm particle under 7.5 kV DC electric field at 5 s with spherical electrode

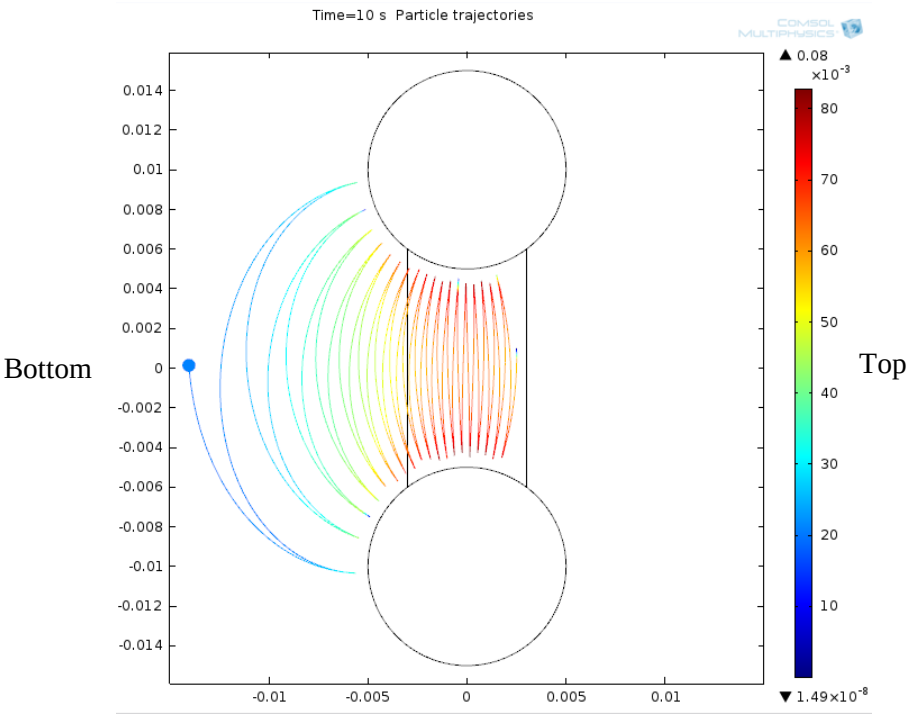

Figure 7:13 Particle trajectory of 200 µm particle under 7.5 kV DC electric field at 10 s with spherical electrode

The above particle trajectory results show that as time progressed, the particle moving close to the mid-point of the electrodes. The velocity is the largest when the particle is in the middle of the electrodes as was shown in Figure 7:4 where the DEP force intensity were also shown. It then

continues towards the left due to gravity. Eventually the particle will fall to the bottom of the tank after ~10 s. It was observed during the experiments that some particles are indeed falling to the bottom of the tank. But as the microscope was focused from the top, it was difficult to monitor the movement of the particles to the bottom of the tank at all the times.

7.4.4 The Effect of Different Particle Sizes

The evolution of the particle size is also investigated for an applied DC voltage of 7.5 kV. The particle sizes used for these simulations are 100 µm, 200 µm and 300 µm and the results are shown in Figure 7:14 , Figure 7:15 and Figure 7:16 respectively.

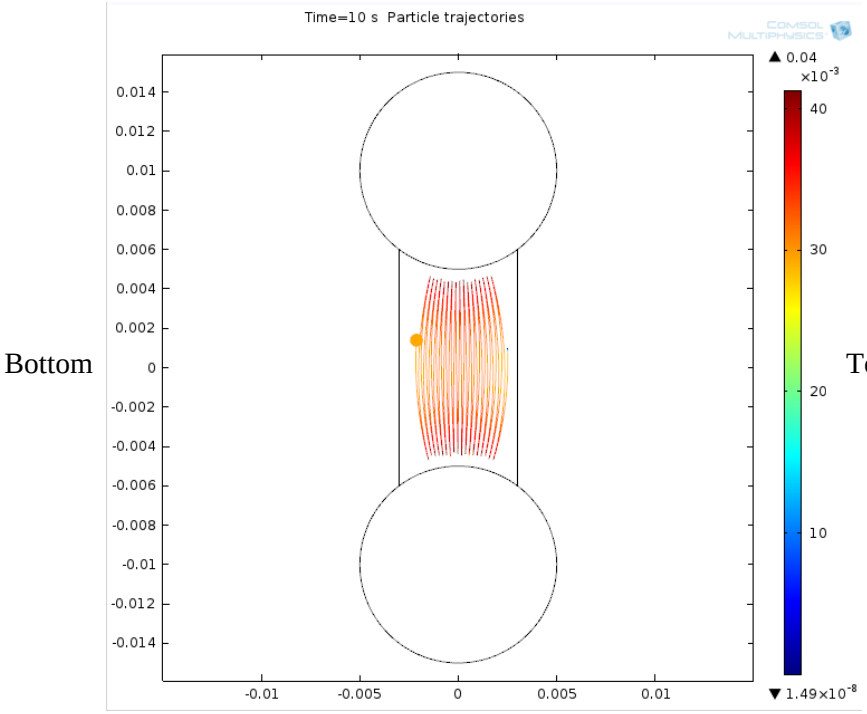

Figure 7:14 Particle trajectory of 100 µm particle under 7.5 kV DC electric field at 10 s with spherical electrode

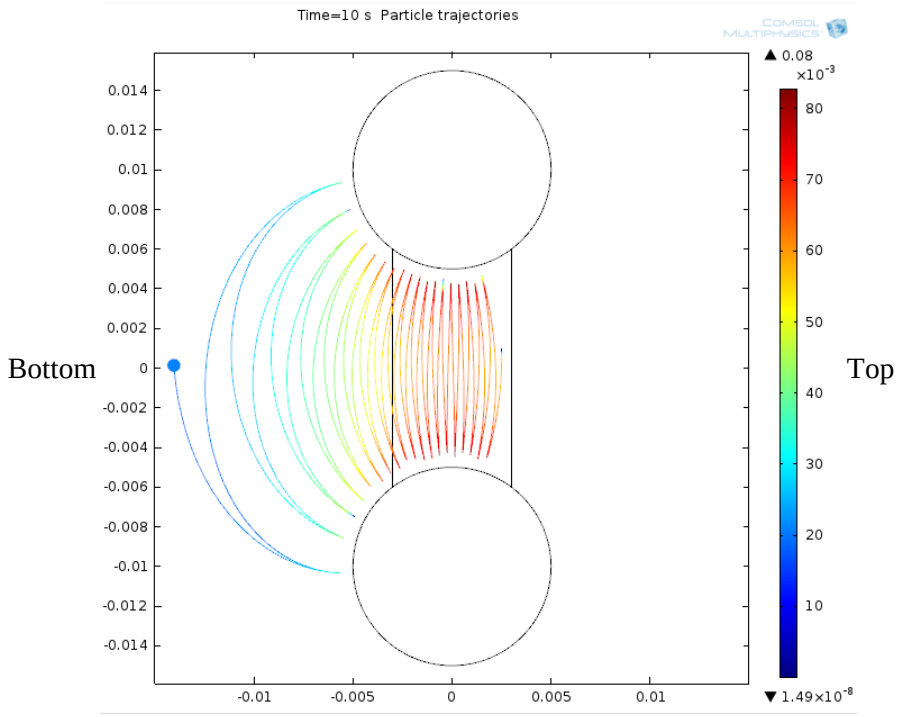

Figure 7:15 Particle trajectory of 200 µm particle under 7.5 kV DC electric field at 10 s with spherical electrode

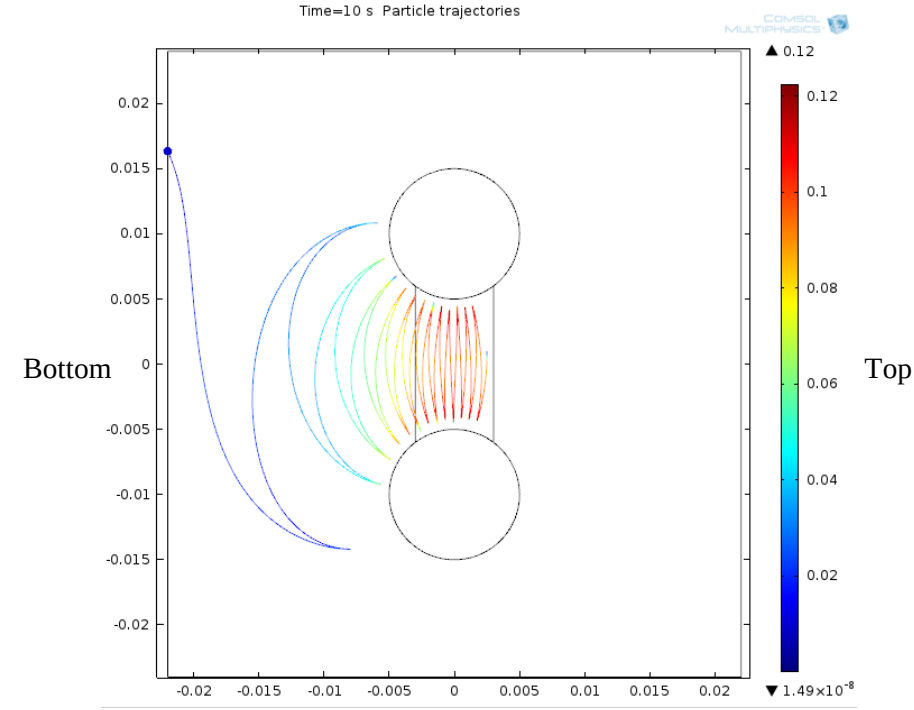

Figure 7:16 Particle trajectory of 300 µm particle under 7.5 kV DC electric field at 10 s with spherical electrode

The results from the different sizes of particle show very similar behavior observed in the experimental section. As the particles became smaller they were subject to only charging and discharging which can be seen in the appendix section where 63 – 150 µm and less than 63 µm

particles results are shown. Most of the time, in the absence of long fibre near the vicinity of the electrodes no bridging were observed and the particles were found to be only charging and discharging. Similar tendency is also observed in the simulations. As the particles getting bigger, there velocity dropped and affected by the gravity quicker than smaller particles.

7.4.5 THE EFFECT OF ELAPSED TIME WITH NEEDLE PLANE ELECTRODE

These simulations and evaluating the effect of time on particle trajectory for needle-plane electrode system. Applied voltage for these results was 6 kV and the particle size was 100 µm. The simulation results for 0 s, 2.5 s, 5 s and 10 s are shown Figure 7:17 , Figure 7:18 , Figure 7:19 and Figure 7:20 respectively.

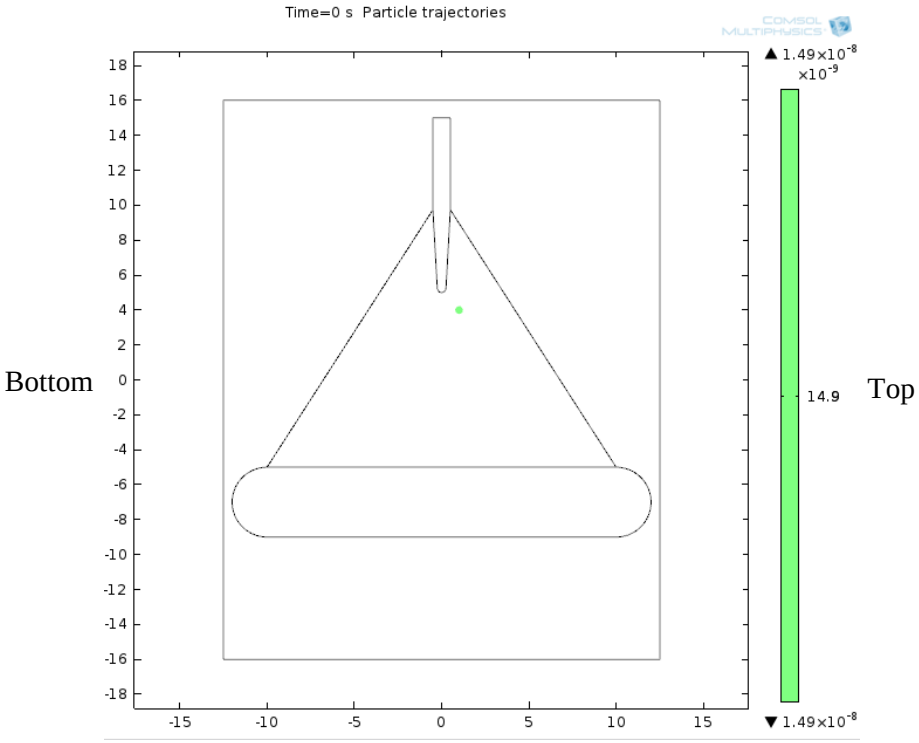

Figure 7:17 Particle trajectory of 100 µm particle under 6 kV DC electric field at 0 s with needle-plane electrode

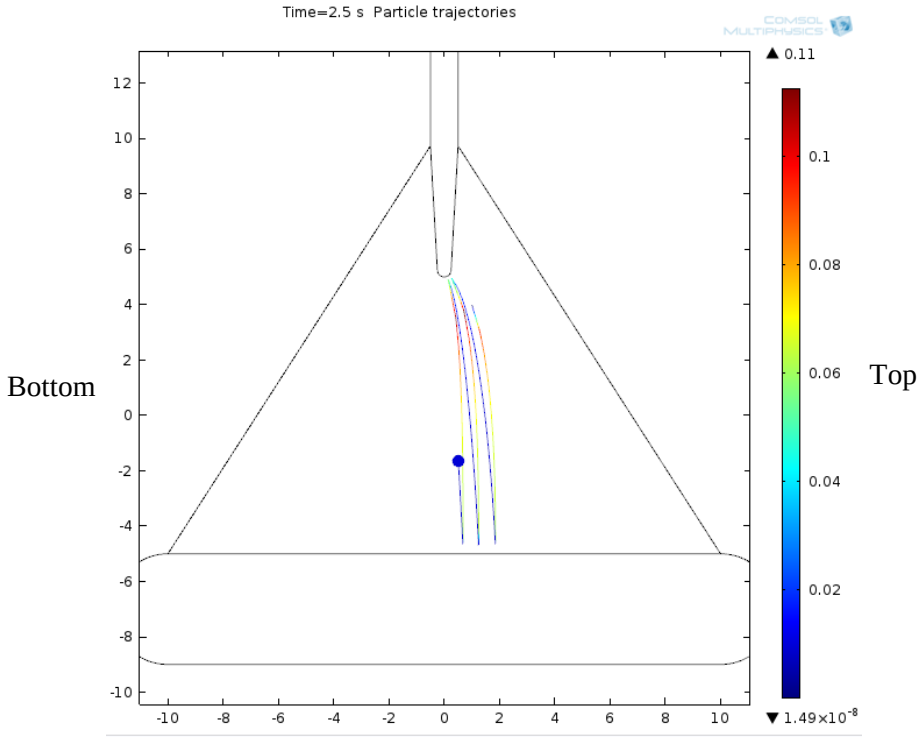

Figure 7:18 Particle trajectory of 100 µm particle under 6 kV DC electric field at 2.5 s with needle-plane electrode

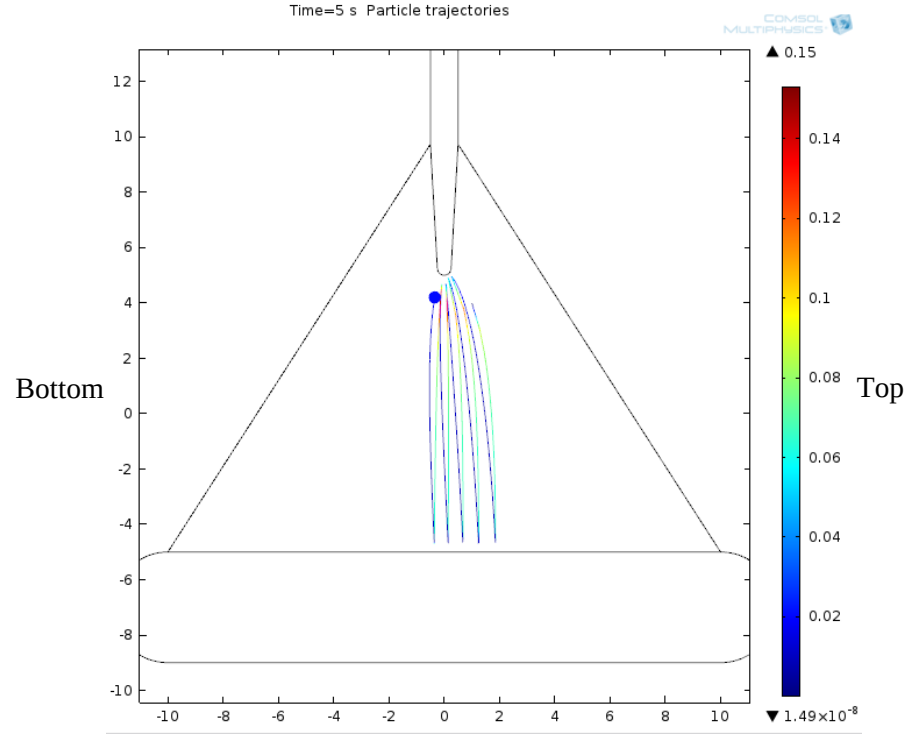

Figure 7:19 Particle trajectory of 100 µm particle under 6 kV DC electric field at 5 s with needle-plane electrode

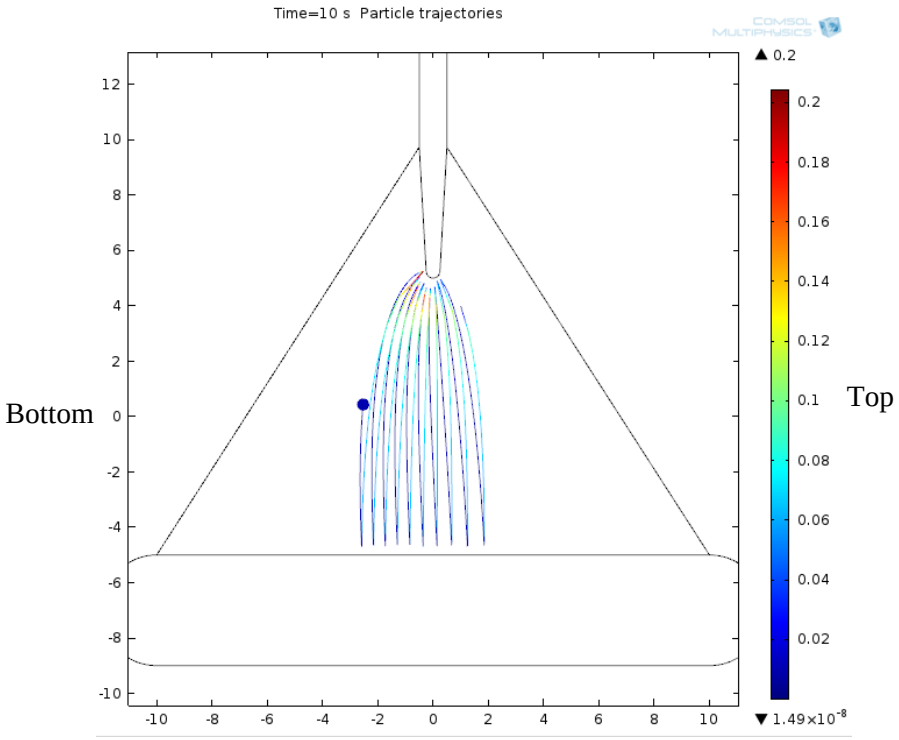

Figure 7:20 Particle trajectory of 100 µm particle under 6 kV DC electric field at 10 s with needle-plane electrode

The above simulation results from needle-plane electrode systems shown that the particle trajectory follow the electric field line as for the simulation result shown in earlier section. The velocity of the particle near the needle-tip is higher than the ground electrode as the gradient of electric field is the highest on the needle-tip. There will be another force which is not considered in this simulation is needle injected by the convection force in the liquid which would have increased the velocity of the particle. Nevertheless, these simulations reflected the observations made in the experiments with regards to the charging and discharging behaviors of the particles closely. Some of the limitations of these simulation are the unknown variable used such as charge reduction, particle size and particle shape.

7.5 Conduction Bridging of the Particles

The conduction current of the mixture of oil and cellulose particles always had higher value than clean oil. Because of the higher current value, it was assumed that the media is partially conducting. So, this simulation model developed by assuming that the media is conducting.

7.5.1 Electric Conductivity of Mixtures

It is assumed that the presence of dust affects the properties of oil. The total conductivity or permittivity depends on the oil and dust conductivity or permittivity. The electric field is calculated

with the dielectric permittivity or the conductivity of the mixture of oil and dust. The concentration of the particles needs to account since the non-uniform presence of particles in oil implies that the conductivity and permittivity of the mixture will also be non-uniform and will depend on where the particles are concentrated.

Three different formulae were derived from the Looyenga formula where permittivity of mixtures are expressed [119]:

$$\sigma_{mix} = a_1 c * \sigma_p + (1 - a_1 c) * \sigma_{oil} \quad \textbf{7:15}$$

$$\sigma_{mix}^{1/\alpha_2} = c * \sigma_p^{1/a_2} + (1 - c) * \sigma_{oil}^{1/a_2} \quad \textbf{7:16}$$

$$\sigma_{mix} = \sigma_p^{a_3 c} \cdot \sigma_{oil}^{1-a_3 c} \quad \textbf{7:17}$$

a_1, a_2 and a_3 are three constants. c is the concentration of the particles.

The same expressions are assumed for the dielectric permittivity of the mixture.

7.5.2 Velocity and Particle Interactions

The experimental study revealed that when dust particles are close enough, they tended to attach themselves and preventing themselves to move. Thus, there is a clear link between the velocity of the particles and their concentration which implies that there should be a critical concentration preventing the particles to move. This can be modeled using the following expression of the modified velocity v'_p (m is a constant) [103]:

$$v'_p = \begin{cases} 0 & if\ c > c_{critical} \\ v_p * \left(1 - \left(\frac{c}{c_{critical}}\right)^m\right) & if\ c \leq c_{critical} \end{cases} \quad \textbf{7:18}$$

The velocity of the particle as a function of the concentration is plotted Figure 7:21 in as an example.

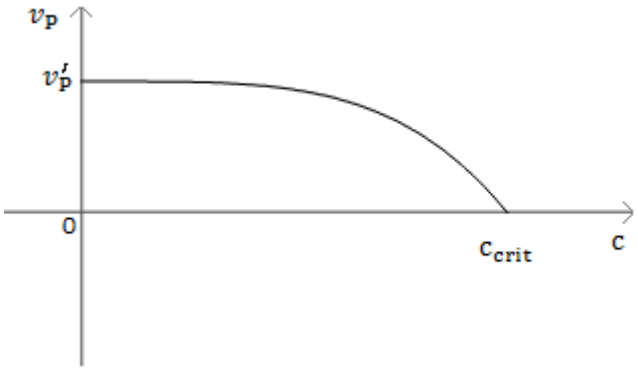

Figure 7:21 Particle Velocity with Particle Interaction Taken into Account, m=4 [103]

Higher value of m will make the transition between v_P and 0 smoother when approaching $c_{critical}$.

7.5.3 THE DIELECTROPHORETIC VELOCITY OF A FIBRE

In [82], they have derived and measured the dielectrophoretic velocity of fibres and examine the applicability of dielectrophoresis for fibre classification.

For the derivation, fibres are considered to be prolate spheroids with the minor axis equal to the fibre diameter d, the major axis equal to the fibre length l and γ the aspect ratio $(\frac{l}{d})$. This assumption is often made in the theoretical derivation of fibre behaviour [82].

A fibre of dielectric constant ε_p, is placed in an electrically insulating medium of lesser dielectric constant ε_m, and viscosity η in an electric field E. The problem is to determine the force on the fibre and the resulting velocity. Placzek [106] originally derived the force for a prolate spheroid in a vacuum, but the notation from Smythe's [120] partial solution is used. The spheroid orients with its length parallel to the field. The dielectrophoretic velocity of a conductive fiber can be expressed as

$$v = \lim_{\gamma \to \infty} \frac{\varepsilon_m \varepsilon_0}{24\eta} L^2 \frac{ln\, 2\gamma - 0.5}{ln\, 2\gamma - 1} \nabla E^2 \qquad \textbf{7:19}$$

which shows that the velocities is a function of aspect ratio only and is nearly unity provided that $\gamma > 5$. The approximation is wholly inappropriate for $\gamma < 2$. The dielectrophoretic velocity is proportional to the square of the length, and is independent of the diameter ignoring the very weak aspect ratio. In conclusion, the conductive fibres can be classified by length even if they are polydisperse in diameter [82].

7.6 MODEL DEVELOPMENT

COMSOL multiphysics software has been chosen for many advantages to simulate the bridging effect which are discussed below. The second step is to simulate the model using the software and compare the results obtained in experimental study.

7.6.1 GEOMETRY OF THE MODEL AND MESHNG

The experimental setup consisted of two 10 mm diameters of spherical electrodes and the gap between them 10mm placed in the middle of a 550 ml glass tank. The exact geometry of experimental setup has been chosen for mathematical model. Therefore, two spherical electrodes drawn and placed in a rectangular oil-filled tank with the following dimensions [103, 105, 110, 111]:

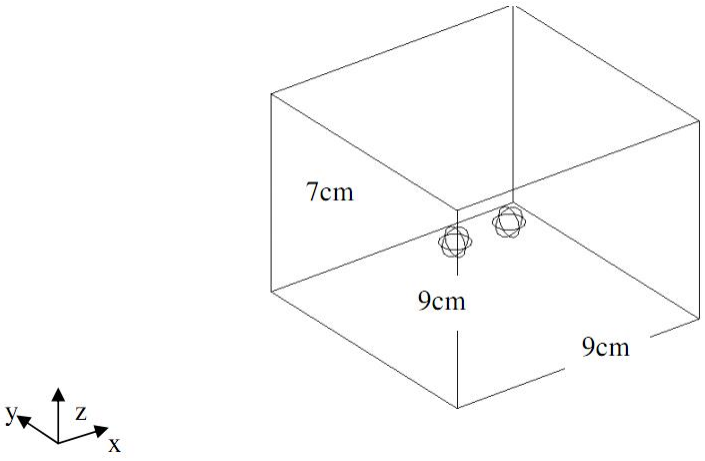

Figure 7:22 Geometrical Model in a 3D Configuration [103]

The rectangular sample tank was initially in 3D. To reduce the simulation time, a 2D model with cylindrical symmetry around the z-axis is chosen as shown below.

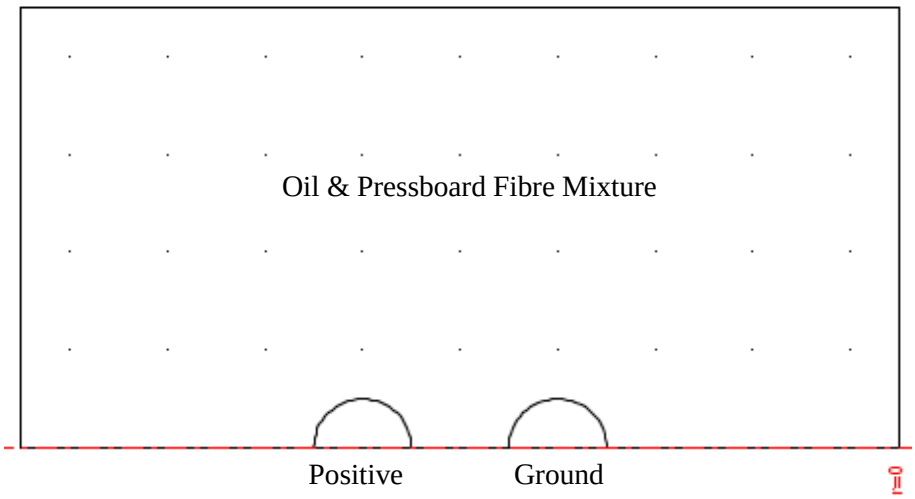

Figure 7:23 2D Model Geometrical in, with Cylindrical Symmetry around z axis

The cylindrical symmetry around the z-axis implies that the tank is cylindrical rather than rectangular. This generates another source of error to the result.

It is important to find an appropriate meshing for the problem as COMSOL uses Finite Element Analysis. Normal mesh is taken for the tank and finer mesh is applied around the electrodes. Finer mesh size slows down simulations.

7.6.2 ELECTROSTATIC MODEL

The particle velocity of the dust particle depends both on the dielectrophoretic and the drag forces. Knowing the value of the time constant can simplify the problem greatly. We know from the literature that:

- ε_0 is the vacuum permittivity $8.85 * 10^{-12} F/m$
- ε_{oil} is the oil dielectric constant and permittivity $2.2\varepsilon_0$
- ε_p is the dust particles dielectric constant and permittivity $4.4\varepsilon_0$
- σ_{oil} is the oil conductivity $2 * 10^{-13} S/m$
- σ_p is the pressboard dust particles conductivity. Currently the value is not known, as the current flows through the bridge, it is assumed that the particle conductivity is greater than the oil conductivity. σ_p is assumed to be equal to $5 * 10^{-5} S/m$ to start with.

The time constant value calculated using equation 7.4 is:

$$\tau = 1.5576 * 10^{-6} s \qquad \textbf{7:20}$$

Since the time interval considered is 3000 s, τ can be considered negligible. The particles interactions with m=4 taking into account equation (7:18) for a smoother transition, the complete expression of the velocity of fibres are given by:

$$v_p = \begin{cases} 0, & c \geq c_{crit} \\ \lim_{\gamma \to \infty} \frac{\varepsilon_m \varepsilon_0}{24\eta_{oil}} L^2 \frac{ln\, 2\gamma - 0.5}{ln\, 2\gamma - 1} \nabla E^2 * \left(1 - \left(\frac{c}{c_{crit}}\right)^4\right), & c < c_{crit} \end{cases} \quad \textbf{7:21}$$

From simulation, the model was best described when $a = 2.3$ and thus:

$$\sigma_{mix} = \sigma_p^{2.3c} * \sigma_{oil}^{1-2.3c} \quad \textbf{7:22}$$

For the calculation of the electric potential two equations can be used depending on whether the media is considered to be conducting or not. From N. N. A. Jaafar's work, the permittivities were considered, no bridge was formed in the time interval considered. So it was assumed that the presence of the dust particles had negligible effect on the total permittivity of the medium. Therefore, it was assumed that dust particles were mainly affecting the total conductivity of the medium rather than permittivity. The calculation of the electric potential was chosen to be (2.6) where [103]:

$$\nabla(\sigma_{mix} \nabla V) = 0 \quad \textbf{7:23}$$

This equation was implemented in COMSOL considering the AC/DC Module and the Conductive Media DC Mode for transient analysis. The electrodes are considered to be inactive. This Mode allows the calculation of the electric field assuming that the mixtures of oil and pressboard dust particles are conductive.

7.7 Convection-Diffusion

The Conductive Media DC Mode allows the computation of the electric field and dust particles conductivity. Knowing this velocity, the Convection-Diffusion Mode under the Chemical Engineering module allows the calculation of the mass balance differential equation given in equation 7:24. The time scaling coefficient δ_{ts} is taken to be 1 and R = 0 assuming no chemical reaction takes place. The evaluation of the diffusion coefficient was a crucial task.

According to [103], when the diffusion coefficient is non-zero, the particles accumulate around the electrode surface. The diffusion coefficient D_p was taken as $10^{-6}\, m^2.s^{-1}$, a small number to produce minimal disturbances.

The final mass balance implemented in COMSOL is:

$$\frac{\partial c}{\partial t} + \nabla \cdot \left(-D_p \nabla c\right) = -v_p \nabla c \quad \text{7:24}$$

The constants and parameters chosen for the model are summarized in the table below.

Constants		Parameters	
ε_0	$8.85 \cdot 10^{-12} F/m$	V_0 (applied DC voltage)	2 kV, 7.5 kV and 15 kV
ε_p	$4.5\varepsilon_0$	σ_p	$5 \cdot 10^{-5}$ S/m
ε_{oil}	$2.2\varepsilon_0$	a	2.3
η_{oil}	$0.02\ kg/m \cdot s$	c_0 (initial particle concentration)	0.0001,2,3 a.u.
σ_{oil}	$2 \cdot 10^{-13} S/m$	d	$100 \cdot 10^{-6}$ m
		l	$1000 \cdot 10^{-6}$
		c_{crit}	0.153 a.u.
		m	4

Table 7-2 Constants and Parameters

7.8 Simulation Results of Particle Bridging

The results obtained from the simulations by focusing on the influence of applied DC voltage, time, the initial and critical particle concentration and the particle size.

7.8.1 Applied DC Voltage

The influence of the applied DC voltage is investigated for the concentration of the particles (compared to the electric field gradient) and the evolution of the current through the bridge as a function of time.

In order to study the influence of the applied DC voltage, the assumed values of the various parameters are shown in Table 7-3.

Table 7-3 Parameters for Influence of the Applied DC Voltage

Parameters	
$\boldsymbol{V_0}$ *(applied DC voltage)*	2 kV, 7.5 kV and 15 kV
T	3000 s
σ_p	$5 \cdot 10^{-5} S/m$
a	2.3
c_0 (initial particle concentration)	0.0003 a.u.
d	$150 \cdot 10^{-6}$ m
l	$1000 \cdot 10^{-6}$ m
c_{crit}	0.153 a.u.
m	4

At 600 s, the concentration of the particles are observed and compared to the electric field. This is shown in Figure 7:24, Figure 7:25 and Figure 7:26 below at 2 kV, 7.5 kV and 15 kV respectively:

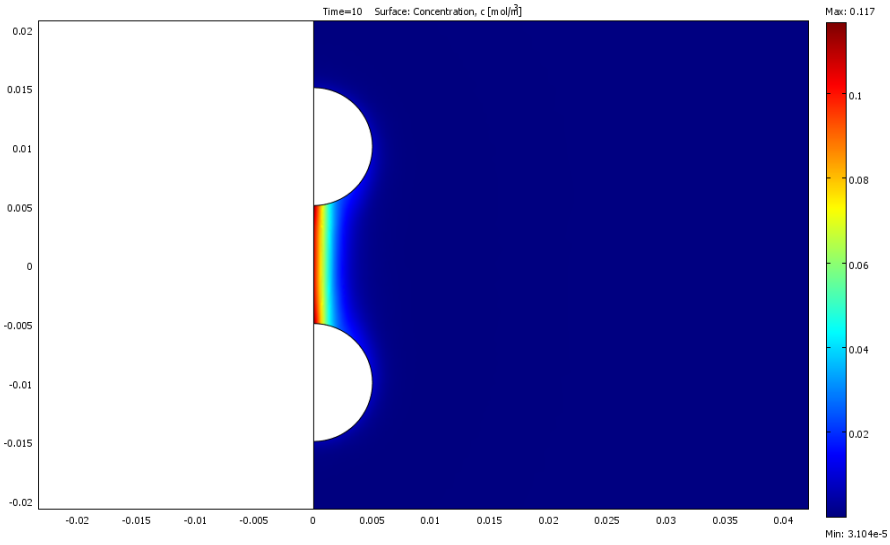

(a) Particle Concentration

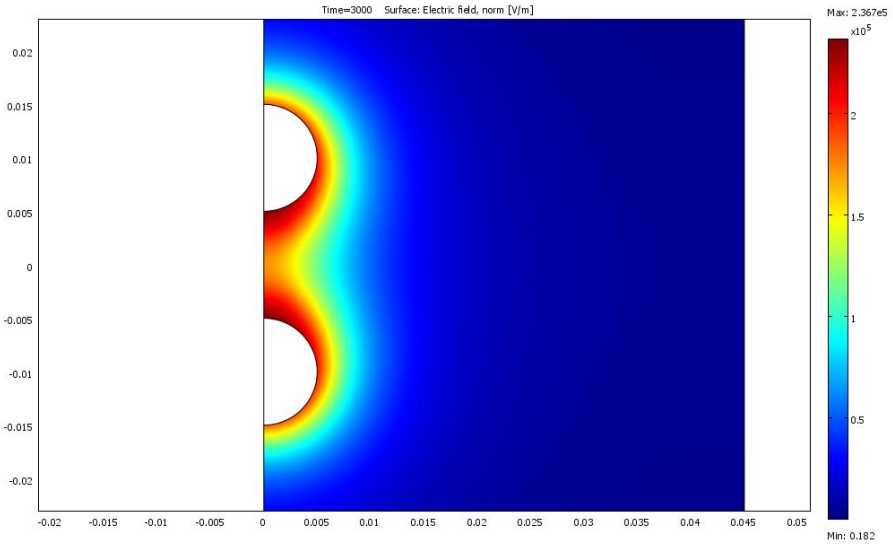

(b) Electric Field Norm

Figure 7:24 Particle Concentration and Electric Field at 2 kV

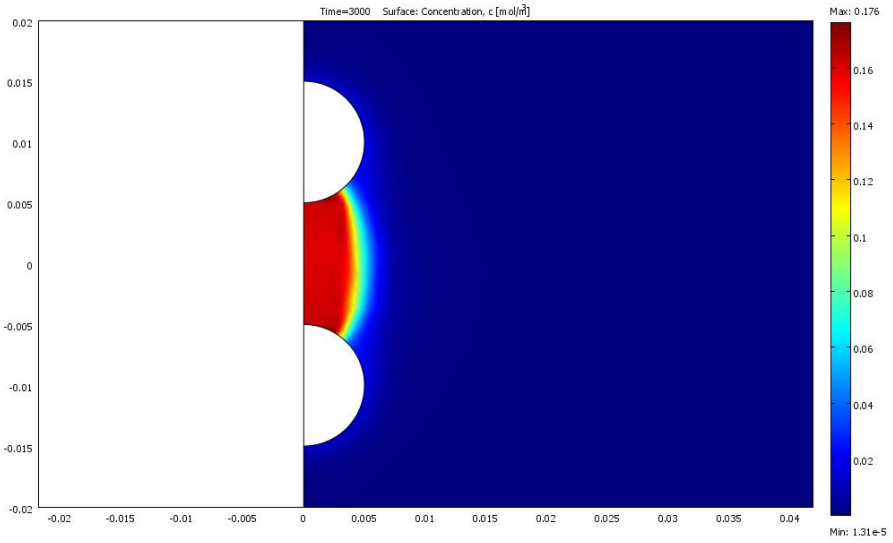

(a) Particle Concentration

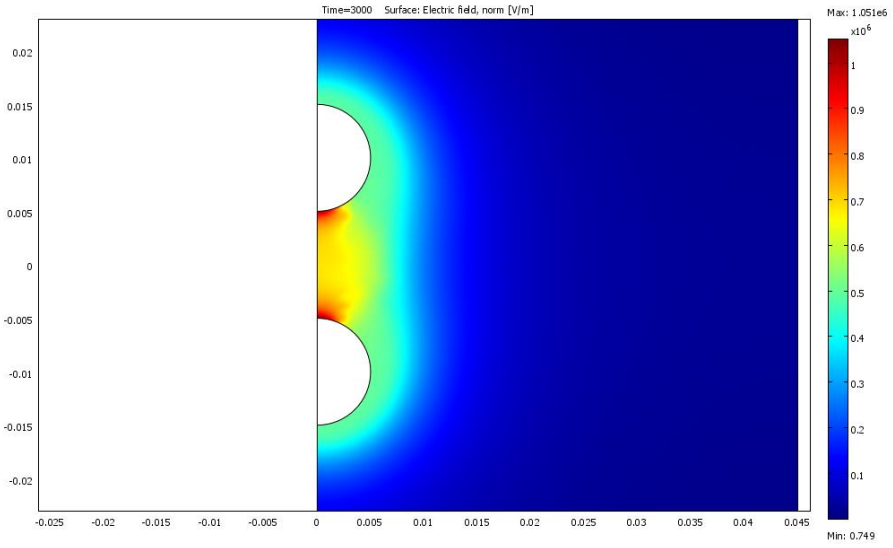

(b) Electric Field Norm

Figure 7:25 Particle Concentration and Electric Field at 7.5 kV

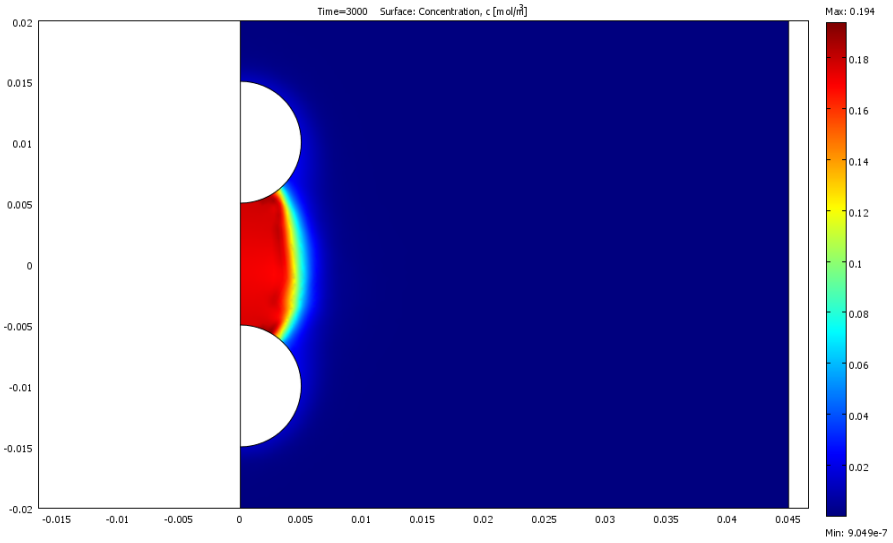

(a) Particle Concentration

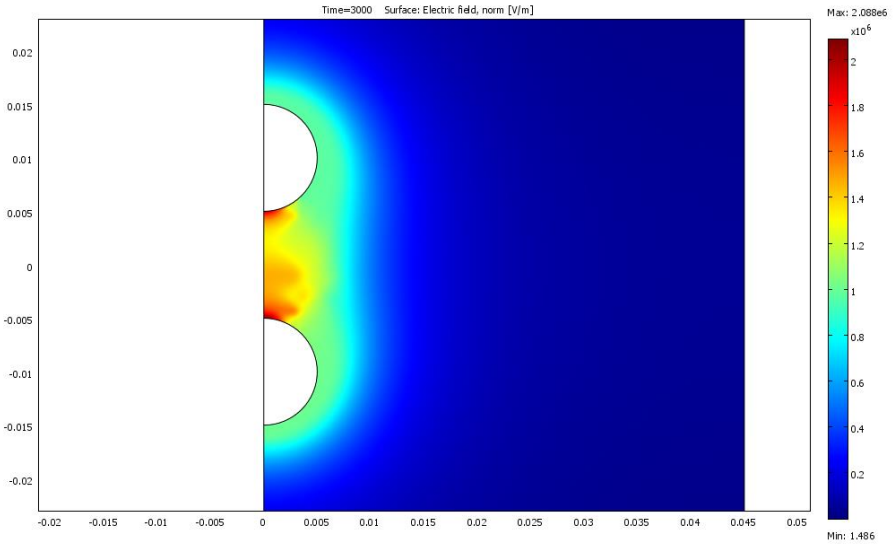

(b) Electric Field Norm

Figure 7:26 Particle Concentration and Electric Field at 15 kV

Figure 7:27 summarizes the values of the saturation currents for the three investigated voltages:

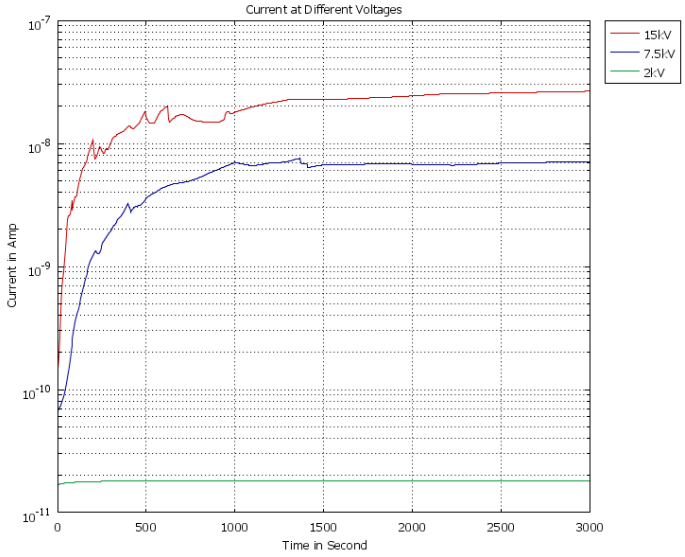

Figure 7:27 Current Flowing through the Bridge at 2 kV (green), 7.5 kV (blue) and 15 kV (red)

7.8.2 TIME

The evolution of the electric field and the particle concentration is also investigated. The parameters considered are summarized in Table 7-4 below.

Table 7-4 Chosen Parameters for the Study of the Influence of Time

Parameters	
V_0 (applied DC voltage)	7.5 kV
T	10s, 90s, 600 s
σ_P	$5 \cdot 10^{-5} S/m$
a	2.3
c_0 (initial particle concentration)	0.0003 a.u.
d	$150 \cdot 10^{-6}$ m
l	$1000 \cdot 10^{-6}$ m
c_{crit}	0.153 a.u.
m	4

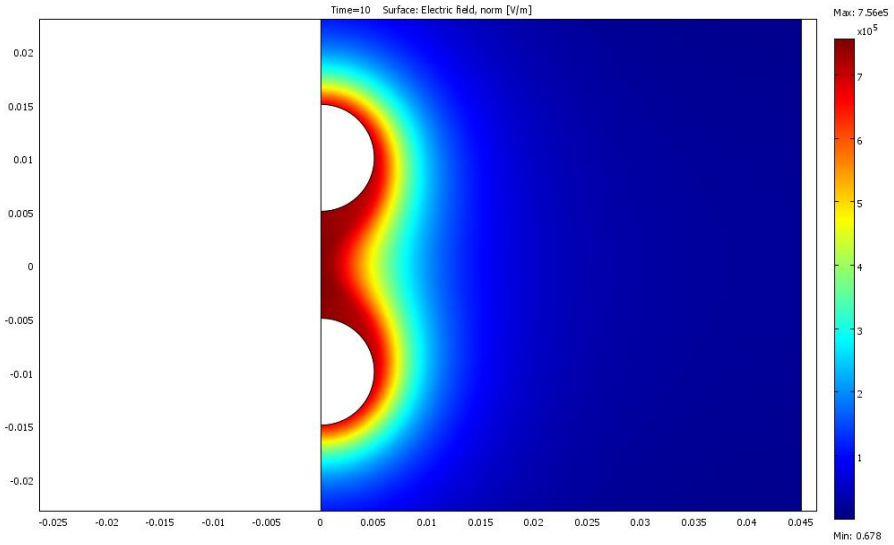

(a) At 10 seconds

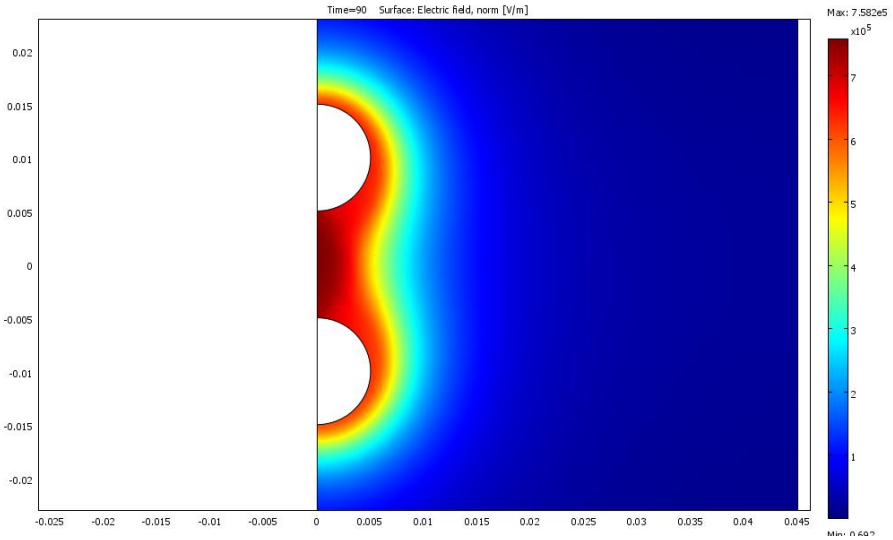

(b) At 90 seconds

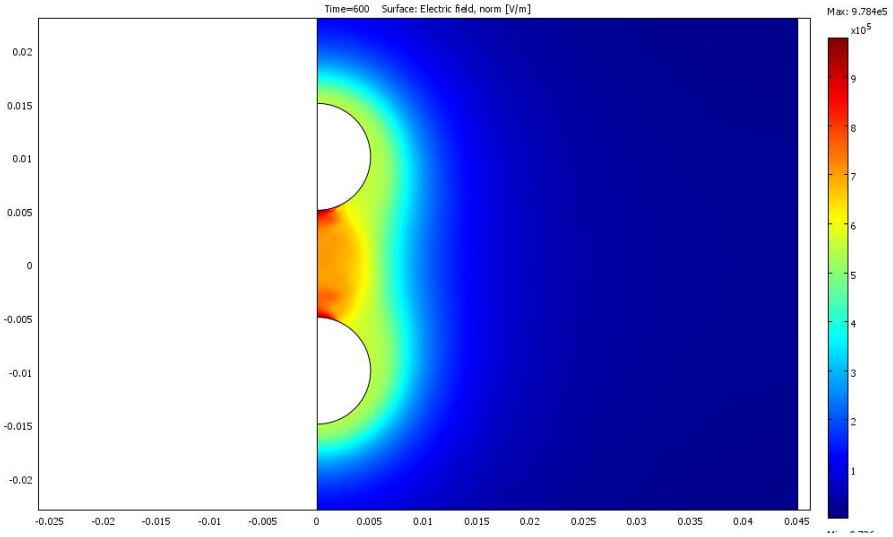

(c) At 600 seconds

Figure 7:28 Evolution of the Electric Field in Function of Time at 7.5 kV

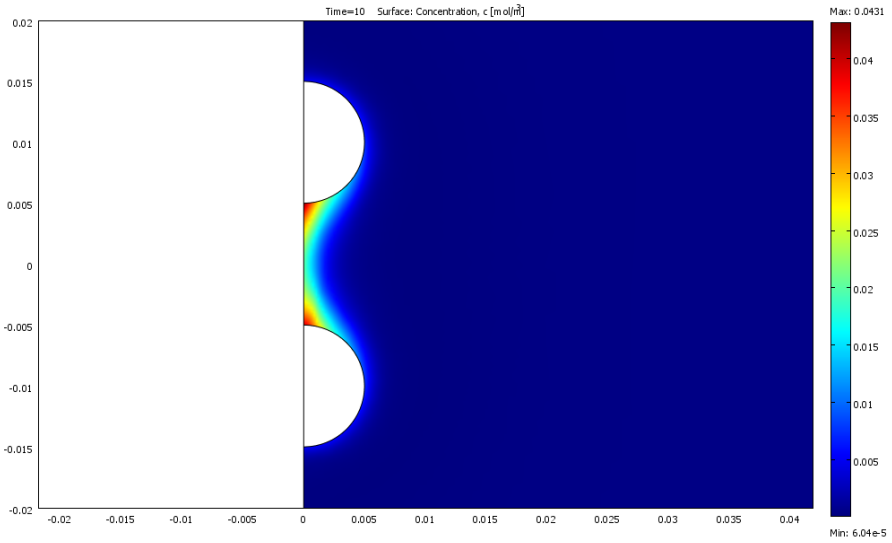

(a) At 10 seconds

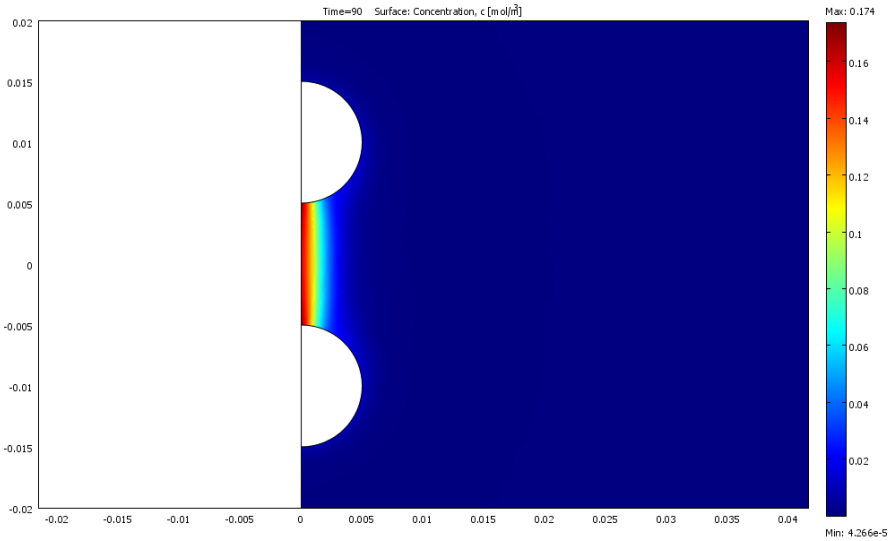

(b) At 90 seconds

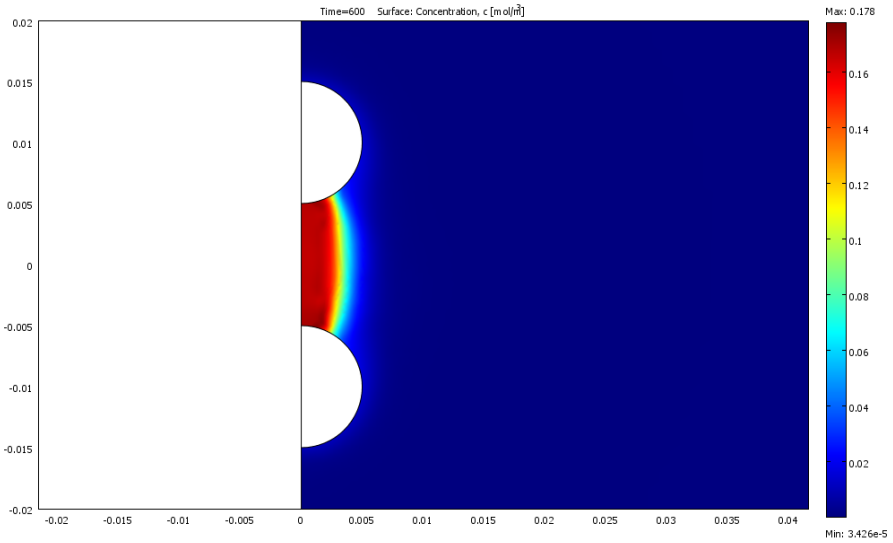

(c) At 600 seconds

Figure 7:29 Evolution of the Particle Concentration in Function of Time at 7.5 kV

7.8.3 INITIAL PARTICLE CONCENTRATION

The evolution of the particle concentration and the current through the bridge as a function of the initial particle concentration is investigated here. The parameters taken into account are summarized in Table 7-5 below.

Table 7-5 Parameters for the Influence of different initial Particle Concentration

Parameters	
V_0 (applied DC voltage)	7.5 kV
t	3000 s
σ_P	$5 \cdot 10^{-5} S/m$
a	2.3
$\boldsymbol{c_0}$ (initial particle concentration)	0.0001 to 3 a.u.
d	$150 \cdot 10^{-6}$ m
l	$1000 \cdot 10^{-6}$ m
c_{crit}	0.153 a.u.
m	4

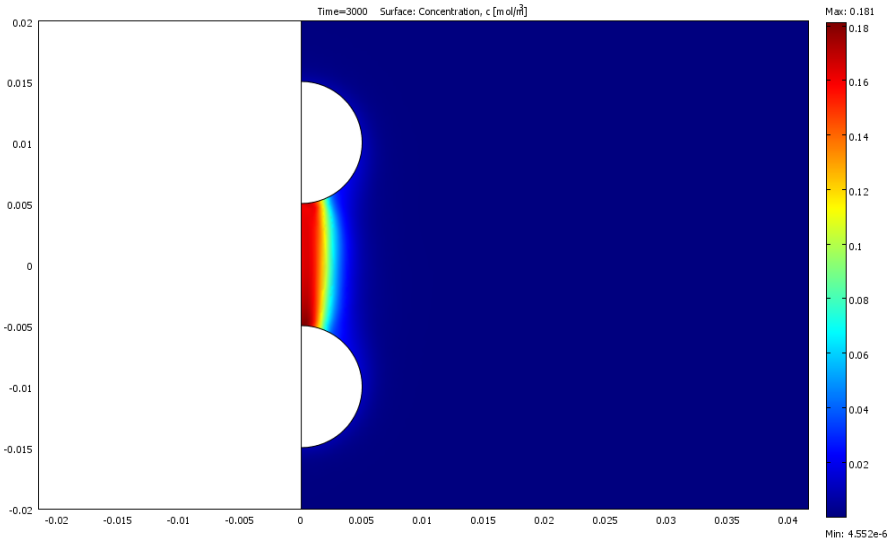

(a) $c_0 = 0.0001$

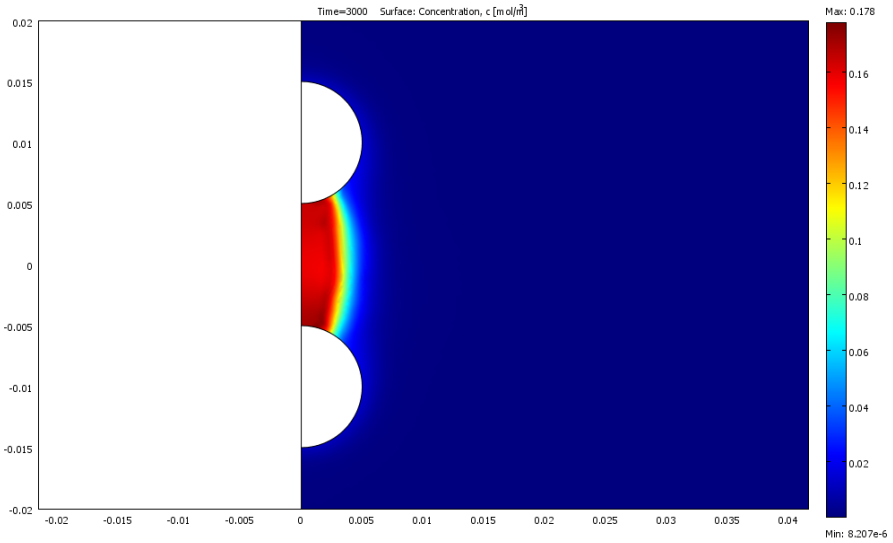

(b) $c_0 = 0.0002$

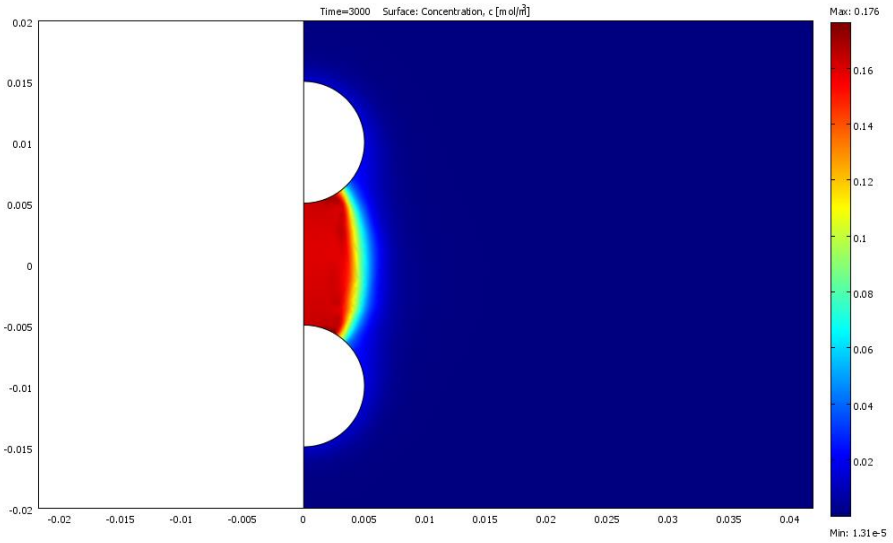

(c) $c_0 = 0.0003$

Figure 7:30 Particle Concentration at Different the Initial Particle Concentration at 7.5 kV

The evolutions of the current flowing through the bridge in function of time are summarized below at the three investigated concentration levels.

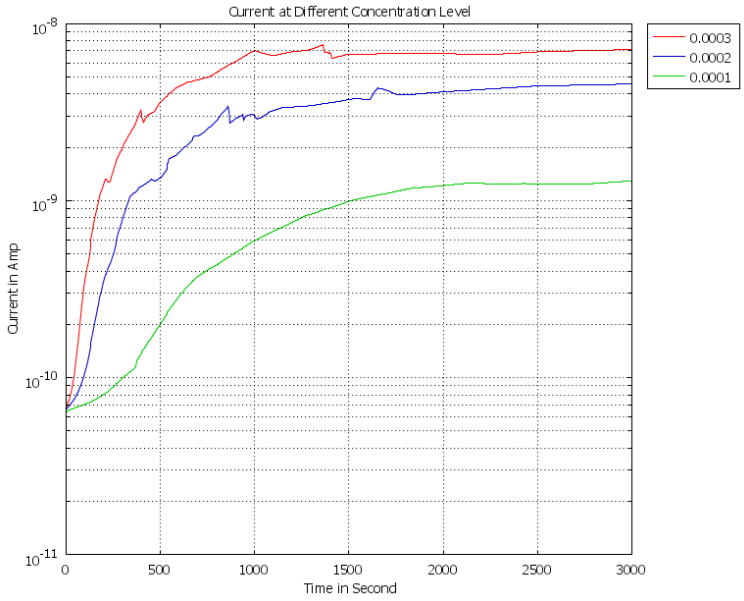

Figure 7:31 Current through the Bridge with the Initial Concentration of 0.0001 (green), 0.0002 (blue) and 0.0003 (red)

7.9 COMPARISONS WITH THE EXPERIMENTAL RESULTS

In the simulation, the particles accumulate in the highest gradient of electric field region which is true for the experimental results as well. Figure 7:24, Figure 7:25 and Figure 7:26 compare the

electric field norm to the particle concentration. The conduction current illustrated in Figure 7:27 for different voltages rises very quickly and then reaches saturation.

The DC voltage has a huge influence on the bridge formation. The bridge is formed much quicker at higher voltage which agrees with the experimental results. A very thin bridge formed at 2 kV experimentally but it was not very clear in simulation. This is because the initial concentration is not known. The experimental study uses concentration level by weight, but it is not possible to have the exact value of concentration by volume as the density of the particles was unknown. The saturation current also increases with voltage. Although the saturation current values obtained experimentally do not match with the simulation model but the bridge formation at different levels of concentrations matches with the experimental results.

The results from simulation correspond well to the experimental results when comparing bridge formation at different times. The bridge becomes thicker and thicker with time. At 7.5 kV, the bridge is formed at approximately 90 seconds. The bridge keeps growing until 600 seconds and then stops at its saturation point.

7.10 Comparisons with Existing Work: Implications and Limitations

This model is the first one describing the bridge formation between the two electrodes and the associated observed phenomena for fiber particles. The model still has many limitations. It is not possible to link the concentrations by weight to the concentrations by volume because the dust particles density is unknown. Several material properties are also unknown which prevented a more accurate analysis of the dust accumulation. The oil impregnated dust particles conductivity is also unknown. So the saturation current values at given voltages and concentrations are not true representation of the experimental work. Overall, the simulation model presented here provided a good understanding of the experimental observations and how the future model should be improved.

CHAPTER EIGHT: CONCLUSIONS AND FUTURE WORK

8.1 SUMMARY OF MAIN FINDINGS AND RESULTS

Through an extensive experimental study on cellulose particle contaminated transformer oil and mathematical modelling, this work has obtained useful results on bridging in transformer oil under the influence of AC, DC, and DC biased AC uniform and divergent fields. Several conclusions are summarized as follows.

Coulomb force is dominant factor for DC bridging. Although the contaminated particles brought to electrodes surfaces due to DEP force, after the contact they acquire charges from the electrodes and move to the other under influence of DC component of electric field. The particles which do not have enough repelling force (small charge) then stay attached to electrodes and they attract other oppositely charged particles. The attachment process is controlled by DEP force. This process leads to form complete bridge between the electrodes gap. As the voltage increased, the velocity of the particles and rate of bridge formation is intensified along with an associated conduction current. With an increase of DC voltage the bridges become wide but not denser. It is a result of the formation of the conductive path along the bridge and associated changes in the direction of DEP force.

The AC case shows absolutely different dynamics. The time averaged DEP force brings the particles to the electrodes surfaces. The particles acquire a charge during one half cycle and change of polarity prevent them to travel to the other electrode. Instead they are shaken in the vicinity of one electrode and form a beard. The particles don't create complete bridge opposite to the DC case. They cover only the electrode surfaces, the points where the DEP force is maximum. The overall rate of particles accumulation for AC case was slower than the DC one at the same voltage levels.

The DEP force and Coulomb force both act on the particles when the DC and AC voltages are combined. DEP force brings the particles to the electrodes surfaces, the particles get a charge, they start to move towards opposite electrode if the charge is large enough to overcome DEP force. As they move, strong DEP force brings them to the central line between the electrodes. The particles collide with each other and discharges between the particles take place. It reduces the particles mobility and creates bridge in the middle of the electrodes. Although the bridging dynamics is slower in comparison with pure DC case, the formed bridges are denser.

The experiments using different sizes of pressboard particles under a DC electric field with spherical electrodes revealed that the particle shape and size has the major impact on the bridge formation and conduction currents. It has been observed from the experiments that the fibre particles are mainly responsible for the creation of the bridge. The time to form the bridge with a smaller particle size was quicker than that of a bigger particle size. The bridges are strongly bonded for smaller particles. It can also be concluded that at higher voltages, the rate of bridge formation is strongly increased along with an associated current increase (non-proportional to voltage). The conduction current with smaller particles was always higher compared with that of bigger particles with the same level of contamination. The other important finding is that if the particles are too small, i.e. less than 63 μm, then the bridge would not be created without a long fibre.

Experiments with a needle-plane electrode system revealed that there were bridges formed for all three different levels of DC voltages and the conduction currents were non-linearly increased with applied voltages. It was observed that a sphere-sphere electrode system with a more uniform electric field created a thicker bridge than a divergent electric field with a needle-plane electrode system. The divergent electric field needed 16 times higher particle contamination to form the bridge than the spherical electrode system.

There was no bridge formed under a pure AC electric field either with spherical or with needle-plane electrode systems that had a more divergent electric field. The particles were accumulated in the both spherical electrodes. A different observation was found for the needle-plane electrode system under AC conditions. The particles were accumulated on the needle tip for 5 kV AC but the particles were going away from the needle and accumulated on the plane electrode for 10 kV and 15 kV AC. The reason is the convective flow in liquid due to the high electric field.

Investigation on DC biased AC voltage with a spherical electrode system revealed that the bridge was always formed under all three different levels of DC offsets combined with three different AC voltages. The results from bridging in a pure DC voltage and that same DC voltage biased with AC voltage showed that the bridges were strongly bonded because of the added AC voltage. The most important finding from these tests is that a bridge will always be created if AC voltages have any levels of DC offset.

There was no bridge formed in the case of a needle-plane electrode system under DC biased AC voltage. The pure DC bridging result were compared with the DC biased AC voltages and it revealed that all the particles were accumulated on the plane electrode, which was similar to an AC electric field. But the quantities of the particles were maximized because of the DC voltage combination.

Covered electrode experiments revealed that when the bond between the electrode surface and the kraft paper is tight, there is always a bridge formed for all the concentration levels tested (0.001% up to 0.003%) under DC and a DC biased AC electric field. The conduction current also increases with the level of contamination for a covered electrode system. A kraft paper barrier between the electrodes also could not prevent bridge formation and the current also increased with the level of concentration, which indicates that there was charge transfer through the paper barrier. The bridge formation was not possible with any of the concentration levels ranging from very low, 0.001%, to very high, 0.024%, when there was a loose bond between the electrode surface and the paper. This suggests that the extra layer of oil between the electrode and paper prevented charge transfer to the particles and hence no bridge formed.

In conclusion, the risk of creating a bridge in a HVDC converter transformer is very likely where there is DC biased AC voltage present. Paper or pressboard insulated metal parts do not stop bridging; oil convection is needed to prevent bridging and particle size if possible should be kept below 63 μm.

The charging and discharging simulation provided a good way of understanding how the current is transferred and hence the bridge formation. The simulation results had a very good overall agreement with experimental results. It predicted the particle the particles' pathway and how the particles are falling down. But the results could not be exactly validated for many factors like the velocity of a known size particle is unknown. They suffer from many unknown variables, i.e. the particle shape and size, charge reduction factor, etc.

The initial bridging simulation model also demonstrated the phenomenon of the bridge formation. The model successfully illustrates the process of particle accumulation between the electrodes matching the bridge size and relative saturation currents observed in the experiments for different applied voltage. The initial stage of the bridging is not described by the model and further refinements are required. The conduction currents from the simulation are not quantifiable with the experiments. This is due to many unknown variables and assumptions made for the model. The contamination levels for the experiments are the percentage by weight while for simulation they are by volume. So the contamination level for simulation could not be a true representation of experiments as the density of the pressboard dust particle is unknown. Nevertheless, the rate of increment in terms of current is similar in the two results, which shows that the model has simulated the same behaviour as the experiment.

8.2 FUTURE WORK

The project will be benefitted from extending the experimental work further to investigate the effect of temperature. As transformers are typically operated at elevated temperatures, it is vital to extend the above research to a higher temperature regime. Particle bridging characteristics as a function of oil viscosity will be revealed as oil viscosity changes with temperature. The viscosity has a direct impact on drag force. There is a possibility of the particle falling down to the bottom due to lower drag force. So, it is very important to investigate this issue further.

This research only considered a hypothetical contamination level of cellulose particles. The contamination level used here might be unrealistic compared to the real data from field. Therefore, it would be really beneficial to perform test with contaminated transformer oil from a real operational transformer.

The current particle trajectory simulation model could be extended with implementation of particle-particle electrostatic force to form the bridge between the electrodes using dielectric particles. The charge exchange mechanism for a dielectric particle has to be calculated using curve fitting technique from experimental velocity curve. A known size particle velocity under the influence of different voltages needs to be captured using a high-speed camera. This method would be more accurate to calculate the amount of charge transfer to the particle. This model could be a very useful tool to predict the behaviour of any other type of particle that might be present in a transformer oil. Transformer designers would be able change the properties of a particle to simulate any other type of particle's behaviour.

Appendix A LABVIEW INTERFACE

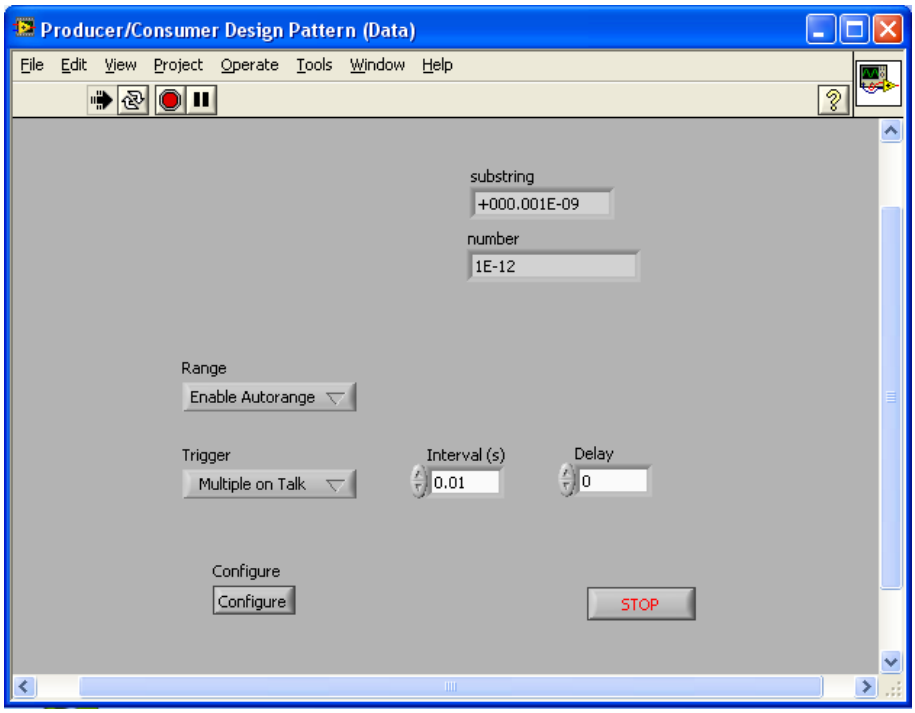

Figure A:1 Current measurement program interface

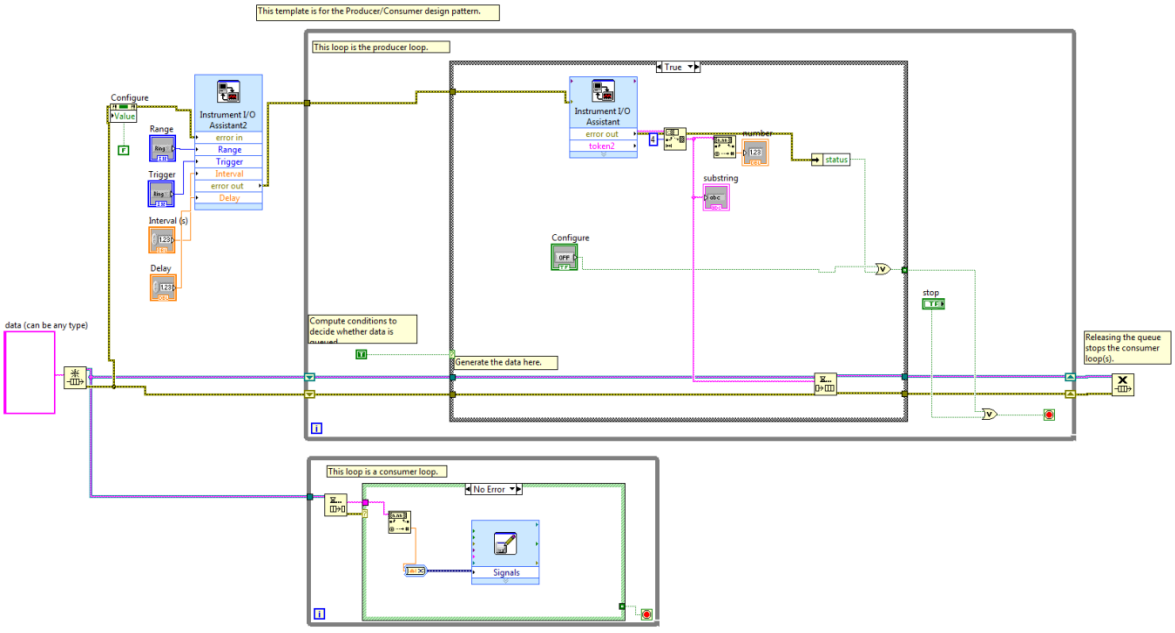

Figure A:2 Block diagram of the LabVIEW current measurement program

Appendix B DC TEST WITH 63-150 µM AND LESS THAN 63 µM

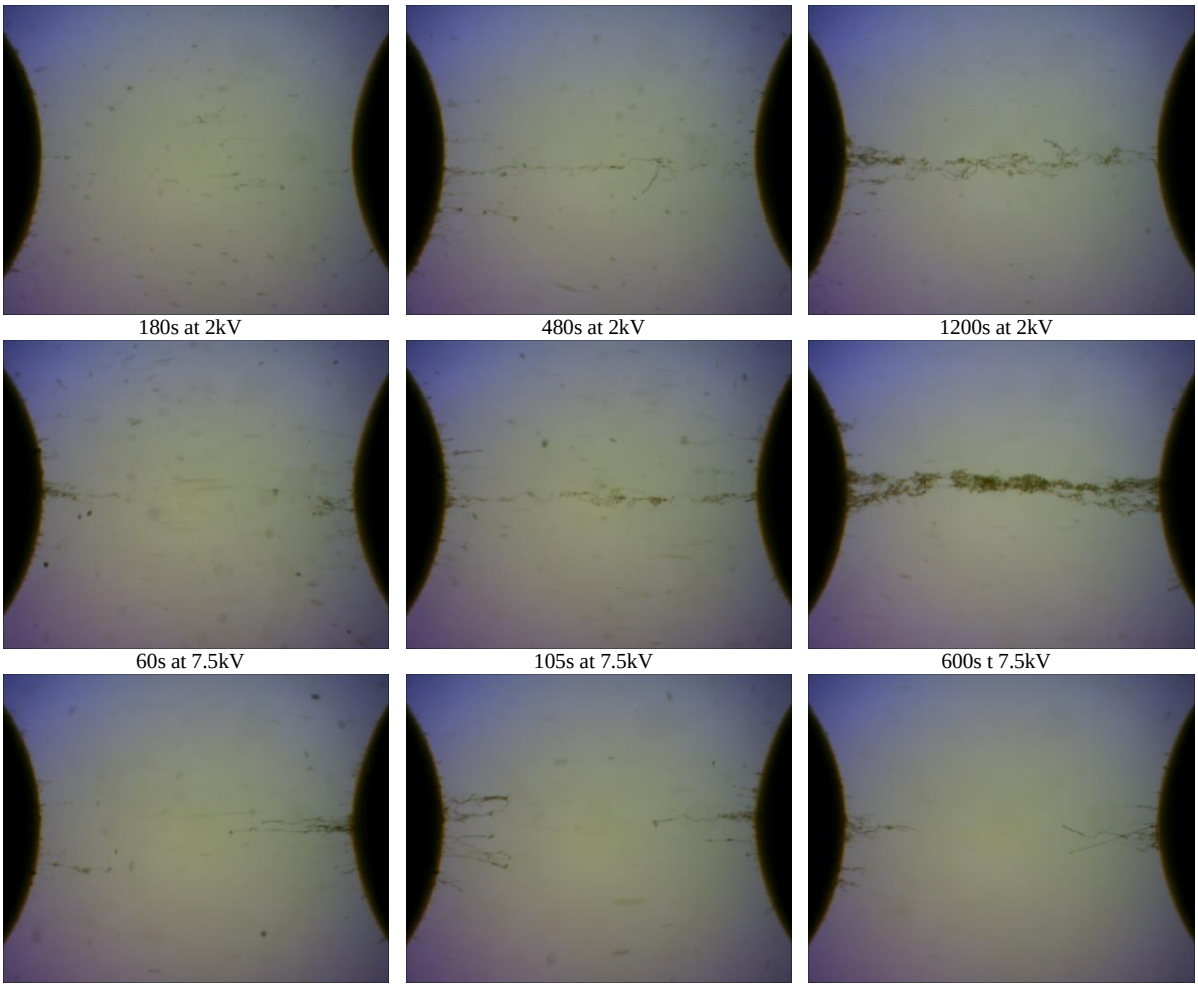

180s at 2kV | 480s at 2kV | 1200s at 2kV

60s at 7.5kV | 105s at 7.5kV | 600s t 7.5kV

30s at 15kV | 90s at 15kV | 180s at 15kV

Figure B:1 Optical microscopic images of bridging in contaminated transformer oil with 63 – 150 µm pressboard fiber, concentration level 0.001%

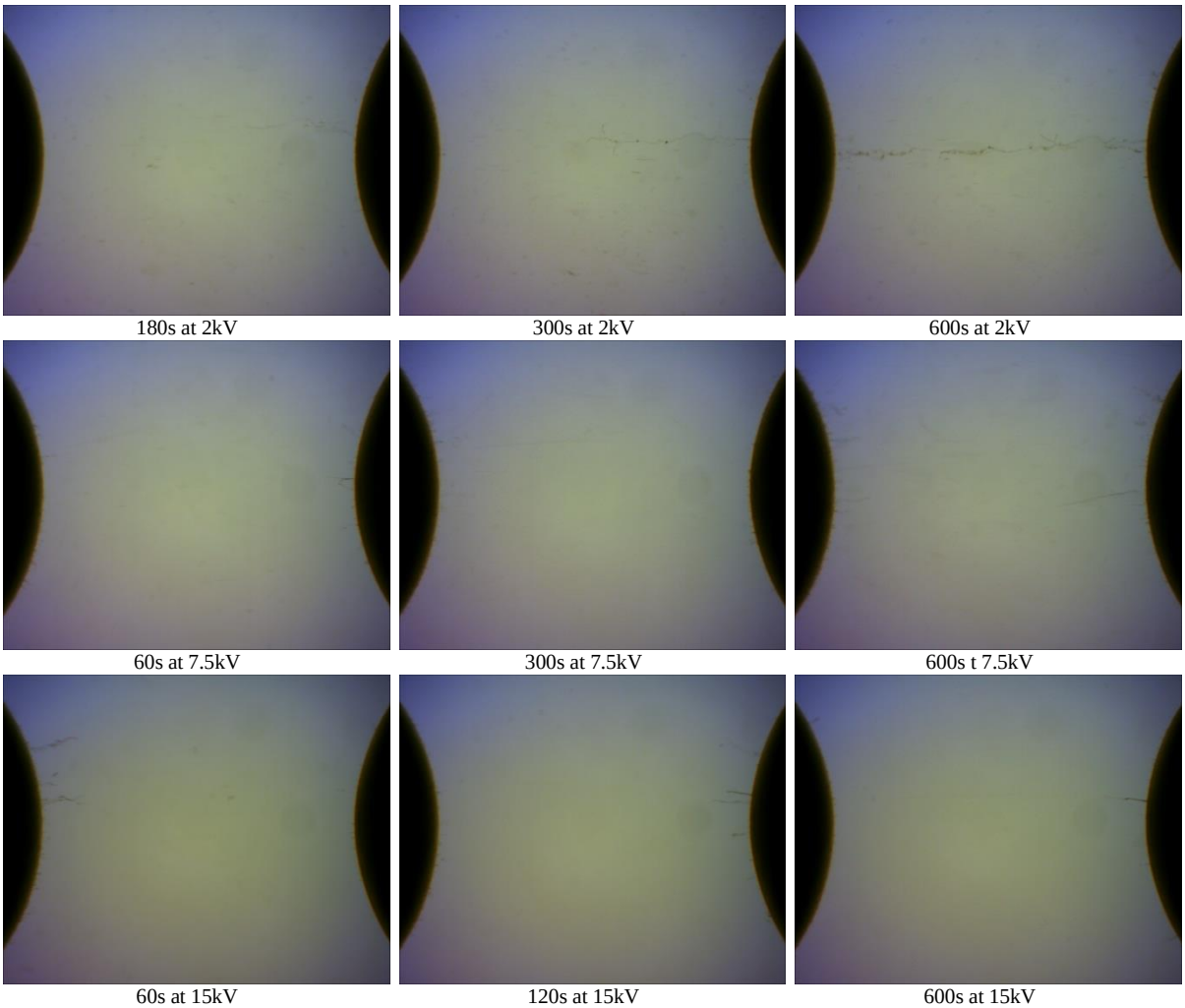

Figure B: 2 Optical microscopic images of bridging in contaminated transformer oil with less than 63 µm pressboard fiber, concentration level 0.001%

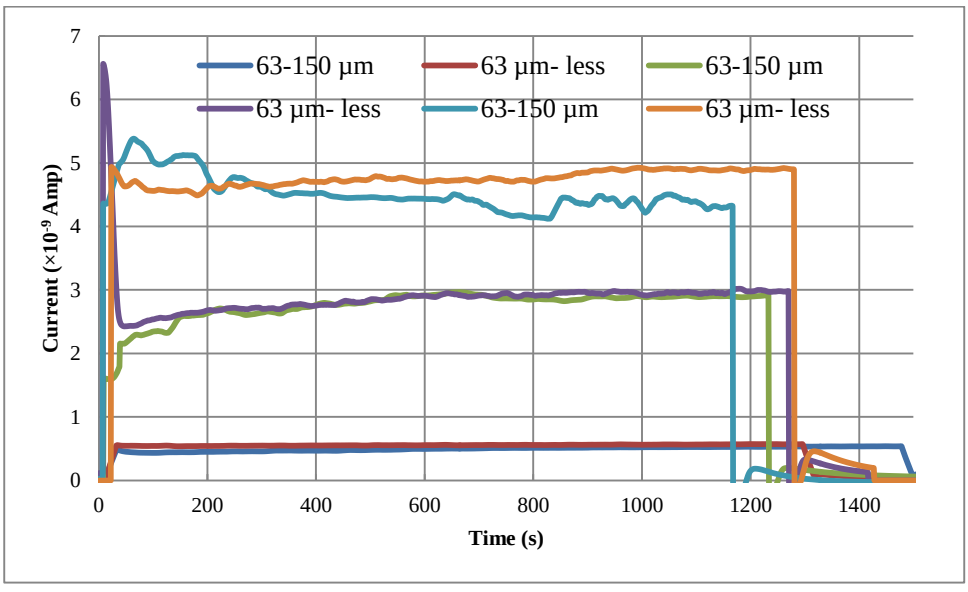

Figure B: 3 Conduction current for 0.001% concentration level for 63 µm – less and 63 – 150 µm

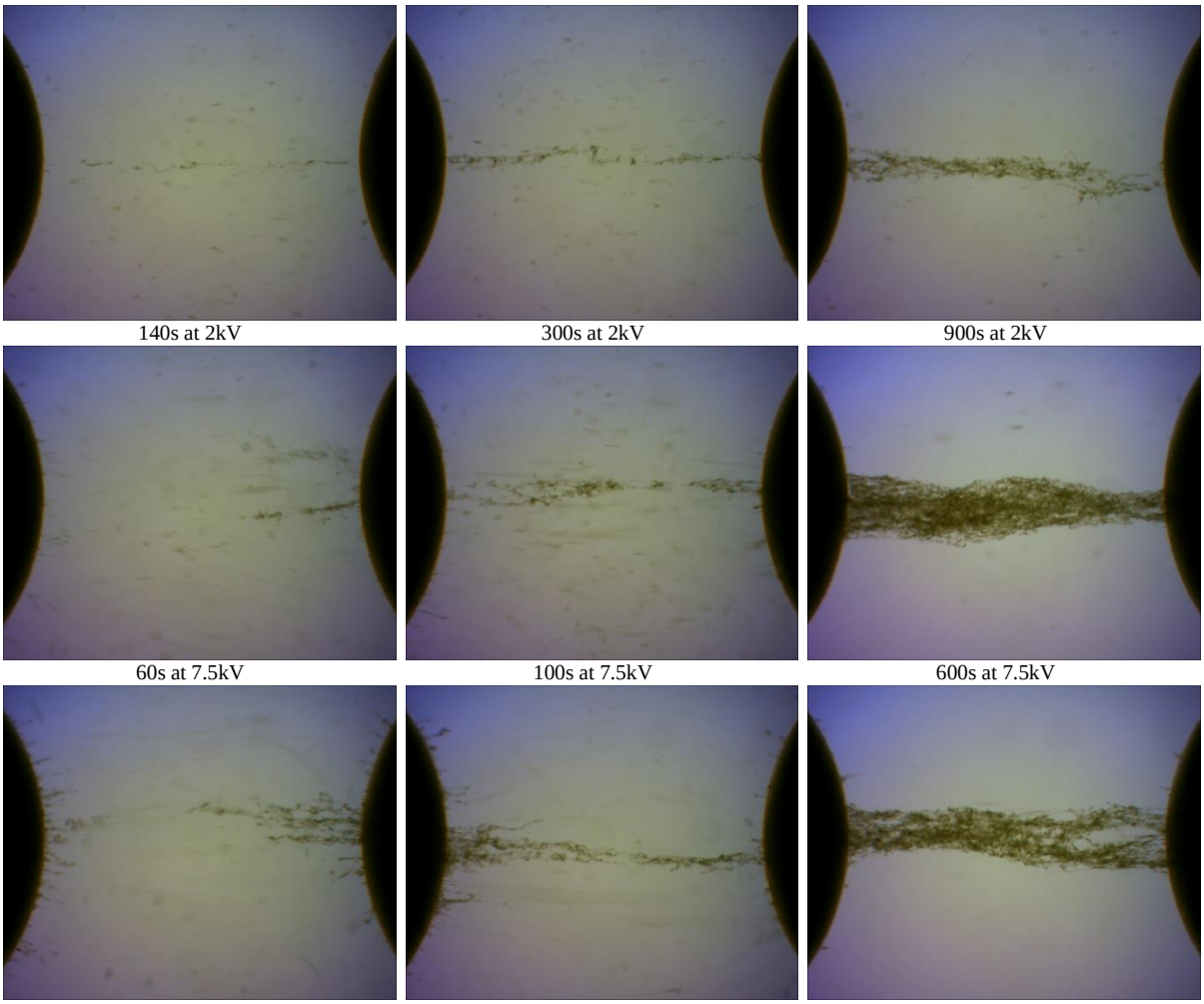

140s at 2kV | 300s at 2kV | 900s at 2kV

60s at 7.5kV | 100s at 7.5kV | 600s at 7.5kV

20s at 15kV | 35s at 15kV | 300s at 15kV

Figure B: 4 Optical microscopic images of bridging in contaminated transformer oil with 63-150 µm pressboard fiber, concentration level 0.002%.

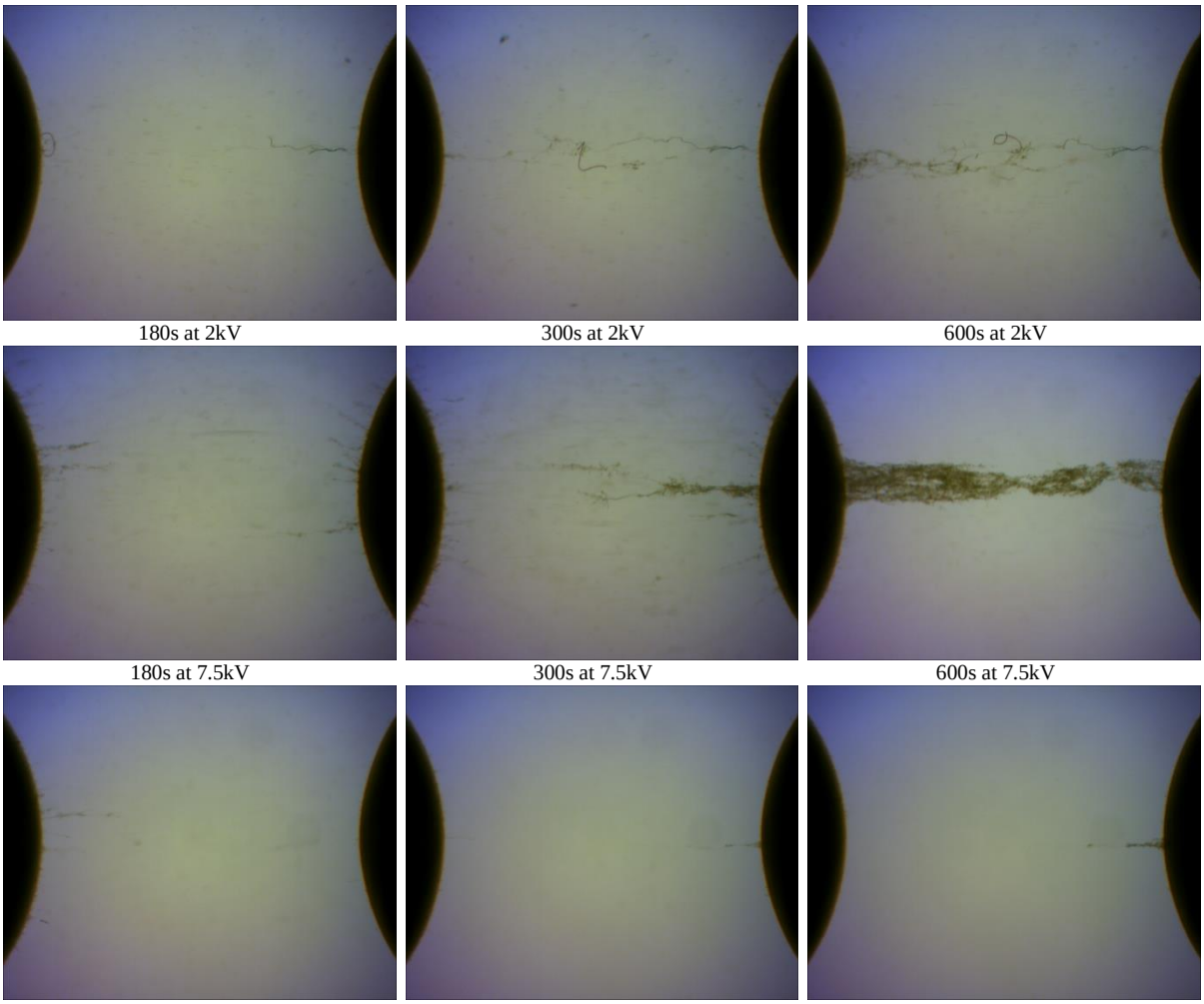

180s at 2kV | 300s at 2kV | 600s at 2kV

180s at 7.5kV | 300s at 7.5kV | 600s at 7.5kV

60s at 15kV | 300s at 15kV | 600s at 15kV

Figure B:5 Optical microscopic images of bridging in contaminated transformer oil with less than 63 µm pressboard fiber, concentration level 0.002%.

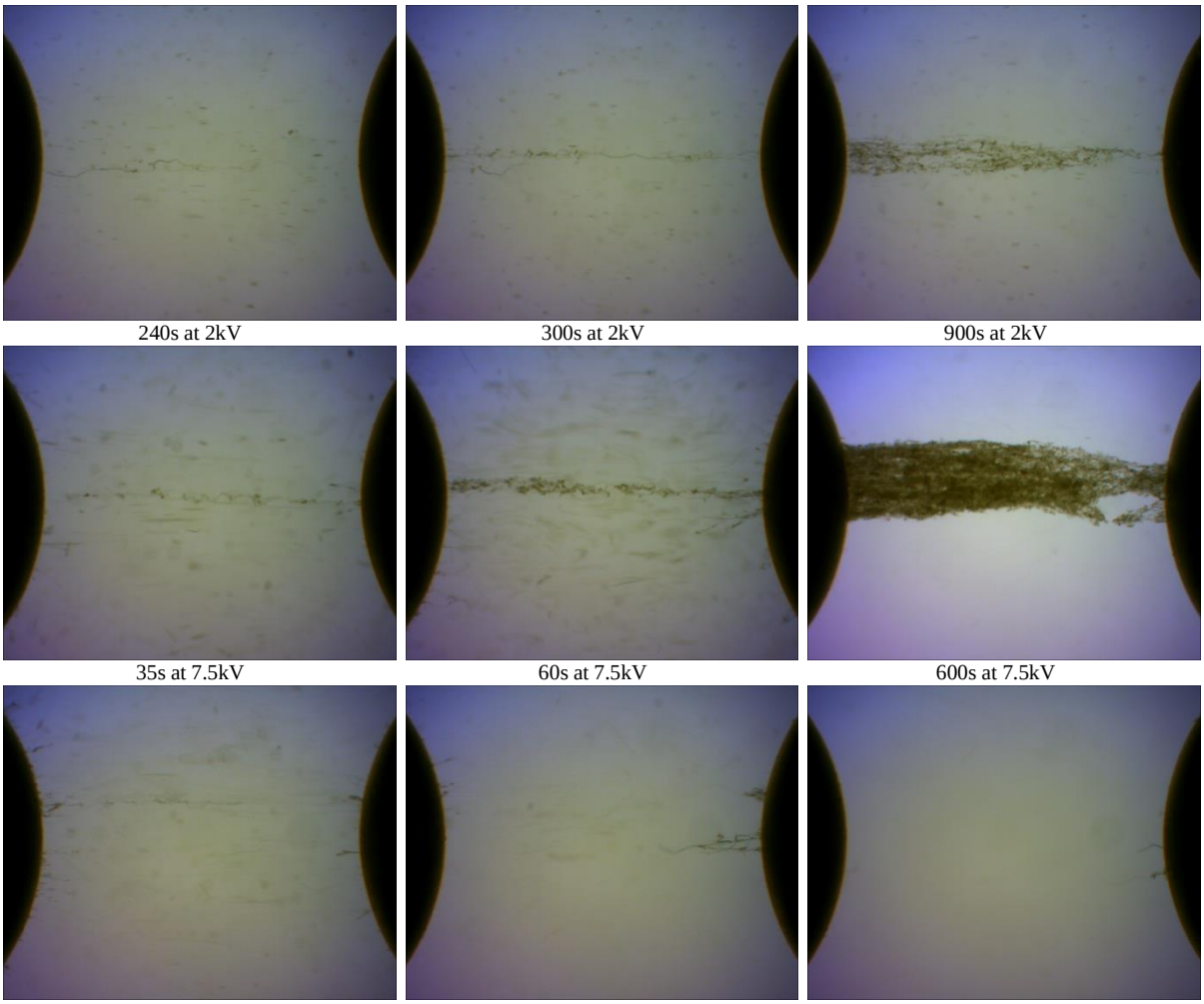

240s at 2kV | 300s at 2kV | 900s at 2kV

35s at 7.5kV | 60s at 7.5kV | 600s at 7.5kV

18s at 15kV | 90s at 15kV | 360s at 15kV

Figure B:6 Optical microscopic images of bridging in contaminated transformer oil with 63-150 µm pressboard fiber, concentration level 0.003%.

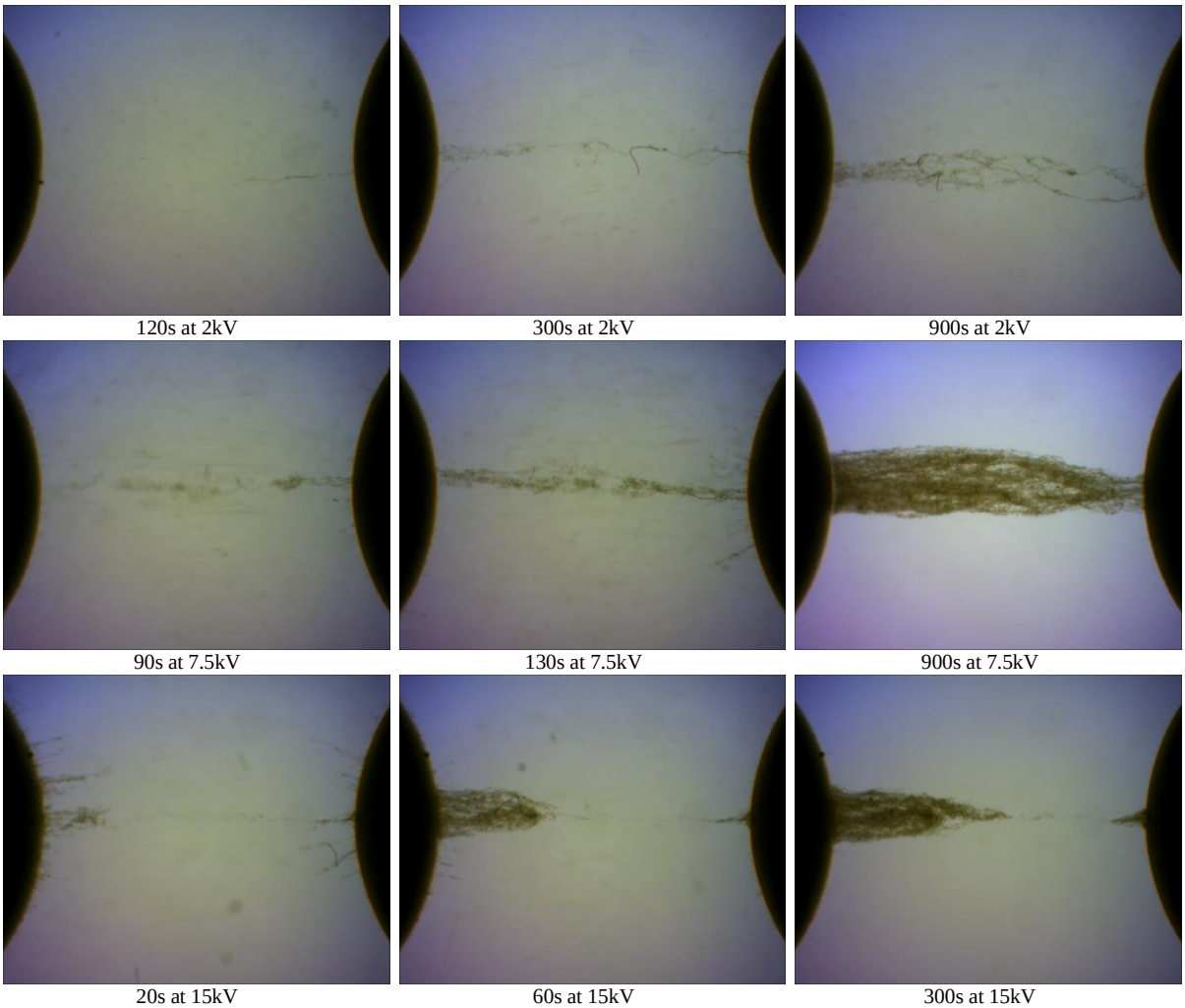

Figure B:7 Optical microscopic images of bridging in contaminated transformer oil with less than 63 µm pressboard fiber, concentration level 0.003%.

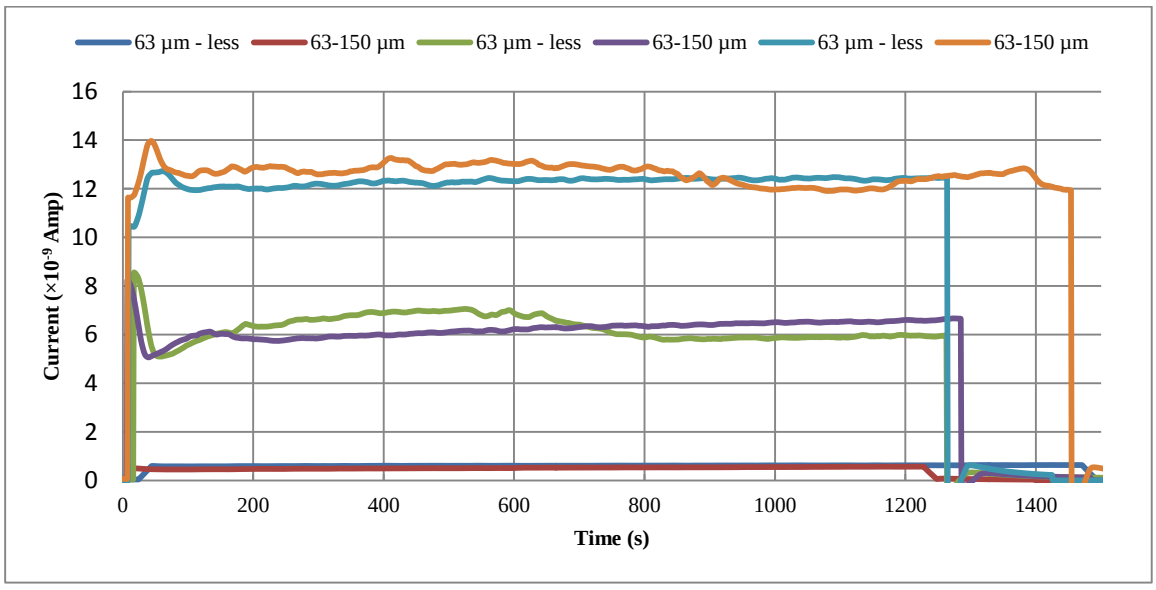

Figure B:8 Conduction current for the 63-150 and less than 63.

Appendix C LOOSELY BONDED COVERED ELECTRODE TEST

The contamination levels tested for loose bonded electrode were 0.001%, 0.002%, 0.003%, 0.004%, 0.006%, 0.008% and 0.016% by weight.

C.1. TEST UNDER DC ELECTRIC FIELD

Each contamination level were tested under the influence of 2 kV, 7.5 kV, 15 kV and 20 kV. The size of particles was 150 – 250 µm.

Figure C:1 shows the images of particle accumulation process for the loosely bonded covered electrodes test with 0.006% concentration. The contaminated pressboard fibres were started to move slowly towards both electrodes as soon as 2 kV supply was turned on. This movement were due to DEP force drawing the particles near to the region with a high gradient of electric field. They started to stick themselves to the surface of the electrodes. The particles were aligned themselves parallel to the electric field. The particles were covering the surface of the covered electrodes until 20 min of the test whereby there was not many particles left near the vicinity of the electrodes.

The movement of the particles were faster with the applied voltage of 7.5 kV. This time particles were sticking to the electrode surfaces with greater speed. A shallow beard like cover of pressboard particles surrounded the electrodes.

After the 15 kV was applied the sample, the particles were violently moving close to the surface of the electrodes. Within 1 min they covered most of the electrode surfaces. The fibre beard cover became thicker with time up to 20 min. The voltage level were increased to 20 kV in hoping that the higher voltage will be able to transfer charge to the particles and will form complete bridge between the electrodes. None of the voltage levels tested were able to create a bridge between the electrodes. The oil layer beneath the kraft paper prevented charge transportation to the other side of the paper surface. So the particles could not get enough charge to detach themselves from the surface to go back and forth as observed for the case of bare electrode test.

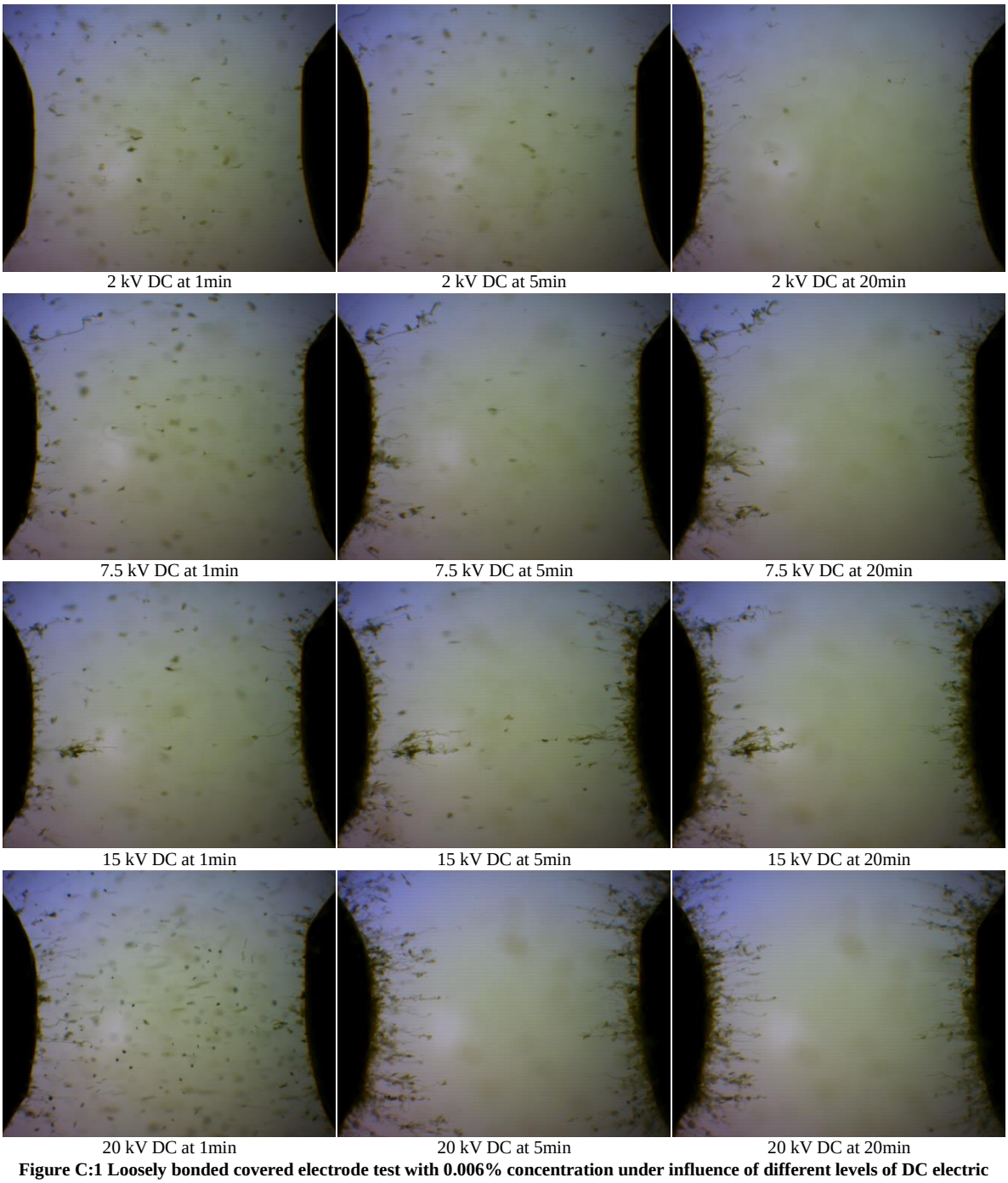

Figure C:1 Loosely bonded covered electrode test with 0.006% concentration under influence of different levels of DC electric field

Figure C:2 shows the images taken from loosely bonded covered electrode test with 0.008% concentration. The particles accumulation to the surface of the electrodes started as soon as the power supply was turned on. For all the voltage levels, the particle accumulation was more than the previous test. Again the particles could not get enough charge to detach from the surface despite of the increment of particle concentration.

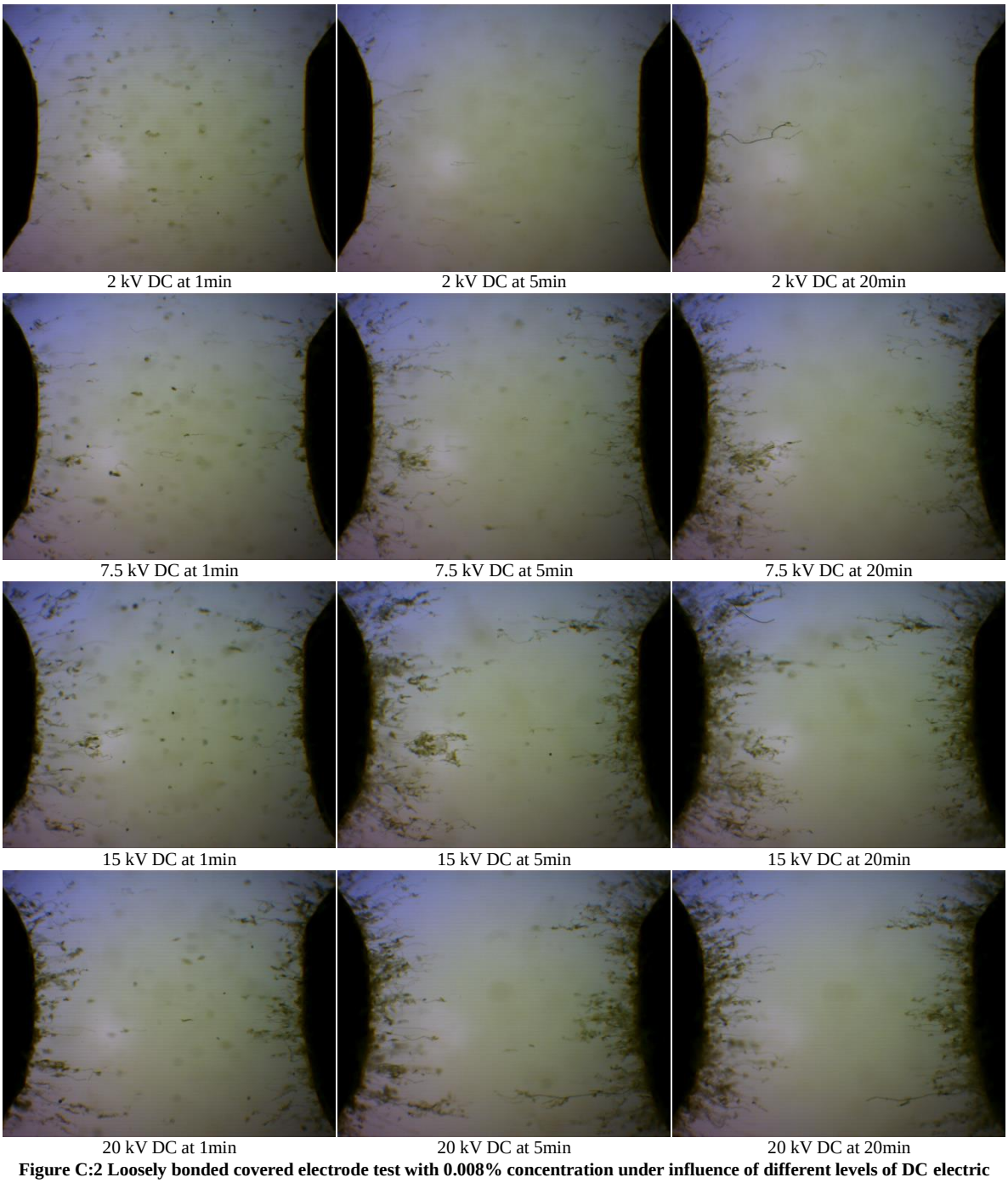

Figure C:2 Loosely bonded covered electrode test with 0.008% concentration under influence of different levels of DC electric field

Loosely bonded paper to the surface of the electrode prevented the charge transportation to the particles for all the concentration levels tested. The images from the highest concentration level of 0.016% is shown in Figure C:3. The higher concentration level only contributed to more particle accumulation of the either electrodes but not formed a complete bridge as for bare electrode system. There was a very thin bridge created very few occasions under 15 kV and 20 kV but it doesn't look like a bridge under DC electric field with bare electrodes.

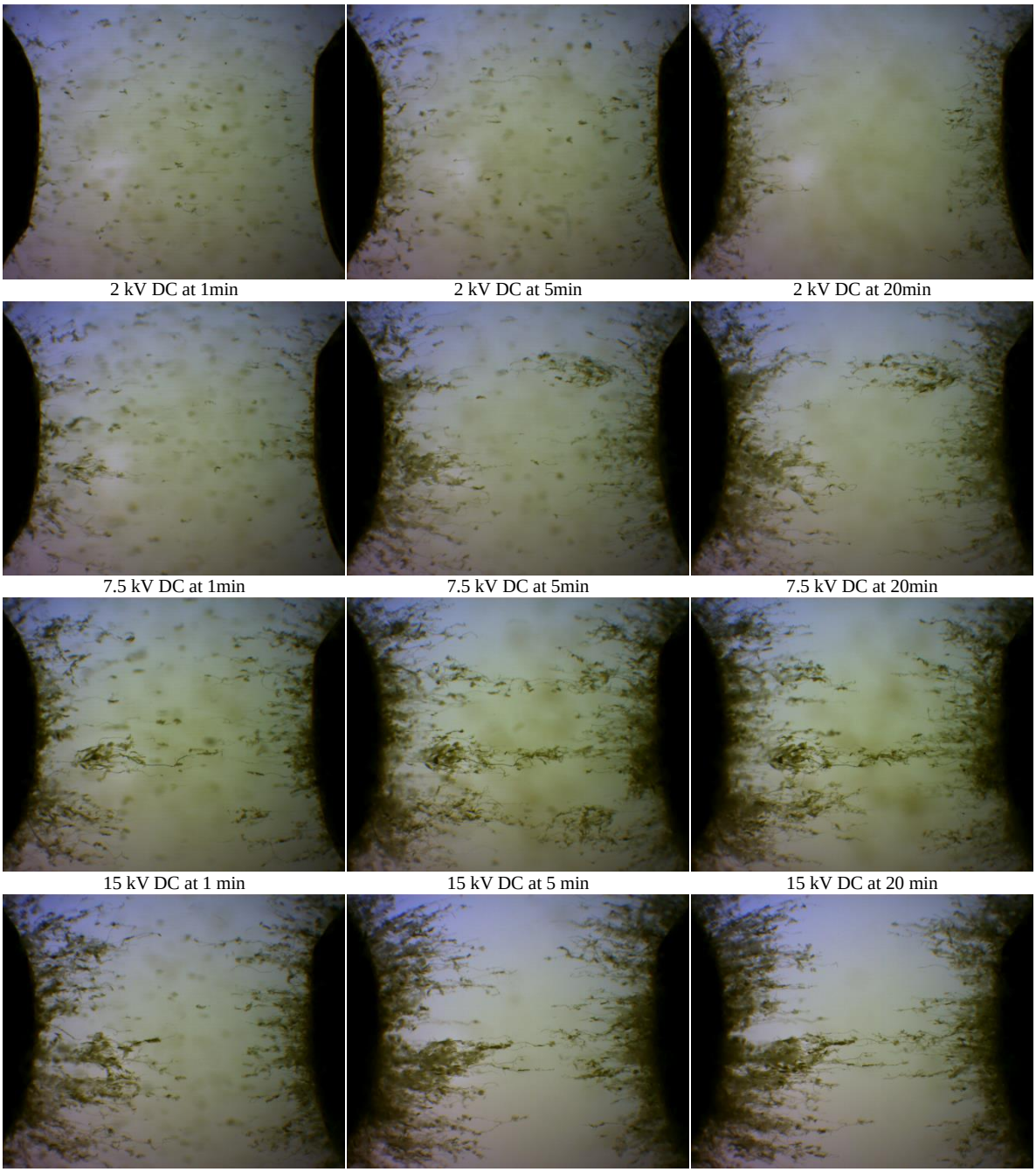

2 kV DC at 1min | 2 kV DC at 5min | 2 kV DC at 20min

7.5 kV DC at 1min | 7.5 kV DC at 5min | 7.5 kV DC at 20min

15 kV DC at 1 min | 15 kV DC at 5 min | 15 kV DC at 20 min

20 kV DC at 1 min | 20 kV DC at 5 min | 20 kV DC at 20 min

Figure C:3 Loosely bonded covered electrode test with 0.0016% concentration under influence of different levels of DC electric field

C.2. Conduction Current Comparison with Different Concentration Levels

The graph below in Figure C:4 shows the conduction current between the electrodes during the tests with different levels of contaminated transformer oil. There is a high polarization current observed for all the concentration levels then the current decayed slowly to steady state after around 600s. These currents are not influenced by contaminated particles as seen in Figure 4:9. It was observed

from previous tests that when there was a bridge between the electrodes, the conduction current increased almost linearly to the level of contamination. But in this case there was no noticeable change in conduction current observed. This is because there was no bridge formed between the electrodes so as the current did not increase.

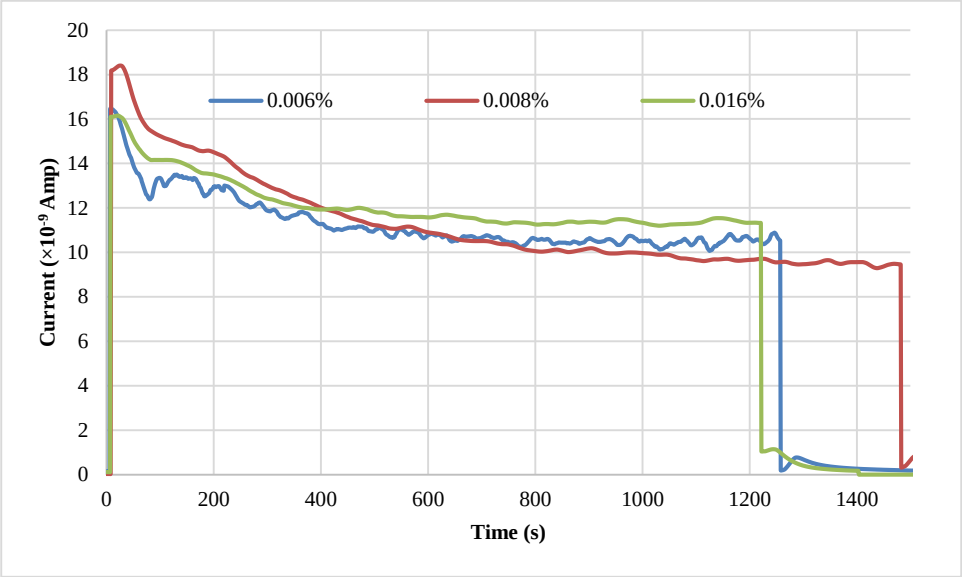

Figure C:4 Conduction currents with loosely bonded electrodes under the influence of 15kV DC electric fields with different concentration levels.

Appendix D BREAKDOWN TESTING

The breakdown strength test is generally used as one of the means of quality check and acceptance tests for transformer oil before filling new transformers or a during routine maintenance procedure. The mean breakdown voltage is commonly reported, and used to evaluate the ability of a transformer liquid to withstand the electric stress.

The purpose of this investigation is to measure the dielectric strengths of clean mineral oil and compare its breakdown voltage with contaminated oil. In order to achieve the purpose, a suitable procedure of sample preparation and breakdown voltage measurement method should be used for all the samples of mineral oil.

D.1. SAMPLE TANK FOR BREAKDOWN TEST

The test cell for breakdown measurement is shown in Figure D:1. This was originally used for a related oil breakdown project and was produced by the technical support team of the Tony Davies High Voltage Laboratory (TDHVL). The cylindrical chamber to hold the oil is made off clear perspex material. A precision micrometer was mounted on the top of the cylinder to achieve accurate gap distance between the electrodes. A piece of magnet was attached to the bottom end of the micrometer to secure the top electrode. Top end of the micrometer was attached to the high voltage power supply. Ground wire was connected to a copper plate placed in the bottom of the cylinder. A pair of spherical ball bearings with a diameter of 25 mm were used as electrodes. The Chrome steel ball bearings were made from Chromium AISI 52100 steel.

The ball bearings were rotated after each breakdown to ensure that any pitting of the electrodes surface was avoided. Each set of ball bearing electrodes were replaced after 10 breakdowns. The samples were stirred before every test to disperse the particles evenly. During the breakdown test all the oil samples were tested for moisture content using Coulometric Karl Fischer Titration equipment. There were 3 consecutive tests were made. The results for moisture test were then averaged. The contaminated oil sample 15 ml was filled in the breakdown test cell and the electrodes were completely submerged in the oil. The used oil was replaced with new oil after each test. The gap for DC breakdown test was chosen by conducted many breakdowns. The micrometer was screwed to the end to enable the electrodes to touch each other. The reading from the micrometer was then became reference for 0 mm and the micrometer was unscrewed to have the desired gap. This procedure of finding 0 mm reference was carried out to ensure that a constant gap between the electrodes achieved before every test as the position changed slightly every time. The

gap started from 10 mm and reduced to 2 mm which enabled all the breakdowns to occur within 55 kV. The voltage ramp rate for the DC breakdown was 100 V per second. The last reading from the power supply LCD display before the breakdown was recorded with a video camera. For AC breakdown, the test rig only had capability of 25 kV. So, the gap distance had been reduced to 1 mm. The ramp rate to AC breakdown was 50 V per second. There were minimum 20 to 30 breakdown tests carried out for each type of sample.

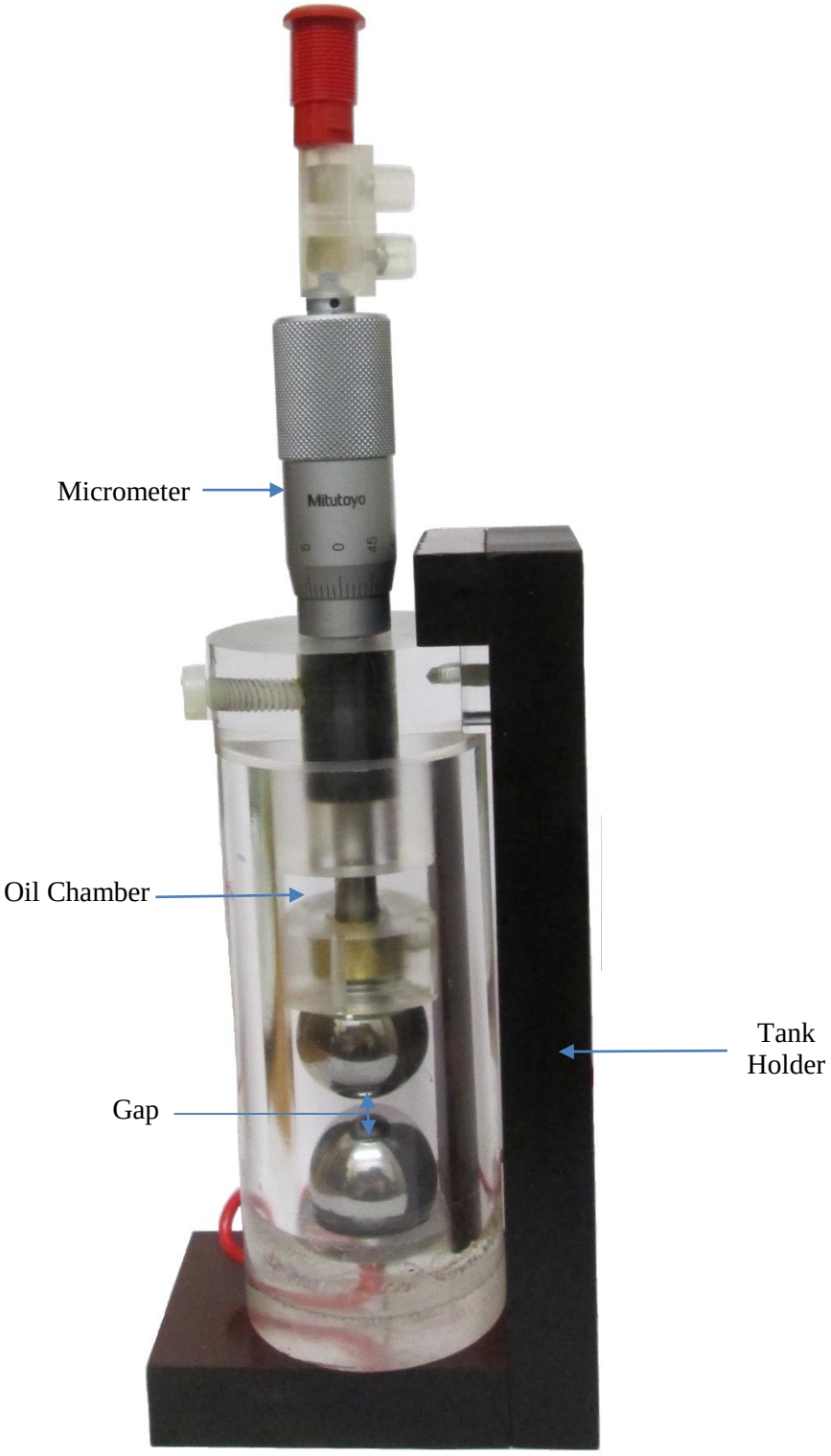

Figure D:1 Sample tank for breakdown test

D.2. BREAKDOWN VOLTAGE DISTRIBUTIONS

The easiest way to determine the withstand voltage of transformer oil is to carry out a lot of breakdown tests. The amount of breakdown tests will determine how accurate the withstand voltage going to be. But the drawback of this method is rather expensive and time-consuming, and is only valid when the breakdown voltage of the test liquid is not influenced by the by-products of frequent breakdowns [121].

Therefore, the experimental measurements should be accompanied by statistical calculations. The main aim of statistical calculation is to find an expected distribution. The withstand voltage can be then predicted using the distributions with limited number tests.

The breakdown process in liquid could be initiated by particles, free water or gas bubbles. The breakdown voltage of a transformer oil is therefore a statistically distributed number. The mean breakdown voltage and standard deviation are used to represent the breakdown voltage distribution, based on the assumption that breakdown voltage follows the normal distribution.

Statistical techniques (parametric and non-parametric) have been used to study the breakdown voltage distribution of transformer dielectric liquids [122, 123]. The most common distributions are normal distribution, minimum Gumbel distribution (Double Exponential distribution), and Weibull distribution [124]. The Gumbel and Weibull distribution are extreme-value distributions. They consider the asymmetry between the low and the high failure rates. Studies of previous researchers concluded that Weibull distribution is the best distribution for transformer mineral oil [125]. The raw breakdown data set had a lot of fluctuations. These data were plotted using Weibull distribution. The equation for Weibull distribution is shown in 5:1.

$$P_W(E;k,\lambda) = 1 - e^{-\left(\frac{E}{\lambda}\right)^k} \qquad \textbf{8:1}$$

D.3. DC BREAKDOWN RESULTS

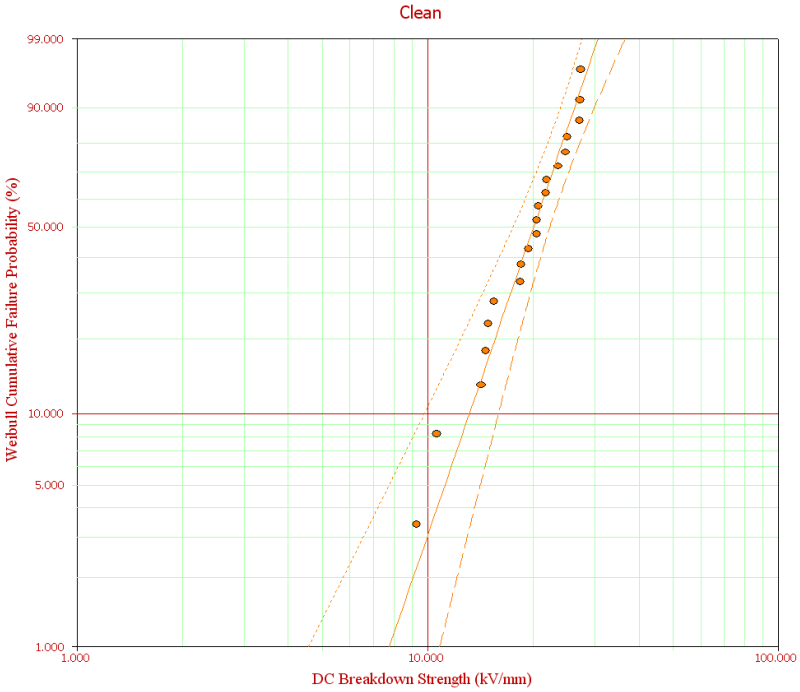

Figure D:2 Weibull parameters with 95% confidence boundaries of clean transformer oil under DC electric field

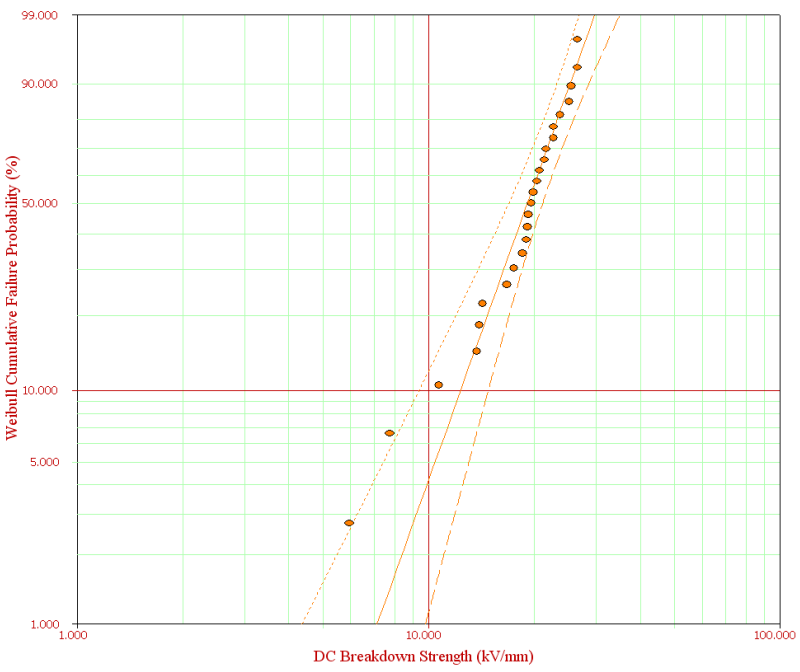

Figure D:3 Weibull parameters with 95% confidence boundaries of transformer oil with 0.003% contamination under DC electric field

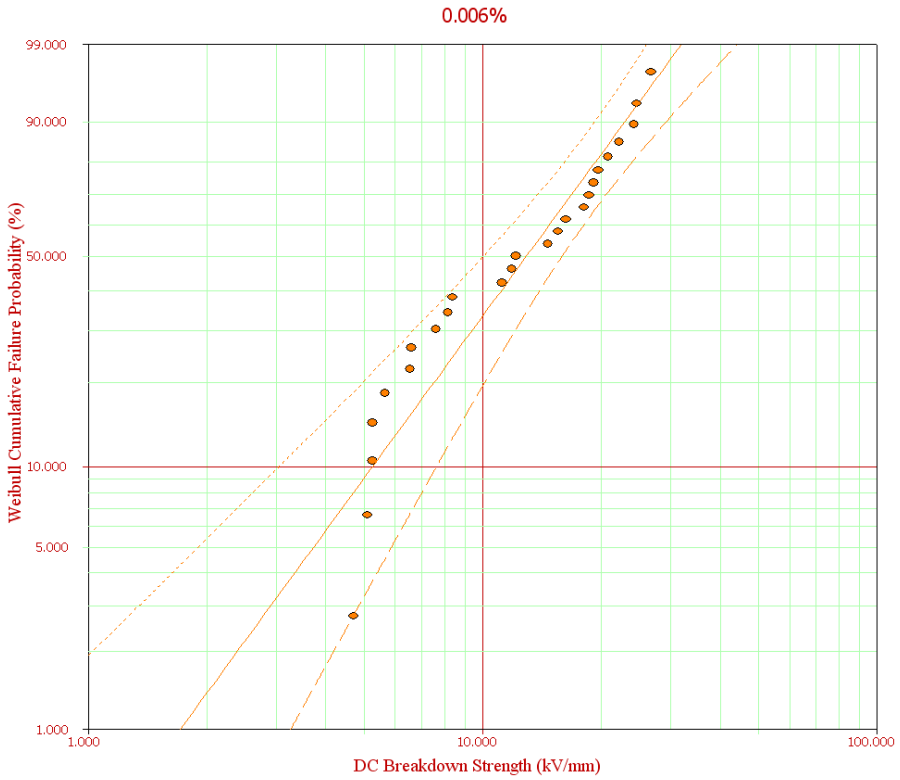

Figure D:4 Weibull parameters with 95% confidence boundaries of transformer oil with 0.006% contamination under DC electric field

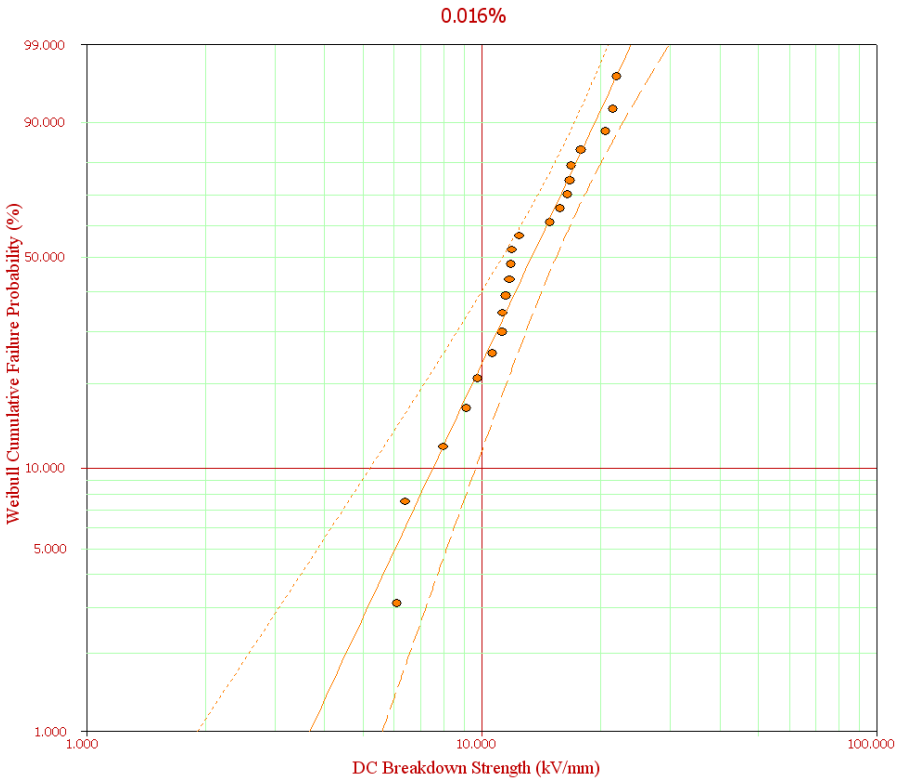

Figure D:5 Weibull parameters with 95% confidence boundaries of transformer oil with 0.016% contamination under DC electric field

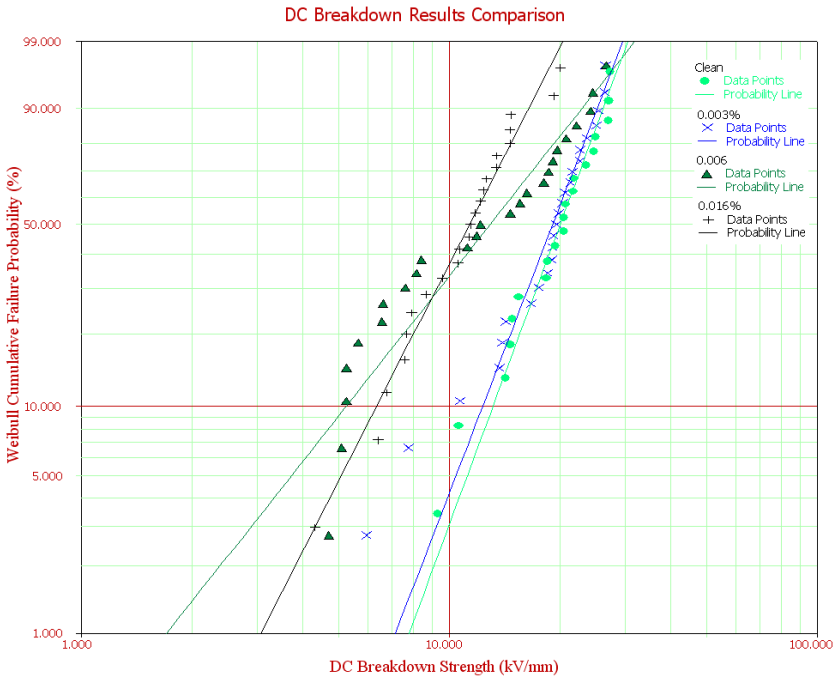

Figure D:6 All the breakdown results of Weibull parameters with different levels of contaminations under DC electric field

The graph showed in Figure D:6 are the breakdown voltages from all the DC tests. The particles size were 150 -250 µm for all the DC and AC breakdown measurement. The breakdown voltage for clean oil was highest 21.71 kV among the other samples. Then the 0.003% had a little less than clean oil of 20.78 kV which is 1 kV less. As the contamination level increased to 0.006%, the breakdown voltage reduced to 15.37 kV. When the contamination level increased to 0.016%, the breakdown voltage further reduced to 12.70 kV. The β value of the plot indicates slope of the curve fitting line. The higher value of β indicates that the data has less scattering. We can observe from the Table D-1 that the β values are higher for clean and 0.003% contaminated samples than the other two results. The higher value of β for clean and lower contaminated oil suggest that there may be different breakdown mechanism present in higher contaminated oil.

Table D-1 Weibull parameters of transformer oil with different levels of contaminations under DC electric field

Oil Sample	Moisture	Air Humidity	Room Temperature	α	β
Clean	15 ppm	69.4%	22.1°C	21.7127	4.4766
0.003%	19 ppm	48.5%	22.5°C	20.7788	4.3043
0.006%	25 ppm	67.3%	23.3°C	15.3684	2.0938
0.016%	20 ppm	60.7%	22.7°C	12.6939	3.2429

D.4. AC BREAKDOWN RESULTS

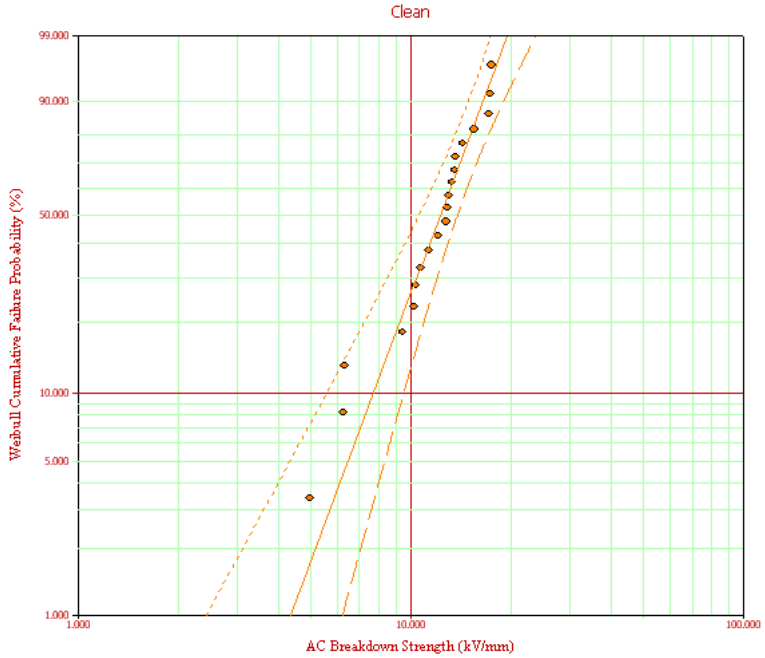

Figure D:7 Weibull parameters with 95% confidence boundaries of clean transformer oil under AC electric field

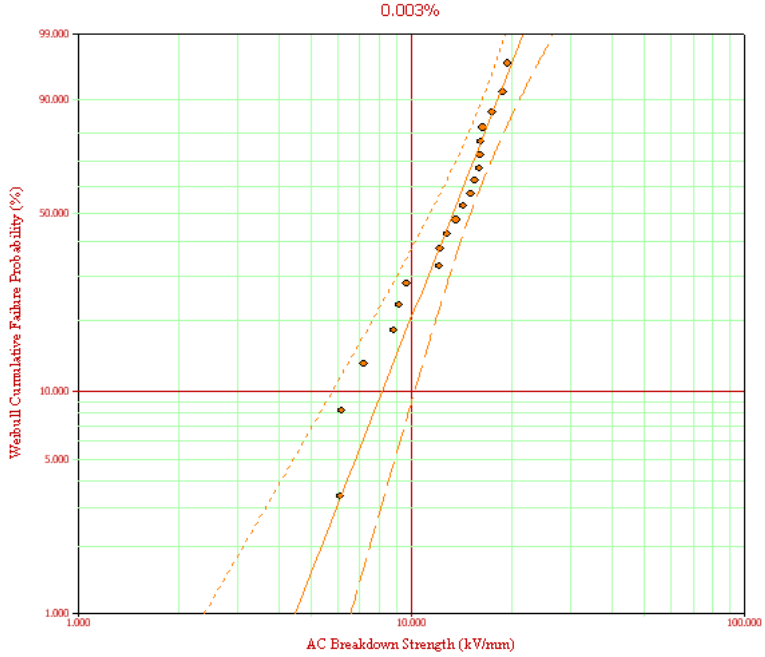

Figure D:8 Weibull parameters with 95% confidence boundaries of transformer oil with 0.003% contamination under DC electric field

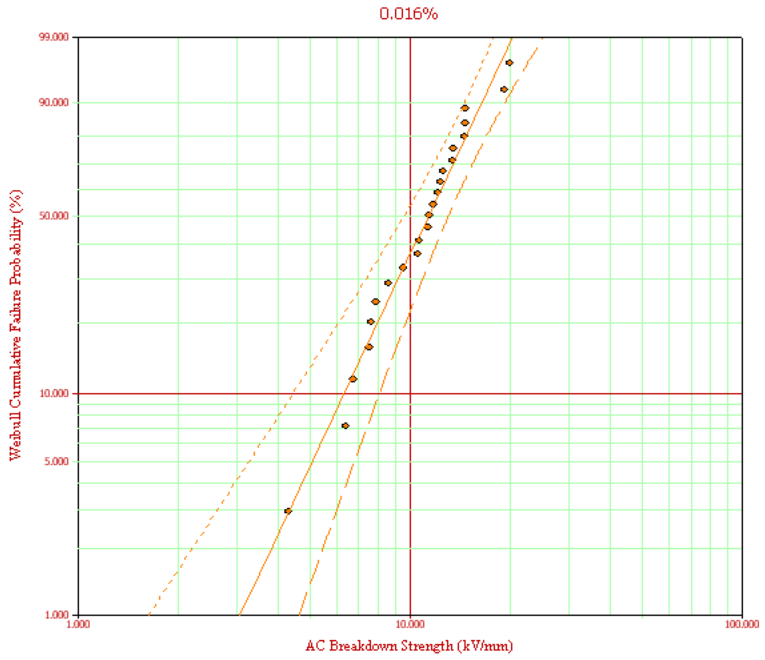

Figure D:9 Weibull parameters with 95% confidence boundaries of transformer oil with 0.016% contamination under DC electric field

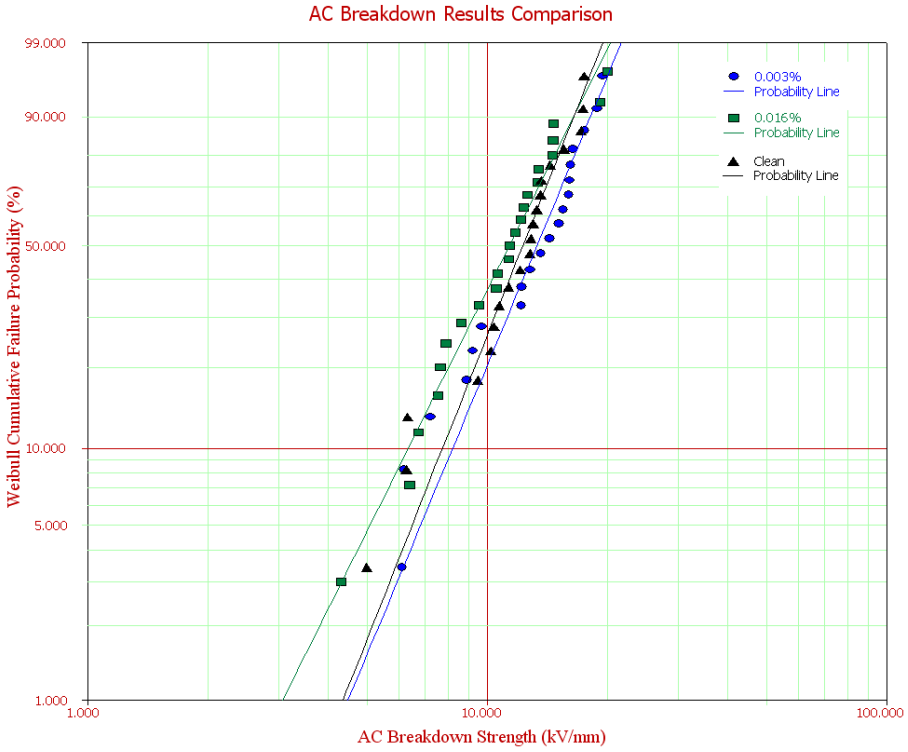

Figure D:10 All the breakdown results of Weibull parameters with different levels of contaminations under AC electric field

The Weibull distribution of breakdown voltages from all the samples are shown in Figure D:10. The breakdown voltage of clean oil was 13.40 kV. But the result from 0.003% had higher breakdown voltage of 14.61 kV which was not expected. It might be the fact that under AC voltage the particles

did not create a bridge between electrodes. It was only covered the surface of the electrodes. On the other hand, when the contamination level was increased to 0.016%, the breakdown voltage were decreased to 12.69 kV. The β values from AC breakdown test are shown in Table D-2. All of these β values are better than DC tests. The overall trend from the breakdown test are of AC and DC shows that as the contamination level in the transformer oil increases, the value of breakdown voltage decreases.

Table D-2 Weibull parameters of transformer oil with different levels of contaminations under AC electric field

Oil Sample	Moisture	Humidity	Temperature	α	β
Clean	15 ppm	60.5%	21.8°C	13.4009	4.0879
0.003%	14 ppm	57.4%	22.1°C	14.6079	3.8909
0.016%	16 ppm	46.5%	23.1°C	12.6939	3.2429

D.5. SUMMARY

The breakdown test were conducted several times but it was not possible to get consisted results. It might be due to the fact that the test cell used for breakdown was holding the electrodes vertically rather than horizontally which should have been more realistic as all the tests of bridging carried out with horizontal electrode arrangement. There is a chance that the particles might be accumulated on the bottom electrode due to gravity. The other reason might be the gap between the electrodes was very small i.e. 1, 2 mm and was not enough for creating a bridge. Therefore the results obtained from DC and AC test is not conclusive and the relation between contamination level and breakdown voltage could not be drawn. Further investigation on breakdown test needed to be carried out.

Appendix E PARTIAL DISCHARGE TEST

Partial discharge in transformer oil with contaminated particles were reported by [11]. It was initially decided that similar measurement of PD should be carried out in the present project. This chapter focuses on PD measurement. The setup of the experiment is based on the Phase resolved partial discharge analysis (PRPDA) technique and the measurement method is explained in this chapter.

E.1. EXPERIMENTAL SETUP

Two different electrode systems were used for these tests which were sphere-sphere and needle-plane. The sample tank for this experiment was same as for DC test. The gap between the electrodes was kept 10 mm for both systems. One side of the electrode was connected to the sinusoidal AC supply via copper tube and the other electrode was attached to the earth. For the needle-plane electrode system, the needle was attached to the AC source and the plane electrode was to the earth. Initially the microscope was used to take the images as well as detecting the partial discharge simultaneously. But presence of the microscope caused a lot of measurement noise. Therefore it was decided to exclude from the PD measurement experiments. This is justified as the earlier tests showed no bridge formation under AC voltage. The PD measurement block diagram is shown in Figure E:1.

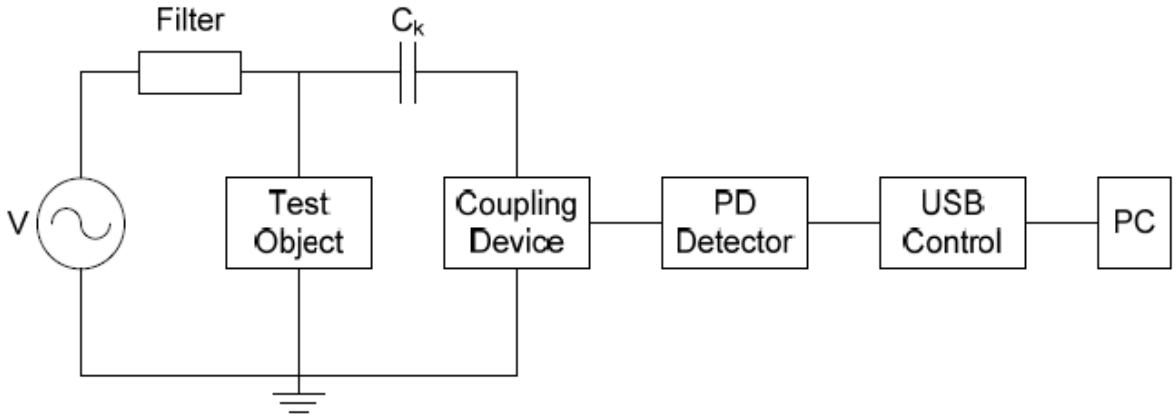

Figure E:1 Block diagram [56] of the PD measurement experiment

The PD measurement unit was calibrated using a calibration unit. The system was calibrated with 20 pC of charge every time before new samples were tested. The center frequency for the PD was set to 350 kHz with the bandwidth of 150 kHz. The voltage was slowly increased to the desired level after the test cell was placed for test. There were three different voltages levels tested for spherical electrodes which were 10 kV, 15 kV and 20 kV at 50 Hz. The breakdown voltage for the

needle - plane electrodes was around 18kV. So the voltage for the entire experiments for the needle - plane electrodes was kept at 15 kV. The threshold level for these experiments was set to 100 fC. Each of the samples was tested for minimum of 30 minutes.

E.2. RESULTS

E.2.1 PARTIAL DISCHARGE OF SPHERICAL ELECTRODE SYSTEM

There was several concentration levels of pressboard fibre tested for PD measurement. The concentration levels were 0.001%, 0.003%, 0.006%, 0.008%, 0.016% and 0.024%. Figure E:2 shows the PD graph with applied voltage 20 kV and particle concentration level 0.024%. There was no PD detected with the spherical electrode system for the entire range of concentration level tested. According to [11], PD were detected with spherical and wrapped electrode system in moistened and pressboard fibre concentrated samples. The applied RMS voltage for their [11] experiments was 6kV for spherical and 8 kV for formed wire electrodes. Several attempts were made to observe any PD activity for spherical electrodes but none of them were successful.

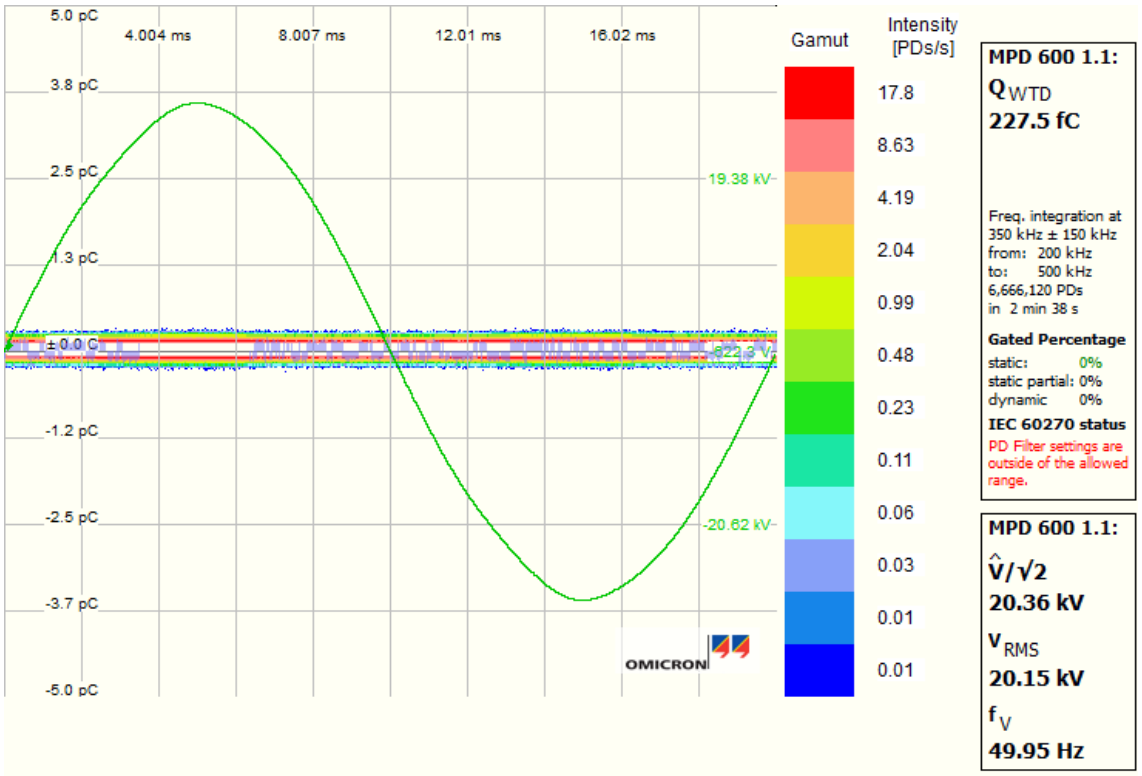

Figure E:2 PD of 0.024% contamination

E.2.2 PARTIAL DISCHARGE WITH NEEDLE – PLANE ELECTRODE SYSTEM

The amounts of pressboard concentration levels for these tests were same as the spherical electrode system. Partial discharge of clean mineral oil was tested before adding the contaminants. The noise level was observed around 200 fC. There were some partial discharge activities detected even for the clean oil with the needle-plane electrode system. There was not noticeable amount of PD detected after adding the fiber particle of 0.001%. There were a few PD activity found with a peak of around 1pC for 0.003% concentration. The PD activities were intensified with 0.006% concentration and the peak was 5 pC. But for the 0.008%, there was not significant PD found. The PD detection was again increased a lot for 0.016% concentration. The peaks of the PD were up to 10 pC. Finally, the PD activities were lower for the 0.024% concentration level.

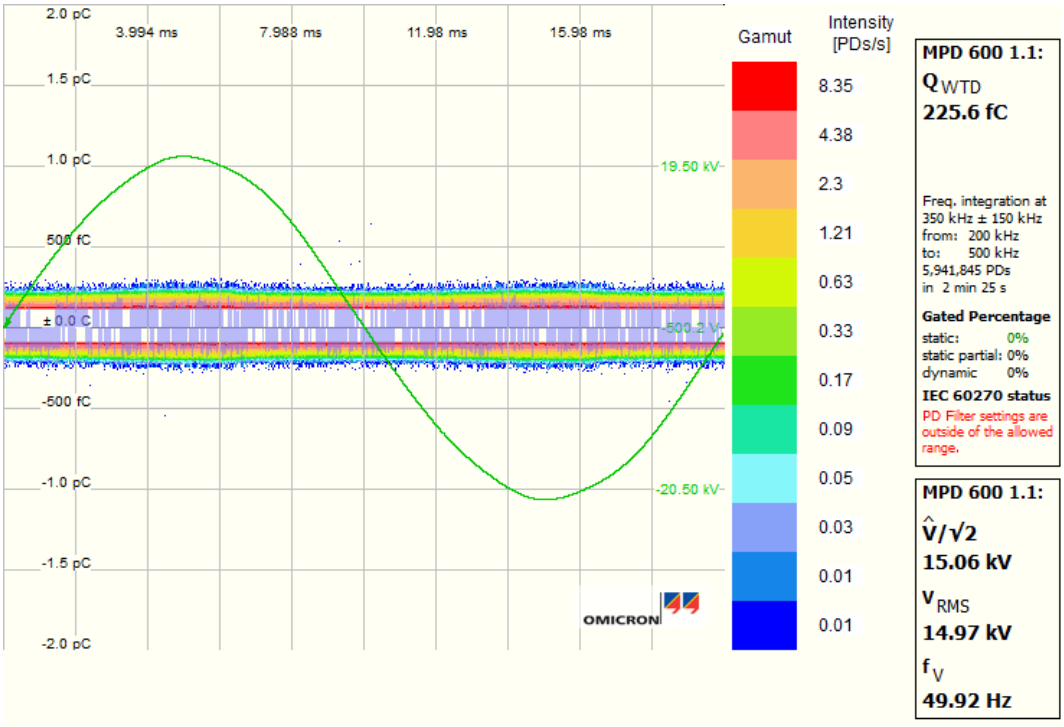

Figure E:3 PD of Clean Oil

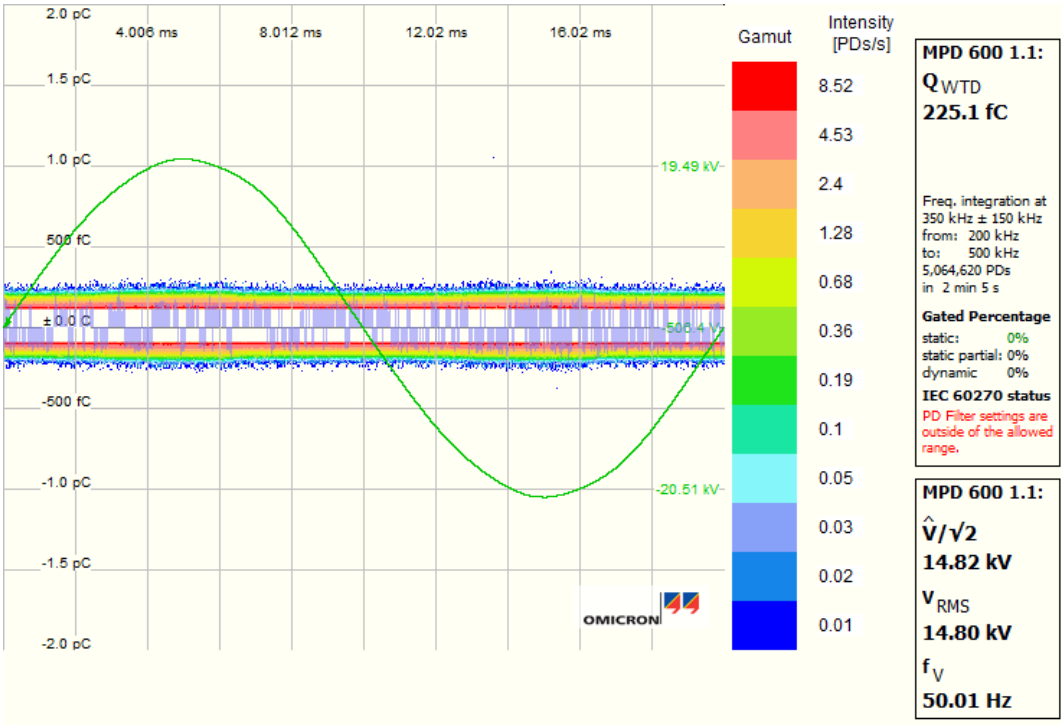

Figure E:4 PD of 0.001% contamination

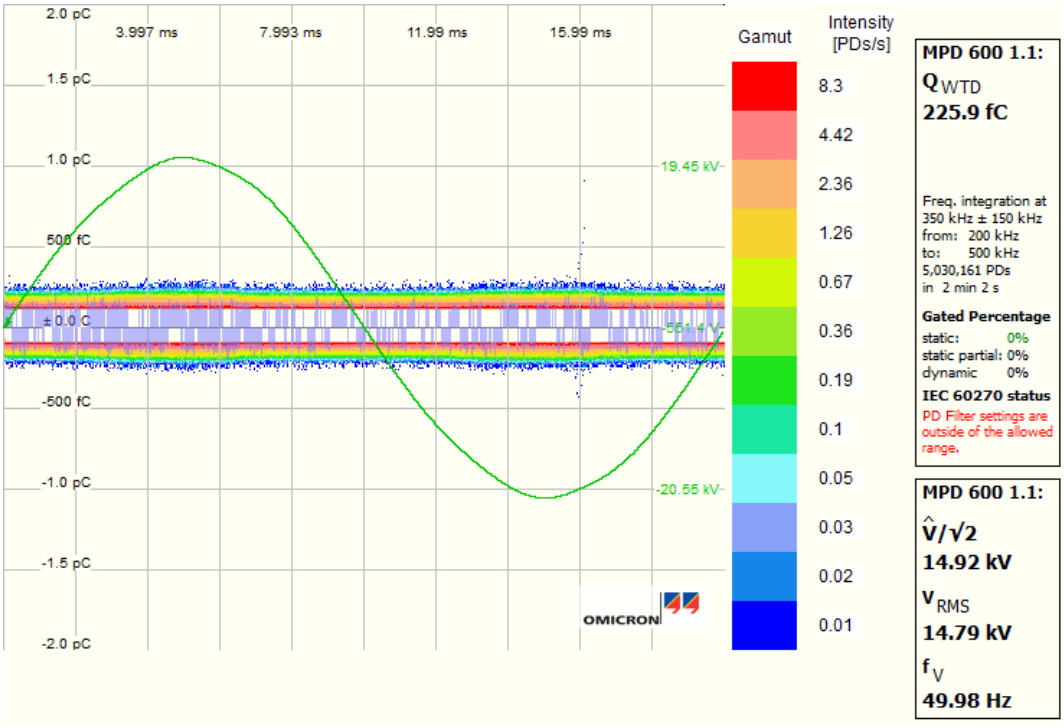

Figure E:5 PD of 0.003% contamination

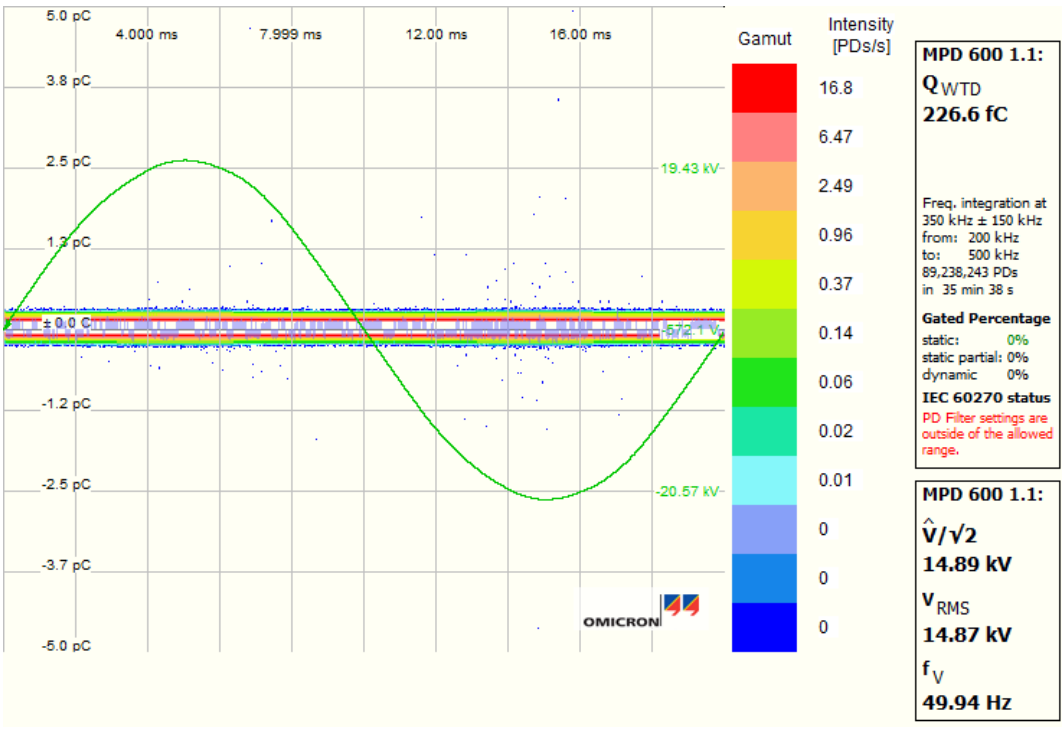

Figure E:6 PD of 0.006% contamination

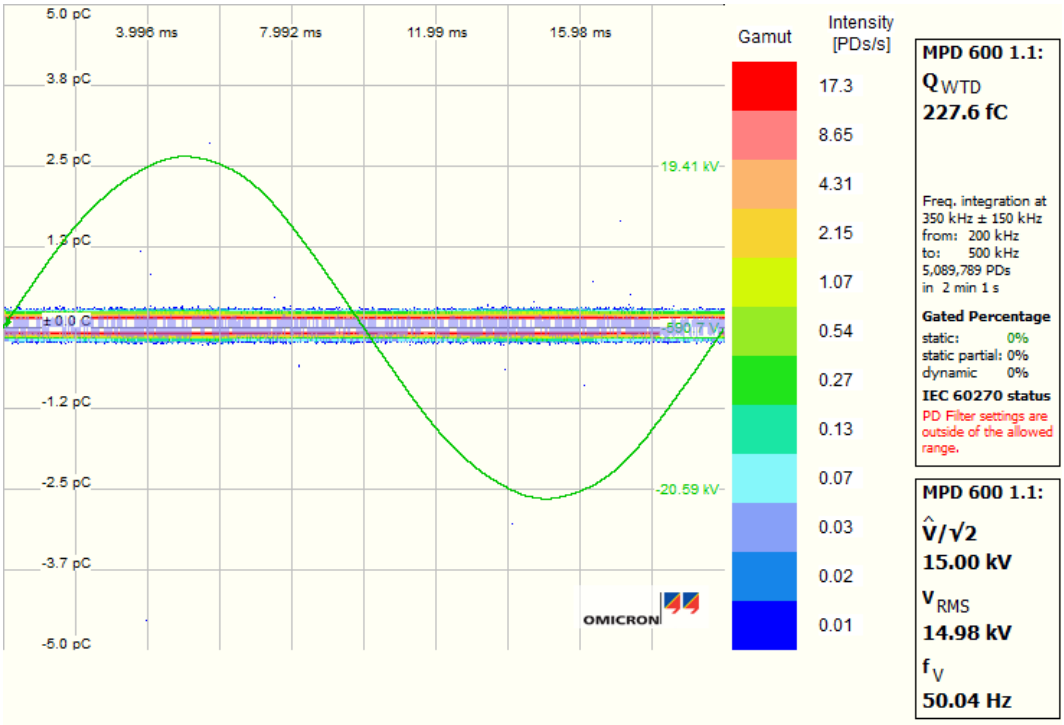

Figure E:7 PD of 0.008% contamination

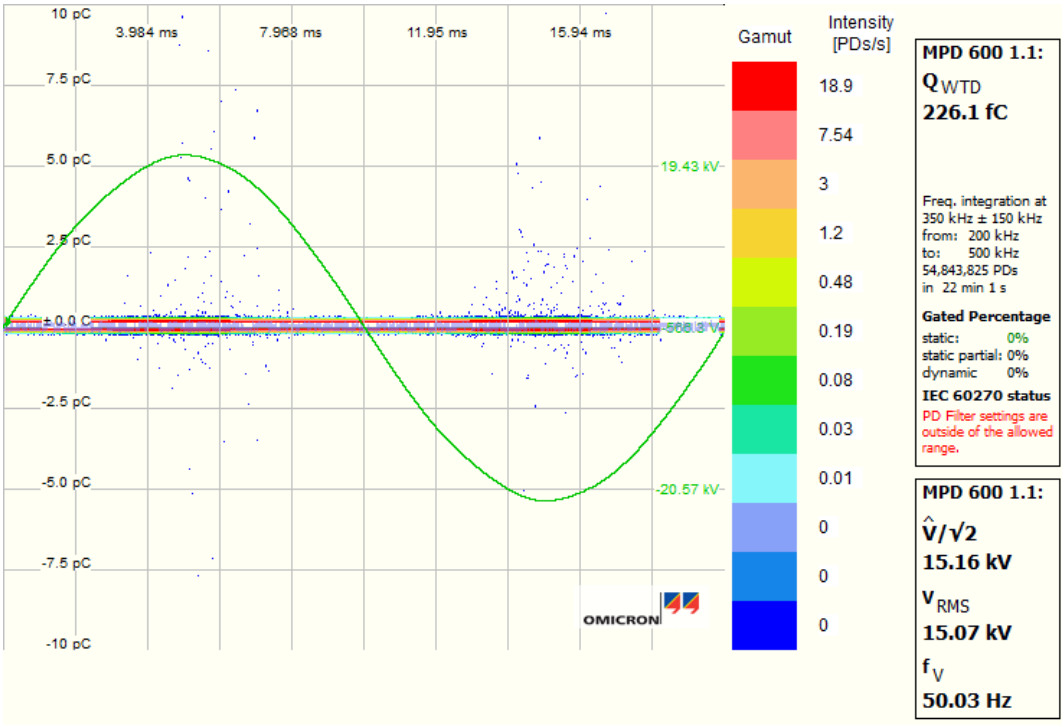

Figure E:8 PD of 0.016% contamination

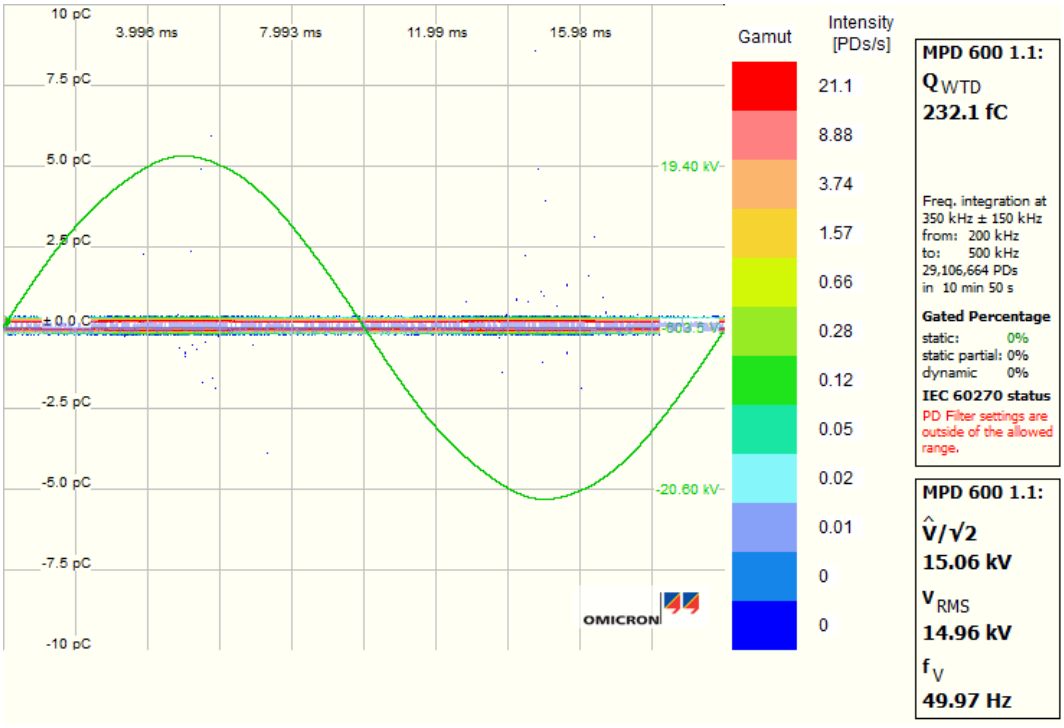

Figure E:9 PD of 0.024% contamination

Partial discharge observed from the above results could not be directly related to pressboard fibre concentration level as the results were inconsistent. It was observed that most of the samples had

more PD at the first 10 minutes then it was reduced. The PD results were not consistent over the range of concentration level tested. So, it was not possible from these scattered PD result to establish the relationship between the particle contaminations with the level of PD detection. The reason for the scattered result might be the as the PD data was not recorded at a regular interval.

E.3. SUMMARY

Several attempts had been made to measure the PD using spherical and needle-plane electrode systems. Successful PD measurements were not accomplished either due to error in experimental setup or mistakes in connecting the connecting the equipment. The PD results were not conclusive from this research and it needs further investigation.

REFERENCES

[1] V. Sokolov, "Experience with the refurbishment and life extension of large power transformers," in *Minutes of the Sixty-First Annual International Conference of Doble Clients*, 1994, pp. 6-4.

[2] V. Kogan, J. Fleeman, J. Provanzana, and C. Shih, "Failure analysis of EHV transformers," *Power Delivery, IEEE Transactions on,* vol. 3, pp. 672-683, 1988.

[3] M. G. Danikas, "Breakdown of transformer oil," *Electrical Insulation Magazine, IEEE,* vol. 6, pp. 27-34, 1990.

[4] T. O. Rouse, "Mineral insulating oil in transformers," *Electrical Insulation Magazine, IEEE,* vol. 14, pp. 6-16, 1998.

[5] G. Chen and M. H. Zuber, "Pre-breakdown characteristics of contaminated power transformer oil," in *Electrical Insulation and Dielectric Phenomena, 2007. CEIDP 2007. Annual Report - Conference on*, 2007, pp. 659-662.

[6] B. R. Andersen, "HVDC transmission-opportunities and challenges," in *AC and DC Power Transmission, 2006. ACDC 2006. The 8th IEE International Conference on*, 2006, pp. 24-29.

[7] W. Youhua, Z. Wenfeng, W. Jianmin, X. Dong, Z. Ping, and L. Jiangui, "Stray Loss Calculation of HVDC Converter Transformer," *Applied Superconductivity, IEEE Transactions on,* vol. 22, pp. 5500604-5500604, 2012.

[8] L. Shu, L. Yilu, and J. De La Ree, "Harmonics generated from a DC biased transformer," *Power Delivery, IEEE Transactions on,* vol. 8, pp. 725-731, 1993.

[9] (25/03/2015). *High-voltage direct current*. Available: http://en.wikipedia.org/wiki/High-voltage_direct_current

[10] C. R. B. Colin Bayliss, Brian J. Hardy, *Transmission and Distribution Electrical Engineering*.

[11] H. Moranda, K. Walczak, and H. M. Grzesiak, "Dynamics of bridge creating in contaminated oil at AC voltage and analysis of accompanying partial discharges," in *XIII International Symposium on High Voltage Engineering Netherlands, 2003.*, 2003.

[12] M. Ossowski, J. Gielniak, H. Moronda, and H. Moscicka-Grzesiak, "Oil resistance at different phases of bridge mechanism development at direct voltage," in *XIII International Symposium on High Voltage Engineering Netherlands*, 2003.

[13] F. M. O'Sullivan, "A model for the initiation and propagation of electrical streamers in transformer oil and transformer oil based nanofluids," PhD, Dept. of Electrical Engineering and Computer Science, Massachusetts Institute of Technology, 2007.

[14] Y. Du, "Measurements and modeling of moisture diffusion processes in transformer insulation using interdigital dielectrometry sensors," PhD PhD Thesis, Dept. of Electrical Engineering and Computer Science, Massachusetts Institute of Technology, 1999.

[15] CIGRE, "Effect of Particles on Transformer Dielectric Strength," *in Working Group 17 of Study Committe 12, June 2000.,* 2000.

[16] V. V. Sokolov, Vanin, B.V.,, "Evaluation of Power Transformer Insulation through Measurement of Dielectric Characteristics," *Proceedings of the Sixty-Third Annual International Conference of Double Clints,* vol. Sec. 8-7.1, 1996.

[17] T. K. Saha, "Review of modern diagnostic techniques for assessing insulation condition in aged transformers," *Dielectrics and Electrical Insulation, IEEE Transactions on,* vol. 10, pp. 903-917, 2003.

[18] V. V. Sokolov, "Failure statistics. Transformer and bushing design review. Typical failure modes and failure causes. What can be learned from post mortem inspection," *Fifth AVO New Zealand International Technical Conference, 2006.,* 2006.

[19] W. G. Cigre, "An international survey on failures in large power transformers in service," *Electra,* pp. 21-47, May 1983 1983.

[20] "IEEE Guide for Reporting Failure Data for Power Transformers and Shunt Reactors on Electric Utility Power Systems," *ANSI/IEEE Std C57.117-1986,* pp. 1-29, 1988.

[21] K. Miners, "Particles and Moisture Effect on Dielectric Strength of Transformer Oil Using VDE Electrodes," *Power Apparatus and Systems, IEEE Transactions on,* vol. PAS-101, pp. 751-756, 1982.

[22] J. A. Kok, *Electrical breakdown of insulating liquids*: Interscience Publishers, 1961.

[23] F. Abgrall and J. Gordon, "Influence of Solid Impurities on the Electric Strength of Transformer Oil," in *Vh International Conference on Conditions and Breakdown in Dielectric Liquids*, 1975, pp. 79-83.

[24] T. J. Gallagher, *Simple dielectric liquids: mobility, conduction, and breakdown*: Clarendon Press Oxford, 1975.

[25] K. Mathes and J. Atkins, "Influence of Particles on Partial Discharge and Breakdown in Oil," in *IEEE 1nt. Symp. on Electrical Insulation Jun*, 1978, pp. 226-231.

[26] N. G. Trinh, C. Vincent, and J. Regis, "Statistical Dielectric Degradation of Large-Volume Oil-Insulation," *Power Apparatus and Systems, IEEE Transactions on,* vol. PAS-101, pp. 3712-3721, 1982.

[27] J. Roach, M. Rosado, and H. Ivey, "Liquid and particle motions in transformer oil under 60 Hz stress," in *Conference Record of the IEEE International Symposium on Electrical Insulation*, 1980, p. 234.

[28] J. Fleszynski, B. Lutynski, and A. Zelek, "Influence of the electrode paper coatings on the electric strength of transformer oil," *Conduction and Breakdown in Dielectric Liquids,* vol. 7, pp. 465-469, 1981.

[29] H. A. Pohl, "Some Effects of Nonuniform Fields on Dielectrics," *Journal of Applied Physics,* vol. 29, pp. 1182-1188, 1958.

[30] B. M. Goswami, L. Angerer, and B. W. Ward, "The Behavior of Impurity Particles in Transformer Oil at Variable Frequencies," *Proc. of the 8th Intern. Conf. on cond. and breakdown in Diel. Liq.,* pp. 218 -223, 1972.

[31] R. T. Harrold, "Electric Discharges from Metallic Slivers and Wire Particles in Mineral Oil," *Proc. of the 1975 Conf. on Elec. Insul. and Diel. Phen., Nat. Acad. Sci.,* pp. 514 -524, 1975.

[32] M. Darvenlza, "A demonstration of the effect of carbon particles on the AC strength of transformer oil," in *Conference record of the 1985 International Conference on Properties and Applications of Dielectric Materials, Shaanxi Guesthouse, Xian, China, June 24-29, 1985*, 1985, p. 154.

[33] T. Dakin and J. Hughes, "The behaviour of individual conducting particles in electric fields," in *1968 Annual report of the conference on electrical insulation and dielectric phenomena*, 1969, pp. 68-72.

[34] J. Fleszynski and B. Lutynski, "Macroparticle - initiated breakdown of insulating oil," *Eight International Conference on Conduction and Breakdown in Dielectric Liquids. IEEE Electr. Insul. Soc. Paria, Italy, 24-27 July 1984.,* pp. 275-279, 1984.

[35] F. Carraz, P. Rain, and R. Tobazeon, "Particle-initiated breakdown in a quasi-uniform field in transformer oil," *Dielectrics and Electrical Insulation, IEEE Transactions on,* vol. 2, pp. 1052-1063, 1995.

[36] S. Birlasekaran and M. Darveniza, "Observations due to particle movement in transformer oil," in *Proc. of the 4th Intern. Conf. on cond. and breakdown in Diel. Liq., Dublin*, 1972, pp. 120-123.

[37] S. Birlasekaran and M. Darveniza, "Microdischarges from Particles in Transformer Oil," *Electrical Insulation, IEEE Transactions on,* vol. EI-11, pp. 162-163, 1976.

[38] G. B. Denegri, G. Liberti, G. Molinari, and A. Viviani, "Field-Enhanced Motion of Impurity Particles in Fluid Dielectrics under Linear Conditions," *Electrical Insulation, IEEE Transactions on,* vol. EI-12, pp. 114-124, 1977.

[39] S. Birlasekaran, "The measurement of charge on single particles in transformer oil," *Electrical Insulation, IEEE Transactions on,* vol. 26, pp. 1094-1103, 1991.

[40] K. Asano, K. Yatsuzuka, and Y. Higashiyama, "The motion of charged metal particles within parallel and tilted electrodes," *Journal of Electrostatics,* vol. 30, pp. 65-74, 1993.

[41] R. Tobazeon, "Behaviour of spherical and cylindrical particles in an insulating liquid subjected to a DC uniform field," in *Conduction and Breakdown in Dielectric Liquids,1993., ICDL '93., IEEE 11th International Conference on*, 1993, pp. 415-420.

[42] A. Stannett, "The conductivity of hydrocarbon transformer oil containing water and solid conducting particles," *British Journal of Applied Physics,* vol. 2, p. 110, 1951.

[43] P. Felsenthal and B. Vonnegut, "Enhanced charge transfer in dielectric fluids containing conducting particles," *British Journal of Applied Physics,* vol. 18, p. 1801, 1967.

[44] Z. Krasucki, "High Field Conduction in Liquid Dielectrics," *Int. Coll. on Conduction Processes in Dielectric Liquids, Grenoble,* p. 311, 1968.

[45] M. D. Butcher, "Mechanisms of charge conduction and breakdown in liquid dielectrics," Thesis (Ph. D.)--Texas Tech University, Dept. of Electrical Engineering, 2005., 2005.

[46] W. G. Chadband, "From bubbles to breakdown, or vice-versa," in *Conduction and Breakdown in Dielectric Liquids,1993., ICDL '93., IEEE 11th International Conference on*, 1993, pp. 184-193.

[47] T. J. Lewis, "A new model for the primary process of electrical breakdown in liquids," *Dielectrics and Electrical Insulation, IEEE Transactions on,* vol. 5, pp. 306-315, 1998.

[48] M. Abdel-Salam, *High-Voltage Engineering: Theory and Practice, Second Edition, Revised and Expanded*: Taylor & Francis, 2000.

[49] T. J. Lewis, "An Overview of Electrical Processes Leading to Dielectric Breakdown of Liquids," in *The Liquid State and Its Electrical Properties*. vol. 193, E. E. Kunhardt, L. G. Christophorou, and L. H. Luessen, Eds., ed: Springer US, 1989, pp. 431-453.

[50] R. Hebner, "Measurement of Electrical Breakdown in Liquids," in *The Liquid State and Its Electrical Properties*. vol. 193, E. E. Kunhardt, L. G. Christophorou, and L. H. Luessen, Eds., ed: Springer US, 1989, pp. 519-537.

[51] R. Tobazeon, "Prebreakdown phenomena in dielectric liquids," *Dielectrics and Electrical Insulation, IEEE Transactions on,* vol. 1, pp. 1132-1147, 1994.

[52] A. Beroual, M. Zahn, A. Badent, K. Kist, A. J. Schwabe, H. Yamashita*, et al.*, "Propagation and structure of streamers in liquid dielectrics," *Electrical Insulation Magazine, IEEE,* vol. 14, pp. 6-17, 1998.

[53] J. G. Hwang, M. Zahn, and L. A. A. Pettersson, "Mechanisms behind positive streamers and their distinct propagation modes in transformer oil," *Dielectrics and Electrical Insulation, IEEE Transactions on,* vol. 19, pp. 162-174, 2012.

[54] D. Linhjell, L. Lundgaard, and G. Berg, "Streamer propagation under impulse voltage in long point-plane oil gaps," *Dielectrics and Electrical Insulation, IEEE Transactions on,* vol. 1, pp. 447-458, 1994.

[55] Y. Torshin, "On the existence of leader discharges in mineral oil," *Dielectrics and Electrical Insulation, IEEE Transactions on,* vol. 2, pp. 167-179, 1995.

[56] O. Lesaint and G. Massala, "Positive streamer propagation in large oil gaps: experimental characterization of propagation modes," *Dielectrics and Electrical Insulation, IEEE Transactions on,* vol. 5, pp. 360-370, 1998.

[57] L. Lundgaard, D. Linhjell, G. Berg, and S. Sigmond, "Propagation of positive and negative streamers in oil with and without pressboard interfaces," *Dielectrics and Electrical Insulation, IEEE Transactions on,* vol. 5, pp. 388-395, 1998.

[58] L. Costeanu and O. Lesaint, "On mechanisms involved in the propagation of subsonic positive streamers in cyclohexane," in *Dielectric Liquids, 2002. ICDL 2002. Proceedings of 2002 IEEE 14th International Conference on*, 2002, pp. 143-146.

[59] N. J. Felici, "Blazing a fiery trail with the hounds (prebreakdown streamers)," *Electrical Insulation, IEEE Transactions on,* vol. 23, pp. 497-503, 1988.

[60] F. O''Sullivan, L. Se-Hee, M. Zahn, L. Pettersson, R. Liu, O. Hjortstam*, et al.*, "Modeling the Effect of Ionic Dissociation on Charge Transport in Transformer Oil," in *Electrical Insulation and Dielectric Phenomena, 2006 IEEE Conference on*, 2006, pp. 756-759.

[61] M. Haidara and A. Denat, "Electron multiplication in liquid cyclohexane and propane," *Electrical Insulation, IEEE Transactions on,* vol. 26, pp. 592-597, 1991.

[62] E. Takahashi, Y. Tsutsumi, K. Okuyama, and F. Ogata, "Partial discharge characteristics of oil-immersed insulation systems under DC, combined AC-DC and DC reversed polarity voltage," *Power Apparatus and Systems, IEEE Transactions on,* vol. 95, pp. 411-420, 1976.

[63] W. Mang-Hui and H. Chih-Yung, "Application of extension theory to PD pattern recognition in high-voltage current transformers," *Power Delivery, IEEE Transactions on,* vol. 20, pp. 1939-1946, 2005.

[64] A. Rajab, K. Umar, D. Hamdani, S. Aminuddin, A. Y. Suwarno, M. Tsuchie*, et al.*, "Partial discharge phase distribution of palm oil as insulating liquid," *TELKOMNIKA,* vol. 9, 2011.

[65] W. N. Kennedy, C. C. Crichton, D. A. Cillies, W. F. Criffard, H. C. Fischer, C. Hurty*, et al.*, "Recommended Dielectric Tests and Test Procedures for Converter Transformers and Smoothing Reactors," *Power Delivery, IEEE Transactions on,* vol. 1, pp. 161-166, 1986.

[66] "IEEE Trial-Use Standard General Requirements and Test Code for Oil-Immersed HVDC Converter Transformers," *IEEE Std C57.129-1999,* p. i, 1999.

[67] A. Cavallini, G. C. Montanari, and F. Ciani, "Analysis of partial discharge phenomena in paper-oil insulation systems as a basis for risk assessment evaluation," in *Dielectric Liquids, 2005. ICDL 2005. 2005 IEEE International Conference on*, 2005, pp. 241-244.

[68] G. P. Cleary and M. D. Judd, "UHF and current pulse measurements of partial discharge activity in mineral oil," *Science, Measurement and Technology, IEE Proceedings -,* vol. 153, pp. 47-54, 2006.

[69] R. Sarathi and G. Koperundevi, "Understanding the Discharge Activities in Transformer Oil under AC and DC Voltage Adopting UHF Technique," *International Journal of Electrical and Computer Engineering,* vol. 3, pp. 878-885, 2008.

[70] M. Krins, H. Borsi, and E. Gockenbach, "Influence of carbon particles on the breakdown and partial discharge inception voltage of aged mineral based transformer oil," in *Dielectric Materials, Measurements and Applications, Seventh International Conference on (Conf. Publ. No. 430)*, 1996, pp. 251-254.

[71] S. Birlasekaran, "The movement of a conducting particle in transformer oil in AC fields," *Electrical Insulation, IEEE Transactions on,* vol. 28, pp. 9-17, 1993.

[72] K. Fischer, "Neues Verfahren zur maßanalytischen Bestimmung des Wassergehaltes von Flüssigkeiten und festen Körpern," *Angewandte Chemie,* vol. 48, pp. 394-396, 1935.

[73] S. Mahmud, G. Chen, I. O. Golosnoy, G. Wilson, and P. Jarman, "Bridging phenomenon in contaminated transformer oil," in *Condition Monitoring and Diagnosis (CMD), 2012 International Conference on*, 2012, pp. 180-183.

[74] S. Mahmud, G. Chen, I. O. Golosnoy, G. Wilson, and P. Jarman, "Bridging in contaminated transformer oil under DC and AC electric field," in *Journal of Physics: Conference Series*, 2013, p. 012007.

[75] S. Mahmud, G. Chen, I. O. Golosnoy, G. Wilson, and P. Jarman, "Bridging in contaminated transformer oil under AC, DC and DC biased AC electric field," in *Electrical Insulation and Dielectric Phenomena (CEIDP), 2013 IEEE Conference on*, Shenzhen, China, 2013, pp. 943-946.

[76] H. A. Pohl, "The motion and precipitation of suspensoids in divergent electric fields," *Journal of Applied Physics,* vol. 22, pp. 869-871, Recieved 15 November 1950 1951.

[77] G. Molinari and A. Viviani, "Analytical evaluation of the electro-dielectrophoretic forces acting on spherical impurity particles in dielectric fluids," *Journal of Electrostatics,* vol. 5, pp. 343-354, 9// 1978.

[78] G. Molinari and A. Viviani, "Experimental results and computer simulation of impurity particles motion in N-hexane under D.C. and A.C. conditions," *Journal of Electrostatics,* vol. 5, pp. 355-367, 9// 1978.

[79] G. Molinari and A. Viviani, "Preliminary results of computer simulation of D.C. conduction due to impurity particles in a dielectric liquid and comparison with experimental data," *Journal of Electrostatics,* vol. 7, pp. 21-26, 8// 1979.

[80] G. Molinari and A. Viviani, "Analysis of the charge exchange mechanism between impurities and electrodes in a dielectric liquid," *Journal of Electrostatics,* vol. 7, pp. 27-32, 8// 1979.

[81] Z. Zapryanov and S. Tabakova, *Dynamics of bubbles, drops and rigid particles* vol. 50: Springer, 1999.

[82] P. J. Lipowicz and H. C. Yeh, "Fiber Dielectrophoresis," *Aerosol Science and Technology,* vol. 11, pp. 206-212, 1989/01/01 1989.

[83] S. Mahmud, G. Chen, I. O. Golosnoy, G. Wilson, and P. Jarman, "Experimental Studies of influence of DC and AC Electric Fields on Bridging in Contaminated Transformer Oil," *Dielectrics and Electrical Insulation, IEEE Transactions on,* 2014.

[84] M. Darveniza, "The Effect of Carbon Particles on the AC Strength of Transformer Oil," *Trans. Electr. Eng. The Institute of Engineers, Australia,,* vol. Vol. 5,, pp. 284-289, 1969.

[85] B. S., "The Study of Prebreakdown Processes in Transformer Oil of Technical Purity," PhD University of Queensland, 1981.

[86] W. Wilson and L. Wetherill, "Operation of Bushings in Carbonized Oil," *American Institute of Electrical Engineers, Transactions of the,* vol. 70, pp. 1398-1407, 1951.

[87] J. H. Harlow, *Electric power transformer engineering*: CRC press, 2007.

[88] Y. Zhou, M. Hao, G. Chen, P. Jarman, and G. Wilson, "Space charge polarization in insulating mineral oil," in *Electrical Insulation and Dielectric Phenomena (CEIDP), 2013 IEEE Conference on*, 2013, pp. 587-590.

[89] Y. Zhou, M. Hao, G. Chen, P. Jarman, and G. Wilson, "A new approach to understanding the frequency response of mineral oil," in *Dielectric Liquids (ICDL), 2014 IEEE 18th International Conference on*, 2014, pp. 1-4.

[90] Y. Zhou, M. Hao, G. Chen, G. Wilson, and P. Jarman, "Study of the dielectric response in mineral oil using frequency-domain measurement," *Journal of Applied Physics,* vol. 115, pp. -, 2014.

[91] S. Mahmud, G. Chen, I. O. Golosnoy, G. Wilson, and P. Jarman, "Effect of Kraft Paper Barriers on Bridging in Contaminated Transformer Oil," in *Electrical Insulation and Dielectric Phenomena (CEIDP), 2014 IEEE Conference on*, Des Moines, Iowa, USA, 2014, p. 4.

[92] S. V. Kulkarni and S. Khaparde, *Transformer engineering: design and practice* vol. 25. New York: Marcel Dekker, Inc, 2004.

[93] A. Castellanos, *Electrohydrodynamics*: Springer, 1998.

[94] Z. Yan, C. Louste, and H. Romat, "Characteristics of an EHD impinging dielectric. Liquid jet in blade-plane geometry," in *Proceedings of the 2012 Electrostatics Joint Conference June*, 2012, pp. 12-14.

[95] Y. Feng and J. Seyed-Yagoobi, "Understanding of electrohydrodynamic conduction pumping phenomenon," *Physics of Fluids (1994-present),* vol. 16, pp. 2432-2441, 2004.

[96] P. Atten, "Electrohydrodynamic instability and motion induced by injected space charge in insulating liquids," *Dielectrics and Electrical Insulation, IEEE Transactions on,* vol. 3, pp. 1-17, Feb 1996.

[97] P. Atten and J. Seyed-Yagoobi, "Electrohydrodynamically induced dielectric liquid flow through pure conduction in point/plane geometry," *Dielectrics and Electrical Insulation, IEEE Transactions on,* vol. 10, pp. 27-36, 2003.

[98] S.-i. Jeong and J. Seyed-Yagoobi, "Experimental study of electrohydrodynamic pumping through conduction phenomenon," *Journal of Electrostatics,* vol. 56, pp. 123-133, 9/26/ 2002.

[99] R. Hanaoka, S. Takata, M. Murakumo, and H. Anzai, "Properties of liquid jet induced by electrohydrodynamic pumping in dielectric liquids," *Electrical Engineering in Japan,* vol. 138, pp. 1-9, 2002.

[100] P. Traoré, M. Daaboul, and C. Louste, "Numerical simulation and PIV experimental analysis of electrohydrodynamic plumes induced by a blade electrode," *Journal of Physics D: Applied Physics,* vol. 43, p. 225502, 2010.

[101] P. Atten, B. Malraison, and M. Zahn, "Electrohydrodynamic plumes in point-plane geometry," *Dielectrics and Electrical Insulation, IEEE Transactions on,* vol. 4, pp. 710-718, 1997.

[102] N. N. A. Jaafar, "Modelling of Dust Accumulation in Transformer Oil," BEng, Electronics and Computer Science, University of Southampton, 2010.

[103] N. Naciri, "FINITE ELEMENT ANALYSIS FOR POWER SYSTEM COMPONENTS: DUST ACCUMULATION IN TRANSFORMER OIL," MSc MSc Thesis, Department of Electronics and Computer Science, , University of Southampton, 2011.

[104] L. Dascalescu, M. Mihailescu, and R. Tobazeon, "Modeling of conductive particle behavior in insulating fluids affected by DC electric fields," *Industry Applications, IEEE Transactions on,* vol. 34, pp. 66-74, 1998.

[105] T. B. Jones, "Dielectrophoretic force calculation," *Journal of Electrostatics,* vol. 6, pp. 69-82, 1979.

[106] G. Placzek, "Zur Dichten- und Gestaltsbestimmung submikroskopischer Probekörper," *Zeitschrift für Physik,* vol. 55, pp. 81-118, 1929/02/01 1929.

[107] H. A. Pohl, "Dielectrophoresis," *Cambridge University Press,* 1978.

[108] F. Du, "Separation of solid-liquid and liquid-liquid phases using dielectrophoresis," PhD, Center for Environmental Research and Sustainable Technology, 2010., Univeristy of Bremen, 2010.

[109] T. B. Jones and G. W. Bliss, "Bubble dielectrophoresis," *Journal of Applied Physics,* vol. 48, pp. 1412-1417, 1977.

[110] L. Benguigui and I. J. Lin, "More about the dielectrophoretic force," *Journal of Applied Physics,* vol. 53, pp. 1141-1143, 1982.

[111] Y. A. Lin, G. Aldaeus, F. Roeraade, J., "Simulation of Dielectrophoretic Motion of Microparticles Using a Molecular Dynamics Approach," 2006.

[112] A. Ramos, *Electrokinetics and electrohydrodynamics in microsystems* vol. 530: Springer Vienna, 2011.

[113] COMSOL Multiphysics, "Particle Tracing for Fluid Flow," in *COMSOL Multiphysics, Finite Element Analysis Software* 4.4 ed, 2014.

[114] N.-J. Felici, "Forces et Charges de Petits Objets en Contact avec une Electrode Affectde d'un Champ Electrique," *Revue GCndrale De L'Clectricitd,* pp. 1145-1157, 1966.
[115] N. Lebedev and I. Skalskaya, "Force acting on a conducting sphere in field of a parallel plate condenser," vol. 7, ed: AMER INST PHYSICS CIRCULATION FULFILLMENT DIV, 500 SUNNYSIDE BLVD, WOODBURY, NY 11797-2999, 1962, pp. 268-&.
[116] J. C. Maxwell, *A treatise on electricity and magnetism*, Third ed. vol. 1: Clarendon press, 1881.
[117] L. Dascalescu, A. Samuila, and R. Tobazéon, "Cylindrical conductive particles in the proximity of an electrode affected by a high-intensity electric field," *Journal of Electrostatics,* vol. 37, pp. 173-196, 1996.
[118] COMSOL, "COMSOL Multiphysics® 2014 " vol. 2014, 4.4 ed. Stockholm, 2014.
[119] S. Sharif, "Chemical and mineral composition of dust and its effect on the dielectric constant," *Geoscience and Remote Sensing, IEEE Transactions on,* vol. 33, pp. 353-359, 1995.
[120] W. R. Smythe, *Static and dynamic electricity*: McGraw-Hill, 1967.
[121] X. Wang, "PARTIAL DISCHARGE BEHAVIOURS AND BREAKDOWN MECHANISMS OF ESTER TRANSFORMER LIQUIDS UNDER AC STRESS," PhD PhD, School of Electrical and Electronic Engineering, University of Manchester, 2011.
[122] H. Hirose, "Maximum likelihood parameter estimation in the extended Weibull distribution and its applications to breakdown voltage estimation," *Dielectrics and Electrical Insulation, IEEE Transactions on,* vol. 9, pp. 524-536, 2002.
[123] D. Martin and Z. D. Wang, "Statistical analysis of the AC breakdown voltages of ester based transformer oils," *Dielectrics and Electrical Insulation, IEEE Transactions on,* vol. 15, pp. 1044-1050, 2008.
[124] F. A. M. Rizk and C. Vincent, "Testing for low breakdown probability with special reference to liquid insulation," *Power Apparatus and Systems, IEEE Transactions on,* vol. 96, pp. 1892-1900, 1977.
[125] H. Z. Ding, Z. D. Wang, and P. Jarman, "Dielectric Strength of Aged Transformer Oils: Experimental Studies and Statistical Analysis of Breakdown voltage," presented at the International Symposium on High Voltage Engineering, China, 2005.